

# **From Polymer End-Group Transformations to Tailored Biosurface Functionalization**

Zur Erlangung des akademischen Grades eines  
DOKTORS DER NATURWISSENSCHAFTEN  
(Dr. rer. nat.)

Fakultät für Chemie und Biowissenschaften  
Karlsruher Institut für Technologie (KIT) - Universitätsbereich

Genehmigte

DISSERTATION

von

**Mathias Christian Dietrich**

aus

Herbolzheim, Deutschland

Dekan: Prof. Dr. M. Bastmeyer

Referent: Prof. Dr. C. Barner-Kowollik

Korreferent: Prof. Dr. M. Wilhelm

Tag der mündlichen Prüfung: 20.10.2011



Die vorliegende Arbeit wurde von November 2008 bis September 2011 unter Anleitung von Prof. Dr. Christopher Barner-Kowollik am Karlsruher Institut für Technologie (KIT) - Universitätsbereich angefertigt.



# Abstract

## End Group Conversion of RAFT-Polymers

The reversible addition fragmentation chain transfer (RAFT) process is currently one of the most established techniques in the field of controlled radical (CRP) polymerization. The RAFT process has proven to be a versatile polymerization method which can be employed on a wide range of monomers as well as offering high solvent compatibility. Since the development of RAFT in the late 1990s, a wide diversity of applications of complex macromolecular architectures have been developed, e.g., diblock copolymers, protein conjugates and star shaped (co)polymers. The RAFT process offers high industrial potential due to its versatility and straightforward application, yet the presence of the sulfur containing control agent is a significant drawback as the products are generally colored materials that may degrade upon UV-light irradiation or that may result in potential toxic and foul smelling bi-products while altering. Although the RAFT group is increasingly seen as a versatile handle in macromolecular architecture design (e.g., *via* RAFT-hetero Diels Alder reactions) for industrial applications, the presence of sulfur is still a drawback. One solution to this problem, which is presented in the current thesis, is the transformation of RAFT polymers into hydroxyl functional polymers. The, herein, developed method can be employed on RAFT polymers ranging from methacrylic to acrylic to styrenic type polymers that possess trithiocarbonate, phenyldithioacetate or dithiobenzoate RAFT group. The transformation is carried out in tetrahydrofuran under atmospheric pressure at 60°C using 2,2'-Azobis(isobutyronitrile) (AIBN) as an initiator. The mechanism consists of an oxidation cycle comparable to the radical autooxidation of ethers with an additional intermediate transfer step yielding hydroperoxide functionalized polymers. After adding triphenylphosphine to the reaction mixture at 40°C, the hydroperoxide group is reduced to the hydroxyl group. The transformation proceeds with very high efficiency and only generates negligible amounts of side products (depending on the type of RAFT agent and polymer employed). Resulting in hydroxyl end functionalized polymers, this simple one pot transformation offers new pathways towards further polymer conjugation reactions, which have already been carried out in the ongoing Ph.D. thesis of C. Schmid (KIT).

# Block Copolymer Architectures via UV-Activation

## The Nitrile Imine-mediated 1,3-Dipolar Cycloaddition of Tetrazole and Ene Coupling (NITEC) Approach for Block Copolymer Formation

Efficient and mild coupling reactions are very important in modern macromolecular architecture design. A significant number of ligation reactions are efficient yet they require a metal catalysts to proceed. However, when working with biological systems all metal catalyst should be avoided. Thus ligation reactions avoiding the need for such catalysts are of great interest. One such reactions is the nitrile imine-mediated tetrazole-ene cycloaddition reaction (NITEC). In the current thesis this reaction is introduced as a powerful and versatile conjugation tool that avoids the use of metal catalysts, which can be utilized to covalently ligate polymer chains yielding block copolymers. The NITEC approach is initiated by UV-light irradiation and proceeds rapidly at ambient temperature yielding a highly fluorescent linkage. The process has already proven to be extremely useful in the field of biochemistry (e.g., for *in vitro* modification of enzymes). Yet, the NITEC has not found applications in synthetic polymer chemistry. Therefore, the formation of block copolymers through a NITEC reaction is studied to demonstrate the efficacy of such a reaction as a macromolecular conjugation tool. This coupling technique employs a tetrazole moiety and an electron deficient or unactivated alkene as a counterpart. Upon UV-light irradiation, the tetrazole group releases nitrogen and forms a nitrile imine. The nitrile imine reacts with alkenes to form pyrazoline linkages. Experiments to determine the efficiency of the coupling reaction was carried out with two polymer systems. First, low molecular weight PEG ( $M_n = 2000 \text{ g mol}^{-1}$ ) was functionalized with a tetrazole and a maleimide end group, respectively. The coupling reaction was performed in ethanol. Evaluation of the coupling reaction was carried out *via* SEC/ESI-MS which proved that the reaction was successful. Furthermore, AB-type block copolymers, consisting of PEG and PMMA units, were synthesized. Although SEC/ESI-MS is not applicable for such a system, a shift in the SEC demonstrated the successful coupling. It was shown that the NITEC reaction could be successfully employed for the synthesis of block copolymers.

## The TEMPO/Photoinitiator Conjugation Approach

As mentioned previously, ligation reactions have become indispensable in constructing complex polymer structures. The, herein, presented ligation reaction combines the concept of photografting with the concept of radical coupling. Upon UV-light irradiation, a photoinitiator generates a radical carbon center, which is captured by a stable nitroxide radical (analog of a modified 2,2,6,6-Tetramethyl-1-piperidinyloxy (TEMPO) molecule). The final aim was to couple a photoinitiator functionalized PEG to its counterpart, the nitroxide functionalized PEG. Thus, low molecular weight PEG ( $M_n = 2000 \text{ g mol}^{-1}$ ) was equipped with a TEMPO derivative or a photoinitiator end group. First, the reactions of the TEMPO functionalized PEG with a small molecule photoinitiator and the photoinitiator functionalized PEG with a small molecule TEMPO were studied. The coupling reactions were investigated by SEC/ESI-MS. After demonstrating the successful coupling of polymer chains and small molecules with the corresponding small molecule, a photoinitiator functionalized PEG and a TEMPO functionalized PEG were coupled together to study this polyme-polymer conjugation method, which would generate AA-type (block) copolymer. Due to the employment of a low molecular PEG chain, the coupling reaction could be investigated by SEC/ESI-MS. The results of this analysis provided evidence for the success of the coupling reaction. It was also discovered that the presence of an oxidizing agent in the reaction mixture significantly improved the yield of the (block) copolymer.

# Tailored Modification of Biosurface Substrates

## The Nitrile Imine-mediated 1,3-Dipolar Cycloaddition of Tetrazole and Ene Coupling (NITEC) Approach for Block Copolymer Formation

The grafting of polymers onto inorganic (i.e, silicon) and bioorganic (i.e., cellulose) surfaces was subsequently carried out employing the optimized reaction conditions obtained from the macromolecular ligation experiments. Surface characterization was performed by X-ray photoelectron spectroscopy and high resolution FT-IR microscopy. In addition, the patterned immobilization of a variety of polymer chains onto profluorescent cellulose was achieved through a simple masking process applied during UV-light irradiation. The patterned cellulose sample showed fluorescence only at the irradiated places demonstrating the success of the reaction. After grafting PMMA onto profluorescent cellulose the surface changed from hydrophilic to hydrophobic, which was demonstrated by contact angle measurements.

## The TEMPO/Photoinitiator Conjugation Approach

The novel TEMPO/photoinitiator coupling approach was applied to a biosurface (i.e., cellulose). To achieve this aim, cellulose sheets decorated with photoinitiator moieties were prepared. The cellulose sheets were irradiated with UV-light in the presence of the TEMPO functionalized polystyrene in order to couple the polymer covalently onto the surface. Indeed, a change of the physical properties could be observed, from small to large, suggested the success of the reaction. Further, the surface was characterized by X-ray photoelectron spectroscopy, the results of which corroborate the conclusion that the polymer grafting reaction was successful. Although it is not discussed in the current thesis, the, herein, presented TEMPO/photoinitiator coupling reaction offers also permits spatial resolution since the grafting only occurs at the locations that are irradiated by the UV-light.

# Contents

Contents	i
<b>1 Introduction</b>	<b>1</b>
1.1 Free Radical Polymerization . . . . .	1
1.1.1 Initiation . . . . .	2
1.2 Controlled Radical Polymerization . . . . .	4
1.2.1 Atom Transfer Radical Polymerization - ATRP . . . . .	5
1.2.2 Reversible Addition Fragmentation Chain Transfer (RAFT) Polymerization . . . . .	7
1.3 End-group Conversion of RAFT-Polymers . . . . .	8
1.3.1 $\alpha$ -End-group Modification . . . . .	10
1.3.2 $\omega$ -End-group Modification . . . . .	10
1.4 Conclusions and Outlook . . . . .	25
1.5 Surface Modification . . . . .	26
1.5.1 Methods for Surface Modification . . . . .	26
1.5.2 Physisorption of Polymers Onto Surfaces . . . . .	26
1.5.3 <i>Grafting-From</i> . . . . .	28
1.5.4 <i>Grafting-To</i> . . . . .	28
1.5.5 Surface Modification of Cellulose . . . . .	29
1.5.6 Cellulose <i>Grafting-From</i> in Heterogeneous Media . . . . .	31
1.5.7 Cellulose <i>Grafting-To</i> in Heterogeneous Media . . . . .	32

---

<b>2</b>	<b>Methods and Materials</b>	<b>33</b>
2.1	Materials . . . . .	33
2.1.1	Chemicals Used in Chapter 3 . . . . .	33
2.1.2	Chemicals Used in Chapter 4 and 5 . . . . .	33
2.2	Characterization Techniques . . . . .	35
2.2.1	<sup>1</sup> H Nuclear Magnetic Resonance Spectroscopy . . . . .	35
2.2.2	Coupled Size Exclusion Chromatography/Electrospray Ionization (SEC/ESI-MS) . . . . .	35
2.2.3	Molecular Weight Analysis <i>via</i> Size Exclusion Chromatography (SEC) . . . . .	36
2.2.4	X-ray Photoelectron Spectroscopy (XPS) . . . . .	36
2.2.5	Contact Angle Measurements . . . . .	37
<b>3</b>	<b>End Group Conversion of RAFT-Polymers</b>	<b>39</b>
3.1	Introduction . . . . .	39
3.2	Experimental . . . . .	40
3.2.1	Polymerizations with cyanoisopropyl dithiobenzoate . . . . .	40
3.2.2	Polymerizations with cumylphenyldithioacetate . . . . .	41
3.2.3	Polymerizations mediated by dibenzyltrithiocarbonate . . . . .	41
3.2.4	Analytical (small scale) end-group conversion . . . . .	41
3.2.5	Larger scale end-group conversion . . . . .	42
3.3	Results and discussion . . . . .	42
3.3.1	Mechanism of the end-group conversion . . . . .	43
3.3.2	End-group conversion of dithiobenzoate functional poly(alkyl acrylate)s and poly(alkyl methacrylate)s . . . . .	44
3.3.3	End-group conversion of phenyldithioacetate functional poly(alkyl acrylate)s . . . . .	48
3.3.4	End-group conversion of symmetrical trithiocarbonate functional poly(alkyl acrylate)s . . . . .	53
3.3.5	Conclusions . . . . .	69

---

<b>4</b>	<b>Block Copolymer Architectures via UV-light Activation</b>	<b>71</b>
4.1	Introduction . . . . .	71
4.2	Efficient Tools for Macromolecular Design . . . . .	72
4.2.1	Azide/Alkyne Cycloadditions . . . . .	72
4.2.2	Cycloadditions with Strained or Activated Alkynes . . . . .	73
4.2.3	Thiol-ene/Thiol-yne Conjugations . . . . .	74
4.2.4	The Chemistry of Thiol-Isocyanate Coupling . . . . .	75
4.2.5	The Chemistry of Thio-Bromo Conjugation . . . . .	76
4.2.6	Inverse Electron-Demand Diels-Alder Cycloaddition . . . . .	77
4.2.7	Nitrile Oxides in Cycloadditions . . . . .	77
4.2.8	Coupling <i>via</i> Oxime Formation . . . . .	78
4.2.9	Atom Transfer Nitroxide Radical Coupling (AT-NRC) . . . . .	79
4.2.10	UV-Light activated Tetrazole-Ene Coupling . . . . .	79
4.3	Experimental Part . . . . .	81
4.3.1	The Nitrile Imine-Mediated 1,3-Dipolar Cycloaddition of Tetra- zole and Ene Coupling (NITEC) Approach . . . . .	81
4.3.2	The TEMPO/Photoinitiator Conjugation Approach . . . . .	86
4.4	Results and Discussion . . . . .	93
4.4.1	The Nitrile Imine-mediated 1,3-Dipolar Cycloaddition of Tetra- zole and Ene Coupling (NITEC) Approach for Block Copolymer Formation . . . . .	93
4.4.2	The TEMPO/Photoinitiator Conjugation Approach . . . . .	100
4.5	Conclusions and Outlook . . . . .	115
4.5.1	The Nitrile Imine-mediated 1,3-Dipolar Cycloaddition of Tetra- zole and Ene Coupling (NITEC) Approach for Block Copolymer Formation . . . . .	115
4.5.2	The TEMPO/Photoinitiator Conjugation Approach . . . . .	116

<b>5 Tailored Modification of Biosurfaces</b>	<b>119</b>
5.1 Introduction . . . . .	119
5.2 Experimental . . . . .	121
5.2.1 The Nitrile Imine-mediated 1,3-Dipolar Cycloaddition of Tetra- zole and Ene Coupling (NITEC) Approach . . . . .	121
5.2.2 The TEMPO/Photoinitiator Conjugation Approach . . . . .	126
5.3 Results and Discussion . . . . .	128
5.3.1 The Nitrile Imine-mediated 1,3-Dipolar Cycloaddition of Tetra- zole and Ene Coupling (NITEC) Approach . . . . .	128
5.3.2 The TEMPO/Photoinitiator Conjugation Approach . . . . .	140
5.4 Conclusion and Outlook . . . . .	144
5.4.1 The Nitrile Imine-mediated 1,3-Dipolar Cycloaddition of Tetra- zole and Ene Coupling (NITEC) Employed for Polymer Grafting on Surfaces . . . . .	144
5.4.2 The TEMPO/Photoinitiator Employed for Polymer Grafting on Surfaces . . . . .	144
<b>References</b>	<b>145</b>
<b>Curriculum Vitae</b>	<b>161</b>
<b>List of Publications and Conference Contributions</b>	<b>163</b>
<b>6 Acknowledgements</b>	<b>167</b>

# 1

## Introduction

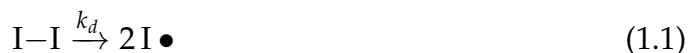
The annual turnover of around 230 million tons of polymer based materials indicates the high demand and importance of this industry. Polymers are more and more replacing classic materials, such as steel and wood, because of their wide range of tunable material properties.<sup>1</sup> Polymers can be synthesized by either step-growth polymerization or chain-growth polymerization. The main focus of this work is placed on the chain-growth polymerization mechanism and especially radical polymerization. While basic information is given as well as information relevant for the current thesis will be provided in here, for further information on polymerization mechanisms, the reader is advised to refer to 'Principles of polymerization' by G. Odian<sup>2</sup> for an in depth coverage of the topic.

### 1.1 Free Radical Polymerization

Free radical polymerization (FRP) contributes approximately 45 % to the world's total production of plastic material,<sup>3</sup> exhibiting the dependance upon polymers produced *via* FRP. Due to the significance of this polymerization process the mechanistic steps will be discussed.

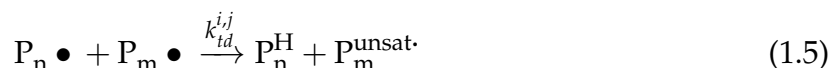
### 1.1.1 Initiation

The first step of a radical polymerization is the initiation process. Active sites are formed which react with the present monomers to start the polymerization. These active sites can be formed *via* various methods, e.g., thermal decomposition and photolysis to name two important examples. The initiation process can be divided into two main parts. The first step is the generation of primary radicals (1.1). Commonly azo-initiators or peroxy-compounds are used which have typical dissociation rate coefficients ( $k_d$ ) in the range of  $10^{-5} \text{ s}^{-1}$ . These primary radicals react with the monomer, mostly *via* a vinyl group (1.2) with a rate coefficient  $k_i$  of about  $10^4 \text{ M}^{-1} \text{ s}^{-1}$ , although this value can vary widely.<sup>4</sup> Further monomer units add to the molecule until the small molecule becomes a macro-radical species which continues to add further monomer units with no influence of the starting radical species on the long chain radical propagation rate coefficient. This part of the polymerization is termed propagation (1.3) with typical propagation rate coefficients around  $10^3 \text{ M}^{-1} \cdot \text{s}^{-1}$  for styrene and methacrylates and  $3 \times 10^4 \text{ M}^{-1} \cdot \text{s}^{-1}$  for acrylates at 60-80 °C,<sup>5-9</sup> for example.



Although these reactions are the main pathways of the polymerization process at low conversion, side reactions inevitably do occur at all stages of the process but are more likely to happen during the end of the process at high conversion. Arguably, the most important side processes are termination reactions where the growing radical species are irreversibly removed from the reaction mixture giving inactive or so called *dead* polymer chains. There are two main termination processes, recombination 1.4 and disproportionation 1.5. Recombination occurs when two active polymer chains react to form a *dead* polymer chain with the length of the chain being equal to the sum of the single chains. Disproportionation occurs when an active polymer chain abstracts a hydrogen atom of another active polymer chain resulting in polymer chains with their initial length. While one polymer chain is not suitable for further polymerization the other polymer chain bears an unsaturated group which can further react, depending on the structure of the unsaturated end-group, and therefore may behave as a macromonomer which can be re initiated with present radical species. The rate coefficient for termination  $k_t$  at low conversions is for many monomers in the range of  $10^8 \text{ M}^{-1} \cdot \text{s}^{-1}$  and therefore considered in the range of diffusion-limited reactions.<sup>10</sup> As the polymer chain grows, the increasing polymer content leads to a higher viscosity in the polymerization solution. Due to reduced mobility of the growing polymer chain, the probability that

two active polymer chains interact and terminate is also reduced and hence the termination rate coefficient  $k_t$  decreases.<sup>11</sup> The decrease in mobility of the polymer chains and less termination reactions lead to an isothermal *autoacceleration* of the polymerization.<sup>12</sup> This effect is called the *gel effect* or *Trommsdorff effect* or *Norrish-Smith effect*. An increase in temperature due to the exothermic polymerization leads to an additional autoacceleration which subsequently leads to even higher polymerization rates.



Dead polymer chains are also formed due to abstraction of hydrogen or other species of macroradicals with molecules present in the polymerization mixture i.e., monomers or solvent. 1.6 shows the general reaction scheme of a transfer reagent, labeled T, with a living polymer chain. The living polymer chain transfers the radical to a transfer reagent and results in dead polymer chain. In 1.7 the transfer agent T re-initiates the polymerization by adding to a monomer unit and thus the cycle starts again. It has to be mentioned that, unlike the termination reaction, the transfer process leads to dead polymer chains but the actual radical concentration is not altered. Although transfer processes do not interfere with the radical concentration it can effect the polymerization process significantly as the rate of re-initiation may be different from the initiator molecule. In addition, the accumulation of short dead polymer chains with T end-groups can lead to altered material properties of the final polymer.



Radical polymerization also allows for co-polymerization with various monomers. The process is quite robust, versatile and works under various reaction conditions as well as for a wide range of monomers and solvents and even allows co-polymerizations between different monomer classes. Despite all these advantages there are some major limitations concerning the control over the macromolecular architecture, composition and the polydispersity. During FRP, polymers can be characterized by the number average molecular mass distribution 1.8 and the weight average molecular weight distribution 1.9. The polydispersity index (PDI) describes the broadness of a polymer sample and depends on the mechanism of the termination process. Termination by recombination leads to a PDI of 1.5, while termination by disproportionation leads to a PDI of 2.<sup>2</sup> Due to the incoherent termination processes, there is a limited end-group functionality and hence the FRP is a limited tool for building complex macromolecular architectures. Often the termination processes occur at the same time and due to the incoherent termination steps there is a limited utility of this method in building complex macromolecular architecture. Scientists made great efforts to gain control over the above mentioned

drawbacks leading to more advanced polymerization techniques.

One of the best examples of controlling macromolecular architecture is anionic polymerization. This technique has the advantage in controlling the end-group functionality during the polymerization and also controlling the molecular weight due to the absence of termination events. Additionally the reaction can be 'paused' when all the monomer is depleted and further monomer can be added successively to re-start the polymerization. Anionic polymerization is therefore also known as a *living* polymerization technique, whereby termination reactions do not occur.<sup>13</sup> Although the control over the polymerization process is exquisite, the major drawbacks are the usage of very high purity solvents and monomers, low temperatures as well as the smaller range of monomers compared to free radical polymerization. Due to the chemical nature of the carbanion, water has to be strictly excluded as it quenches the polymerization immediately. A significant body of work has been carried out to combine the advantages of FRP with *living* polymerization techniques. These efforts lead to the development of controlled radical polymerization techniques.

$$M_n = \frac{\sum N_i M_i}{\sum N_i} \quad (1.8)$$

$$M_w = \frac{\sum N_i M_i^2}{\sum N_i M_i} \quad (1.9)$$

$$PDI = \frac{M_w}{M_n} \quad (1.10)$$

where  $N_i$  = number of molecules with mass  $M_i$

## 1.2 Controlled Radical Polymerization

Reversible-Deactivation Radical Polymerization (RDRP) or the abbreviated term Controlled Radical Polymerization (CRP)<sup>14</sup> offer the opportunity to combine the characteristics of *living* polymerization with the versatility of free radical polymerization *via* a careful selection of reaction conditions and control reagents. The advantages of CRP compared to anionic *living* polymerization techniques are the relatively low sensitivity toward impurities, wide range of monomers and mild reaction conditions. Compared to conventional free radical polymerization, there is a more uniform molecular mass distribution and control over the polymer end-groups. These functional polymer end-groups can be exploited for further reactions. Although CRP exhibits a living character during the polymerization process, there is still the possibility of chain terminations to occur which cannot be completely suppressed. To make this distinction clear, the term '*controlled*' is used rather than '*living*'. It is advisable to refer to such processes as radical

polymerization with living characteristics. The most prominent representatives for CRP are the Nitroxide Mediated Polymerization (NMP), the Atom Transfer Radical Polymerization (ATRP) process and the Radical Addition Chain Transfer Polymerization (RAFT) process.

### 1.2.1 Atom Transfer Radical Polymerization - ATRP

ATRP first described 1995 by Sawamoto and colleagues<sup>15</sup> and Matyjaszewski and coworkers<sup>16</sup> and is one of the most studied CRP methods used in synthetic polymer chemistry. In ATRP the control over the polymerization is achieved by a careful selection of an organic halide initiator reacting with a solubilized transition metal complex. The first step is a simultaneous single electron transfer from the metal complex and halogen abstraction from the initiator generating the starting radical. The initiator radical starts the polymerization process, while the oxidized metal complex acts as a 'stable' radical or in this context 'deactivator' is a more appropriate term.<sup>17</sup> This so-called *dormant* species reacts with the *active* polymer chain radical species in a catalytic redox reaction rebuilding the *active* transition metal complex and a *dormant* polymer chain. The equilibrium between activated species and dormant species is the key in providing the livingness of this reaction. Livingness can be achieved if the amount of activated radicals is kept at very low and constant concentrations, which minimizes the termination reactions. To provide a reasonable polymerization the equilibrium constant  $K_{\text{ATRP}} = k_{\text{act}} / k_{\text{deact}}$  has to fulfill certain prerequisites. It must be small enough to suppress bimolecular termination reactions but at the same time large enough to keep the propagation of the polymer chain at an acceptable rate. For a typical ATRP the equilibrium constant  $K_{\text{ATRP}}$  is between  $10^{-4}$  to  $10^{-9}$ .<sup>18</sup> Although the termination reaction is shown in the reaction scheme, under appropriate conditions its contribution will be less than a few percent of total number of chains. One great advantage of ATRP compared

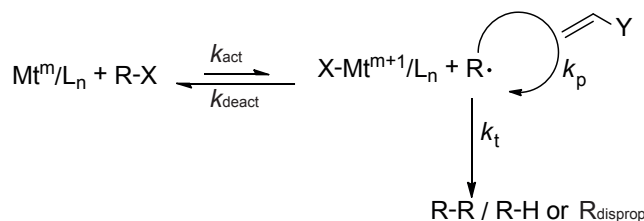


**Figure 1.1:** General mechanism of ATRP. With  $\text{Mt}^m$  = transition metal,  $\text{L}_n$  = complexing Ligand

to conventional FRP is the possibility of post polymerization reactions on the polymer chain end-group moieties. Ideally, more than 90 % of the polymer chains should contain the halide atom which can be substituted. To achieve such high end functionalizations, the conversion has to be stopped at low monomer concentration (< 40 %) as

the chain-end functionality decreases due to side reactions. If one employs an initiator bearing a functional group, the variety of post polymerization reactions increases, as will be shown later. The transition metal complexes consist of iron, nickel, ruthenium, rhodium, palladium, rhenium or most commonly copper. Ligands used in ATRP mostly consist mostly of nitrogen based compounds and as initiators usually halogenated alkanes, benzylhalogenides are used. The monomers should stabilize the growing chain end radical and therefore the following important monomer classes have been used in ATRP with success: Styrene, (meth)acrylates, (meth)acrylamides, butadiene or acrylnitriles. For high reactive monomers, such as vinyl acetate, ATRP is not suitable due to only a small stabilization of the propagating radical. Although the above mentioned polymers are generally appropriate for the ATRP process, each monomer exhibits a unique set of rate coefficients  $k_{act}$ ,  $k_{tr}$  and  $k_{tr}^*$  which has to be tuned to the ATRP system of initiator and catalyst to maintain good control over the polymerization. Over the past years there have been modifications of the original ATRP process to improve its versatility. Examples of modified ATRP processes include:

- **'reverse' ATRP**

The ATRP initiator is generated *in-situ* from a higher oxidation state metal complex by the decomposition of conventional free radical initiators.

Advantages: Less sensitivity of the active catalyst complexes against air compared to conventional ATRP.

Limits: Only linear polymers can be synthesized. Lower end-group functionality than in conventional ATRP due to side reactions of the growing polymer chain with the conventional initiator. The amount of metal complex is still employed in the same magnitude than conventional ATRP.<sup>19</sup>

- **Activator Generated by Electron Transfer (AGET) ATRP**

Stoichiometric amounts of reducing agents, such as zero-valent copper, tin(II) 2-ethyl hexanoate, ascorbic acid and triethylamine, are added to the ATRP mixture containing the alkyl halide, monomer and an air stable higher oxidation state catalyst. The deactivated high oxidation state catalyst is regenerated by the reducing agent.

Advantages: The technique was successfully applied in aqueous and miniemulsion systems.

Limits: The amount of metal complex is still employed in the same magnitude than conventional ATRP.<sup>20-23</sup>

- **Activator ReGenerated by Electron Transfer (ARGET) ATRP**

The ARGET ATRP is similar to AGET ATRP, with the exception of using a much lower concentration of the active metal catalyst. The active catalyst is regenerated by a large excess of a present reducing agent, such as ascorbic acid, glucose and tin(II) 2-ethyl hexanoate.

Advantages: The rate of polymerization is comparable to standard ATRP with

the benefit of using a much lower amount (as low as 10 ppm) of active catalyst compared to traditional ATRP (1000-10000 ppm).<sup>20,24,25</sup>

- **Initiators for Continuous Activator Regeneration (ICAR) ATRP**

Free radicals are slowly and continuously generated by a conventional free radical initiator, such as AIBN, in order to scavenge oxidants and decrease the amount of active metal catalyst by regenerating the active catalyst. Therefore the metal catalyst can be employed in very low concentration (as low as 1 ppm) but still keeping good control over the ATRP polymerization.<sup>26</sup>

For a comprehensive overview over the ATRP process the reader is referred to the reviews by de Lina and Matyjaszewski,<sup>27</sup> Xia and Matyjaszewski,<sup>17</sup> and Pintauer and Matyjaszewski.<sup>28</sup>

Although there have been great improvements in reducing the active metal catalyst employed for ATRP polymerizations, there will always be at least the risk of contamination of a small amount of metal catalyst present in the final product. Another very important polymerization technique will be introduced in the next chapter avoiding the limitations of metal catalyst systems. Not saying that the remaining metal catalyst in polymerization is always not desirable, the metal free controlling polymerization technique offers new opportunities in new materials where a present metal catalyst has to be avoided under all circumstances.

## 1.2.2 Reversible Addition Fragmentation Chain Transfer (RAFT) Polymerization

The RAFT process was invented 1998 by a group from the Commonwealth Scientific and Industrial Research Organisation (CSIRO). They showed the controlled polymerization process of various monomers using dithioesters as controlling agents.<sup>29</sup> The livingness of this method can be further confirmed by building block copolymer using the initial RAFT polymers in subsequent polymerizations.<sup>30</sup> RAFT polymerization has several advantages compared to the before mentioned ATRP process such as the absence of a transition metal complex. Removing the metal complexes after the ATRP can include a tedious work up before the obtained polymer is free of the catalyst. Also the RAFT process opens the controlled living polymerization to a wider monomer range, as it is robust toward acidic groups, such as (meth)acrylic acids, while acidic groups poison the ATRP catalyst and hence interfere with the control of the polymerization. At the same time Corpart and co-workers developed a mechanistic same procedure which is based on xanthates as control agents, named *macromolecular design by interchange of xanthates* (MADIX) and can be utilized for monomers with high reactivity where dithioesters are not applicable.<sup>31-34</sup> The RAFT mechanism is shown in Figure 1.2 (modified from reference<sup>30</sup>). First, the initiator **1** generates radicals which react with the monomer to

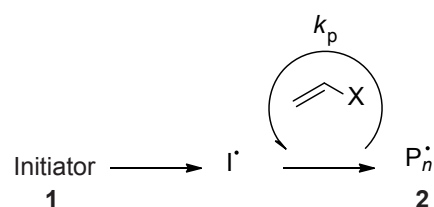
oligomers bearing active radical end-groups **2**. These radicals add to the RAFT agent **3** building an intermediate radical **4** which degenerates through fragmentation into a RAFT agent bearing a polymer/oligomer group **5** and re-initiating a radical **6**. If its radical reactivity is chosen carefully, this radical initiates a new polymerization generating reactive oligomers **7**. Once all of the RAFT agent's R-groups are released, the polymerization is (ideally) controlled by the main equilibrium where the active chain ends **7** are added to the macro RAFT agent **5**. The intermediate macro RAFT radical **8** plays an important role as deactivates the active polymer chain, while 'releasing' the before attached polymer chain to re-generate an active polymer chain radical **2**. The newly activated polymer chain continues with the polymerization until it is deactivated by the macro RAFT agent and the cycle restarts. The controlling nature of the RAFT process is caused by the short lifetime of an active polymer end-group radical and therefore its small probability of terminating with another active polymer end-group radical. The number of active radicals is the same as in FRP - provided the intermediate radicals **4** and **8** are unstable - while in ATRP the number of radicals is reduced during the polymerization. As a result, the propagation rate should not be reduced when comparing the RAFT process with a conventional free radical polymerization. However, sometimes rate retarding can be observed, specifically when dithiobenzoates are employed as mediating agents. A wide range of explanations exist for the phenomena, e.g., radical coupling between the intermediate dithioester radical and an active polymer chain end radical and a slow or delayed fragmentation of the intermediate radical step during the transfer reaction. It also has to be noted that the given rate coefficients for the RAFT process are (potentially) depending on the chain length of the polymer chain. For a deeper insight of effects on propagation rate coefficients, the reader is referred to the article by Dervaux *et al.*<sup>35</sup>

Beside dithioesters, certain trithiocarbonates and dithiocarbamates can be employed as RAFT agents.<sup>36-41</sup> It should be further mentioned that the RAFT process has been proven to be compatible not only to various monomers but also with a variety of solvents.<sup>42-45</sup>

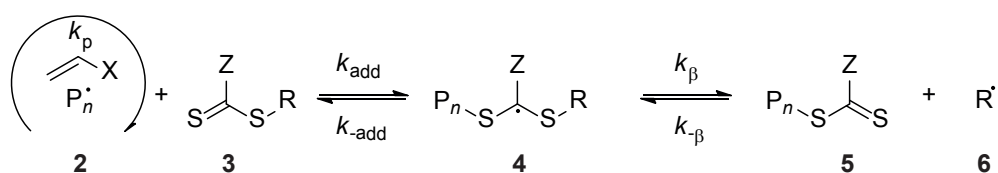
### 1.3 End-group Conversion of RAFT-Polymers

Beside being a versatile tool for excellent control over radical polymerizations, the RAFT process also offers the possibility of synthesizing a wide range of complex polymer architectures such as block copolymers,<sup>46</sup> stars,<sup>47</sup> hyperbranched polymers<sup>48</sup> and higher order supramolecular structures.<sup>49-51</sup> As a CRP the RAFT process allows the incorporation of functional end-groups during the polymerization. There are two approaches how one can access polymer end-group functionalization, i.e., the  $\alpha$  or the  $\omega$  approach. Figure 1.3 shows the resulting main product of a RAFT polymerization process highlighting the two end-groups. The  $\alpha$ -end is the polymer chain end bearing the

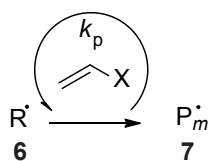
Initiation



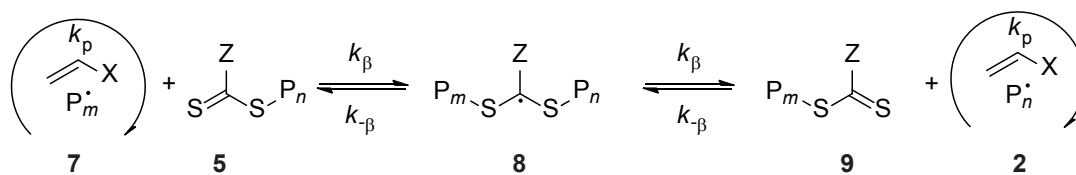
Reversible Chain Transfer (Pre-Equilibrium)



Reinitiation



Main Equilibrium



Termination

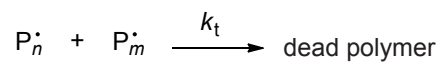


**Figure 1.2:** General RAFT mechanism of a polymerization mediated by dithioesters.

R-group, while the  $\omega$ -end is bearing the Z-group. There are multitude of successful syn-

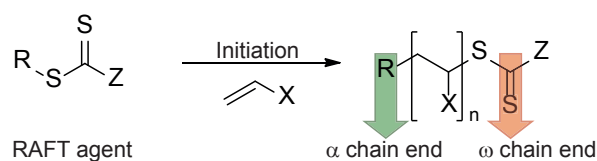


**Figure 1.3:** The RAFT polymerization process highlighting the  $\alpha$ - and  $\omega$ -chain end in the final polymer.

thetic pathways for introducing a wide range functional groups into thiocarbonyl thio capped polymers by the  $\alpha$ - and  $\omega$ -end-group approach of which some examples will be given.<sup>52-54</sup>

### 1.3.1 $\alpha$ -End-group Modification

The incorporation of functional groups into the  $\alpha$ -end-group of RAFT polymers follows the same paths, as in other CRP methods such as ATRP or NMP (see the comprehensive reviews<sup>55</sup> and<sup>56</sup>). There are many examples of chain end functionalization *via* the  $\alpha$ -end-group approach in the RAFT process i.e., carboxylic acids,<sup>52</sup> peptides<sup>57</sup> as well as lipid groups,<sup>58</sup> the *in-situ* formation of protein-polymer conjugates *via* RAFT polymerization using a bioconjugated RAFT agent<sup>59</sup> and other examples, e.g ionic dithioester based RAFT agents, bis(2,2':6',2''-terpyridine)ruthenium(II)-connected diblock polymers and cationic surfactants containing a cleavable group to name a few.<sup>44,54,60-62</sup> While the R-group approach is similar in RAFT as in the other CRP methods, the new feature of RAFT polymers is the  $\omega$ -chain end bearing a thiocarbonyl moiety. As useful the labile C-S bond in the thiocarbonylthio group is in aspects of controlling a polymerization, it may be a problem for industrial applications. These problems include the odor and color due to the potential degradation of the end-group, even including the release of toxic volatile sulfur compounds. Thus, a great amount of investigations has been conducted to address this problem by removing the thiocarbonyl group in post polymerization reactions.<sup>63,64</sup> Since these reports, a paradigm shift seems to have taken place. Instead of removing the thiocarbonyl group it is now also considered as a valuable tool in macromolecular architecture design, e.g., in Hetero Diels Alder reactions.<sup>65,66</sup> The exploration of further  $\alpha$ -end-group modification is beyond the scope of the current thesis and the reader is directed to detailed reviews for more insight into this area.<sup>42,44,45,67,68</sup>

### 1.3.2 $\omega$ -End-group Modification

The following section elucidates some aspects of RAFT end-group transformations and shows the current state of the art methods which will be explained step by step. Due

to the well established small molecule chemistry on thiocarbonylthio groups,<sup>69</sup> most of these reactions can also be applied to RAFT polymers. Figure 1.4 shows some important RAFT end-group transformations and related subsequent reactions opening the path to new block copolymers which are not accessible *via* sequential RAFT processes. These typically include nucleophilic substitution reactions which produce a polymer with a thiol moiety. Such thiol moieties can be coupled to an alkene using the thiol-ene reaction. Unfortunately, except the useful reaction, the thiol group, if left in the polymer without further reaction, is prone to UV-light irradiation or other oxidizing agents leading to the same problems as noted before, i.e., toxic small sulfur molecules. Complete desulfurization can be achieved *via* thermolysis or radical-induced reactions. If the sulfur content of the resulting polymer is not an issue, then the focus of end-group removal shifts to make use of the thiocarbonylthio group in subsequent reactions. Examples include the block copolymer formation by RAFT polymerization using the previously synthesized RAFT polymer as a macro RAFT agent with another monomer or combining RAFT with ATRP or NMP in order to synthesize new block copolymers.<sup>70-74</sup> A new strategy involves the use of a universal RAFT agent for a wider range of monomer classes. These new discoveries enhance the RAFT process as a tool for macromolecular architectures. In the next sections these methods will be explained in detail.

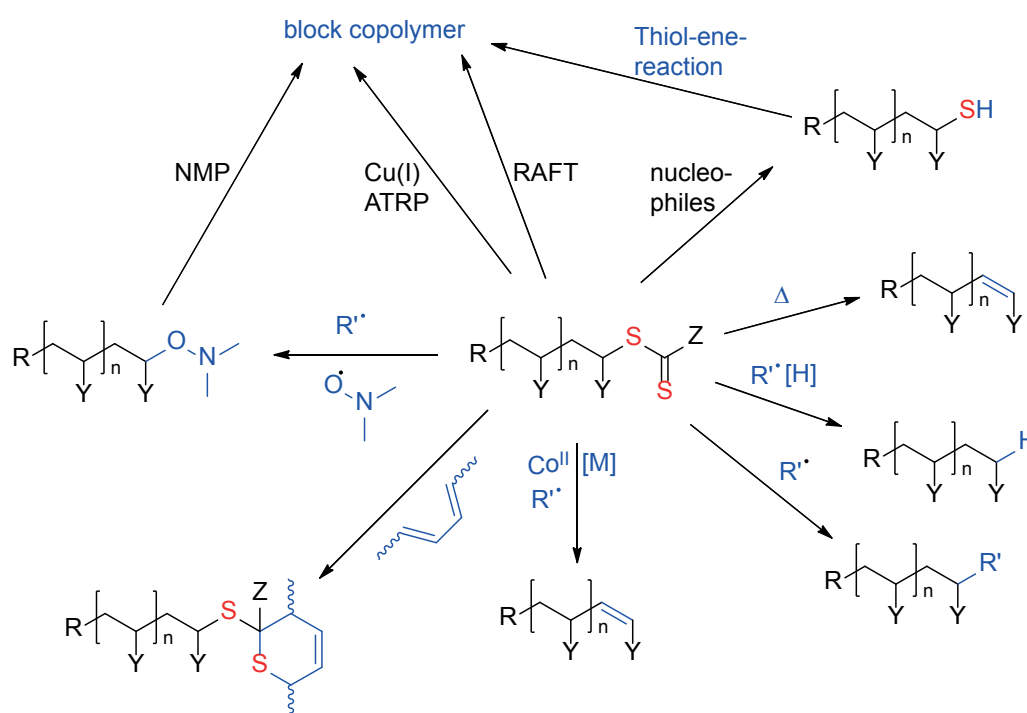


**Figure 1.4:** RAFT end-group transformations - Overview ( $R'\bullet$ =Radical, [H]=Hydrogen donor, [M]=Monomer).

## End-group modification using nucleophiles

Nucleophiles, such as amines,<sup>64,75–81</sup> thiols<sup>82</sup> or hydroxides<sup>77,82–86</sup> and ionic reducing agents, such as boron hydrides<sup>84,85,87–89</sup> can be applied to react with the thiocarbonylthio group to give thiol groups at the end of the polymer chain. The hydrolysis reaction occurs also during RAFT polymerization in aqueous media. However, the macro RAFT agents are more stable in water than their small molecule analogs.<sup>80</sup> The resulting thiols can be used in subsequent reaction, i.e. gold nanoparticle formation,<sup>88</sup> biopolymer conjugates,<sup>90</sup> as well as thiol-ene reactions.<sup>83</sup> The synthesis of a macro thiol can be hindered by the occurrence of a side reaction occurring, i.e., disulfide coupling of two polymer chains yielding in a bimodal molecular weight distribution showing twice the molecular weight of the initial polymer. The extent depends on the polymer used and the specific reagents and reaction conditions used.<sup>64,84,91</sup> Disulfide coupling can be reduced by performing the reaction in an inert atmosphere. Already formed disulfides can be reformed into thiols by using reducing agents in subsequent reactions.<sup>67,78</sup> If performing an aminolysis in the presence of a reducing agent, such as sodium dithionite<sup>91,92</sup> or phosphine,<sup>93,94</sup> the disulfide formation can almost be eliminated. Thiols are prone to oxidation once there is base present and therefore one should take the necessary precautions when working with these polymers. The oxidation problem can be bypassed by a new promising technique which includes the use of hydrazine as a nucleophile even if the reaction is carried out in air.<sup>95</sup> These thiol polymers have found various applications in thiol-ene reactions, biopolymer conjugations, as well as in the subsequent preparation of sulfonic acid-terminated polymers.<sup>96</sup> For further information of subsequent reactions the reader is referred to Thang *et. al.*<sup>97</sup>

## End-group modification by radical induced reduction

The main aim of radical induced reduction is the replacement of the thiocarbonylthio group with a hydrogen atom.<sup>63,98–100</sup> Figure 1.5 shows the general mechanism where the thiocarbonylthio group of the macro-RAFT agent **5** undergoes an addition initiated by a radical  $R\bullet$  **10** to generate an intermediate thiocarbonylthio radical **12**. The intermediate radical **11** is not stable and rapidly fragments to produce a propagating radical  $P_n\bullet$  **2** and the thiocarbonylthio side product **12**. In the presence of a hydrogen atom donor, the propagating radical abstracts a hydrogen atom to give the desired saturated product **13**. Once the reaction is started with an initiator, the reaction is a catalytic process, as  $R'\bullet$  **14** reinitiates the reduction of further RAFT polymer molecules. Side reactions include the radical coupling of the initiator with an active polymer chain **15** as well as the radical coupling of two active polymer **16**. The radical reduction of RAFT polymers is a versatile method, because the reducing agent is not restricted to hydrogen-atom donors, as in principle other non-hydrogen donors can be used. A well known example

of a radical induced reduction is based on the Barton-McCombie reaction for deoxygenation of secondary alcohols<sup>101,102</sup> and can be applied in the reduction of xanthates. For the reduction of low molecular weight thiocarbonylthio groups, tin compounds as hydrogen donors have also been successfully employed, but due to their toxicity and sometimes difficult purification methods, substitutes have been explored.<sup>103</sup> Although disproportionation occurs instead of the reduction of the end-group, the most prominent side reaction is the termination reaction in which two reactive polymer chains react with each other to form a product with a bimodal distribution, one equal to the starting molecular weight and one equal to the double molecular weight of the starting material. The success of the reduction of the RAFT polymer depends on the specific polymers but as a trend the hydrogen atom donors increase in the following order: toluene < 2-propanol < triethylsilane < triphenylsilane \ tris(trimethylsilyl)silane \ *N*-ethylpiperidine hypophosphite < tri-*n*-butylstannane.<sup>63</sup>

While *N*-ethylpiperidine hypophosphite are less attractive hydrogen donors compared to tin hydrides, they still exhibit the advantage of a more environmental friendly reagent and are used therefore as substitutes for tin hydrides.<sup>104</sup> Another important issue is the choice of the radical initiator. It has been shown that generally peroxide initiators should be preferred over azo compounds such as AIBN.<sup>63</sup> Peroxide radicals replace the propagating radical more effective than the azo compounds. Although peroxide radicals are more effective in replacing the thiocarbonylthio group, it has to be kept in mind that they are also prone to provide end-groups by transfer to the initiator.

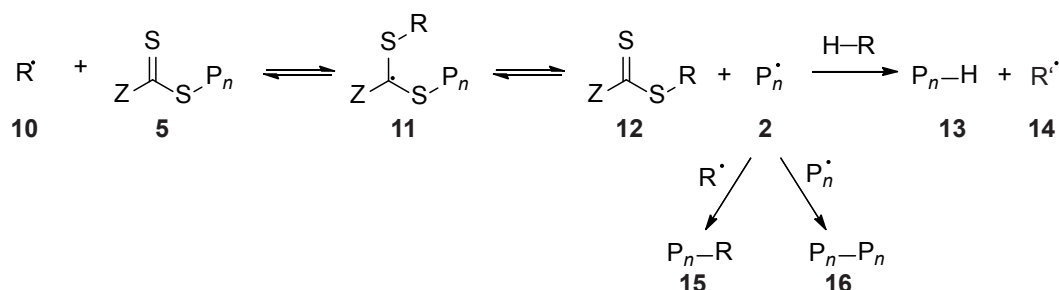


**Figure 1.5:** Radical-induced reduction of thiocarbonylthio compounds.

### End-group modification *via* catalytic chain transfer

The catalytic chain transfer (CCT) process is an important polymerization technique which was invented in the 1970s in order to gain control over the end-group functionality and the molecular weight. For further insight of the CCT process the following review is pointed out.<sup>105</sup> The CCT process is not only an important technique for polymerization but can also be used for RAFT polymer end-group modification. Figure 1.6 shows the reaction steps occurring during this modification process.<sup>106</sup> CCT agents are

often square planar Co(II) or Co(III) complexes. It has been shown that a small amount of CCT agent added at latter stages of the RAFT mediated methyl methacrylate (MMA) or butyl methacrylate polymerization resulted in the complete end-group removal and a high purity low dispersity macromonomer product **22**. The active cobalt(II) complex is reduced during this process to a Co(I) species **23** which is subsequently reoxidized to the active Co(II) complex by the monomer present in the reaction mixture, i.e., MMA or BMA respectively. The resulting macromonomer **22** can subsequently be used in further copolymerizations to obtain e.g., graft copolymers.

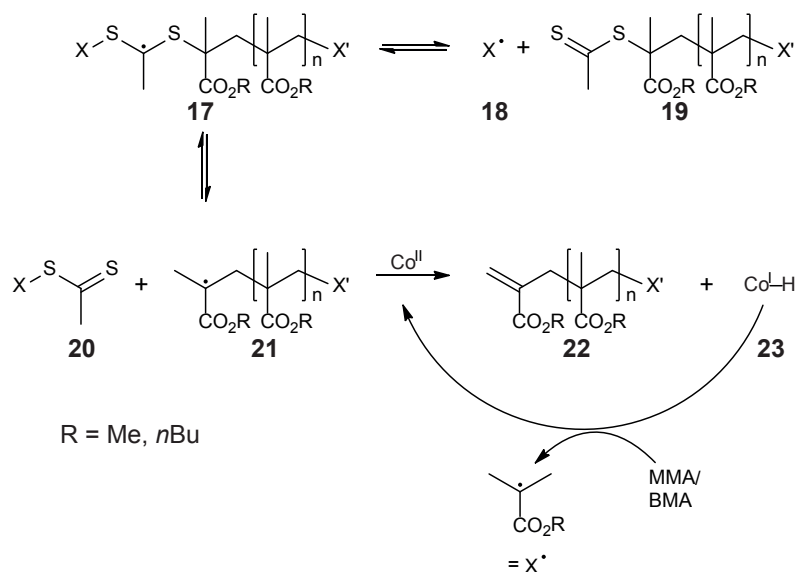


**Figure 1.6:** RAFT catalytic chain transfer process \ radical-induced oxidation of thiocarbonylthio compounds.

### End-group modification *via* radical addition-fragmentation-coupling

Heating a given RAFT-polymer in a solution of an excess of a thermal radical initiator will remove the dithioester group and result in a radical initiator capped polymer. The underpinning mechanism is depicted in Figure 1.7. On a small molecule scale, this reaction can be employed to e.g., prepare 2-cyanoprop-2-yl dithiobenzoate with more than 90% yield.<sup>63</sup> The process can also be applied in end-group polymer modification to remove the thiocarbonylthio group of RAFT polymers.<sup>10745</sup> The first step is the addition of the radical  $R\bullet$  **10** to the thiocarbonylthio end-group followed by the fragmentation of the intermediate radical to result in a polymer chain end-group radical  $P\bullet$  **2**. Side reactions include the disproportionation of the active polymer resulting in an unsaturated polymer **24** as well as the combination of two active polymer chains **16**. If the radical source is in excess, there is a high probability of this polymer chain radical to terminate with the radical source and result in radical end functionalized polymer chain **15**. The reaction is versatile as it can be applied on a wide range of polymer classes (i.e.,

poly(methyl methacrylate) PMMA,<sup>107,108</sup> poly(styrene) (PS),<sup>109,110</sup> poly(methyl acrylate) PMA<sup>107</sup> or even poly(*N*-isopropylacrylamide) PNIPAM<sup>111</sup>). A further advantage is the possibility of the recovery of the RAFT agent. The process involves heating the polymer in presence with the initiator (often AIBN) and works most effective with dithiobenzoates and trithiocarbonates. The xanthate end-group of poly(vinyl acetate) can not be removed using this process. Due to the nature of the cyanoisopropyl radical which is more stable than the PVAc radical which is therefore not generated.<sup>100</sup> One problem of this reaction involves incomplete conversion of the thiocarbonylthio group, due to the relative stability of the radicals present in the reaction. The radical source and its concentration has to be chosen in a manner that the resulting radicals readily add to the trithiocarbonyl group but also do not enhance the coupling of two polymer chains giving a bimodal distribution, therefore  $k_{tr}$  should be small. One step toward the solution of the polymer-polymer coupling side reaction is the combination of two radical sources. It has been demonstrated that a mixture of lauroyl peroxide (LPO) (2 molar equivalents) and AIBN (20 molar equivalents) gave the best results in removing the thiocarbonylthio end-group as well as keeping the amount of a potential bimodal side product (16) on a negligible level.<sup>112</sup> An additional side reaction, which has to be considered, is the disproportionation reaction of an active polymer chain resulting in an unsaturated end-group (24). The disproportionation reaction is not a desired reaction, but can be suppressed if the ratio between combination/disproportionation ( $k_{tc}/k_{td}$ ) is very high. While the disproportionation reaction still allows for the removal of the thiocarbonylthio group it has to be taken into account that a high end-group fidelity will not be achieved. In summary this method - if applied cautiously - is one of the more widely used techniques in RAFT end-group modification which can be attributed to its versatility.

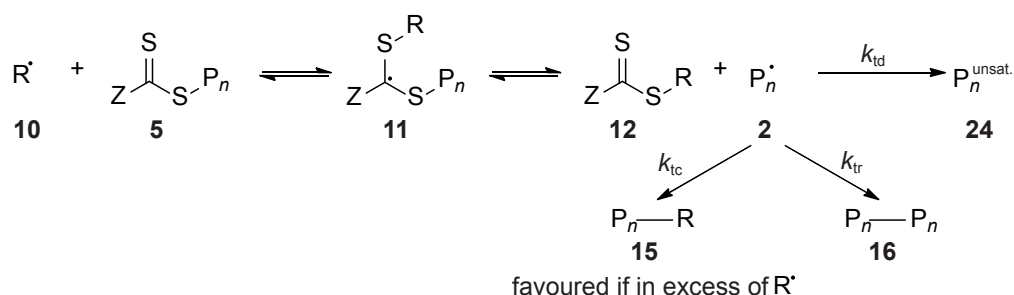


**Figure 1.7:** General mechanism of the radical addition-fragmentation-coupling using an excess of a thermal radical initiator.

### End-group modification combined with ATRP

The thiocarbonylthio group can also be used in ATRP as a pseudo halogen instead of a halogen atom. One of the first catalysts reported for such a system was copper(I)(*N,N*-dialkyl dithiocarbamate) ( $\text{Cu}(\text{S}_2\text{CNET}_2)$ ).<sup>71,72,113</sup> As dithiocarbamates are not suitable

for controlling more activated monomers *via* the RAFT process e.g., MMA, styrene, or acrylonitril (AN),<sup>97</sup> they exhibit control over the polymerization using a copper catalyst system. Therefore the mechanism for polymerizations employing the before mentioned components are more likely of an ATRP type than a RAFT mediated type. The latest developments in combining RAFT and ATRP employs - besides dithiobenzoates<sup>114,115</sup> - more activated RAFT agents, such as *N,N*-diaryldithiocarbamates<sup>116,117</sup>, 1-pyrrolicarbodithioates<sup>118</sup> and 1-dithionaphthalates<sup>119,120</sup> (see Figure 1.9). These RAFT agents are effective in polymerizing activated monomers and once they are used in ATRP the reaction mechanism has to be questioned. Instead of a *pure* ATRP it appears to that a mixture of ATRP and RAFT with the controlling mechanism evolving from the RAFT part while the initiating part is more an ATRP-like mechanism. The general mechanism for the concurrent RAFT/ATRP process is shown in Figure 1.8. The red color highlights the RAFT mechanism part while the blue color highlights the ATRP part of the polymerization process. For a more detailed information about the concurrent ATRP/RAFT mechanism, the reader is referred to the publications of Kwak *et al.*<sup>114,115</sup>

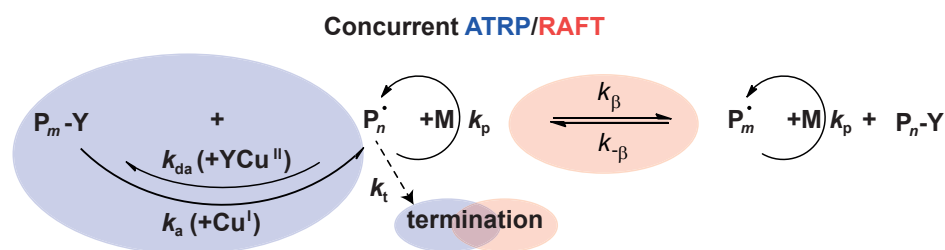


**Figure 1.8:** General Mechanism for a concurrent ATRP/RAFT polymerization.

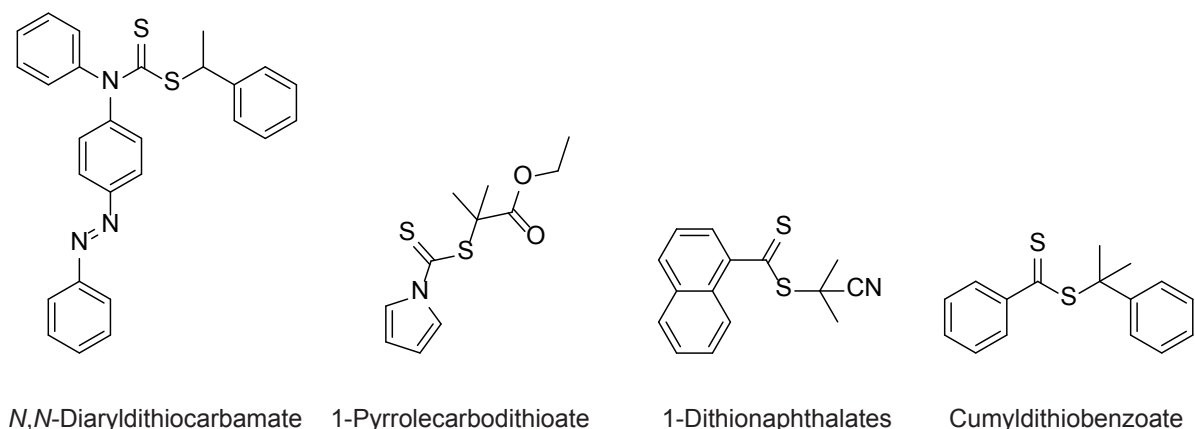


**Figure 1.9:** RAFT agents employed in ATRP processes.

## End-group modification combined with NMP

Another interesting method in end-group modification of RAFT polymers is the combination of addition fragmentation coupling in the presence of nitroxide yielding an alkoxyamine end-group. The process is termed 'exchange of substituents between (macro)alkoxyamines and macro(RAFT) agents' (ESARA) and was developed by Favier *et al.*<sup>73</sup> The mechanism is depicted in Figure 1.10. The first step is the dissociation of an alkoxyamine  $SG_1$  into a radical  $A\bullet$  and a stable nitroxide radical.  $A\bullet$  adds to the RAFT agent and generates an intermediate radical. The R-group and A-group have to be carefully selected and fulfill certain requirements.  $R\bullet$  has to be less stabilized/sterically hindered compared to  $A\bullet$ , otherwise the formation of an A-RAFT adduct would be favoured. In this case a temperature range can be defined where the dissociation of  $A-SG_1$  is favoured over the dissociation of the desired product  $R-SG_1$ . Also, the radical  $A\bullet$  has to be stable enough to allow the release of  $R\bullet$ . If these requirements are fulfilled,  $R\bullet$  is irreversibly trapped by  $SG_1$ . The efficiency is controlled by the high combination rate coefficient of  $SG_1$  with alkyl radicals as well as the excess of  $SG_1$  compared to  $R\bullet$ . Both effects make the end-group transformation reaction efficient and no bimodal distribution was observed. Applying the before mentioned method in end-group transformation of RAFT polymers connects the two controlled polymerizations RAFT and NMP and provides an efficient pathway to new materials, although the design of the reagents has to be chosen carefully.<sup>73</sup>

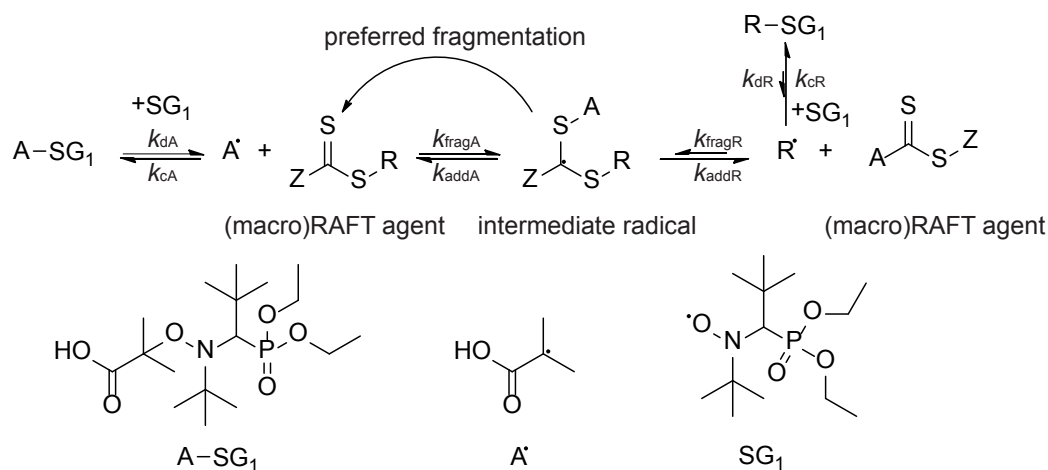


**Figure 1.10:** General scheme for NMP agents employed in end-group modification of RAFT polymers.

## End-group modification employing switchable RAFT agents

As shown before, the RAFT process is a versatile technique for controlling radical polymerizations. However, the RAFT agents have to be designed according to the activity of the monomer. Less activated monomers (e.g., vinylacetate) are not controlled using trithiocarbonates or dithioesters, respectively. On the other side xanthates and dithiocarbamates control these less activated monomers, but fail in controlling more activated monomers, such as methyl methacrylate or styrene. Therefore the synthesis of a RAFT block copolymer with the first block consisting of a more activated monomer and the second block consisting of a less activated monomer is difficult to almost impossible using conventional RAFT agents. Such an incompatibility is related to the lower reactivity toward radical addition and therefore these substances possess lower transfer constants.<sup>121</sup> The character of the double bond is reduced due to zwitterionic canonical form of the *N*-4-pyridinyl-*N*-methyldithiocarbamate **25a** localizing a positive charge on the nitrogen and a negative charge on the sulfur **25b** as shown in Figure 1.11a.<sup>36,121</sup> The tendency of dithioesters and trithiocarbonates in inhibiting polymerizations with less activated monomers originates - at least imparts - from the poor leaving group ability of the propagating radical of the terminal unit of less activated monomers compared to the R-group of the RAFT agent. Dithiocarbamates possessing an electron withdrawing group attached to the nitrogen or where the lone pair of the nitrogen is part of an aromatic system are effective with more activated monomers but inhibit polymerizations of less activated monomers. Benaglia *et al.*<sup>122</sup> introduced the concept of a 'switchable' RAFT agent which can polymerize less activated monomers as well as more activated monomers after protonation. The ability of polymerizing the less activated monomers, as well as the more activated monomers, is achieved by employing *N*-4-pyridinyl-*N*-methyldithiocarbamates **25a** which are similar in reactivity to *N*-phenyl-*N*-methyldithiocarbamates. These RAFT agents **26** control the polymerization of less activated monomers but lack in control of more activated monomers. Though, once the *N*-4-pyridinyl-*N*-methyldithiocarbamates are protonated **27a** (canonical form **27b**), they offer good control over more activated monomers but inhibit the polymerization of less activated monomers as their activity is in the range of aromatic dithiocarbamates such as 1-pyrrolicarbodithioates. The concept and the process of the diblock formation is shown in Figure 1.11b. Employing a switchable RAFT agent strategy, it is now possible to synthesize block copolymers of more activated monomers and less activated monomers using one RAFT agent which is readily transformed *in-situ* by adding base **26** during the two polymerization steps. It is important to perform the two subsequent polymerizations according to the reaction sequence shown in Figure 1.11b. Employing such a strategy it is possible to synthesize a poly-(methyl methacrylate)-*block*-poly(vinyl acetate) **31** by polymerization of vinyl acetate controlled with a poly(methyl methacrylate) RAFT agent **30**. The R-group of the RAFT/macro-RAFT agent still needs to be chosen according to the monomer which is polymerized. The radical of the less acti-

vated monomer is a poor leaving group compared to the radical of the polymer of the more activated monomer. Therefore retardation can be observed if one attempts to extend a more activated macro-RAFT agent (e.g., polystyrene macro-RAFT agent) with a less activated monomer (e.g., vinyl acetate). The retardation is due to the very low addition rate of the active polymer chain to the less activated monomer. In order to synthesize such block copolymers despite the retardation problem, an intermediate block copolymer can be formed with a polymer radical reactivity between the more activated and the less activated monomer (e.g., methyl acrylate). The intermediate block can now be further extended with the less activated monomer.

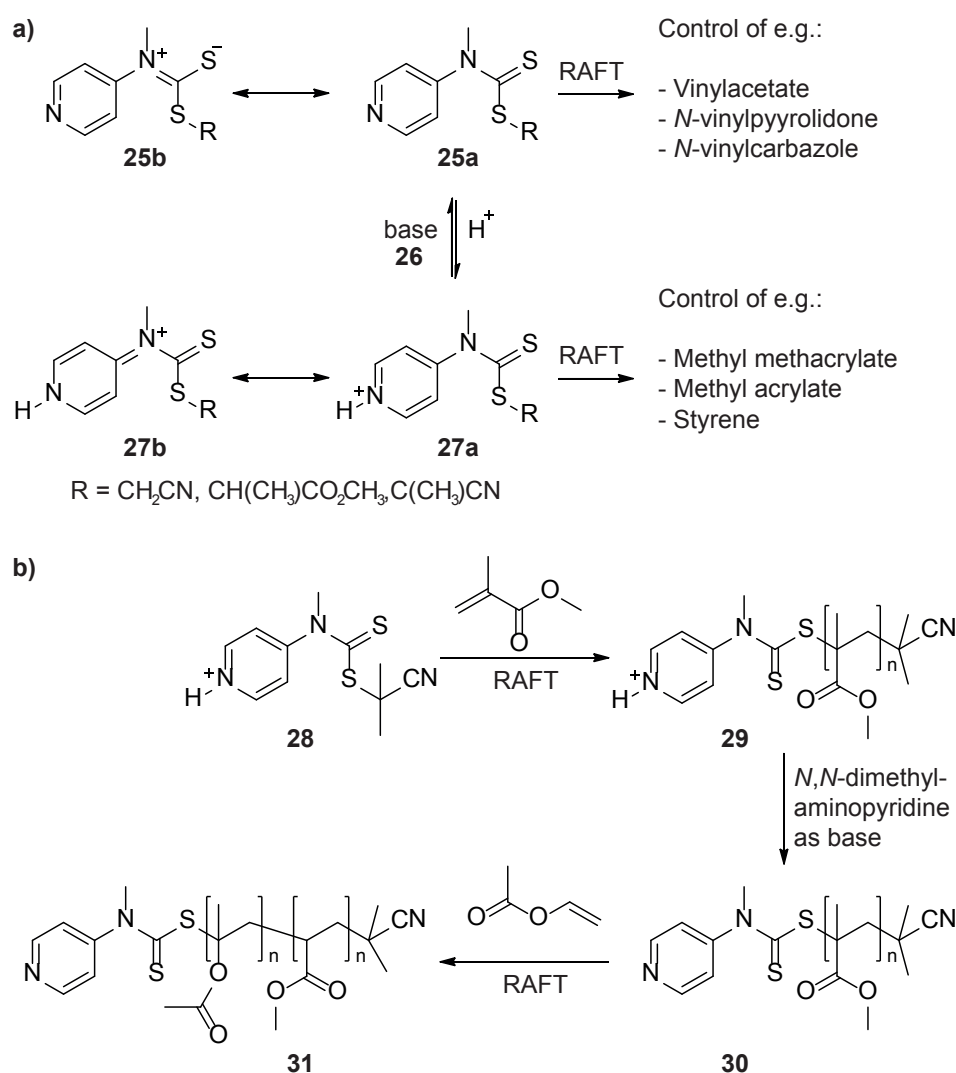


**Figure 1.11:** Concept of switchable RAFT agents and reaction pathway to poly-(methyl methacrylate)-*block*-poly(vinyl acetate).

## End-group modification by thermolysis

Thermolysis is a widely employed tool to provide complete thiocarbonylthio group removal.<sup>64,109,123–125</sup> The advantages of thermolysis compared to other transformation reactions is the absence of a chemical treatment. It does, however, require sufficient stability of the polymer and the desired end-group in order to achieve high purity products. Although the resulting polymer bears a unsaturated end-group, the mechanism depends on the type of the particular polymer and the thiocarbonylthio group. Figure 1.12 shows the thermolysis at 180 °C under nitrogen of a poly(butyl acrylate), synthesized *via* controlled polymerization employing butyl trithiocarbonate as RAFT agent **32**, resulting in a purity between 65 and 90% for the macromonomer **35a** and **35b**.<sup>123</sup> The macromonomer consists of an *exo*-methylene double bond which is build *via* consecutive C-S bond homolysis to form a chain end radical **33**. Backbiting of the chain end radical **33** leads to a more stable mid chain radical **34** followed by  $\beta$ -scission to give the macromonomer **35a** and **35b** and another end chain radical **36a** and **36b**. The mechanism is identical to the proposed mechanism for degradation of conventional polymerized poly(butyl acrylate) and other poly(acrylates) at higher temperatures (304–370 °C).<sup>126,127</sup> The isothermal thermolysis of butyl trithiocarbonate poly(styrene) **37** is finished at a temperature range of 210–250 °C of and removes the trithiocarbonate group to give a colorless product **39**.<sup>64,109,124</sup> In this case the proposed mechanism seems to be similar to the concerted Chugaev elimination process.<sup>128,129</sup> The mechanism of the Chugaev elimination is shown in Figure 1.13. It involves a stereospecific *syn*-elimination through a six membered transition state where the proton is transferred to the sulfur and the desired macromonomer. Another possible intermediate is the thiol terminated polymer **38**, which is not stable under the reaction conditions and eliminates hydrogen sulfide yielding in the unsaturated product. A significant reduction of temperature (onset temperature of 165 °C) during the reaction is achieved by performing the thermolysis in the presence of copper powder. The major product possesses also an *exo*-methylene double bond, which was identified *via* <sup>1</sup>H NMR.<sup>109</sup> The copper catalyzed process seems to involve the homolytic cleavage of the C-S bond resulting in an poly(styrene) radical which can decay through backbiting and chain scission similar to the mechanism shown in Figure 1.12.<sup>109</sup> Interestingly, poly(methyl methacrylate) synthesized *via* controlled polymerization with dithiobenzoate end-groups **40** is more stable to weight loss, than poly(methyl methacrylate) formed by conventional polymerization processes. Applying a suitable temperature range, thermolysis is a convenient method in cleanly removing dithiobenzoate end-groups yielding polymers with an unsaturated end-group **41**. There are a variety of applications where the thermolysis method was employed.<sup>81,91,125,130</sup> The mechanism for the reaction seems to be similar to the concerted Chugaev elimination and is shown in Figure 1.14. It has to be taken care of the polymer purification before thermolysis reactions are performed. Due to radical initiator residues or contaminations of metal, as poly(methyl methacrylate) is less stable

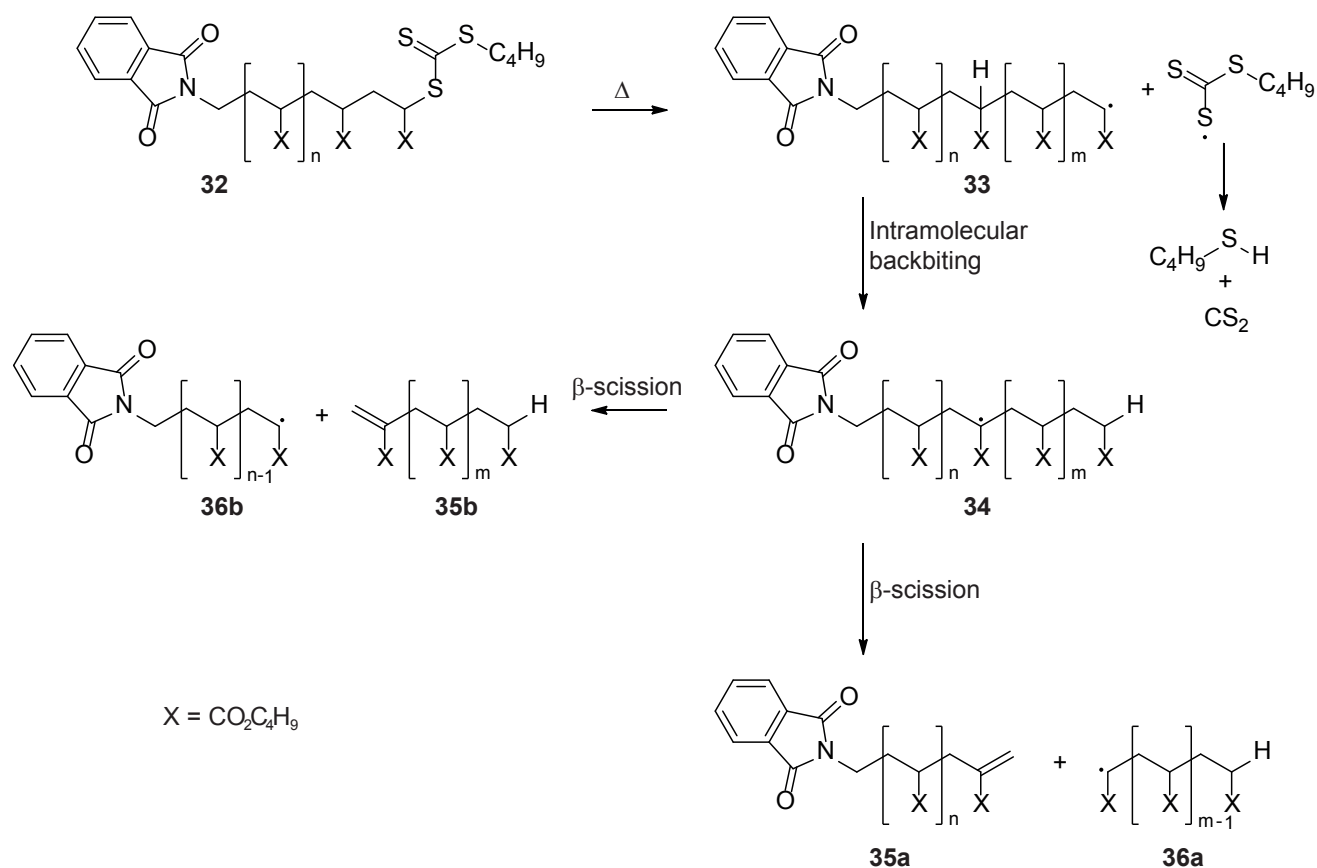


**Figure 1.12:** Thermolysis of a butyl trithiocarbonate *via* direct Chugaev elimination or intermediate thiol formation.

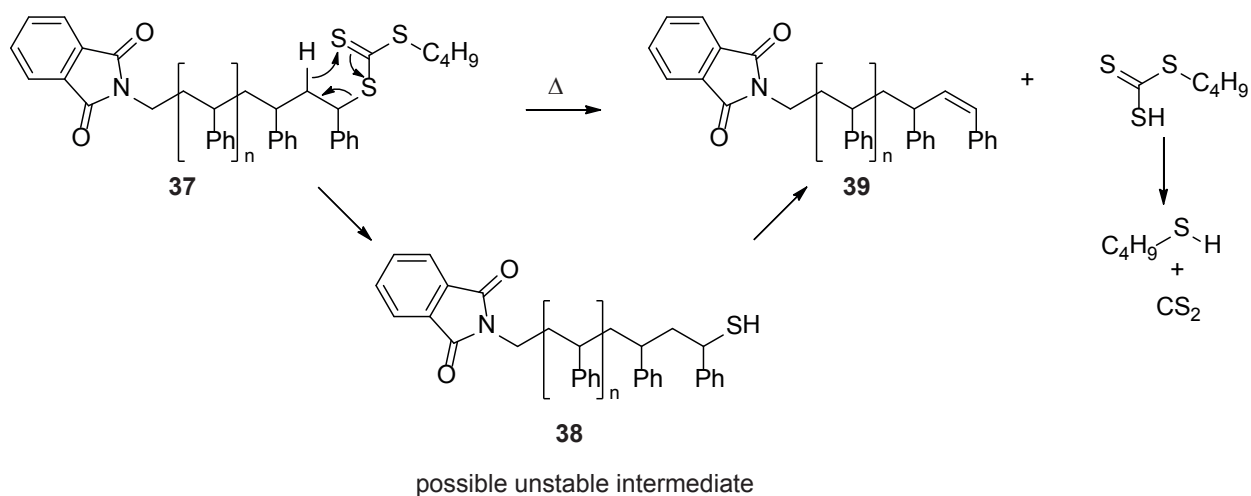


**Figure 1.13:** Thermolysis of a polystyrene with an S-butyl trithiocarbonate end.

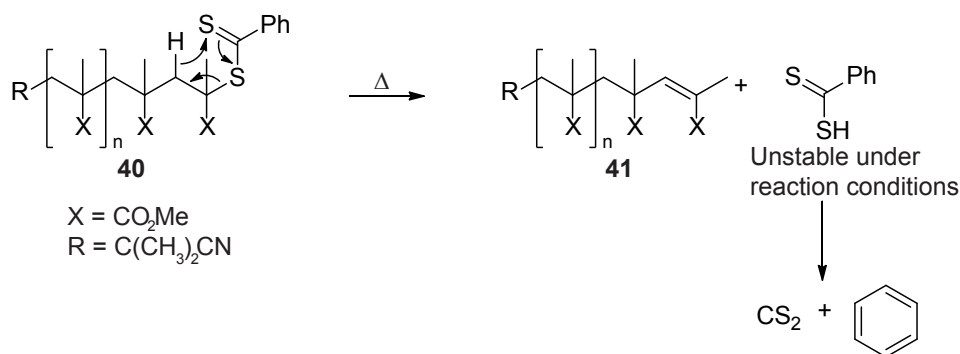


**Figure 1.14:** Thermolysis of a dithiobenzoate end-group *via* Chugaev elimination.

in the presence of such impurities. It has also to be kept in mind that thermolysis reactions performed with poly(methyl methacrylates) bearing trithiocarbonate end-groups **42** tend to promote the polymer degradation, thus resulting in a lower molecular weight than the starting material.<sup>125</sup> The side reaction is triggered by the homolysis of the C-S bond generating a poly(methyl methacrylate) chain end radical **43**, which can further degrade by an 'unzipping' mechanism as shown in Figure 1.15 to produce another chain end radical with the loss of one MMA unit **44**. The 'unzipping' of the polymer chain can continue until the chain end radical reacts in a disproportionation reaction yielding in a polymer with an unsaturated chain end **45**. The thermolysis reaction is not only restricted to dithioesters and trithiocarbonates, but can be extended to xanthates yielding in thiol terminated or unsaturated products depending on the Z-group.<sup>123,131</sup>

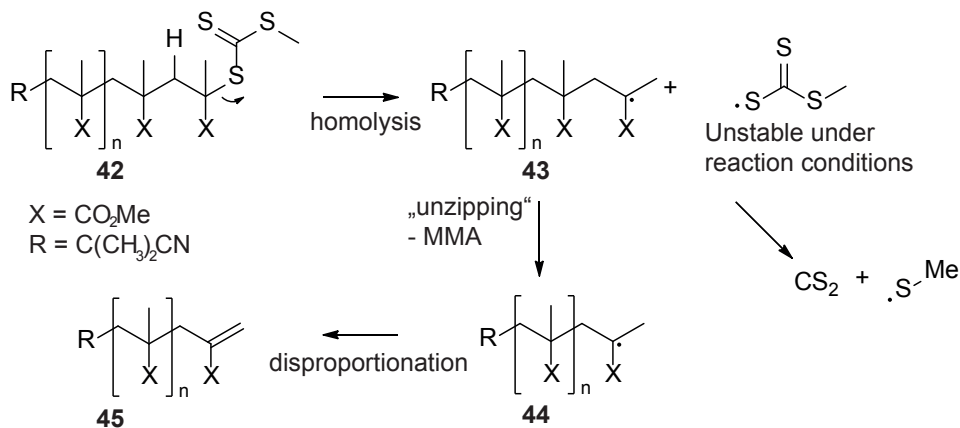


**Figure 1.15:** Thermolysis of PMMA with S-methyl-trithiocarbonate end.

## End-group modification by 'click'-type reactions

As in other fields of chemistry, the application of *click* chemistry<sup>132</sup> has grown extensively and is now a powerful tool in achieving advanced polymer architectures. The area of *click*-reactions is too wide to cover in the content of the present thesis, thus the

focus on the current chapter is on reactions employing the RAFT end-group of thiocarbonylthio compounds as *click*-moieties. For a further insight on *click*-reactions in macromolecular chemistry, the reader is referred to the following articles on azide alkyne *click*-reactions,<sup>133–135</sup> the review by Binder *et al.*,<sup>136</sup> the review by Inglis *et al.*,<sup>137</sup> as well as the review by Harvison and Lowe.<sup>138</sup> It has to be mentioned that the criteria of *click*-type reactions in polymer chemistry differ from criteria applied in biochemistry. While some of the original criteria are suggested by Sharpless *et al.*<sup>132</sup> (e.g., stereospecificity) are more important for certain fields of chemistry than for other fields of chemistry, modification of these *click*-criteria are proposed toward the needs of polymer-polymer conjugations. These modifications include new principles (e.g., equimolarity, large scale purification and fast time scale of the reaction). For example, in the case of polymer-polymer conjugation, the stereospecificity is not of a great concern compared to the bio-related fields of chemistry. More important for polymer-polymer conjugations is the employment of equimolar amounts of reagents in order to sufficiently synthesize block copolymers. The reactions of thiols derived from thiocarbonylthio end-groups have been mentioned above and many of these subsequent reactions employing the thiol group are described as *click*-type reactions. The so-called thiol-ene chemistry extended macromolecular design toward biopolymer conjugates<sup>139</sup> as well as into the optoelectric field.<sup>140</sup> One of the latest approaches in polymer conjugation/end-group modifications is the [4+2] cycloaddition of heterodienophiles with dienes to form a six-membered heterocycle. In the specific case of RAFT polymers, the thiocarbonyl group can act as a heterodienophile and open a path to dihydrothiopyrans.<sup>141,142</sup> The general mechanism for this reaction is shown in Figure 1.16. It has been shown by Barner-Kowollik and co-workers that RAFT agents and macro-RAFT agents **46** conjugate with polymers bearing diene-end-groups **47** in a hetero-Diels-Alder (HDA) reaction if the Z-groups are chosen carefully resulting in well defined block copolymers. The HDA-reaction increases in efficiency and reaction time when more electron withdrawing Z-groups are employed. Suitable Z-groups are pyridyl, phosphonate and phenylsulfonyl. The diene employed in the HDA reaction also influences the kinetics of the conjugation reaction. Due to its permanent *s-cis* conformation, cyclopentadiene is a highly reactive diene in this type of cycloaddition.<sup>143</sup> Using the RAFT-HDA approach, it has been possible to synthesize block copolymers,<sup>65,143,144</sup> star polymers,<sup>66,145</sup> graft copolymers,<sup>65</sup> modified surfaces.<sup>146,147</sup> and even biofunctional surfaces.<sup>148</sup> The reaction rates can be further increased by employing trifluoroacetic acid as a catalyst. HDA-chemistry is a versatile and powerful tool in polymer architecture because there is no requirement of a metal catalyst as well as carrying out the reaction at ambient temperatures with fast reaction times.

### End-group modification using oxidizing agents and irradiation

The thiocarbonylthio group of RAFT polymers reacts with various oxidants to cleave its functionality or being modified into another molecule. Reagents employed in

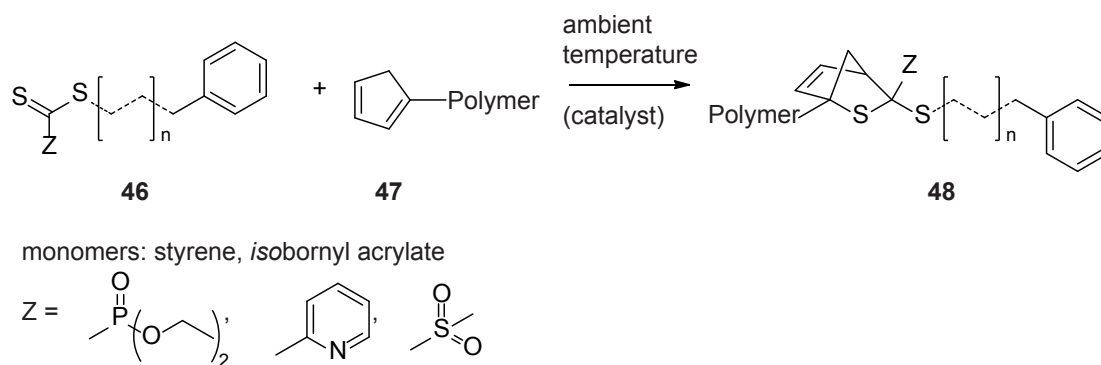


**Figure 1.16:** Hetero-Diels-Alder reactions employing RAFT polymers as hetero-dienophiles.

such processes are ozone,<sup>149,150</sup> air,<sup>151</sup> hydrogen peroxide,<sup>152</sup> hydroperoxide,<sup>153</sup> and peracids.<sup>142,154</sup> In addition - as mentioned before - RAFT end-groups are not stable under UV-light irradiation as they degrade upon irradiation.<sup>155,156</sup> On exposure to ozone xanthate end-groups of RAFT polymers **49** are transformed into thiocarbonate end-groups **50**. Although there is no knowledge about the mechanism, the thiocarbonyl group exchanged with a carbonyl and sulfuric acid is formed as a side product (see Figure 1.17). The authors submit that the process is also applicable to other RAFT end-groups such as trithiocarbonates and dithioesters and therefore a patent has been filed covering the process.<sup>149,150</sup> It has been shown by Metzner<sup>157</sup> and Cerreta *et al.*<sup>154</sup>

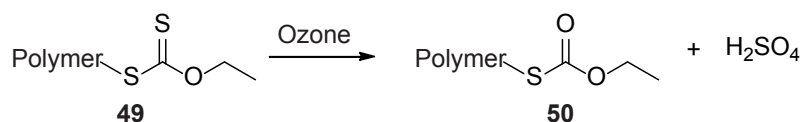


**Figure 1.17:** Reaction of Xanthate end-groups

that low molecular weight trithiocarbonate and dithioester compounds can be directly transformed into sulfine end-groups using hydroperoxides. This process can also be applied to polymeric materials where hydroperoxides (especially *t*-butylhydroperoxide) can directly transform dithioester end-groups of RAFT polymers in high yield into sulfine end-groups.<sup>151</sup> Another route requiring hydrogen peroxide is the employment of the direct transformation of poly(*N*-vinylpyrrolidone) with xanthate chain ends and poly(styrene) with dithiobenzoate end-groups *via* heating to 60 °C. The proposed mechanism is similar to the addition-fragmentation-coupling shown before in Figure 1.7. A transformation reaction - although not always a desired reaction pathway for RAFT polymers - is the degradation/transformation of dithioesters *via* UV-light radiation. A reaction mechanism was proposed by Quinn *et al.*<sup>156</sup> and is shown in Figure 1.18. Upon UV-light irradiation of the dithioester **51** a homolytic cleavage occurs leaving two radicals (**52** and **53**) which decompose further (*via* **54**) and finally lead to toluene **55** and styrene **56**. If polymers are included in the reaction mixture, the polydispersity is in-

creased due to coupling reactions between polymer chains. Hence, the reaction is not acceptable as a synthetic tool for designing complex polymer architectures.

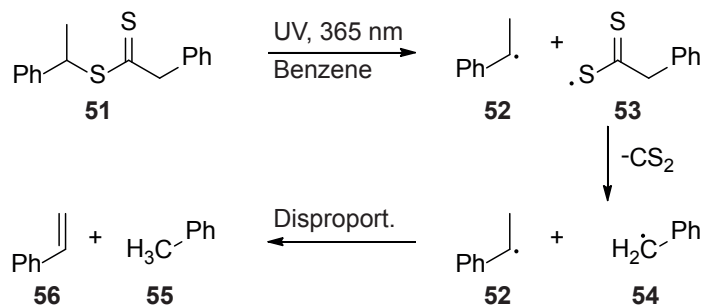


**Figure 1.18:** Decomposition of 1-phenylethyl phenyldithioacetate under irradiation of UV-light.

## 1.4 Conclusions and Outlook

One major advantage of the RAFT process compared to the mostly copper mediated polymerization *via* ATRP is the lack of transition metals. However - so far - the applications of the RAFT process in industry are limited, due to the color of the resulting polymers, yet the unstable nature of RAFT polymers under UV-light radiation. To overcome these drawbacks, techniques have been developed which introduce new functionalities instead of the RAFT group leading to more stable polymers. As shown in the current literature review, there is a growing interest in academia as well as in industry in transforming or removing polymers based on the RAFT process. Although substantial work has been carried out in this field there is a need for further reactions on RAFT end-groups to expand the usefulness of RAFT polymers in subsequent reactions. Specifically, the complete removal of sulfur from the polymer would be highly desirable. The work conducted in the present thesis introduces a new and versatile method for transformations of RAFT polymers into sulfur free entities featuring a versatile oxygen-based functional handle as well as taking advantage of controlled polymerization techniques in order to synthesize well defined polymers for subsequent coupling reactions in homogeneous and heterogeneous media such as functionalization of surfaces.

## 1.5 Surface Modification

Functional polymers with reactive terminal groups, such as the examples given in the section before, can be employed in subsequent coupling reactions with variable surfaces in order to change their chemical and physical properties. The aim of the current section is to give an insight of how polymers in general - specifically functional polymers - can be used to alter surfaces. The focus will be on the general techniques available for covalently attaching of polymers onto surfaces, followed by a more detailed view on cellulose as an important bio-substrate, which has been employed as a grafting base in the current thesis.

### 1.5.1 Methods for Surface Modification

Since the stone age mankind has been working on techniques to modify surfaces in order to transform substances into more valuable materials.<sup>158</sup> Since then the modification of surfaces of all kinds of materials did not loose any of its attractiveness and there is a wide range of surface techniques ranging from mechanical grinding,<sup>159,160</sup> electrochemical modification<sup>161</sup> to applying laser systems.<sup>162</sup> The beauty of surface modification is that it leaves the bulk properties of the material untouched while the physical, chemical and mechanical properties of the surface are changed during the modification processes. Since there exists such a great variety of materials all with specific surfaces and modification techniques, the current overview can only include and discuss certain aspects. Tailoring surfaces *via* decoration of polymers onto surfaces has been employed since the invention of synthetic (poly)oxybenzylmethylenglycolanhydride - bakelite - and its modification with wood fibers.<sup>163</sup> Today, the main purpose of such modifications is the change of surface properties, such as adhesion, wettability or lubrication, while keeping the mechanical properties of the bulk material unchanged. In general there are three techniques available to modify surfaces with polymers which are presented in Figure 1.19 and are explained individually.

### 1.5.2 Physisorption of Polymers Onto Surfaces

One of the simplest methods for modifying surfaces is the physisorption of (co)polymers with the above mentioned bakelite/wood fiber mixture being a first example. The general mechanism is shown in Figure 1.19a. As there is no covalent bond between the polymer and the surface, the process is reversible and the surface can often readily be cleaved from the deposited polymer. In more sophisticated decoration of surfaces using such a technique, the self assembly is accomplished by polymeric surfactants or end-functionalized polymers.<sup>164</sup> Although kinetic control is possible, the

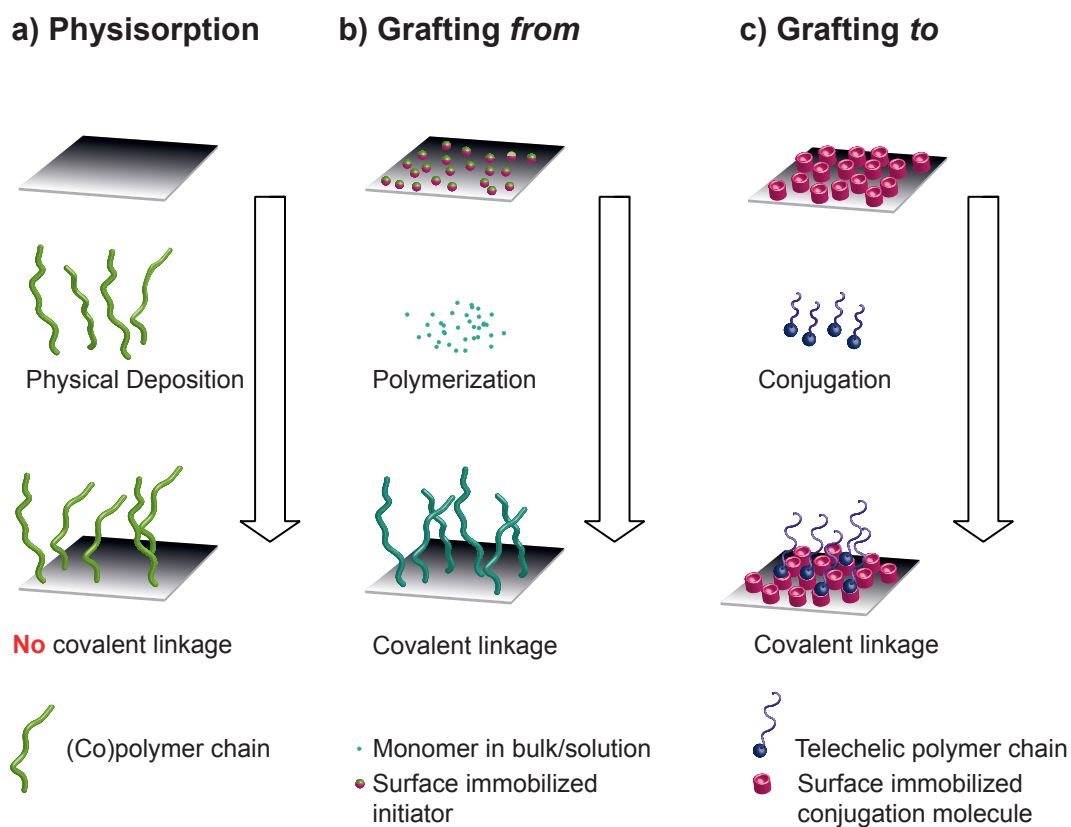


**Figure 1.19:** General scheme of surface modification with polymers employing a) physical adsorbed polymer, b) polymerization from the surface from a covalently bound initiator and c) conjugation of pre-made telechelic polymers with covalently bound active molecules on the surface.

grafting density and other characteristic dimensions are mostly governed by thermodynamics. Initially, a fast coverage of the polymer is observed which is becoming very slow due to the barrier to adsorption posed by the polymer layer already present.<sup>165</sup> State of the art techniques for physisorption of polymers onto surfaces include the use of block copolymers in combination with a selective solvent. The solvent should be chosen to be a good solvent for one block and a precipitant for the other block.<sup>166</sup> While the precipitated block builds an anchor layer on the surface, the dissolved block builds the structure while the solvent is removed. An ideal surface exhibits preference of adsorption toward one block of the block copolymer. For more in depth information about physisorption of polymers on surfaces, the reader is referred to the review by Netz and Andelman.<sup>164</sup>

### 1.5.3 *Grafting-From*

A common problem of physisorbed polymer on a surface is its often ready removal by washing of the substrate with a solvent. Such a loss of surface coverage is undesirable for certain applications. The solution is generating a covalent linkage between the polymers and the substrate. One way to achieve this goal is to covalently anchor of initiators onto the surface or radical generation on the surface *via* irradiation followed by polymerization of monomers from the surface yielding covalently bound polymer chains. Therefore, the above technique is referred to *grafting-from*. The general mechanism is shown in Figure 1.19b. There are various initiators known for such processes, e.g., anionic,<sup>167</sup> cationic,<sup>168</sup> ATRP.<sup>169</sup> The review by Zhao and Brittain<sup>170</sup> as well as by Edmondson *et al.*<sup>171</sup> give an excellent overview over the *grafting-from* techniques. It should be noted that the *grafting-from* technique often achieves a higher grafting density compared to the *grafting-to* technique (explained in the following section), yet causes problems in characterization of the covalently bond polymer, e.g., with respect to their molecular weight distribution.<sup>172</sup>

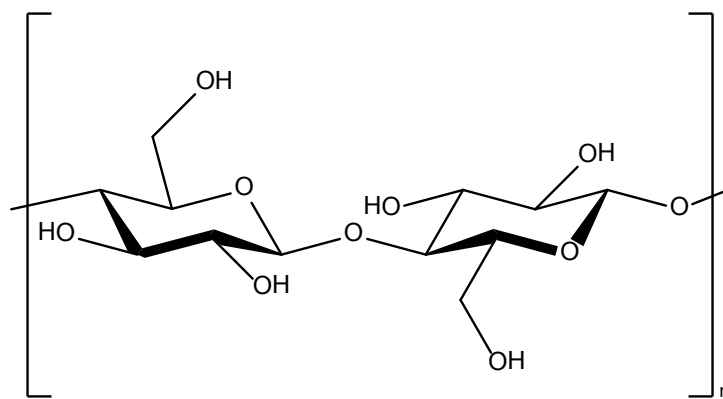
### 1.5.4 *Grafting-To*

The *grafting-to* technique employs already prepared end functional polymers which couple with a pre-functionalized surface. If one utilizes the *grafting-to* technique, the polymer may be analyzed thoroughly before the coupling with wet analysis methods - e.g., NMR or SEC - exhibiting a great advantage over the before introduced *grafting-from* technique. In addition, *grafting-to* approaches can be more readily applied in an industrial context, as pre-made building blocks can be employed. Although the characterization is more straight forward, it has to be noted that the grafting density may be smaller compared to the *grafting-from* technique due to slow diffusion of the polymer chains

through the existing polymer film before coupling to the reactive sites on the surface.<sup>172</sup> Yet, the method is very versatile as the reactive polymers can be synthesized *via* various methods, e.g., free radical polymerization, controlled/living free radical polymerization or ring-opening polymerization.<sup>173</sup> The general concept of the *grafting-to* technique is depicted in Figure 1.19c. The technique was successfully employed on various surfaces, such as flat substrates,<sup>174</sup> porous structures,<sup>175</sup> fibers/textiles<sup>176</sup> and nanoparticles.<sup>177</sup> Due to the widespread nature of the surface modification field, the following section focuses on the modification of cellulose. For a deeper insight into the general surface modification *via* the *grafting-to* technique, the reader is referred to the excellent review by Zdyrko and Luzinov.<sup>173</sup>

### 1.5.5 Surface Modification of Cellulose

Cellulose is an important class of bio-material. Since thousands of years cellulose is a large part of man's diet as it exists in fruits and other plants. Cellulose - although not digestible for humans - is an important dietary fiber and helps in maintaining healthiness.<sup>178</sup> Further, cellulose can readily be transformed into various derivatives. Unmodified cellulose is a polysaccharide which consists of a linear chain of several hundred to over ten thousand  $\beta$ -1,4-linked D-glucose units (see Figure 1.20). A further very impor-



Structure of native cellulose

**Figure 1.20:** Structure of native cellulose consisting of  $\beta$ -1,4-linked D-glucose units.

tant advantage of cellulose as starting material for subsequent reactions is its abundant occurrence in nature, as all plant life contains cellulose. It is difficult to give concrete numbers for the total amount of cellulose which is produced each year, however it is estimated that the total biomass production on the planet is around 170 billion tons per year of which around 6 billion tons are utilized by humans for food (3.9 billion tons) as well as wood for energy, paper and construction (1.98 billion tons) and finally non-food use (0.3 billion tons).<sup>179</sup> Eventually, the fossil raw materials (crude oil and coal) will be depleted and therefore new sustainable materials have to replace them.

Due to the large production of cellulose in nature it can help to open new pathways in replacing the existing fossil based materials, such as synthetic fibers. As mentioned above, cellulose is harmless toward humans and therefore it is recognized as one of the safest and most accepted polymer classes for use in food and pharmaceutical products.<sup>180</sup> Beside the use of native cellulose, it is advantageous and indeed necessary to alter its surface properties (e.g., hydrophobicity) for a greater variety of applications. Modification processes of cellulose are either conducted in homogeneous or heterogeneous media. The first results of grafting of polymers onto cellulose were presented by Waltcher *et al.* at a IUPAC meeting in Stockholm 1953.<sup>181</sup> One advantage of performing reactions on cellulose in homogeneous media is the higher degree of functionalization as well as the more uniform distribution of grafts. Cellulose exhibits a poor solubility in most organic solvents. A mixture of *N,N*-dimethylacetamide/lithium chloride (DMAc/LiCl)<sup>182</sup> or ionic liquids<sup>183</sup> can be employed for solubilizing native cellulose. In order to achieve a high degree of functionality, the reactions have to be carried out in anhydrous conditions as the main problem is the low acylation of the active cellulose sites due to small amounts of water which is still present in the reaction and very difficult to remove. Therefore only a handful of reactions have so far been carried out in such media. Reactions of cellulose in DMAc/LiCl include the polymerization of 2-methacryloyloxyethyl phosphorylcholine<sup>184</sup> as well as MMA<sup>185</sup> mediated by an ATRP-initiator. Examples of functionalizations of cellulose in ionic liquids include the polymerization of MMA,<sup>186,187</sup> 2-(dimethylamino)ethyl methacrylate<sup>188</sup> and styrene<sup>186</sup> mediated by ATRP-initiators. Further examples of work conducted on cellulose in homogeneous medium include the attachment of RAFT agents onto hydroxyisopropyl cellulose with subsequent controlled polymerization,<sup>189</sup> polysaccharide attached with NMP initiators and subsequent controlled polymerization, attaching an ATRP initiator with subsequent controlled polymerization, as well as polysaccharide-based comb copolymers.<sup>190</sup> While all these methods work with cellulose which is completely dissolved in a medium, in the process of heterogeneous chemical modification of cellulose, the cellulose pieces are dispersed and swollen in the surrounding solvent. One great drawback of performing reactions in homogeneous media on cellulose is the lack of spatial resolution. Spatial resolution means the functionalization only occurs at specific sites leaving protected parts of the surface free. The focus of the current thesis is on heterogeneous functionalization which opens a pathway for applying spatial resolution techniques. For a further insight into homogeneous functionalization of cellulose - not exclusively with polymers - the reader is referred to the review by Heinze and Petzold<sup>191</sup> as well as Heinze and Liebert.<sup>192</sup> The next section of the current chapter presents state of the art modification techniques of cellulose in heterogeneous media.

### 1.5.6 Cellulose *Grafting-From* in Heterogeneous Media

As most natural polymers, cellulose exhibits poor solubility in most common solvents and therefore the modification under heterogeneous conditions has been under investigation for almost a century.<sup>190</sup> Beside the traditional chemical transformation of cellulose, such as cellulose xanthate, cellulose esters and regenerative cellulose, which find applications from textiles to pharmaceuticals, there is a steady growth of synthetic polymer grafting onto polysaccharides making use of the *grafting-from* technique. This method offers an attractive route to new material properties, as well as keeping the intrinsic properties of the unmodified cellulose. The *grafting-from* technique in heterogeneous media of cellulose has been conducted with free radical polymerization techniques.<sup>193</sup> However, one drawback of applying free radical polymerization in the *grafting-from* technique is a lack of control of the polymer strands on the surface as well as a lack of control of molecular weight and *PDI*.<sup>194</sup> Recently, new methods were developed to overcome the before mentioned problems, i.e., the combination of controlled free radical polymerization with the *grafting-from* technique for the synthesis of cellulose-polymer hybrids. The control agent may consist of a RAFT- or ATRP-agent. Covalently bound ATRP initiators on different cellulose substrates with subsequent controlled polymerization of (i) methyl acrylate was shown by Castelvetro *et al.*,<sup>195</sup> (ii) glycidyl methacrylate has been shown by Malmström and coworkers<sup>196–198</sup> and (iii) 2-(dimethylaminoethyl methacrylate) was shown by Lee *et al.*<sup>199</sup> Recently, the concept of RAFT polymerization was combined with the *grafting-from* method on cellulose substrates. In this case, the RAFT agent was not immobilized on the cellulose, but added as free RAFT agent in the dispersion consisting also of dispersed cellulose, dissolved monomer and RAFT agent. The cellulose was irradiated with  $\gamma$ -rays as an initiator for the controlled polymerization. Not only did the  $\gamma$ -rays start the initiation but also created radicals on the surface where the desired controlled polymerization took place. It was proposed that the molecular weight of the graft polymer is almost the same as the polymer generated in the free solution. This issue was addressed by dissolving the grafted cellulose and subsequently analyzing the residual polymer *via* size exclusion chromatography. The comparison of the size exclusion chromatograms of the free generated polymer and the grafted polymer were almost identical, showing proof for the presumption of an identical polymerization rate in solution as well as on the surface. Combining RAFT-agents immobilized on cellulose with controlled polymerization of (i) styrene was shown by Barsbay *et al.*<sup>200</sup> and (ii) 2-(dimethylaminoethyl) methacrylate was shown by Roy *et al.*<sup>189</sup> One of the most recent examples of cellulose modification is given by Bongiovanni *et al.* where fluorinated monomers were polymerized *via* UV-light activation from the surface of a cellulose surface generating a hydrophobic polymer layer grafting.<sup>201</sup>

### 1.5.7 Cellulose *Grafting-To* in Heterogeneous Media

As mentioned earlier, the *grafting-to* technique bears the advantage of using thoroughly characterized polymers although the grafting densities appear to be lower than with the *grafting-from* technique. While for the most *grafting-to* reactions this statement seems to be correct, it has been shown for a range of efficient reactions (some of which adhere to the *click*-type reactions) that the grafting densities can be in a comparable range. Examples for such reactions are the copper-catalyzed Huisgen cycloadditions, Michael additions, as well as (hetero) Diels-Alder cycloadditions.<sup>202-204</sup> Compared to the *grafting-from* technique, the *grafting-to* technique has - so far - obtained only little attention. Actually only a few examples are known using such *click*-type reactions. One example is given by Zhao *et al.*, which employed the UV-light activated radical thiol-ene reaction for surface functionalization on cellulosic derivatives yielding inter alia poly( $\epsilon$ -caprolactone) grafted cellulosic hybrid material.<sup>205</sup> The azide alkyne cycloaddition was first demonstrated by Lieber *et al.* on cellulose surfaces with small molecules.<sup>206</sup> For the same type of coupling reaction, Krouit *et al.* introduced poly( $\epsilon$ -caprolactone) on cellulose.<sup>207</sup> A recent example of combining a *click*-type reaction with cellulose surface modification is the functionalization of cellulose surfaces employing the hetero Diels Alder reaction which was demonstrated by Tischer *et al.*<sup>148</sup> The authors showed the grafting of well-defined poly(*isobornyl* acrylate) onto a solid cellulose substrate which was confirmed by IR-microscopy as well as X-ray photoelectron spectroscopy. While the given examples are a valuable addition to the variety of surface modification of cellulose, they exhibit no possibility of spatial resolution during the functionalization process. To overcome this deficiency, two *grafting-to* techniques will be presented in the current thesis which offer the possibility of spatial resolution and thus offer new avenues for cellulose modification in the heterogeneous phase. It will be demonstrated that the combination of controlled free radical polymerization techniques with UV-light activated *click*-type reactions are a powerful tool to modify surfaces.

# 2

## Methods and Materials

### 2.1 Materials

#### 2.1.1 Chemicals Used in Chapter 3

Styrene (99 % extra pure stabilized, Acros), methyl acrylate (99 %, Acros Organics), butyl acrylate (99 %, Acros Organics), *tert*-butyl acrylate (99 %, Acros Organics), and *isobornyl* acrylate (technical grade, Sigma Aldrich) were freed from inhibitor by percolating through a column of basic alumina prior to use. The RAFT agents cyanoisopropyl dithiobenzoate (CPDB),<sup>208</sup> cumyl phenyldithioacetate<sup>209</sup> and dibenzyl trithiocarbonate,<sup>46,210</sup> were synthesized according to literature procedures and their purity was confirmed *via* <sup>1</sup>H NMR. 2,2'-Azobis(isobutyronitrile) (AIBN, 98 %, Sigma Aldrich) was recrystallized twice from ethanol prior to use. Sodium iodide (puriss. p.a., Fluka), tetrahydrofuran (multisolvant, 250 ppm BHT, Scharlau), triphenylphosphine (Merck), methanol (chromasolv, Sigma Aldrich), hydrogen peroxide (30 %, rotipuran, Roth) and acetonitrile (99 % extra pure, Acros) were used as received.

#### 2.1.2 Chemicals Used in Chapter 4 and 5

Poly(ethylene glycol) methyl ether (PEG, Sigma Aldrich, average  $M_n$  2000 g mol<sup>-1</sup>) was dried just prior its use *via* azeotropic distillation in toluene. Copper (I) bromide (CuBr, Fluka) was purified *via* sequential washing with sulfuric acid, acetic

acid, and ethanol, followed by drying under reduced pressure. Methyl methacrylate (MMA, 99 %, Acros) and 2-(dimethylamino)ethyl methacrylate (DMAEMA, 98 %, Sigma Aldrich) were passed through a short plug of basic alumina to remove inhibitors and stored at -19 °C. *N,N'*-dicyclohexylcarbodiimide (DCC, 99 %, Acros), 4-(dimethylamino)pyridine (DMAP, 99 %, ABCR), 2,2'-bipyridyl (bpy,  $\geq 99$  %, Sigma-Aldrich copper (II) bromide ( $\text{CuBr}_2$ ,  $\geq 99$  %, Fluka), 3-aminopropyltriethoxysilane (APTS, 98 %, ABCR), bromoethane (98 %, ABCR), sulfuric acid ( $\text{H}_2\text{SO}_4$ , 95 %, Roth), hydrogen peroxide (30 %, rotipuran, Roth), sodium hydrogencarbonate ( $\text{NaHCO}_3$ , 99 %, Roth), magnesium sulfate ( $\text{MgSO}_4$ , 99 %, Roth), lithium bromide ( $\text{LiBr}$ ,  $\geq 99$  %, Alfa Aesar), acetone (for synthesis, VWR), tetrahydrofuran (THF, for synthesis: multisolvent, 250 ppm BHT, Scharlau; SEC ESI/MS: HPLC grade, VWR), *N,N,N',N'',N''*-pentamethyldiethylenetriamine (PMDETA, for synthesis, Merck), and *N,N*-dimethylacetamide (DMAc, HPLC grade, Sigma Aldrich) were used as received. Carboxy-functionalized tetrazole (methyl 4-(2-phenyl-2*H*-tetrazol-5-yl)benzoic acid),<sup>211</sup> tetrazole-functionalized PEG (1),<sup>211,212</sup> 2-bromo-2-methyl propionic acid 2-(3,5-dioxo-10-oxa-4-azatricyclo[5.2.1.0<sup>2,6</sup>]dec-8-en-4-yl) ethyl ester (Fur-Mal-ATRP),<sup>213</sup> 4-(2-[(3-acetyl-7-oxabicyclo[2.2.1]hept-5-en-2-yl)carbonyl]aminoethoxy)-4-oxobutanoic acid (Ful-Mal-COOH) and maleimide functionalized PEG were synthesized according to previously published procedures.<sup>214</sup> 2-Hydroxyethyl 2-bromo-2-methylpropanoate (HBMP) was synthesized according to a literature procedure by Wolf et al.<sup>215</sup> Dichloromethane (DCM, p.a. grade, VWR) and toluene (p.a. grade, VWR), and ethanol (p.a. grade, VWR) were dried (when stated) on appropriate molecular sieves (4 and 3 Å, respectively). Styrene (99 % extra pure stabilized, Acros) was freed from inhibitor by percolating through a column of basic alumina prior to use. Tungstate dehydrate (99 %, Sigma Aldrich), acetonitrile (99 %, extra pure, Acros), 2,2,6,6-tetramethyl-4-piperidone (98 %, ABCR), tosylmethyl isocyanide (97 %, ABCR), diethylether (normapur, Merck), dimethoxyethane (for synthesis, VWR), potassium *tert*-butoxide (97 %, Sigma Aldrich), *tert*-butyl alcohol (rectapur, VWR), cyclohexane (rectapur, VWR), ethyl acetate (p.a. grade, VWR), barium hydroxide monohydrate (99 %, Acros), sodium hydroxide (99 %, Roth), hydrochloric acid, (32 % solution in water, pure, Acros), magnesium sulfate (extra pure, Acros), *N,N*-diisopropylethylamine (99 %, Roth), succinic anhydride (99 %, Acros), acetone (for synthesis, VWR), 4-dimethylaminopyridine (99 %, Acros) and 2,2,6,6-tetramethyl-1-piperidinyloxy (98 %, Sigma Aldrich). Irgarcure 2959<sup>TM</sup> was kindly provided by BASF.

## UV-Lamps

### The Nitrile Imine-Mediated 1,3-Dipolar Cycloaddition of Tetrazole and Ene Coupling (NITEC) Approach

Hand-held UV-lamp emission at 254 nm with 8 W output (Camag, Switzerland).

## TEMPO/Photoinitiator Approach

UV low-pressure light bulb with emission from 290 to 350 nm and a maximum emission between 300-320 nm and 36 W output (Cosmedico Medical Systems, Germany).

## 2.2 Characterization Techniques

### 2.2.1 $^1\text{H}$ Nuclear Magnetic Resonance Spectroscopy

$^1\text{H}$  NMR spectra were recorded either in  $\text{CDCl}_3$  or dimethyl sulfoxide  $d_6$  (specified in each chapter) at ambient temperature on a Bruker Advance 400 NMR spectrometer operating at 400 MHz for hydrogen nuclei or a Bruker AM250 spectrometer at 250 MHz for hydrogen nuclei. The  $\delta$  scale is referenced to tetramethylsilane ( $\delta = 0.00$ ) as an internal standard.

### 2.2.2 Coupled Size Exclusion Chromatography/Electrospray Ionization (SEC/ESI-MS)

Spectra were recorded on an LXQ mass spectrometer (ThermoFisher Scientific, San Jose, CA, USA) equipped with an atmospheric pressure ionization source operating in the nebulizer assisted electrospray mode. The instrument was calibrated in the  $m/z$  range 195-1822 using a standard containing caffeine, Met-Arg-Phe-Ala acetate (MRFA) and a mixture of fluorinated phosphazenes (Ultramark 1621) (all from Aldrich). A constant spray voltage of 4.5 kV and a dimensionless sweep gas flow rate of 2 and a dimensionless sheath gas flow-rate of 12 were applied. The capillary voltage, the tube lens offset voltage and the capillary temperature were set to 60 V, 110 V and 275 °C respectively. The LXQ was coupled to a Series 1200 HPLC-system (Agilent, Santa Clara, CA, USA) consisting of a solvent degasser (G1322A), a binary pump (G1312A), a high-performance autosampler (G1367B), followed by a thermostatted column compartment (G1316A). Separation was performed on two mixed bed size exclusion chromatography columns (Polymer Laboratories, Mesopore 250  $\times$  4.6 mm, particle dia. 3  $\mu\text{m}$ ) with pre-column (Mesopore 50  $\times$  4.6 mm) operating at 30 °C. THF at a flow rate of 0.30 mL  $\text{min}^{-1}$  was used as the eluent. The mass spectrometer was coupled to the column in parallel to a RI-detector (G1362A with SS420x A/D) in a setup described previously.<sup>216</sup> 0.27 mL  $\text{min}^{-1}$  of the eluent were directed through the RI-detector and 30  $\mu\text{L min}^{-1}$  infused into the electrospray source after post-column addition of a 100  $\mu\text{M}$  solution of sodium iodide in methanol at 20  $\mu\text{L min}^{-1}$  by a micro-flow HPLC syringe pump (Teledyne ISCO, Model 100DM). 20  $\mu\text{L}$  of a polymer solution with a concentration of approximately 3 mg  $\text{mL}^{-1}$  were injected into the HPLC system. Measurements can also be

conducted *via* direct infusion ESI-MS. However, pre-separation *via* SEC provides an improved ionization due to the absence of low molecular weight impurities and the slice by slice ionization of the investigated polymers.

### 2.2.3 Molecular Weight Analysis *via* Size Exclusion Chromatography (SEC)

For the determination of molecular weight distributions (MWD), a SEC system (Polymer Laboratories PL-GPC 50 Plus) comprising an auto injector, a guard column (PLgel Mixed C, 50 × 7.5 mm) followed by three linear columns (PLgel Mixed C, 300 × 7.5 mm, 5 μm bead-size) and a differential refractive index detector was employed. THF was used as the eluent at 40 °C with a flow rate of 1 mL min<sup>-1</sup>. The SEC system was calibrated using narrow polystyrene standards ranging from 160 to 6 × 10<sup>6</sup> g mol<sup>-1</sup> (Polymer Standard Service). The resulting molecular weight distributions were reassessed by universal calibration using Mark-Houwink parameters for *p*iBoA ( $K = 5.00 \times 10^{-5} \text{ dL g}^{-1}$ ,  $\alpha = 0.745$ ),<sup>35</sup> poly(methyl acrylate) *p*MA ( $K = 19.5 \times 10^{-5} \text{ dL g}^{-1}$ ,  $\alpha = 0.66$ ),<sup>217</sup> poly(butyl acrylate) *p*BA ( $K = 12.2 \times 10^{-5} \text{ dL g}^{-1}$ ,  $\alpha = 0.70$ ),<sup>218</sup> and for polystyrene *p*Sty ( $K = 14.1 \times 10^{-5} \text{ dL g}^{-1}$  and  $\alpha = 0.70$ ).<sup>219</sup> Mark-Houwink-Kuhn-Sakurada parameters were not known at the time of experimental investigation for poly(*tert*-butyl acrylate) *pt*BA, therefore *p*Sty equivalent molecular weights were employed.

### 2.2.4 X-ray Photoelectron Spectroscopy (XPS)

XPS-investigations were performed on a K-Alpha spectrometer (ThermoFisher Scientific, East Grinstead, U.K.) using a microfocused, monochromated Al K $\alpha$  X-ray source (200 μm spot size). Up to 30 separated spots were measured to prevent the samples from X-ray damage, each at minimum acquisition time. All spectra were finally collapsed to one single spectrum with a sufficient signal/noise ratio. The kinetic energy of the electrons was measured by a 180° hemispherical energy analyzer operated in constant analyzer energy mode (CAE) at 50 eV pass energy for elemental spectra. The photoelectrons were detected at an emission angle of 0° with respect to the normal of the sample surface. The K-Alpha charge compensation system was employed during analysis, using electrons of 8 eV energy and low-energy argon ions to prevent any localized charge build-up. Data acquisition and processing using the Thermo Avantage software is described elsewhere.<sup>220</sup> The spectra were fitted with one or more Voigt profiles (BE uncertainty: ±0.2 eV). The analyzer transmission function, Scofield<sup>221</sup> sensitivity factors, and effective attenuation lengths (EALs) for photoelectrons were applied for quantification. EALs were calculated using the standard TPP-2 M formalism.<sup>222</sup> All

spectra were referenced to the C1s peak of hydrocarbon at 285.0 eV binding energy controlled by means of the well-known photoelectron peaks of metallic Cu, Ag, and Au, respectively.

### 2.2.5 Contact Angle Measurements

Contact angle measurements were performed on a Kruess DSA 100 using Kruess DSA 2 software. Method employed: Sessil drop method, droplet phase: Water, environment phase: Air, dispensing volume: 4.0  $\mu\text{L}$ , dosing rate: 100  $\mu\text{L}/\text{min}$ , manual baseline detection.



# 3

## End Group Conversion of RAFT-Polymers

### 3.1 Introduction

As stated in the literature review in chapter 1, the reversible addition fragmentation chain transfer (RAFT) process is currently one of the most established techniques applied for controlling radical polymerizations.<sup>42–44,223,224</sup> The RAFT process has proven itself to be a flexible method, featuring a broad range of polymerizable monomer systems as well as a high solvent compatibility.<sup>42–45,224</sup> Recent examples of the employment of the RAFT process include pathways towards thermo-responsive protein conjugates,<sup>62</sup> the synthesis of surface initiated stimuli-responsive diblock co-polymers,<sup>225</sup> applications in polymer therapeutics and drug delivery<sup>226</sup> as well as the synthesis of surface functional nanomaterials.<sup>227</sup>

The living nature and control over the molecular weight is achieved by a reversible chain transfer step of the propagating polymer radical onto a dormant polymer chain. Usually a dithioester or trithiocarbonate group is employed as the controlling agent. The RAFT process thus yields polymers bearing the leaving- or R-group of the controlling agent as the initiating chain end and the thiocarbonyl thio as the terminating functional group (see chapter 1 for a further insight).

Although the RAFT process has high industrial potential, the presence of thioester or trithiocarbonate groups in the synthesized polymer is a significant drawback of the technique. These functional groups also lead to a generally colored material and further problems with potentially toxic or ill-smelling end-group degradation products. Even though the dithioester group is a highly reactive functional group, there is a shortage of chemical transformations in the literature that are of synthetic industrial interest.<sup>45,107</sup>

These characteristics of the RAFT process are disfavored in commercial applications and have led to research into developing an efficient and low cost reaction to eliminate the Z-group or transform it into a more desirable functional group, which enables further reaction steps with the functionalized polymer. Recently, Perrier and colleagues have shown an elegant approach for the end-group modification of RAFT polymers. Their employed procedure requires the polymer to be reacted with a functional azo-initiator after isolation of the polymer. The advantage of this procedure is that it allows the recovery of the chain transfer agent.<sup>107</sup> In addition, dithioesters and trithiocarbonates may undergo the reactions as shown in the introduction chapter.

The degradation of dithiobenzoate capped poly(methyl methacrylate) in peroxide-containing tetrahydrofuran has been reported by Gruendling *et al.*<sup>153</sup> Surprisingly, it was found that polymer degradation did not proceed towards the formation of sulfines and thioesters, but instead the single product of this degradation reaction appeared to be hydroperoxide functional polymer. It was further shown that for dithiobenzoate capped poly(methyl methacrylate) pMMA and pyridine-2-carbodithioate poly(*isobornyl* acrylate) (*piBoA*) the conversion into hydroperoxide- or hydroxyl-functional polymers can easily be achieved in a quantitative fashion.<sup>153</sup> The conversion reaction was performed in a simple one-pot procedure, employing an azo-initiator and tetrahydrofuran as solvent and reagent.

In the current chapter, a versatile method for the conversion of RAFT polymers into sulfur free yet hydroxy terminal macromolecules will be presented.<sup>228,229</sup>

## 3.2 Experimental

### 3.2.1 Polymerizations with cyanoisopropyl dithiobenzoate

Solutions of cyanoisopropyl dithiobenzoate (CPDB) and 2,2'-azobis(isobutyronitrile) in the monomer (50 mL) were degassed by purging with nitrogen for 15 min. The solutions were heated to 60 °C for variable time intervals, after which the reactions were stopped by cooling in liquid nitrogen. The residual monomers were removed under vacuum and the polymers precipitated in cold methanol. Polymerization times and exact concentrations are collated in Table 3.1. Molecular weight averages were determined by SEC after precipitation.

**Table 3.1:** Reaction conditions for the CPDB mediated polymerizations of various monomers at 60 °C as well as the obtained molecular weights and polydispersities, where  $c^0_{\text{CPDB}}$  is the concentration of the employed RAFT agent,  $c^0_{\text{AIBN}}$  is the initial concentration of AIBN.

Monomer	$c^0_{\text{CPDB}}/\text{mmol L}^{-1}$	$c^0_{\text{AIBN}}/\text{mmol L}^{-1}$	$t/\text{min}$	$M_n/\text{g mol}^{-1}$	$PDI$
MMA	48.70	5.11	150	3500	1.18
MA	7.85	3.41	150	3100	1.09
BA	7.89	3.61	120	2300	1.18
<i>i</i> BoA	21.08	2.19	300	3100	1.20

### 3.2.2 Polymerizations with cumylphenyldithioacetate

The same experimental procedure as with CPDB was employed. Polymerization times and exact concentrations are shown in Table 3.2. Molecular weight averages were determined by SEC after precipitation.

**Table 3.2:** Reaction conditions for the CPDA mediated polymerizations of various monomers at 60 °C as well as the obtained molecular weights and polydispersities, where  $c^0_{\text{CPDA}}$  is the concentration of the employed RAFT agent,  $c^0_{\text{AIBN}}$  is the initial concentration of AIBN.

Monomer	$c^0_{\text{CPDA}}/\text{mmol L}^{-1}$	$c^0_{\text{AIBN}}/\text{mmol L}^{-1}$	$t/\text{min}$	$M_n/\text{g mol}^{-1}$	$PDI$
MA	8.84	3.65	40	3100	1.30
BA	8.80	3.74	30	6300	1.23

### 3.2.3 Polymerizations mediated by dibenzyltrithiocarbonate

An identical experimental procedure as in the case of the CPDB mediated polymerization was employed. The polymerization times and exact concentrations are collated in Table 3.3. Molecular weight averages were determined by SEC after precipitation.

### 3.2.4 Analytical (small scale) end-group conversion

A solution of 2,2'-azobis(isobutyronitrile) (10 mmol L<sup>-1</sup>) in THF was heated to 60 °C for 60 min in the presence of ambient air. A solution of the RAFT-polymer (5-10 mmol L<sup>-1</sup> based on  $M_n$ ) in 2 mL of the pre-treated THF was prepared in a 4 mL glass vial under ambient atmosphere. The vial was heated to 60 °C. After a discoloration of the solution indicated full conversion, the temperature was reduced to 40 °C and 3 eq. triphenylphosphine (with respect to the molar amount of polymer) were added. The reader

**Table 3.3:** Reaction conditions for the DBTC mediated polymerizations of various monomers at 60 °C as well as the obtained molecular weights and polydispersities, where  $c_{\text{DBTC}}^0$  is the concentration of the employed RAFT agent,  $c_{\text{AIBN}}^0$  is the initial concentration of AIBN.

Monomer	$c_{\text{CPDA}}^0/\text{mmol L}^{-1}$	$c_{\text{AIBN}}^0/\text{mmol L}^{-1}$	$t/\text{min}$	$M_n/\text{g mol}^{-1}$	$PDI$
Styrene	10.27	4.36	960	20000	1.33
MA	29.52	3.65	35	3500	1.32
MA	17.06	5.05	45	34100	1.07
BA	12.00	3.50	60	1800	1.41
BA	6.10	1.83	60	56800	1.12
<i>t</i> Ba	29.48	3.71	60	1000	1.34
<i>i</i> BoA	7.31	3.74	20	3600	1.30

is cautioned that although triphenylphosphine acts as a quenching agent, formation of small amounts of potentially explosive THF-peroxides during the reaction is possible and liquid solvent waste should be tested and treated accordingly.

### 3.2.5 Larger scale end-group conversion

A solution of 2,2'-azobis(isobutyronitrile) (10 mmol L<sup>-1</sup>) in THF was heated to 60 °C for 60 min under ambient air. A solution of 500 mg RAFT polymer in the pre-treated THF (10 mmol L<sup>-1</sup> based on  $M_n$ ) was prepared in a 50 mL round flask under ambient atmosphere. The flask was heated to 60 °C under vigorous stirring. After a discoloration of the solution indicated full conversion, the temperature was reduced to 40 °C and 3 equiv. triphenylphosphine were added. After 15 min the polymer was precipitated in cold methanol. Please refer to the note of caution in the previous paragraph; it applies similarly to this procedure.

## 3.3 Results and discussion

Figure 3.1 depicts the general procedure for the conversion of dithioester functional (meth)acrylate polymers: A dilute solution of the RAFT polymer and a radical initiator (2,2'-azobisisobutyronitrile, AIBN) in THF is stirred at elevated temperatures ( $T = 60$  °C) in the presence of atmospheric oxygen to yield hydroperoxide functional polymer. Subsequent reduction by triphenylphosphine leads to a quantitative conversion into the hydroxide.

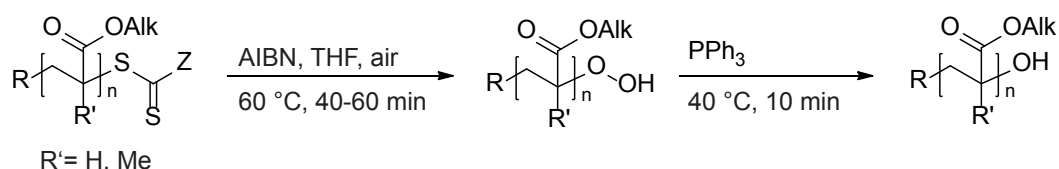


**Figure 3.1:** Synthetic transformation sequence of the dithioester end-group of RAFT polymers into a hydroperoxyl or hydroxyl end-group.

### 3.3.1 Mechanism of the end-group conversion

Based on earlier experiments<sup>155</sup> and on the results from SEC/ESI-MS analysis of the degraded polymer solutions, a tentative mechanism for the end-group conversion has already been proposed (see Figure 3.2).<sup>155,228</sup> The mechanism consists of a radical oxidation cycle similar to the radical autoxidation of ethers,<sup>230,231</sup> yet comprises an intermediate chain transfer step.

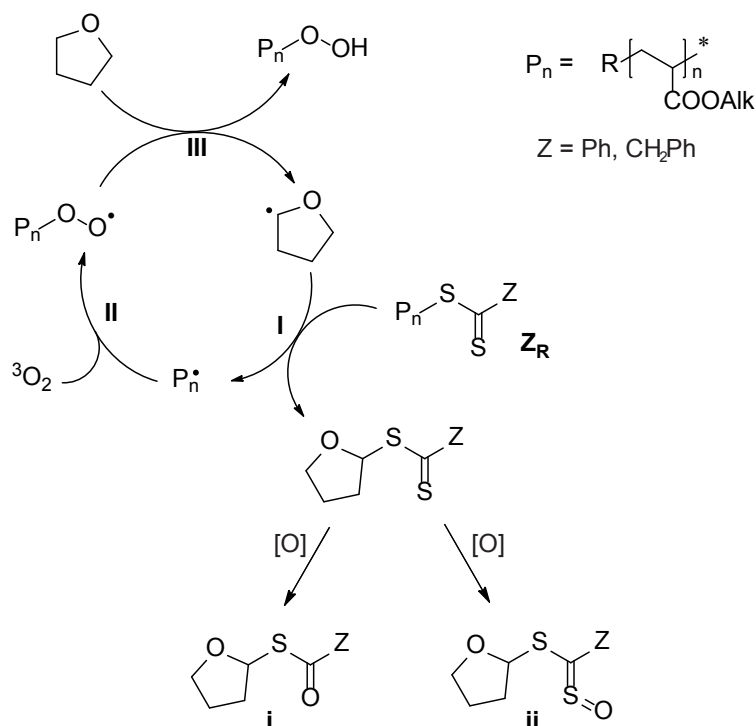


**Figure 3.2:** The pathway for the radical conversion of the dithioester group into a hydroperoxyl group.

Initially the dithioester functional vinyl polymer  $Z_R$  is cleaved by a tetrahydrofuranyl radical, yielding the macroradical  $P_n \cdot$  and the tetrahydrofuranyl dithioester in a degenerative chain transfer step [Figure 3.2 (I)]. The formed dithioester is relatively inert against radical attack, because of the low leaving group ability of the tetrahydrofuranyl substituent. It may be further oxidized to the sulfoxide (ii) or the thioester (i) by molecular oxygen or by hydroperoxide [Figure 3.2 (IV)]. As shown by Gruendling *et al.*,<sup>228</sup>

these species were identified during the SEC/ESI-MS analysis of the raw polymer solution after end-group conversion. The polymer radical undergoes irreversible addition to oxygen dissolved in the solution with close to diffusion controlled rates [Figure 3.2 (II)].<sup>232</sup> Finally, the hydroperoxide functional polymer is expelled by radical chain transfer to THF (III), starting a new oxidation cycle. Initiation of the radical oxidation process is most likely achieved by addition of oxygen onto a cyanoisobutyryl radical and subsequent chain transfer to THF, analogous to steps II and III of the reaction mechanism but with the cyanoisobutyryl radical instead of the macroradical. The proposed conversion mechanism is most likely to work with macroradicals  $P_n\bullet$  that have a good leaving group ability. The leaving group ability depends on the stability of the formed macroradical  $P_n\bullet$ . The better the macroradical  $P_n\bullet$  is stabilized, the better is its leaving group ability. Thus, the stability of the macroradical is based on the class of monomer, and therefore only monomer classes that yield stable polymer radicals are most likely to work in the conversion mechanism. Monomers which adhere to this requirement include functional acrylates, methacrylates and styrene. Highly reactive monomers such as vinylacetate are not capable to undergo the conversion into hydroxyl functional polymers using the here applied method because the degenerative chain transfer step yielding the destabilized macroradical  $P_n\bullet$  [Figure 3.2 (I)] is not favourable. Employing a reagent/solvent forming a less stable radical than THF may provide a solution to overcome this limitation.

### 3.3.2 End-group conversion of dithiobenzoate functional poly(alkyl acrylate)s and poly(alkyl methacrylate)s

The quantitative conversion of dithiobenzoate functional poly(methyl methacrylate) (pMMA) into hydroxyl functional pMMA was previously demonstrated.<sup>228</sup> Here the ability of various poly(alkyl acrylate)s prepared *via* cyanoisopropyl dithiobenzoate (CPDB) mediated RAFT polymerization to undergo conversion into hydroxyl functional poly(alkyl acrylate)s is examined. Figure 3.4 displays the SEC/ESI-MS spectra of dithiobenzoate functional poly(methyl acrylate) (pMA) before (top) and after conversion into the hydroxyl functional pMA (bottom). Inspection of the figure indicates that the conversion towards the hydroxyl functional pMA involves the formation of some side products. At the start of the reaction ( $t = 0$ ), the only species present in the spectrum is the dithiobenzoate capped pMA  $Z_R$  (see Figure 3.3 for structural formulas). After 60 min reaction time the dithiobenzoate capped pMA  $Z_R$  has disappeared.

The main product is the hydroperoxide functional pMA  $P_R\text{OOH}$ , yet some thioester functional polymer  $Z_R''$  can also be identified. (see Figure 3.5 for a full overview of the SEC/ESI-MS spectra).

It is already known that hydroperoxides are able to oxidize dithiobenzoate functional polymers to sulfine and thioester capped polymers.<sup>151,157</sup>

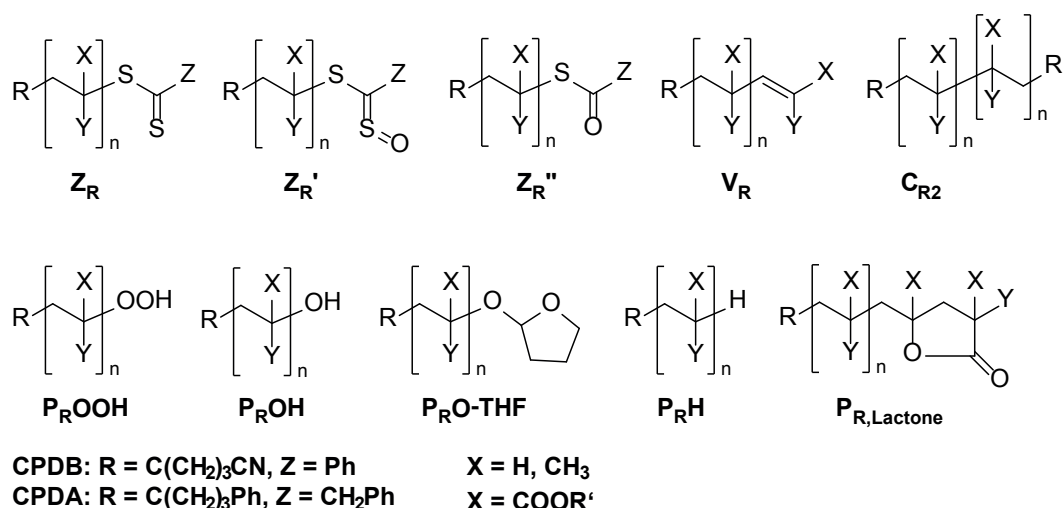


**Figure 3.3:** Possible species involved in the transformation of the dithiobenzoate or phenyldithioacetate end-group of various poly((meth)acrylate)s into a hydroxyl end-group.

The theoretical  $m/z$  ratios of the involved species are collated in Table 3.4. Within experimental error, excellent agreement between the measured  $m/z$  ratios and the theoretical  $m/z$  ratios of the expected structures is observed. From the above observations it can be concluded that although CPDB functionalized poly(acrylate)s are adequate precursors for the synthesis of hydroxyl functional poly(acrylate)s, some thioester functional poly(acrylate) **Z<sub>R</sub>''** side product will always be present during subsequent reaction steps (e.g., ring opening polymerization) that maybe conducted with the transformed polymer. These evolving side products are a drawback compared to the conversion of CPDB functionalized pMMA.<sup>228</sup> Poly(acrylate)s are more susceptible to oxidation compared to pMMA, as was previously shown.<sup>228</sup> An explanation can be found in the radical leaving group abilities of the macroradicals associated with different RAFT polymers. As the macroradical **P<sub>n</sub>•** derived from pMA is less stable than the macroradical **P<sub>n</sub>•** of pMMA, radical reactions occur slower and hence non-radical reactions play a more important role for poly(acrylate)s.

**Table 3.4:** Theoretical and measured  $m/z$  ratios of the main species involved in the end-group conversion of pMA carrying a dithiobenzoate end-group into hydroxyl functional pMA.

Structure	[M + Na] <sup>+</sup>		
	$m/z^{\text{theo}}$	$m/z^{\text{exp}}$	$\Delta m/z$
Z <sub>R</sub>	1362.50	1362.58	0.08
Z <sub>R</sub> ''	1346.52	1346.67	0.15
P <sub>R</sub> OOH	1328.55	1328.58	0.03
P <sub>R</sub> OH	1312.55	1312.75	0.20

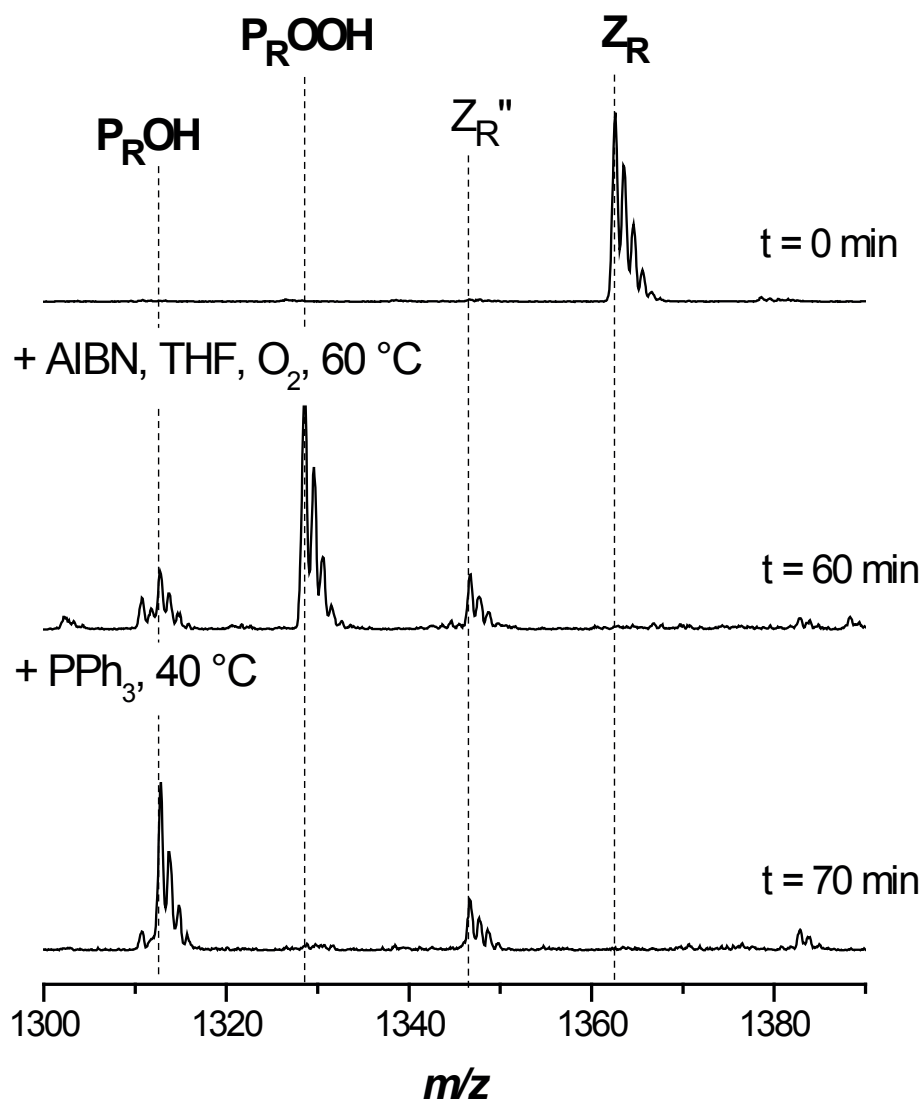


**Figure 3.4:** Electrospray ionization mass spectra of the end-group transformation of poly(methyl acrylate) carrying a dithiobenzoate end-group into hydroxyl functional pMA in the charge state  $z = 1$ . The reagents AIBN/THF and  $\text{PPh}_3$  were added sequentially at  $t = 0$  and 60 min. Full conversion was reached after 70 min. The  $\text{PPh}_3$  acts as the reducing agent from  $-\text{OOH}$  to  $-\text{OH}$ .

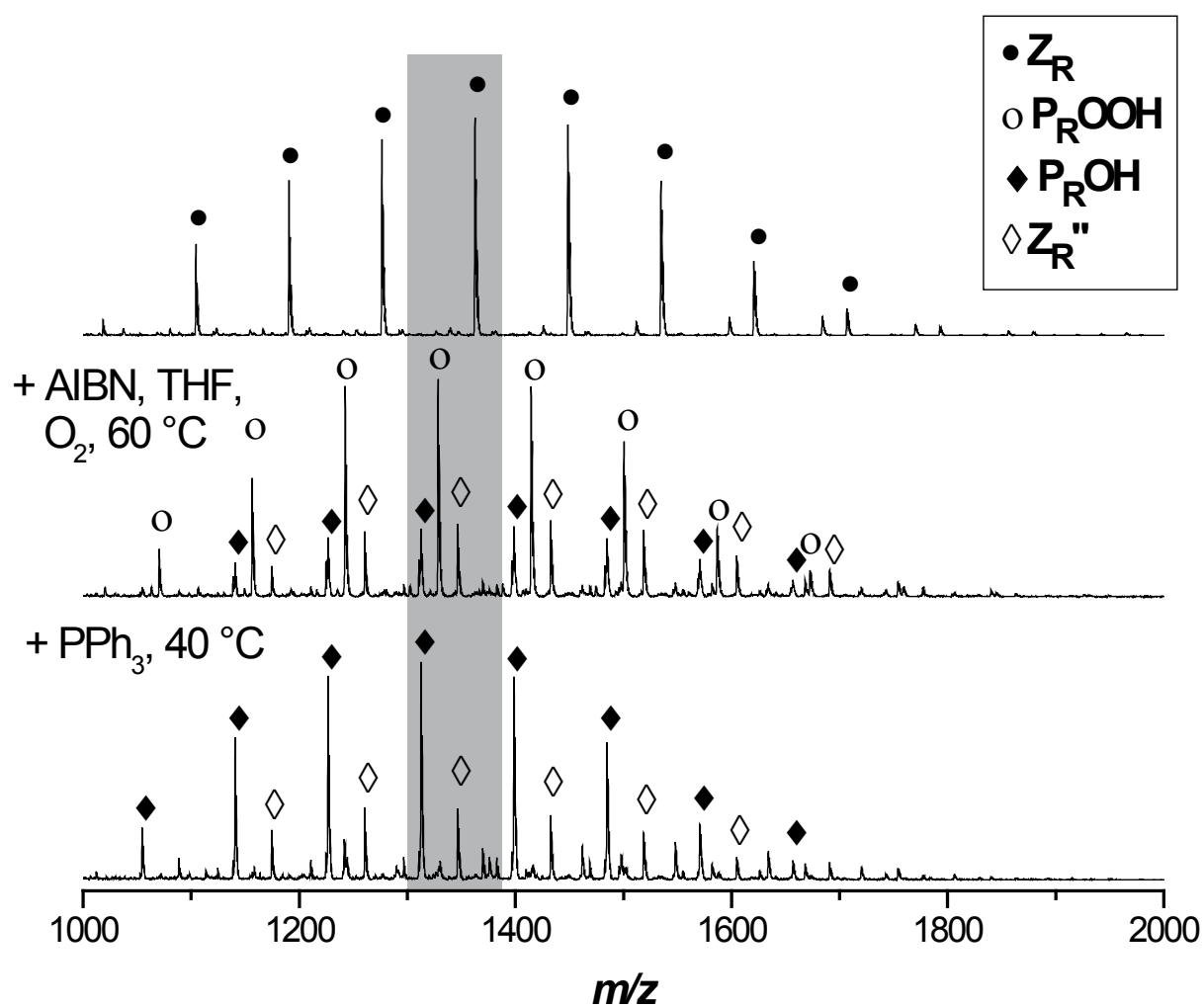


**Figure 3.5:** Electrospray ionization mass spectra of the end-group transformation of poly(methyl acrylate) carrying a dithiobenzoate end-group into hydroxyl functional pMA in the charge state  $z = 1$ . The range highlighted in grey is shown in Figure 3.4.

A similar result is obtained in the case of alternative polymers prepared from acrylic monomers, *i.e.* *pi*BoA and pBA. The results are shown in Figure 3.6 and 3.7. The comparison of the theoretical and experimental  $m/z$  values are depicted in the tables 3.5 and 3.6.

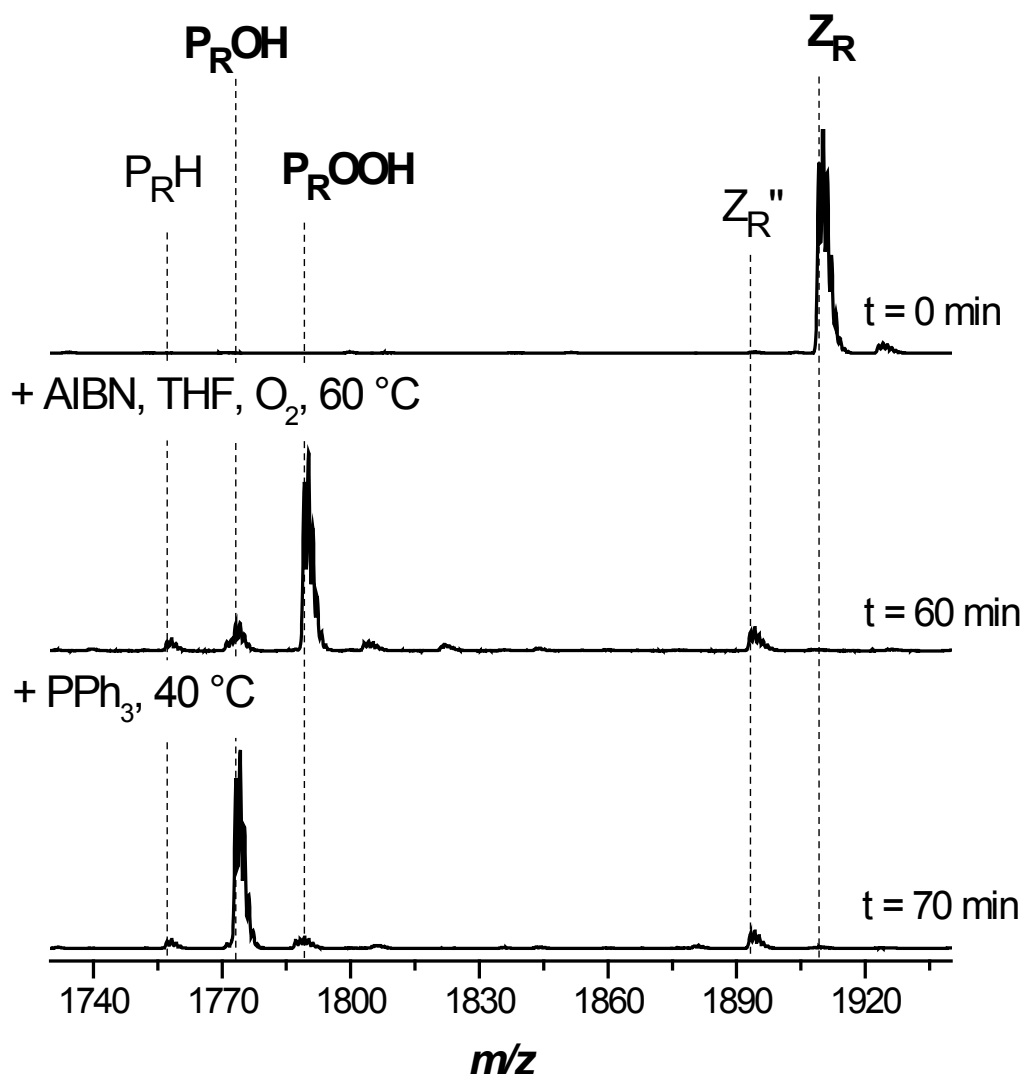


**Figure 3.6:** Electrospray ionization mass spectra of the end-group transformation of poly(*isobornyl acrylate*) carrying a dithiobenzoate end-group into hydroxyl functional *pi*BoA in the charge state  $z = 1$ . The reagents AIBN/THF and  $PPh_3$  were added sequentially at  $t = 0$  and 60 min. Full conversion was reached after 70 min.

### 3.3.3 End-group conversion of phenyldithioacetate functional poly(alkyl acrylate)s

As the conversion of dithiobenzoate functional pMA, *pi*BoA and pBA into hydroxyl functional polymer leads to formation of the thioester  $Z_R''$  as a side-product,

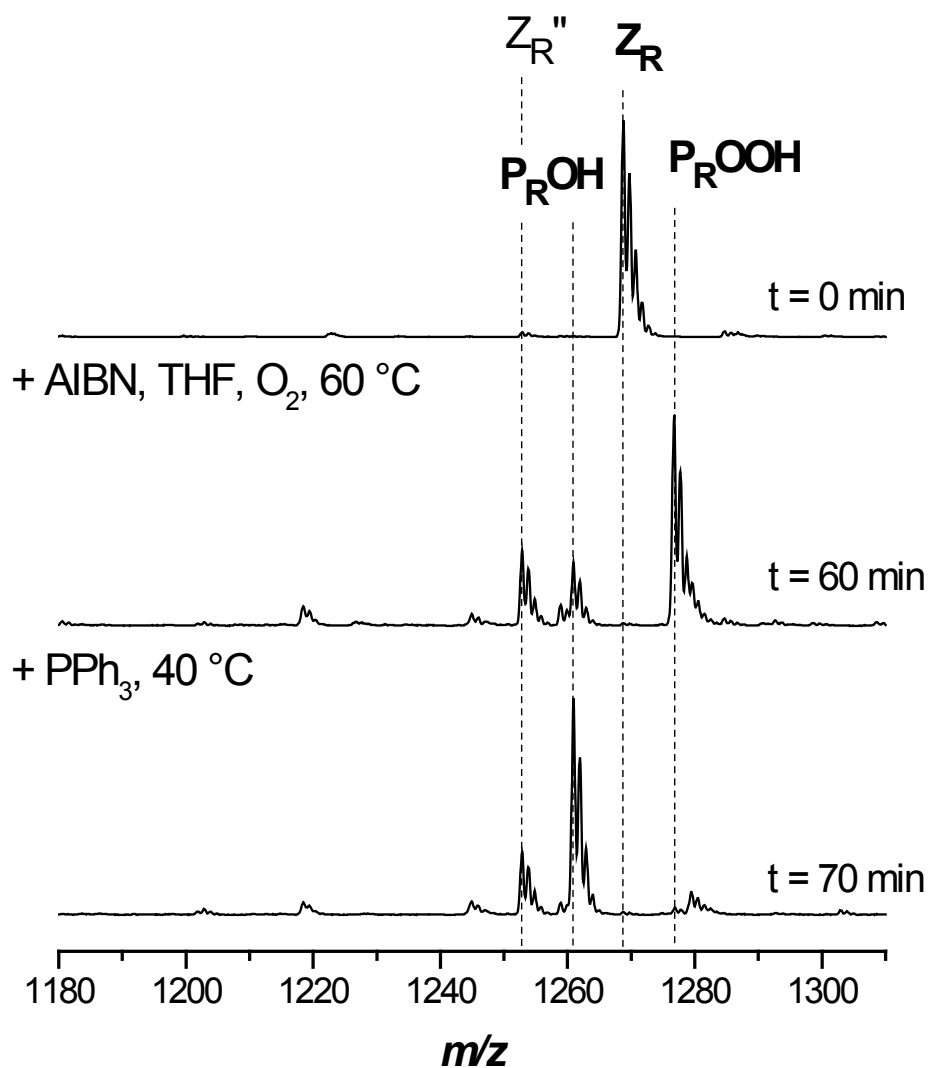


**Figure 3.7:** Electrospray ionization mass spectra of the end-group transformation of poly(butyl acrylate) carrying a dithiobenzoate end-group into hydroxyl functional pBA in the charge state  $z = 1$ . The reagents AIBN/THF and PPh<sub>3</sub> were added sequentially at  $t = 0$  and 60 min. Full conversion was reached after 70 min.

**Table 3.5:** Theoretical and measured  $m/z$  ratios of the main species involved in the end-group conversion of *pi*BoA carrying a dithiobenzoate end-group into hydroxyl functional *pi*BoA.

Structure	[M + Na] <sup>+</sup>		
	$m/z^{\text{theo}}$	$m/z^{\text{exp}}$	$\Delta m/z$
Z <sub>R</sub>	1909.19	1909.17	0.02
Z <sub>R</sub> ''	1893.22	1893.17	0.05
P <sub>R</sub> OOH	1789.21	1789.17	0.04
P <sub>R</sub> OH	1773.21	1773.25	0.04
P <sub>R</sub> H	1757.22	1757.25	0.03

**Table 3.6:** Theoretical and measured  $m/z$  ratios of the main species involved in the end-group conversion of pBA carrying a dithiobenzoate end-group into hydroxyl functional pBA.

Structure	[M + Na] <sup>+</sup>		
	$m/z^{\text{theo}}$	$m/z^{\text{exp}}$	$\Delta m/z$
Z <sub>R</sub>	1268.69	1268.75	0.06
Z <sub>R</sub> ''	1252.72	1252.83	0.11
P <sub>R</sub> OOH	1276.79	1276.75	0.04
P <sub>R</sub> OH	1260.80	1260.92	0.12

phenyldithioacetate was employed as an alternative RAFT agent for the preparation of dithioacetate capped pMA and pBA to study the influence of the Z-group on the conversion process. Figure 3.8 displays the SEC/ESI-MS spectra of phenyldithioacetate functional pMA before (top) and after conversion into the hydroxyl functional pMA (bottom).

The thioester functional poly(acrylate) Z<sub>R</sub>'' (see Figure 3.3 for structural formulas) is generated in noticeable amounts. In addition, species corresponding in mass to the hydrogen terminated pMA P<sub>R</sub>H can be observed. From the chain transfer reaction of a macroradical P<sub>n</sub>• with a THF molecule, a hydrogen terminated pMA P<sub>R</sub>H and a THF radical both evolve, which is plausible in light of the reactive nature of acryloyl radical species. Table 3.7 collates the experimental  $m/z$  ratios, which are in very good agreement with the theoretical  $m/z$  ratios of the involved species.

Similarly to the observation when using dithiobenzoate functionalized pMA, it can be observed that the conversion is not fully quantitative towards the hydroxyl functional pMA, which also applies to the conversion of pBA. The ESI-MS spectra for the conversion of phenyldithioacetate functional pBA and the theoretical and measured  $m/z$  ratios are shown in Figure 3.9 and Table 3.8.

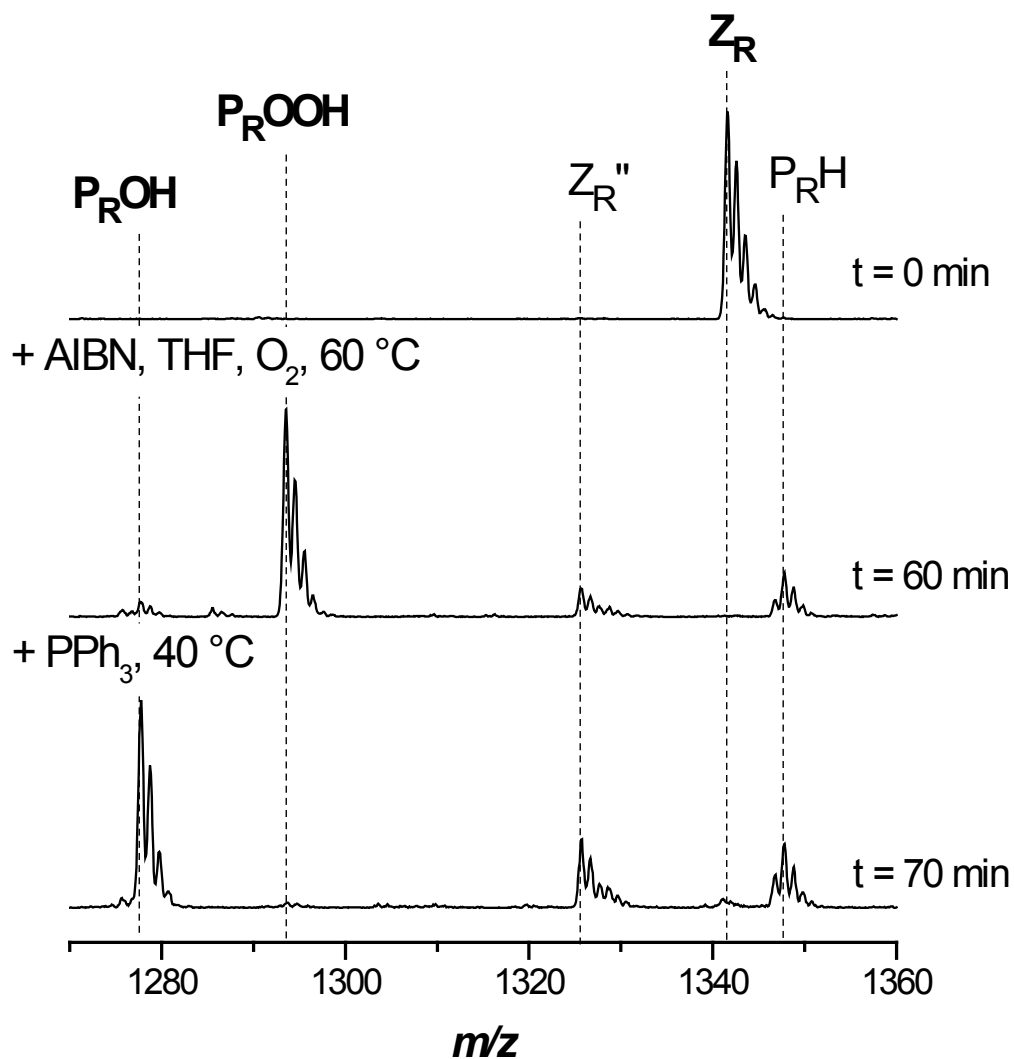


**Figure 3.8:** Electrospray ionization mass spectra of the end-group transformation of poly(methyl acrylate) carrying a phenyldithioacetate endgroup into hydroxyl functional pMA in the charge state  $z = 1$ . The reagents AIBN/THF and  $PPh_3$  were added sequentially at  $t = 0$  and 60 min. Full conversion was reached after 70 min.

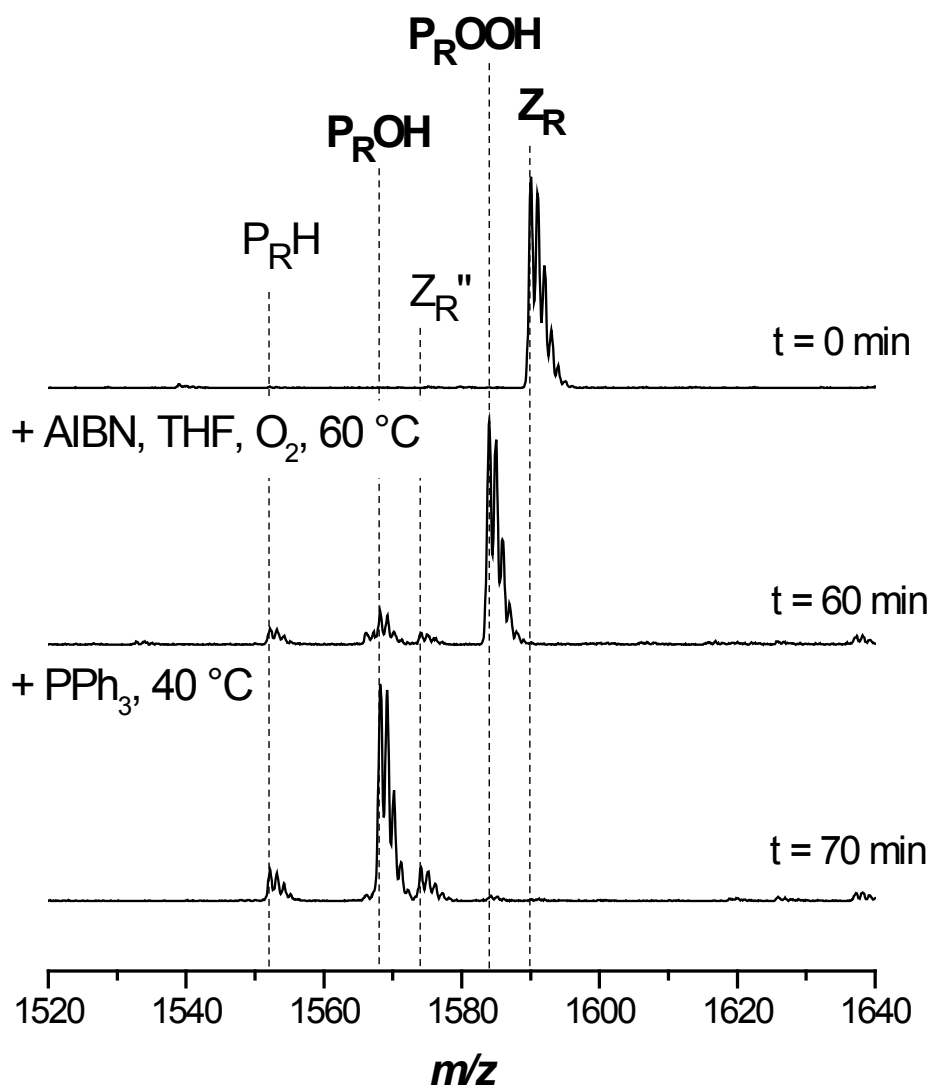


**Figure 3.9:** Electrospray ionization mass spectra of the end-group transformation of poly(butyl acrylate) carrying a phenyldithioacetate end-group into hydroxyl functional pBA in the charge state  $z = 1$ . The reagents AIBN/THF and PPh<sub>3</sub> were added sequentially at  $t = 0$  and 60 min. Full conversion was reached after 70 min.

**Table 3.7:** Theoretical and measured  $m/z$  ratios of the main species involved in the end-group conversion of pMA carrying a phenyldithioacetate end-group into hydroxyl functional pMA.

Structure	[M + Na] <sup>+</sup>		
	$m/z^{\text{theo}}$	$m/z^{\text{exp}}$	$\Delta m/z$
P <sub>R</sub> H	1347.67	1347.60	0.07
Z <sub>R</sub>	1341.52	1341.58	0.06
Z <sub>R</sub> ''	1325.54	1325.67	0.13
P <sub>R</sub> OOH	1293.55	1293.58	0.03
P <sub>R</sub> OH	1277.55	1277.75	0.20

**Table 3.8:** Theoretical and measured  $m/z$  ratios of the main species involved in the end-group conversion of pBA carrying a phenyldithioacetate end-group into hydroxyl functional pBA.

Structure	[M + Na] <sup>+</sup>		
	$m/z^{\text{theo}}$	$m/z^{\text{exp}}$	$\Delta m/z$
Z <sub>R</sub>	1589.91	1590.08	0.17
P <sub>R</sub> OOH	1584.00	1584.00	0.00
Z <sub>R</sub> ''	1573.94	1574.00	0.06
P <sub>R</sub> OH	1568.00	1568.17	0.17
P <sub>R</sub> H	1552.00	1552.17	0.17

### 3.3.4 End-group conversion of symmetrical trithiocarbonate functional poly(alkyl acrylate)s

In an attempt to optimize the conversion procedure, a symmetrical trithiocarbonate was investigated as an alternative end-group for the quantitative conversion of acrylate based RAFT-polymers. For this purpose dibenzyltrithiocarbonate (DBTC) was employed as RAFT agent. Using such a symmetrical trithiocarbonate, the polymer chain is inserted on both sides of the RAFT agent, placing the trithiocarbonate in the middle of the polymer chain. Therefore the mechanism of transformation into hydroxyl functional polymers is slightly different to that proposed for the case when dithiobenzoates and phenyldithioacetates are employed as RAFT agents. As shown in Figure 3.10, in the first step the tetrahydrofuranyl radical cleaves the trithiocarbonate capped polymer  $Z_{R,R}$  to leave a macroradical  $P_n\bullet$  and the tetrahydrofuranyltrithio functional polymer  $Z_{\text{THER}}$ . The tetrahydrofuranyltrithio functional polymer  $Z_{\text{THER}}$  subsequently reacts with a further tetrahydrofuranyl radical, yielding another macroradical  $P_n\bullet$  and a ditetrahydrofuranyltrithiocarbonate molecule. The macroradicals  $P_n\bullet$  undergo irreversible addition to oxygen dissolved in the solution, analogue to the case of the dithiobenzoate and

phenyldithioacetate conversion mechanism [see 3.2 (II)].<sup>232</sup> Eventually, the hydroperoxide functional polymer is expelled by radical chain transfer to THF (III), starting a new oxidation cycle.

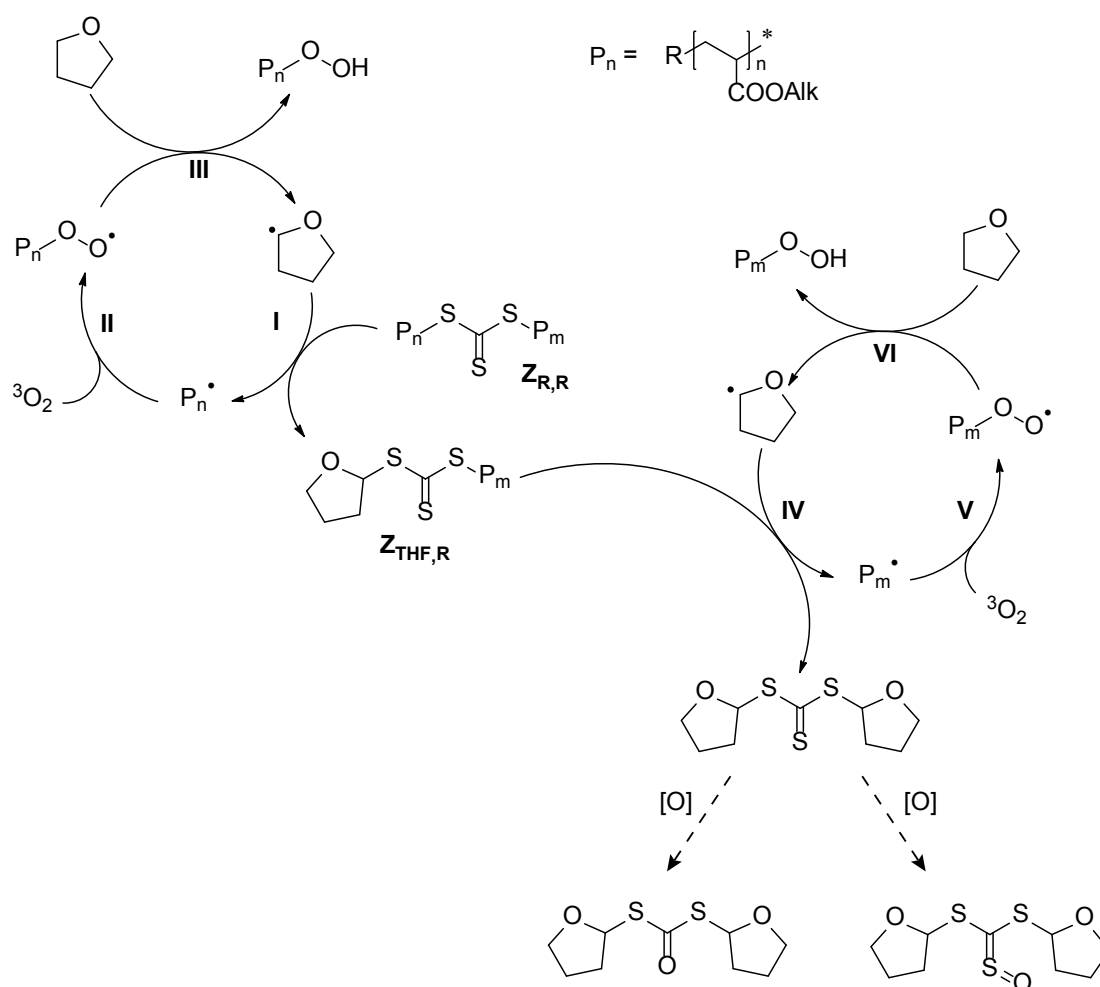


**Figure 3.10:** Pathway for the radical conversion of the symmetrical trithiocarbonate group into a hydroperoxyl group.

Upon inspection of Figure 3.10, it can be observed that the  $M_n$  of the polymer after the conversion should be half the  $M_n$  of the polymer before conversion into a hydroxyl functional polymer. To assess this theoretical expectation, SEC traces before and after the conversion sequence were recorded for variable polymers carrying a trithiocarbonate function in the mid-chain position. In Figure 3.11 the SEC traces of the trithiocarbonate functional and the degraded polymers are depicted. To map the progress of the reaction, samples of the reaction mixture were taken at preset time intervals.

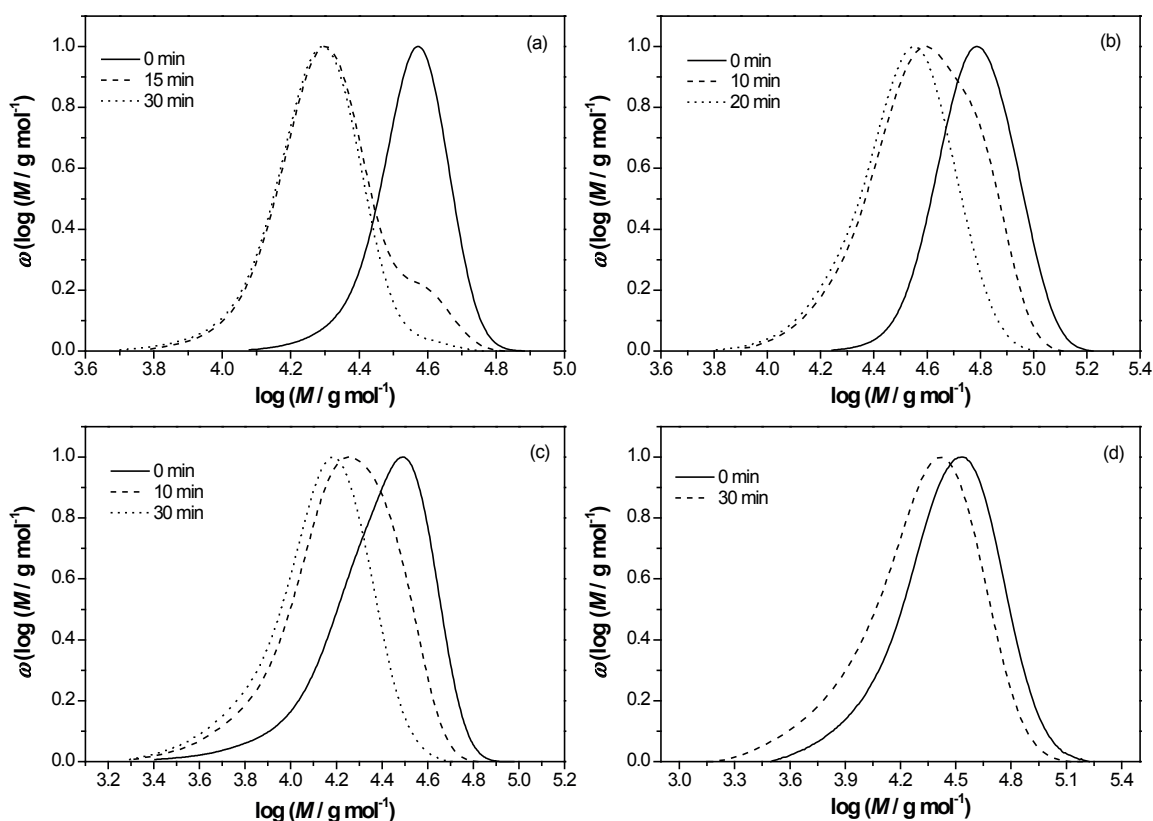


**Figure 3.11:** SEC traces of variable polymers with a trithiocarbonate moiety in the middle of the chain after reaction with AIBN/THF as a function of time. (a) pMA, (b) pBA, (c) pSty, (d) piBoA. Samples were taken at preset time intervals and precipitated in methanol.

It can be observed that  $M_n$  decreases with time, congruent with the proposed conversion mechanism. Table 3.9 depicts the different polymer classes, molecular weights of the polymers before and after the conversion and the ratios of the number average molecular weights  $M_n^{\text{RAFT}}/M_n^{\text{OH,exp}}$ . The ratio  $M_n^{\text{RAFT}}/M_n^{\text{OH,exp}}$  is close to two for pMA and pBA.

**Table 3.9:** Number average molecular weights,  $M_n$ , and  $PDI$ , for variable polymers with a trithiocarbonate moiety in the middle of the chain before and after conversion into hydroxy functional polymers.

	pMA	pBA	pSty	piBoA
$M_n^{\text{RAFT}}/\text{g mol}^{-1}$	34000	56800	19900	23300
$M_n^{\text{OH,theo}}/\text{g mol}^{-1}$	17000	28400	9950	11650
$M_n^{\text{OH,exp}}/\text{g mol}^{-1}$	17600	28900	11000	13300
$M_n^{\text{RAFT}}/M_n^{\text{OH,exp}}$	1.93	1.96	1.81	1.75
$PDI^{\text{RAFT}}$	1.07	1.12	1.30	1.47
$PDI^{\text{OH}}$	1.11	1.20	1.31	1.80

This observation underpins the proposed conversion mechanism in Figure 3.10. The ratios  $M_n^{\text{RAFT}}/M_n^{\text{OH,exp}}$  for pSty and p*t*BoA are not as close to two as for pMA and pBA. The derivation may be explained by side reactions, such as recombination of macroradicals  $\mathbf{P}_n\bullet$  or oxidation of the trithiocarbonate capped polymer  $\mathbf{Z}_{\text{R,R}}$  to the dithiocarbonate capped polymer  $\mathbf{Z}_{\text{R,R}}''$  (see Figure 3.12 for structural formulas).

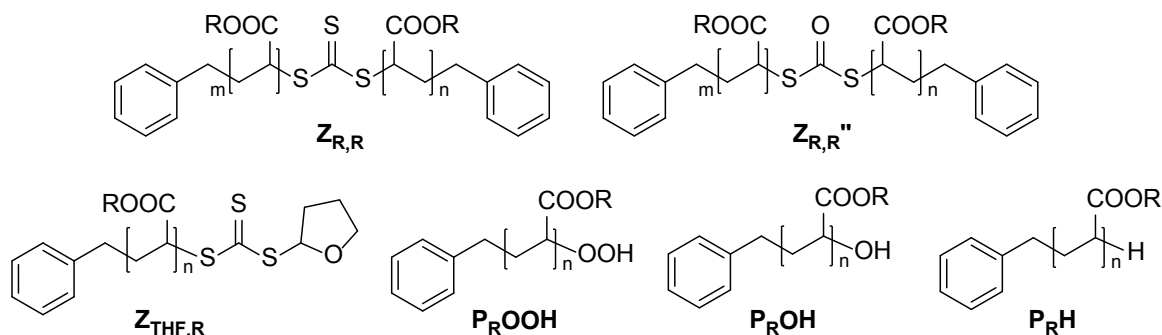


**Figure 3.12:** Possible species involved in the transformation of various poly(acrylate)s, synthesized with DBTC as RAFT agent, into hydroxyl functional polymers.

For further investigations into the mechanism an SEC/ESI-MS analysis was performed on the polymers. Employing SEC/ESI-MS, polymers of a molecular weight of up to 15 kDa (up to 4 kDa in the charge state  $z = 1$ ) can be investigated with quadrupole ion trap mass spectrometry.<sup>145,216</sup> To achieve high resolution spectra, lower molecular weight polymers were synthesized to study their conversion into hydroxyl capped entities. Ionization of non-polar polymers such as polystyrene is achieved only with some difficulties by soft ionization methods, i.e., ESI.<sup>233</sup> Although there is an existing method available for the ionization of dithioester capped polystyrene, only very low ion counts were obtained, disallowing a meaningful spectral data interpretation.<sup>233</sup>

Figure 3.13 displays the SEC/ESI-MS spectra of the symmetrical trithiocarbonate functional pMA before and after conversion into the hydroxyl functional pMA recorded at variable reaction times. It can be seen that after the conversion reaction, there are nearly quantitative amounts of the hydroxyl functional pMA  $\mathbf{P}_{\text{R,OH}}$  present. There are only traces of hydrogen terminated  $\mathbf{P}_{\text{R,H}}$  present in the spectrum.

The state of the reaction can conveniently be monitored by SEC/ESI-MS. After five minutes reaction time the intermediate tetrahydrofuran functional polymer  $\mathbf{Z}_{\text{THF,R}}$  can be observed. Ten minutes later,  $\mathbf{Z}_{\text{THF,R}}$  is only present in trace amounts. The intermediate appearance of  $\mathbf{Z}_{\text{THF,R}}$  further supports the proposed mechanism depicted in Figure 3.10.

Table 3.10 displays the experimental  $m/z$  ratios, which are in good agreement with the theoretical  $m/z$  ratios of the involved species. However, the difference between the the-

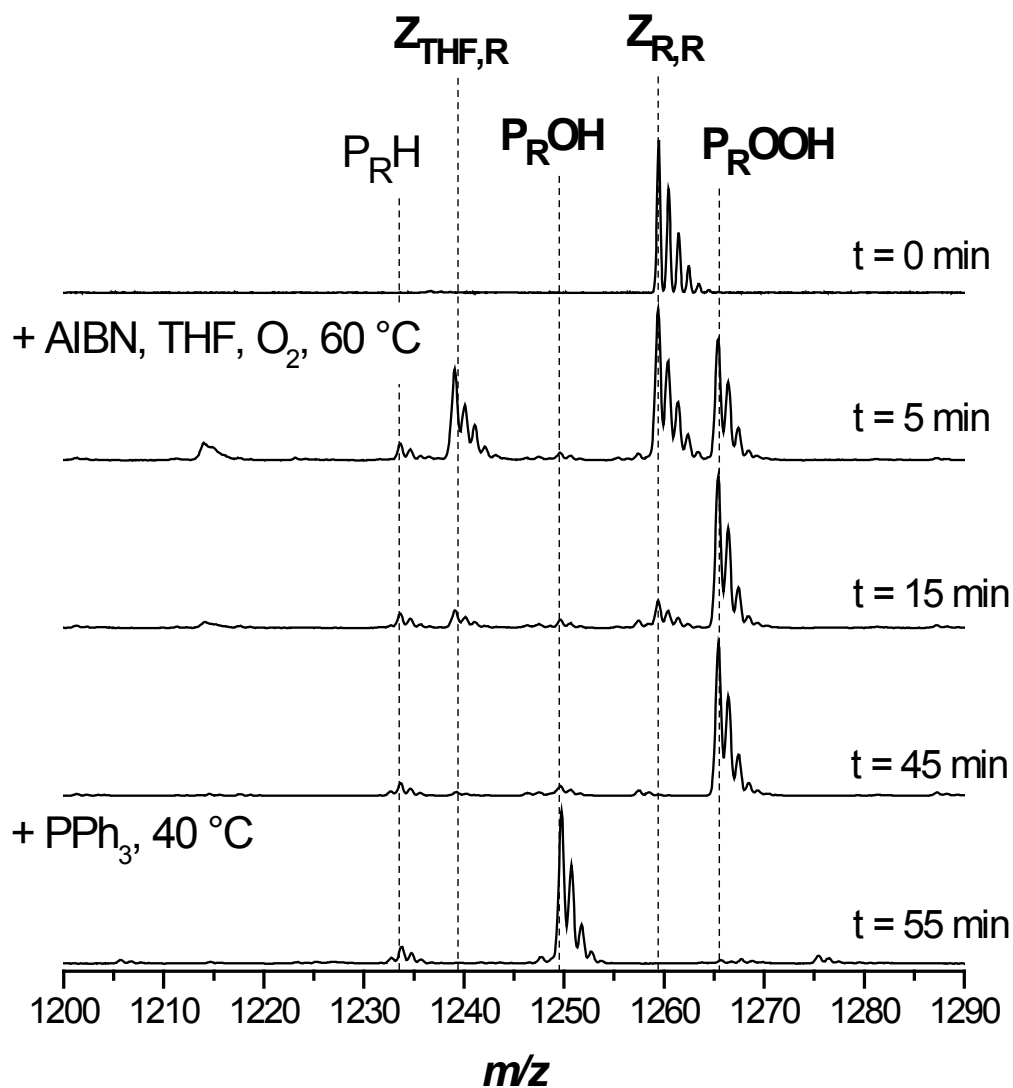


**Figure 3.13:** Electrospray ionization mass spectra of the transformation of poly(methyl acrylate) with a trithiocarbonate moiety in the middle of the chain into hydroxyl functional pMA in the charge state  $z = 1$ . The reagents AIBN/THF and PPh<sub>3</sub> were added sequentially at  $t = 0$  and 45 min. Full conversion was reached after 55 min.

oretical and measured  $m/z$  of the species  $Z_{\text{THF,R}}$  was somewhat enhanced compared to the other species.

**Table 3.10:** Theoretical and measured  $m/z$  ratios of the main species involved in the conversion of pMA with a trithiocarbonate moiety in the middle of the chain into hydroxyl functional pMA.

Structure	$m/z^{\text{theo}}$	$[\text{M} + \text{Na}]^+$	
		$m/z^{\text{exp}}$	$\Delta m/z$
$Z_{\text{R,R}}$	1259.42	1259.50	0.08
$Z_{\text{THF,R}}$	1239.42	1239.08	0.34
$P_{\text{R}}\text{OOH}$	1265.52	1265.42	0.10
$P_{\text{R}}\text{OH}$	1249.53	1249.67	0.14
$P_{\text{R}}\text{H}$	1233.53	1233.67	0.14

A great advantage of quadrupole ion trap instrumentation is the ability to perform multi-stage dissociation experiments, yielding valuable information about the chemical structure of unknown species in the mass spectrum. Therefore collision induced dissociation experiments were performed on the putative species with  $m/z^{\text{meas}} = 1239.1$  to obtain proof of the intermediate product structure. As can be observed in Figure 3.14, a neutral loss of  $m/z^{\text{meas}} = 69.9$  corresponding to a loss of dihydrofuran ( $m/z^{\text{theo}} = 70.0$ ) in the first dissociation step (see Figure 3.15), followed by a loss of  $m/z^{\text{meas}} = 75.8$  corresponding to  $\text{CS}_2$  ( $m/z^{\text{theo}} = 76.0$ ) in the second dissociation step proves the species to be the THF trithioester-capped polymer  $Z_{\text{THF,R}}$ .

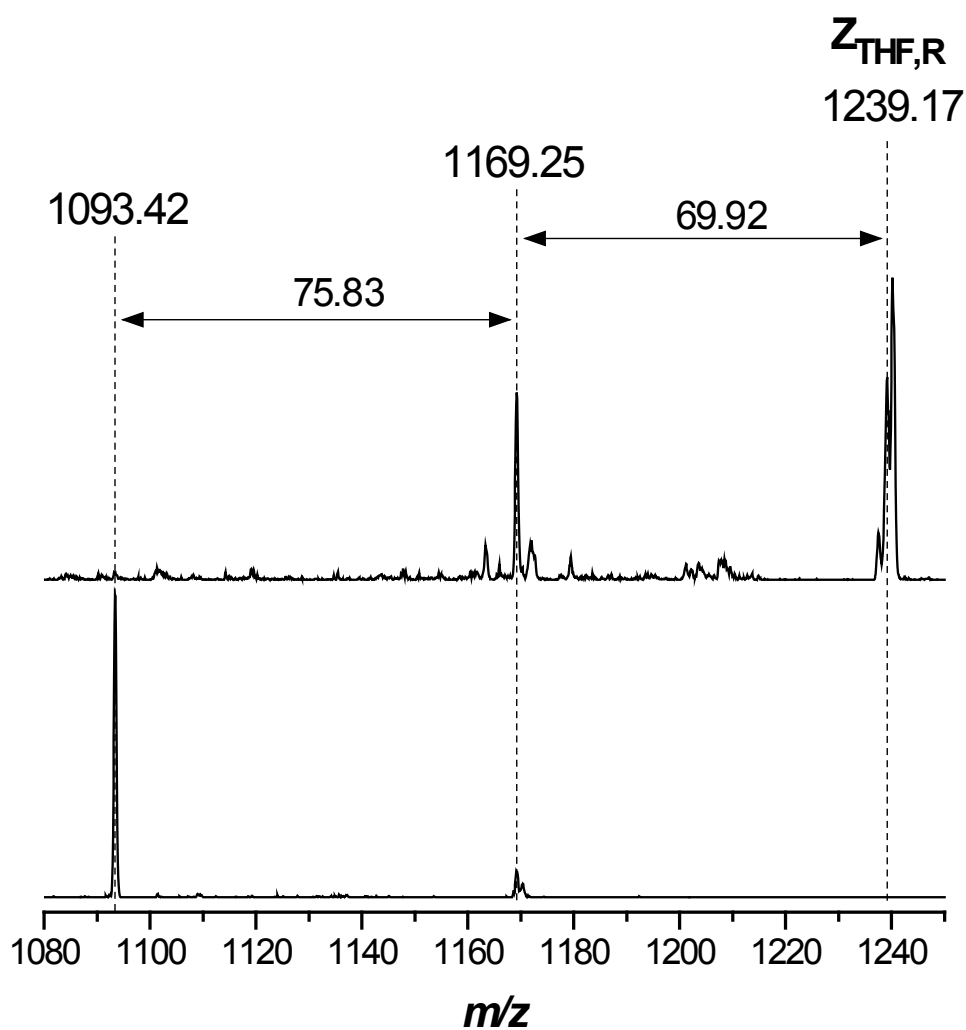


**Figure 3.14:** Collision induced dissociation electrospray ionization mass spectra (CID-ESI-MS) of the intermediate involved in the transformation of poly(methyl acrylate) with a trithiocarbonate moiety in the middle of the chain into hydroxyl functional pMA in the charge state  $z = 1$ .

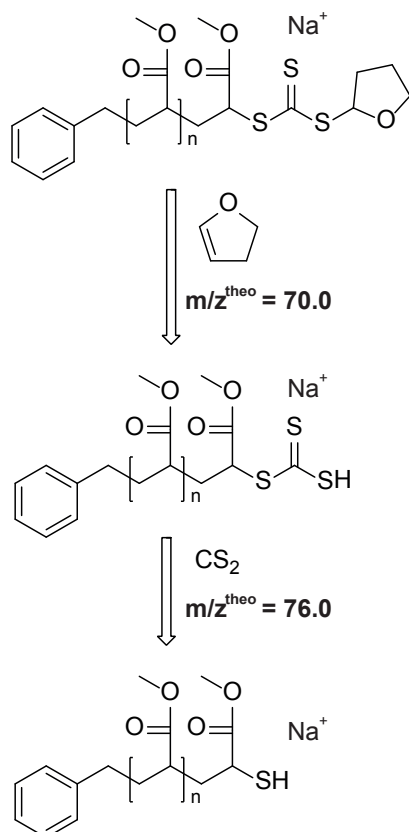


**Figure 3.15:** Dissociation pathway and theoretical masses of the neutral losses during the collision induced dissociation of the intermediate THF-trithiocarbonate carrying poly(methyl acrylate)  $Z_{\text{THFR}}$ . MS<sup>2</sup> of  $Z_{\text{THFR}}$  leads to loss of dihydrofuran ( $m/z^{\text{theo}} = 70.0$ ,  $m/z^{\text{meas}} = 69.9$ ), MS<sup>3</sup> of the product species leads to loss of a CS<sub>2</sub> molecule ( $m/z^{\text{theo}} = 76.0$ ,  $m/z^{\text{meas}} = 75.8$ ) confirming the structure of the intermediate.

In Figure 3.16 the  $^1\text{H}$  NMR spectra before the transformation reaction ( $t = 0$  min) of the symmetrical trithiocarbonate functional pMA and at full conversion ( $t = 55$  min) are depicted. Disappearance of peak (a) at 4.7 ppm, corresponding to the proton in geminal position to the trithioester sulfur indicates the complete replacement of the trithiocarbonate group.

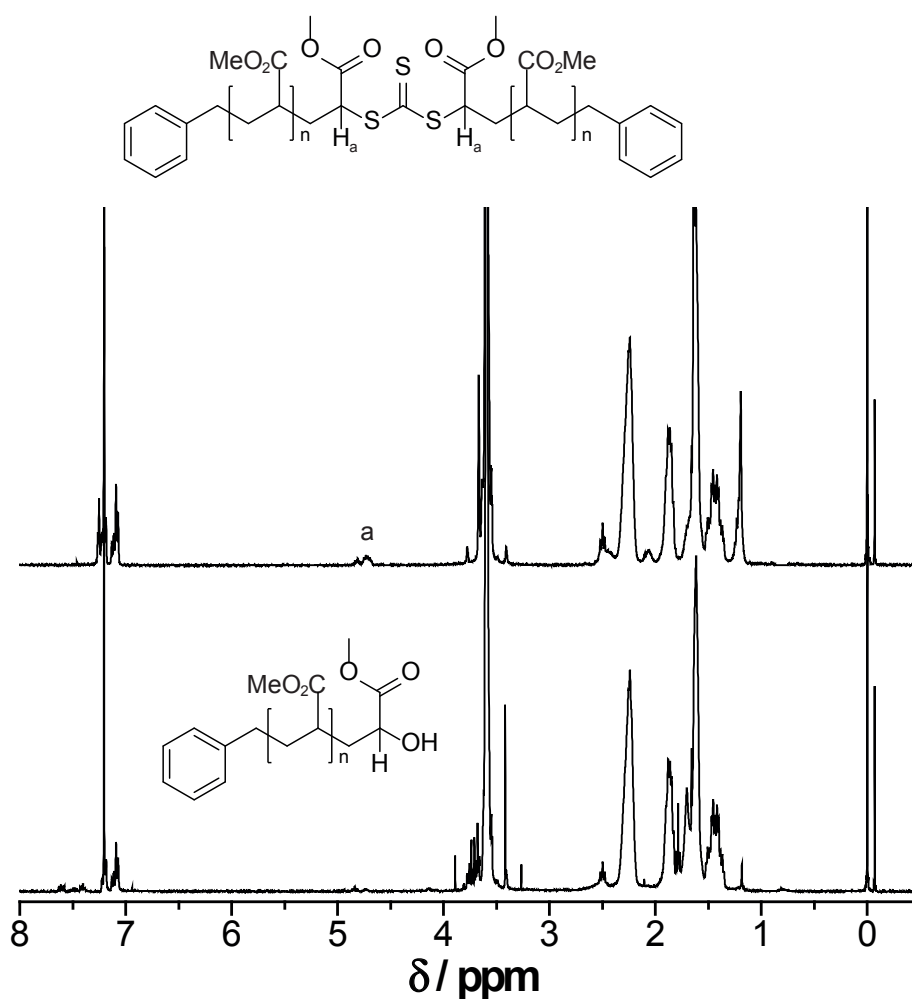


**Figure 3.16:** (Top)  $^1\text{H}$  NMR spectra of poly(methyl acrylate) with a trithiocarbonate moiety in the middle of the chain. (Bottom) Spectrum of the same polymer after 70 min reaction time at the end of the transformation reaction. Disappearance of peak (a) corresponding to the proton  $\text{H}_a$  in geminal position to the trithioester sulfur indicates complete conversion of the RAFT endgroup.

Figure 3.17 displays the SEC/ESI-MS spectra of symmetrical trithiocarbonate functional pBA before (top) and after conversion to the hydroxyl functional pBA (bottom). It can be seen that the conversion is nearly quantitative towards the hydroxyl functional  $\text{P}_R\text{OH}$  and only traces of hydrogen terminated  $\text{P}_R\text{H}$  are present in the spectrum. Table 3.11 displays the experimental  $m/z$  ratios, which are in very good agreement with the theoretical  $m/z$  ratios of the involved species.

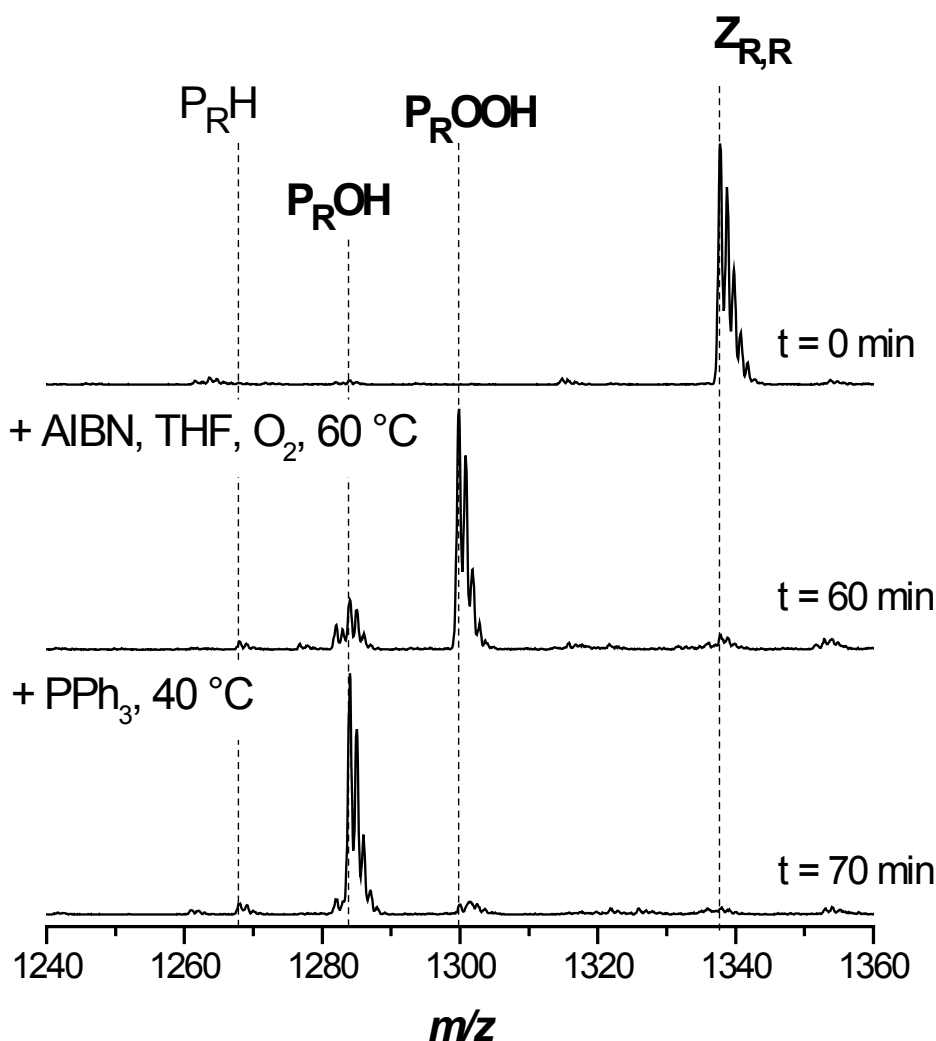


**Figure 3.17:** Electrospray ionization mass spectra of the transformation of poly(butyl acrylate) with a trithiocarbonate moiety in the middle of the chain into hydroxyl functional pBA in the charge state  $z = 1$ . The reagents AIBN/THF and  $\text{PPh}_3$  were added sequentially at  $t = 0$  and 60 min. Full conversion was reached after 70 min.

**Table 3.11:** Theoretical and measured  $m/z$  ratios of the main species involved in the conversion of pBA with a trithiocarbonate moiety in the middle of the chain into hydroxyl functional pBA.

Structure	$m/z^{\text{theo}}$	[M + Na] <sup>+</sup>	
		$m/z^{\text{exp}}$	$\Delta m/z$
Z <sub>R,R</sub>	1337.69	1337.75	0.06
P <sub>R</sub> OOH	1299.83	1299.80	0.03
P <sub>R</sub> OH	1283.80	1284.00	0.20
P <sub>R</sub> H	1267.81	1268.00	0.19

Figure 3.18 depicts the SEC/ESI-MS spectra of symmetrical trithiocarbonate functional *pi*BoA before (top) and after conversion to the hydroxyl functional *pi*BoA (bottom). One can conclude from Figure 3.18 that there is also an almost quantitative conversion towards the hydroxyl functional *pi*BoA. The symmetrical trithiocarbonate functionalized *pi*BoA after conversion has a slightly higher content of hydrogen terminated P<sub>R</sub>H than the pMA and pBA. This could be due to saturation of the macroradical P<sub>n</sub>• with a THF molecule. Table 3.12 displays the experimental  $m/z$  ratios, which are in good agreement with the theoretical  $m/z$  ratios of the involved species.

**Table 3.12:** Theoretical and measured  $m/z$  ratios of the main species involved in the conversion of *pi*BoA with a trithiocarbonate moiety in the middle of the chain into hydroxyl functional *pi*BoA.

Structure	$m/z^{\text{theo}}$	[M + Na] <sup>+</sup>	
		$m/z^{\text{exp}}$	$\Delta m/z$
Z <sub>R,R</sub>	1353.75	1353.75	0.00
P <sub>R</sub> OOH	1187.78	1187.75	0.03
P <sub>R</sub> OH	1171.78	1171.75	0.03
P <sub>R</sub> H	1363.93	1363.92	0.01

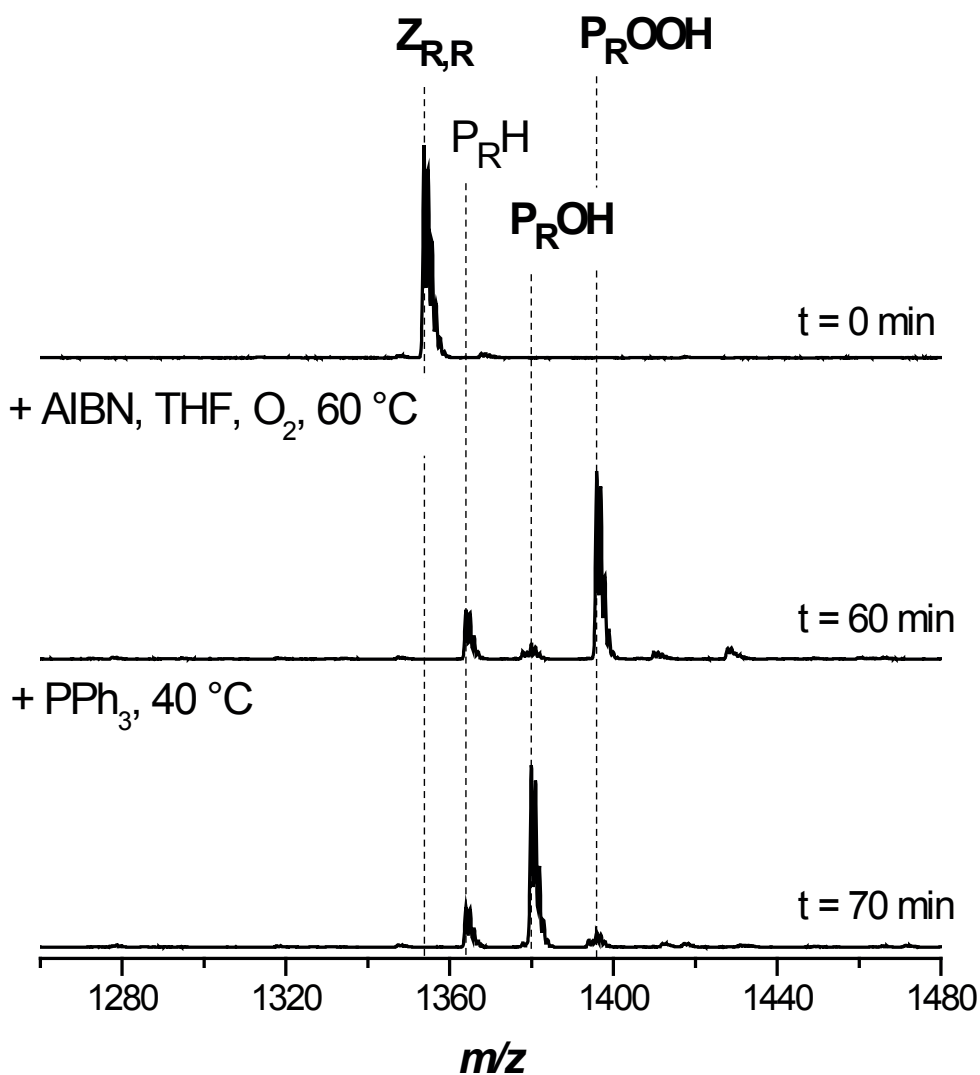


**Figure 3.18:** Electrospray ionization mass spectra of the transformation of poly(*isobornyl acrylate*) with a trithiocarbonate moiety in the middle of the chain into hydroxyl functional *piBoA* in the charge state  $z = 1$ . The reagents AIBN/THF and PPh<sub>3</sub> were added sequentially at  $t = 0$  and 60 min. Full conversion was reached after 70 min.

Water soluble polymers, such as poly(acrylic acid) pAA, are interesting due to their potential use in *e.g.*, the construction of nano-containers.<sup>234</sup> Thus, it seemed important to investigate the suitability of pAA precursor polymers such as ptBA for the conversion process, as ptBA can readily be transformed *via* hydrolysis into pAA under mild conditions. Concerning the symmetrical trithiocarbonate functional ptBA, it can be seen in Figure 3.19 that the conversion is almost quantitative and there is only a small amount of hydrogen terminated  $\mathbf{P}_R\mathbf{H}$  evolving during the reaction. Table 3.13 displays the experimental  $m/z$  ratios, which are in excellent agreement with the theoretical  $m/z$  ratios of the concerned species. The conversion process does not affect the *tert*-butyl group.

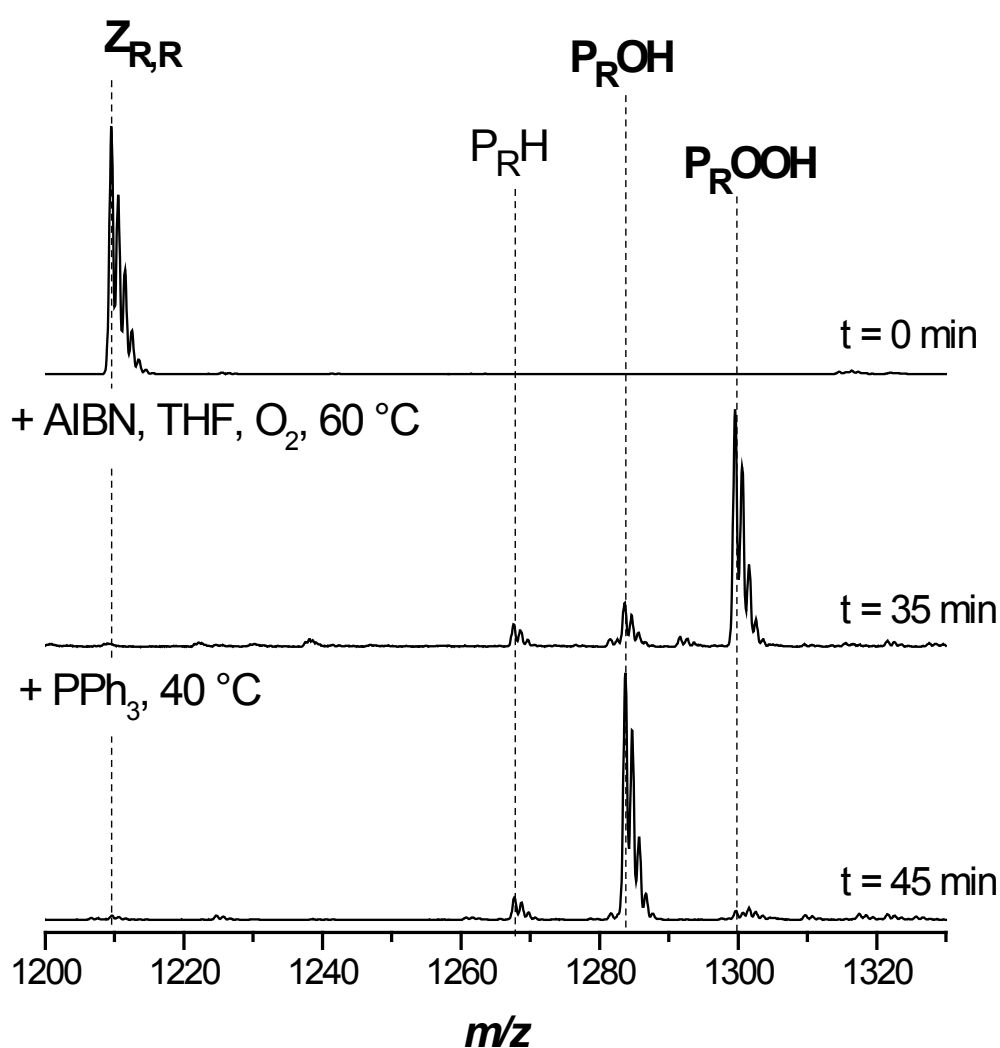


**Figure 3.19:** Electrospray ionization mass spectra of the transformation of poly(*tert*-butyl acrylate) with a trithiocarbonate moiety in the middle of the chain into hydroxyl functional ptBA in the charge state  $z = 1$ . The reagents AIBN/THF and PPh<sub>3</sub> were added sequentially at  $t = 0$  and 35 min. Full conversion was reached after 45 min.

**Table 3.13:** Theoretical and measured  $m/z$  ratios of the main species involved in the conversion of  $p\text{iBoA}$  with a trithiocarbonate moiety in the middle of the chain into hydroxyl functional  $p\text{iBoA}$ .

Structure	$m/z^{\text{theo}}$	$[\text{M} + \text{Na}]^+$	
		$m/z^{\text{exp}}$	$\Delta m/z$
$Z_{\text{R,R}}$	1209.60	1209.50	0.10
$P_{\text{R}}\text{OOH}$	1299.80	1299.67	0.13
$P_{\text{R}}\text{OH}$	1283.80	1283.75	0.05
$P_{\text{R}}\text{H}$	1267.81	1267.75	0.06

Poly(2-ethylhexyl acrylate) (p(2-EHA)) is an industrial important polymer for copolymer-based pressure-sensitive adhesives, coatings and finishes.<sup>235</sup> Therefore the symmetrical trithiocarbonate p(2-EHA) was investigated to consider the usability of the developed process. It can be depicted from Figure 3.20 that the conversion reaction did not proceed in a clean fashion which can be seen by the considerable amounts of  $P_{\text{R}}\text{H}$  visible in the spectrum, as well as two unidentified side products. Table 3.14 depicts the experimental  $m/z$  ratios, which are in excellent agreement with the theoretical  $m/z$  ratios of the concerned species.

**Table 3.14:** Theoretical and measured  $m/z$  ratios of the main species involved in the conversion of p(2-EHA) with a trithiocarbonate moiety in the middle of the chain into hydroxyl functional p(2-EHA).

Structure	$m/z^{\text{theo}}$	$[\text{M} + \text{Na}]^+$	
		$m/z^{\text{exp}}$	$\Delta m/z$
$Z_{\text{R,R}}$	1233.77	1233.85	0.12
$P_{\text{R}}\text{OOH}$	1251.94	1251.82	0.12
$P_{\text{R}}\text{OH}$	1235.95	1235.87	0.08
$P_{\text{R}}\text{H}$	1219.95	1219.72	0.23
$P_{\text{R}}\text{Z-THF}$	1213.76	1213.66	0.10

To enable the application of the hydroxyl functional polymer in further reaction steps the conversion procedure was carried out on a larger scale using close to ten times more material (500 mg) of the trithiocarbonate capped pMA. The polymer was isolated by precipitation and subsequently investigated by SEC/ESI-MS. It can be elucidated from Figure 3.21 that the conversion reaction is also almost quantitative towards the hydroxyl functional pMA, as shown before in Figure 3.13. It was observed that the only difference between performing the reaction on a small and larger scale was the longer reaction time (by a factor of approx. 1.5) required for the large scale process. The dissolved oxygen in the reaction mixture is depleted more rapidly than it is replaced by oxygen from

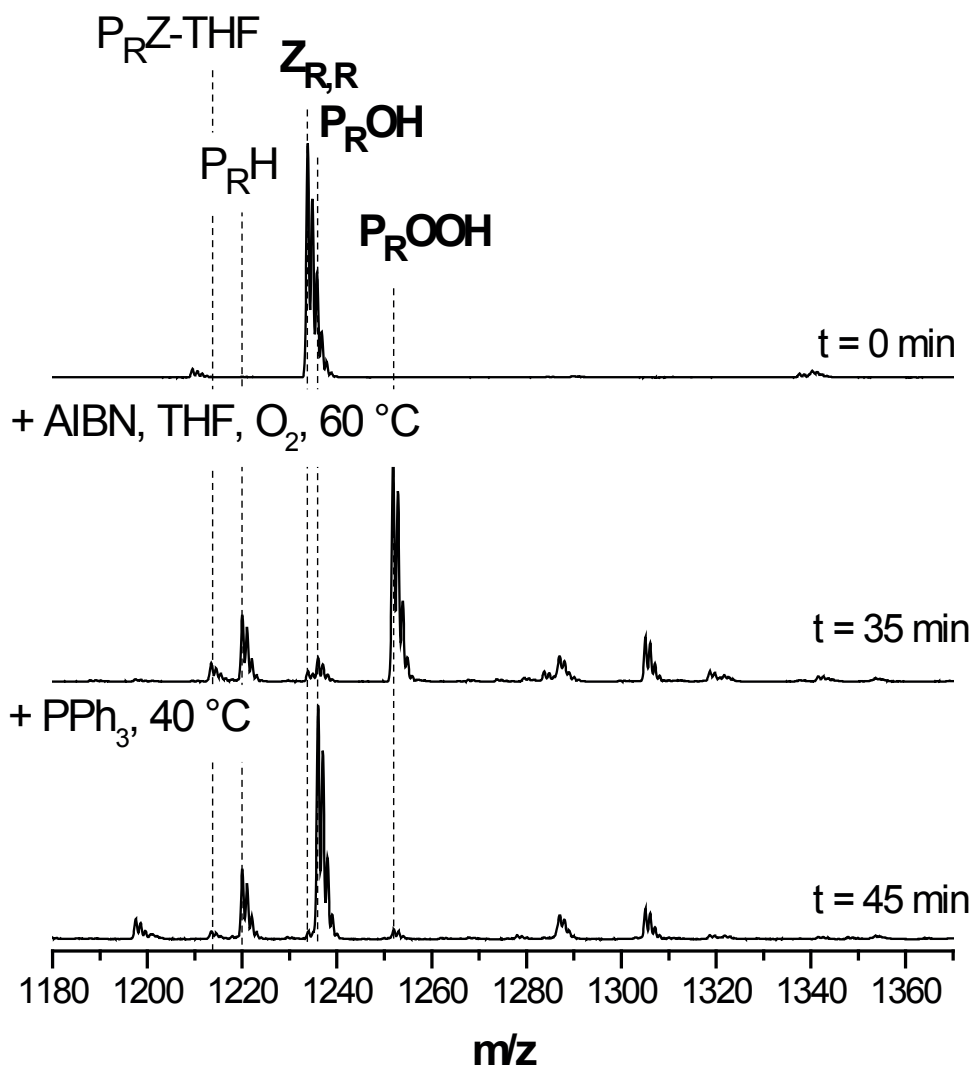


**Figure 3.20:** Electrospray ionization mass spectra of the transformation of p(2-EHA) with a trithiocarbonate moiety in the middle of the chain into hydroxyl functional p(2-EHA) in the charge state  $z = 1$ . The reagents AIBN/THF and  $PPh_3$  were added sequentially at  $t = 0$  and 35 min. Full conversion was reached after 45 min.

the atmosphere. The results additionally confirm the introduced method as a useful strategy for converting trithiocarbonate functional polymers into hydroxyl functional polymers.

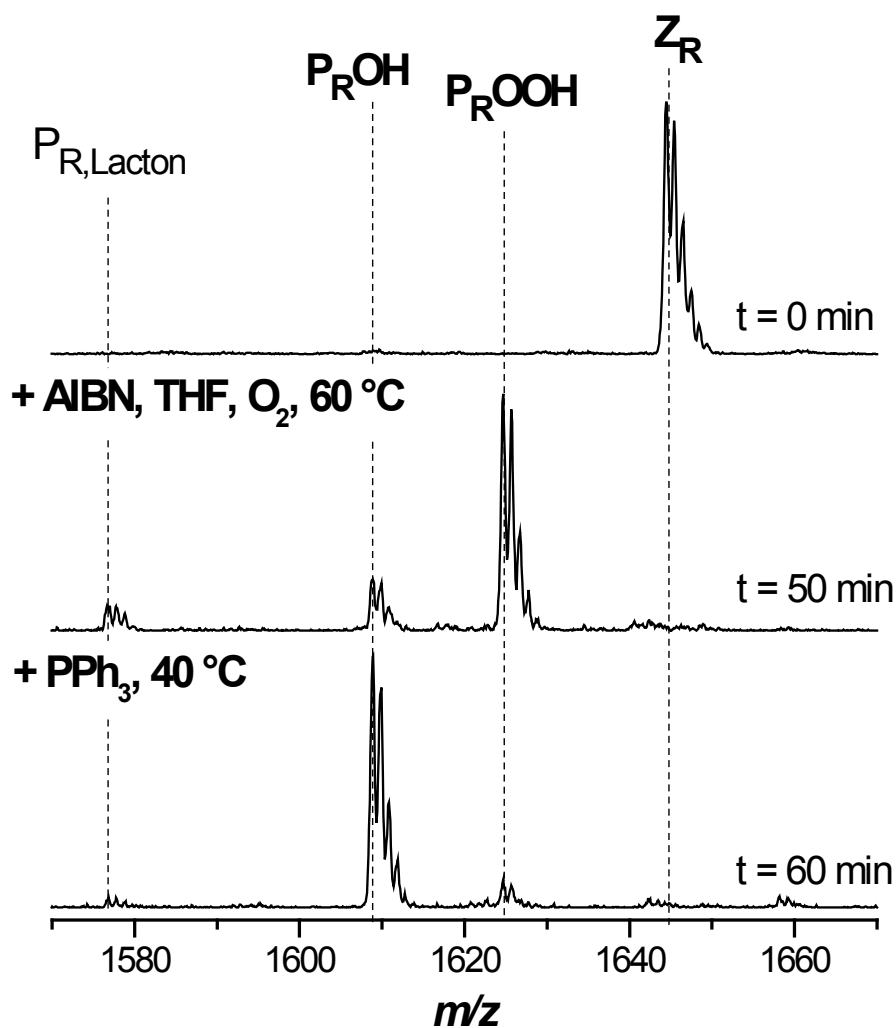


**Figure 3.21:** Electrospray ionization mass spectra of the preparative transformation of poly(methyl acrylate) with a trithiocarbonate moiety in the middle of the chain into hydroxyl functional pMA in the charge state  $z = 1$ . DBTC was used as RAFT agent. The reagents AIBN/THF and PPh<sub>3</sub> were added sequentially at  $t = 0$  and 90 min. Full conversion was reached after 100 min. The transformation was carried out with 500 mg pMA. The resulting polymer was precipitated in methanol.

### 3.3.5 Conclusions

It has been demonstrated that transformation reactions of trithiocarbonate functional acrylate polymers into hydroperoxide and hydroxyl functional polymers proceed with a very high efficiency. The amount of side products is negligible and the conversion is almost quantitative. A mechanism for the transformation is proposed which is supported by mass spectrometric evidence. A further advantage of symmetrical trithiocarbonates lies in the fact that they can be synthesized in one pot reactions and are mostly easily purified.<sup>46,210</sup> Additionally it has been demonstrated that the presented one-pot conversion method is applicable to a number of different monomer systems and can also be carried out on a larger scale. The transformation reaction can also be performed with dithiobenzoate and phenyldithioacetate capped acrylate polymers, however there is a small amount of side products evolving. The above described one-pot procedure is simple and versatile, as only low cost solvents and chemicals are utilized. Having access to a stable and versatile hydroxyl functional group allows for the first time the direct use of RAFT polymers in certain end-group conjugation and block-copolymer formation reactions: ring-opening polymerization (ROP) with ethylene oxide and lactones or, after tosylation, cationic ROP of oxazolines for the formation of well defined block co-polymers are imaginable and have indeed been carried out in our group by C. Schmid<sup>236</sup> in an ongoing Ph.D. thesis.



# 4

## Block Copolymer Architectures via UV-light Activation

### 4.1 Introduction

In the current chapter the results of the evaluation of two UV-light activated conjugation techniques toward their employment in synthetic polymer chemistry are presented. In order to investigate the coupling techniques, model reactions have been carried out where end-group functionalized polymers were reacted with small molecules as well as functionalized polymers with the aim to generate AA-type (block co)polymers and AB-type block copolymers. The first investigated coupling reaction was the nitrile imine-mediated 1,3-dipolar cycloaddition of tetrazole and ene coupling (NITEC) while the second method comprised a radical coupling technique. Before these methods will be explained in detail, important state of the art conjugation techniques are explained with an emphasis on reactions lacking of transition metals as catalysts.

As already noted before in the introduction to chapter 1, there is a growing demand for functional polymeric material due to 'high value added' applications in the fields of e.g., biomedicine and nanoscience. Complex macromolecular architectures - as we know today - would not have been possible without the substantial developments achieved in living/controlled radical polymerization techniques as well as highly orthogonal and

efficient conjugation techniques of the generated polymers.<sup>135–137</sup> Specifically, these two methodologies have given chemists the ability to control macromolecular properties with unprecedented precision. While controlled radical polymerization techniques (CRP) such as RAFT<sup>14</sup> or ATRP<sup>15,16</sup> have already led the way in producing well defined polymeric materials, the development of the *click*-type reactions brought a significant increase of creativity in designing and synthesizing polymeric materials.<sup>132,136,237</sup> Furthermore, in the context of polymer conjugations, *click*-type chemistry allows building of polymeric structures in combination with virtually any polymerization methodology. The chemists' perspective of polymers has changed from macromolecules being simple individual polymer chains to viewing the individual polymer species as building blocks for larger structures, such as star block copolymers, multi-block copolymers and e.g., their formation into micelles in solution as well as the formation of nano-structured surfaces.<sup>17,137,143,238,239</sup> It should be mentioned that the term *click* has been used inflationary over the last decade for reactions which do not meet the high standards proposed by Sharpless.<sup>240</sup> The criteria for *click*-type reactions in polymer chemistry have been adapted and recently extended from the original criteria proposed by Sharpless.<sup>132</sup> *Click*-criteria extended to polymer conjugations include the employment of equimolar amounts of starting materials, fast timescales and large-scale purification techniques.<sup>240</sup> In the forthcoming section important efficient coupling techniques - some of which adhere to the *click*-criteria - with possible applications in polymer chemistry are briefly presented. The emphasis of the coupling reactions is on transition metal-free techniques, showing the wide variety and versatility of such conjugation reactions.

## 4.2 Efficient Tools for Macromolecular Design

### 4.2.1 Azide/Alkyne Cycloadditions

1,3-dipolar reactions employing azides represent a long known reaction class.<sup>241</sup> However, it was not until 1963, when this type of reaction was 'rediscovered' by Huisgen.<sup>242</sup> The 1,3-dipolar cycloadditions of azides and alkynes are carried out at elevated temperatures which makes the reaction for temperature sensitive materials less attractive. Although not a transition metal-free technique, the copper catalyzed reaction of the 1,3-dipolar cycloaddition of azides and alkynes is presented due to its high impact on polymer science. In 2002 Sharpless and co-workers<sup>243</sup> introduced a modification of 1,3-dipolar cycloadditions employing a Cu(I) catalyst. By adding copper as a catalyst in the cycloaddition reaction, it is now possible to perform the pericyclic reaction between an azide and an alkyne at ambient temperature. The copper catalyzed modification of the azide/alkyne Huisgen cycloaddition is without doubt one of the most accepted and applied coupling reactions employed in polymer chemistry.<sup>135</sup> The overall reaction

scheme is depicted in Figure 4.1. Advantages of the copper mediated cycloaddition include its versatility and orthogonality as well as the wide variety of solvents in which the reaction can be performed (e.g., water, alcohols).<sup>244</sup> A detailed overview on the application of azide/alkyne chemistry in the context of polymer chemistry can be found in the reviews by Binder and Sachsenhofer,<sup>135,136</sup> Inglis and Barner-Kowollik<sup>137</sup> as well as Hawker et.al.<sup>245</sup>

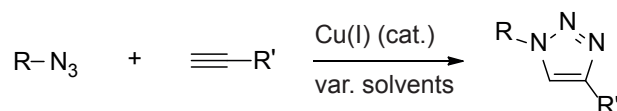


**Figure 4.1:** Overall reaction scheme of the copper mediated azide alkyne 1,3-cycloaddition.

## 4.2.2 Cycloadditions with Strained or Activated Alkynes

As mentioned in section 4.2.1, azides and alkynes do not react in a 1,3-cycloaddition at ambient temperature unless a transition metal catalyst is present. Sometimes certain applications forbid the use of such catalysts. Activation of the alkyne can help to overcome the employment of a transition metal catalyst, which can be achieved by introducing ring-strain to an alkyne, the attachment of an electron-withdrawing group (EWG) or the combination of both techniques. Wittig and Krebs<sup>246</sup> were the first to show the ring-strained promoted 1,3-cycloaddition of cyclooctynes and azides. Further research was conducted by Bertozzi and co-workers who applied the technique in living cells.<sup>247</sup> In general, reaction rates were much slower and also a lack regioselectivity could be observed compared to the copper catalyzed azide alkyne 1,3-cycloaddition. Although lacking of regioselectivity, there are areas in chemistry where strict regioselectivity is not crucial, especially in macromolecular chemistry. Further improvement in reactivity has been achieved by the subsequent introduction of electron withdrawing groups, such as propargylic fluorine groups, to the ring-strained cyclooctyne with the best result being a 20-fold faster reaction rate than without the electron withdrawing group.<sup>248</sup> The biocompatibility of the fluorinated cyclooctynes are proven, yet a drawback in employing these cyclooctynes in applications is the low yield during their synthesis. Although the synthesis of fluorinated cyclooctynes is still investigated for improvement, to date it remains at least a 6-step process with a yield of only 36%.<sup>249</sup> The overall reaction scheme of the process is depicted in Figure 4.2. Due to the before mentioned drawbacks, no application in synthetic polymer chemistry, such as synthesizing block copolymers, employing these activated alkynes has been described so far. For a detailed review of cycloadditions with strained or activated alkynes the reader is referred to the review by Inglis and Barner-Kowollik.<sup>137</sup>



**Figure 4.2:** Overall reaction scheme of 1,3-cycloaddition incorporating ring-strained and fluorinated alkynes.

### 4.2.3 Thiol-ene/Thiol-yne Conjugations

The general concept of the reaction between thiols and alkenes/alkynes is well known since the 1900s.<sup>250</sup> Within the last decade, two main approaches are specifically under investigation, i.e., the catalyzed ionic reaction of thiols and electron deficient alkenes (Michael-type additions)<sup>251</sup> and the radical reaction pathway of electron rich/electron poor alkenes. The general mechanism is depicted in Figure 4.3. Regardless whether the Michael or radical reaction is utilized for thiol-ene chemistry, both types can exhibit - under certain circumstances - some attributes of *click*-type reactions, such as modularity, high yield and chemoselectivity. The most prominent thiols employed in thiol-ene reactions are alkyl thiols, thiophenols, thiol propionates and thiol glycolates. The highest yields of thiol-ene conjugations are achieved, if the Michael-type addition is applied. For example, Dove and colleagues<sup>252</sup> showed block copolymer conjugation as well as 3-arm star formation of small molecule thiol linkers and maleimide functionalized polymers. Although the reaction was successful, the reaction time can be as long as one week, disqualifying the reaction as a *click*-type reaction.<sup>240</sup> An interesting alternative route is the combination of polymers prepared *via* RAFT mediated processes and Michael type thiol-ene chemistry. Lowe, Hoyle and co-workers have established a one pot procedure employing dithioester capped polymers, alkene and a hexylamine/dimethylphenylphosphine with consecutive aminolysis and Michael addition to finally synthesize 3-arm polymers at ambient temperature.<sup>253,254</sup> The noted examples and the amount of reviews about thiol-ene reactions show the importance of the reaction, which sometimes even adheres to the *click*-criteria. For an in-depth coverage, the reader is referred to the excellent review by Hoyle and Bowman<sup>255</sup> as well as the broader scope review by Summerlin and Vogt.<sup>239</sup> Although the radical thiol-ene reactions are very efficient when employing small molecules (including their grafting on surfaces), the formation of block copolymers or higher order macromolecular architectures, such as stars, has limited scope due to side reactions. In a recent work by Koo *et al.*<sup>256</sup> the formation of star polymers employing the radical thiol-ene reaction as a polymer-polymer conjugation method was evaluated. If an excess of a small molecule is used in polymer grafting reactions, the process performs well due to simple removal of small molecule side products. In contrast, the polymer-polymer conjugation largely fails if the starting materials are employed in equimolar ratios. Separating polymer-

polymer-conjugates from unreacted starting polymer is almost not possible.<sup>256</sup> Due to employment of an excess of small molecule thiol, the radical type thiol-ene reaction does not fit in the scope of *click*-type reactions for polymers.<sup>240</sup>

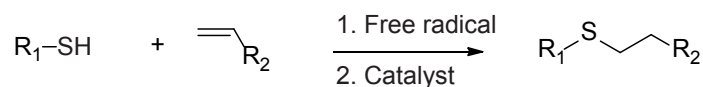


**Figure 4.3:** Overall reaction scheme of the thiol-ene coupling by: 1. Free radical reaction pathway and 2. Michael addition reactions.

Thiols can not only react with alkenes, they can also be employed in conjugation reactions with alkynes. The so-called thiol-yne reaction follows *via* the same general mechanism as the radical-based mechanism of the thiol-ene reaction. The general reaction scheme is a two step addition of thiols to the alkyne triple bond which is depicted in Figure 4.4. Chan *et al.*<sup>257</sup> showed the combined coupling of small molecules resulting in multi functional thioethers. Perrier and coworkers demonstrated the step-growth formation of high molecular weight materials, employing molecules functionalized with a thiol end-group and an alkyne end-group.<sup>258</sup> The lack of orthogonality of the thiol-yne reaction toward the radical thiol-ene reaction is one disadvantage of the thiol-yne reaction. Therefore it has to be kept in mind, when combining a thiol-yne reaction with a Michael type thiol-ene reaction, to perform the later before the thiol-yne reaction. Otherwise the thiol-ene reaction and the thiol-yne reaction would occur at the same time.

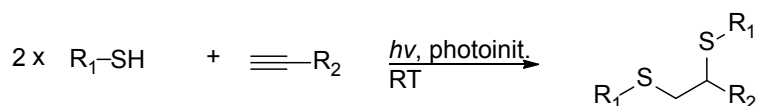


**Figure 4.4:** Overall reaction scheme of the radical induced thiol-yne coupling.

#### 4.2.4 The Chemistry of Thiol-Isocyanate Coupling

A further interesting reaction involving thiols is their base catalyzed reaction with isocyanates. The reaction was utilized by Klemm and Stöckl<sup>259</sup> who synthesized thiol- and isocyanate-terminated thiocarbamate prepolymers. The reaction could be tuned to either thiol or isocyanate end-groups depending on the initial ratio of both moieties. Figure 4.5 depicts the scheme of the reaction pathway, showing the two main products of the poly(thiourethane)s prepolymer synthesis. The reaction itself is very fast and proceeds within one hour at ambient temperature following a the step-growth polymerization but exhibiting a significant disadvantage. Although being a fast and efficient reaction, the high reactivity of the isocyanate group toward nucleophiles and even itself - and therefore the lack of orthogonality - is a severe drawback for applications in synthetic polymer architecture design.

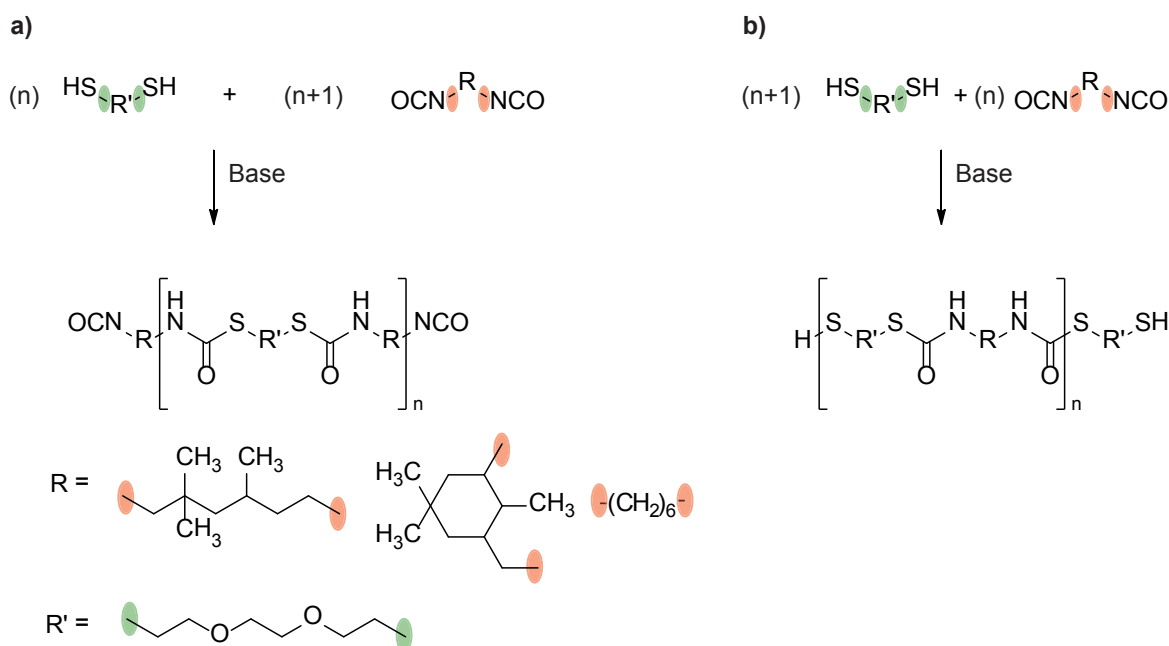


**Figure 4.5:** Step-growth polymerization of dithiols with diisocyanates using a) an excess of the diisocyanate and b) an excess of the dithiol yielding poly(thiourethane)s.

#### 4.2.5 The Chemistry of Thio-Bromo Conjugation

The nucleophilic thio-bromo reaction is a promising new method for polymer conjugation. A thiol reacts in a base (e.g., triethyl amine) catalyzed reaction with  $\alpha$ -bromoesters yielding thioesters (see the general reaction scheme in Figure 4.6). Rosen and coworkers showed an efficient pathway synthesizing dendrimers at ambient temperature by employing the thiol-bromo reaction.<sup>260</sup> Further, the reaction has been utilized and extended by Davis and Lowe. They demonstrated a combination of RAFT mediated polymerization with a thio-bromo conjugation. Initially a RAFT polymer bearing two  $\alpha$ -bromoesters at the R-group was synthesized. Subsequently the dithioester was transformed into a thiol end-group. The following thio-bromo conjugation of the  $\alpha,\omega$ -functionalized polymer was conducted at ambient temperature resulting in well defined highly branched polymers. With its high efficiency, the thio-bromo reaction has the potential to be a versatile addition to the already established *click*-type reactions.

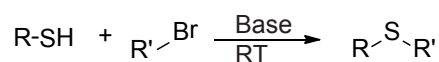


**Figure 4.6:** General reaction scheme of the thio-bromo conjugation of thiols with bromide functionalized molecules.

### 4.2.6 Inverse Electron-Demand Diels-Alder Cycloaddition

Despite the inherent advantages of (reversible) Diels-Alder cycloadditions, certain applications require irreversible conjugations. An efficient way of achieving this aim is *via* the utilization of the inverse electron-demand Diels-Alder (IVED-DA) cycloaddition where an electron-deficient tetrazine derivative and various alkenes are conjugated.<sup>137</sup> The transformation reaction is initiated without catalyst starting a [4+2] cycloaddition with the subsequent release of nitrogen through a retro-[4+2] cycloaddition. *Trans*-cyclooctenes as well as maleimide capped molecules are to date the most efficient alkenes which can be employed in such IVED-DA cycloadditions.<sup>261</sup> Nitrogen as only non toxic side product, fast reaction rates and the wide range of available solvents in which the reaction can be performed highlight the advantages of the IVED-DA cycloaddition. The reaction pathway is depicted in Figure 4.7. It has to be mentioned that although the reaction rate is high, they are greatly influenced by the employed solvent. Even though the IVED-DA cycloaddition is not regioselective, it is a very fast and mild conjugation technique, thanks to performing the reaction at ambient temperatures. To date the IVED-DA cycloaddition has only been applied in a *macromolecular sense* by Fox and colleagues during the modification of proteins. Apart from that IVED-DA cycloadditions did not have not a great impact on synthetic macromolecular chemistry - such as the copper catalyzed azide alkyne cycloaddition - which is probably due to the limited availability of tetrazines.

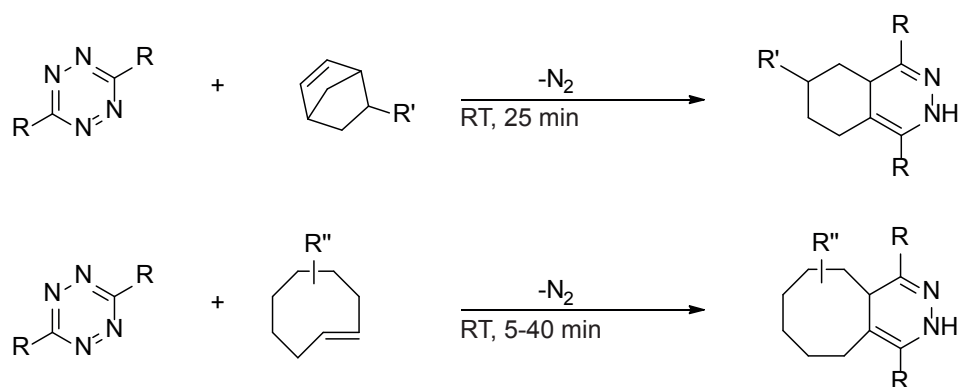


**Figure 4.7:** General reaction scheme of the inverse electron-demand Diels-Alder (IVED-DA) cycloaddition between alkenes and tetrazines.

### 4.2.7 Nitrile Oxides in Cycloadditions

The cycloaddition of nitrile oxides and alkynes or norbornenes forming isoxazoles or isoxazolines, respectively, is a versatile coupling reaction with no need for a catalyst. The nitrile oxide is generated *in situ* from an oxime precursor using a mixture for a dipole forming agent as well as a weak base. The overall reaction scheme is depicted in

Figure 4.8. The mild and efficient reaction has been applied in the modification of DNA as shown by Carrel and colleagues.<sup>262</sup> The nitrile oxide cycloaddition is also applied in synthetic polymer chemistry by introducing functionalities at the polymer end-group as demonstrated by Lutz and coworkers,<sup>263</sup> as well as modifications on the polymer backbone as shown by Meyer and colleagues.<sup>264</sup> In terms of macromolecular conjugation of block copolymers, the method has not proven its versatility, especially because the reaction appears to fail the equimolarity requirement combined with the lack of orthogonality of the nitrile oxide toward nucleophiles. For a deeper insight the reader is referred to the recent review by Qin and colleagues.<sup>265</sup>

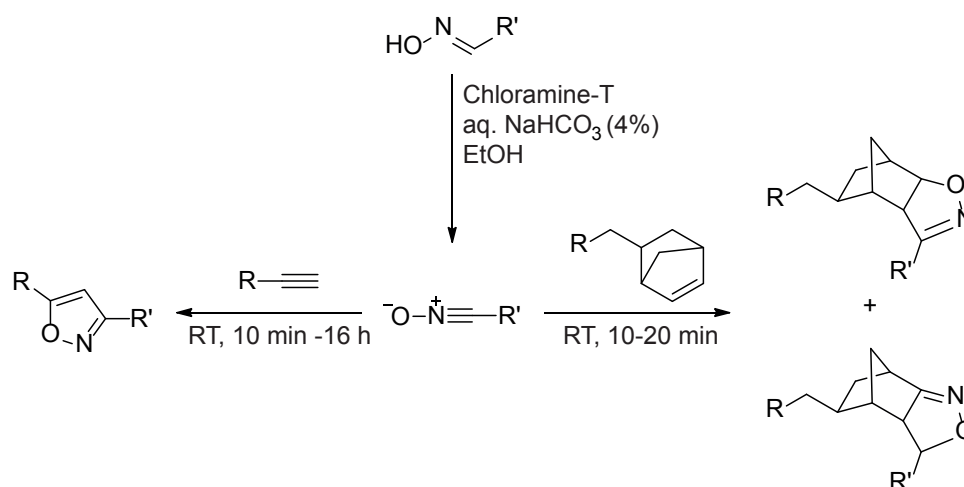
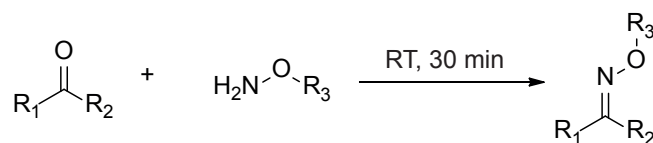


Figure 4.8: General pathway of the nitrile oxide cycloaddition.

#### 4.2.8 Coupling *via* Oxime Formation

A further versatile conjugation reaction is the catalyst-free oxime formation of aldehydes/ketones with aminoxy functionalities at ambient temperature as shown in Figure 4.9. The reaction has - so far - not found a broad range of applications in macromolecular architecture design. Nevertheless, there are two excellent examples making use of oxime conjugation. The first one has been reported by Maynard and coworkers.<sup>266</sup> After an ATRP polymerization bearing an aminoxy end-group, they coupled the bromine-terminal polymer with *N*-levinyl lysine employing the oxime reaction in 30 minutes reaction time at ambient temperatures. The second example describes the coupling of a propionaldehyde-derivative of a poly(ethylene glycol) monomethyl ether with an amino functionalized protein.<sup>267</sup> The oxime reaction has to be further investigated for possible applications in macromolecular conjugations, as the oxime linkage is prone to cascade reactions with nucleophiles or rearrangements (Beckmann-rearrangement<sup>268</sup>) which could potentially reverse the conjugation.



**Figure 4.9:** Oxime formation employing amino oxides and aldehydes/ketones.

### 4.2.9 Atom Transfer Nitroxide Radical Coupling (AT-NRC)

The atom transfer nitroxide radical (AT-NRC)-coupling reaction combines the advantages of ATRP and nitroxide chemistry. The coupling reaction involves the formation of a carbon-centered radical with  $\text{Cu}^{\text{I}}\text{Br}$  and the trapping of the radical with a persistent nitroxide radical at close to diffusion-controlled rates. The general reaction route is shown in Figure 4.10.

Not only the fast kinetics, but also its reversibility make the AT-NRC reaction attractive for several applications. The nitroxide can readily be removed by heating the nitroxide capped radical at elevated temperatures (approx. 100 °C when TEMPO-derivatives are employed).<sup>269–271</sup> The method has been employed in synthesizing degradable and reversibly coupled linear multiblock copolymers, block and graft copolymers in the presence of a 10-fold molar excess of copper species per halide end-group.<sup>272</sup> The process has been modified by Monteiro and colleagues in order to improve its efficiency and combined with a classical copper catalyzed azide alkyne conjugation.<sup>273</sup>

### 4.2.10 UV-Light activated Tetrazole-Ene Coupling

Recently, a new conjugation method for selective functionalization of proteins was demonstrated by Song *et al.*<sup>274</sup> The nitrile imine-mediated 1,3-dipolar cycloaddition of tetrazoles and alkenes (NITEC) is initiated by UV-light irradiation of a tetrazole-containing compound. Upon exposure to UV-light irradiation, nitrogen is released from the molecule and a reactive nitrile imine moiety is formed *in situ* (see Figure 4.11). Nitrile imines have been shown to readily undergo reactions with various electron-deficient and unactivated terminal alkenes to form a stable pyrazoline-based covalent linkage.<sup>275</sup> The advantage of this method over other more established ligation reactions is the absence of metal catalyst, the fast reaction time and its bio-orthogonality. For instance, it was possible to modify a genetically engineered protein in *E. coli* with a poly(ethylene glycol) tetrazole derivative.<sup>276</sup> The work already conducted in the field of NITEC reactions seems to have potential for further applications in the field of macromolecular conjugations.

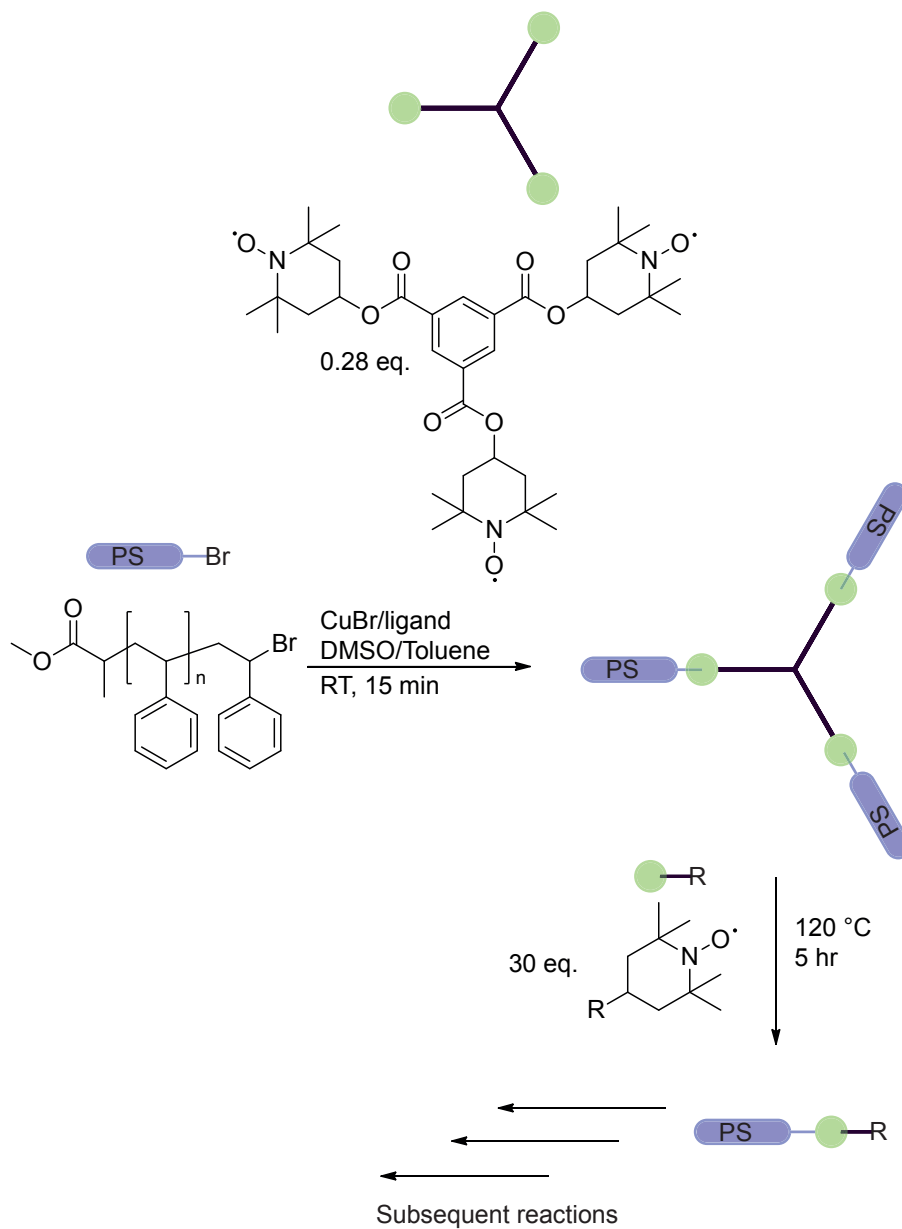


**Figure 4.10:** Employing the atom transfer nitroxide radical (AT-NRC) - coupling technique as a macromolecular conjugation method.

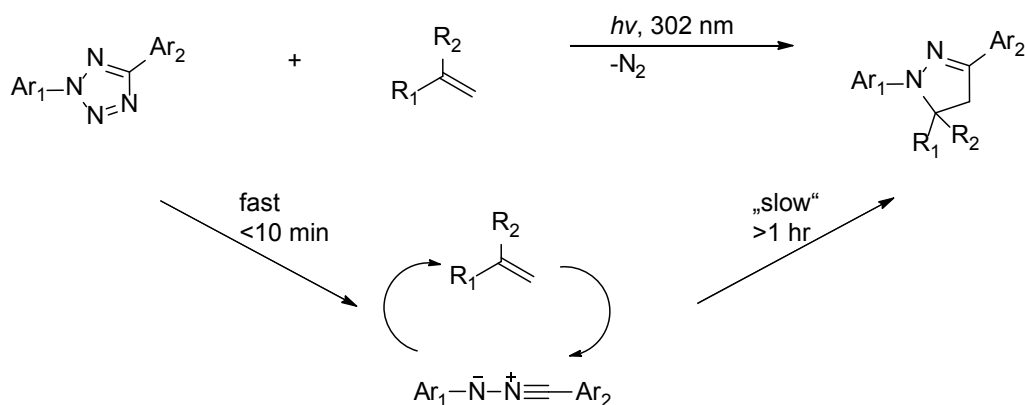


**Figure 4.11:** Schematic representation of the UV-induced formation of the nitrile imine from a tetrazole and its subsequent 1,3-dipolar cycloaddition with dipolarophiles.

As explained in the beginning of the current chapter, the following work shows evaluations of two ligation techniques employed in synthetic macromolecular architecture design. The first method which is described, is the NITEC approach, while the second approach is the combination of radical capturing nitroxide chemistry combined with photoinitiation. The outstanding characteristic of both reactions is the use of triggering the reaction with light. During the evaluation process, the ligation techniques were investigated with regard to their efficiency by employing test systems. These test systems consisted of well defined polymers with high end-group fidelities which were conjugated to small molecules. Studies of these test systems are explained in detail in the following sections. Furthermore, the test systems are extended toward polymer-polymer conjugation of telechelic polymeric starting material. The final aim of the work was to extend the conjugation techniques toward the possible decoration of bioactive surfaces, such as cellulose. The light activated conjugations opens the pathway for functionalization of surfaces with spatial resolution and hence shows the great potential of the presented ligation reactions.

## 4.3 Experimental Part

### 4.3.1 The Nitrile Imine-Mediated 1,3-Dipolar Cycloaddition of Tetrazole and Ene Coupling (NITEC) Approach

#### Tetrazole functionalized PEG 1

The synthesis of the tetrazole functionalized PEG was carried out *via* a DCC esterification of poly(ethylene glycol) methyl ether (PEG). The success of the reaction was confirmed by ESI-MS and the spectrum is shown in Figure 4.13. There is only a negligible amount of unreacted PEG remaining. The structure of **1** and the unreacted PEG **1a** is

depicted in Figure 4.12. Table 4.1 depicts the comparison of the theoretical and experimental  $m/z$  values of the tetrazole functionalized PEG, which are in excellent agreement.

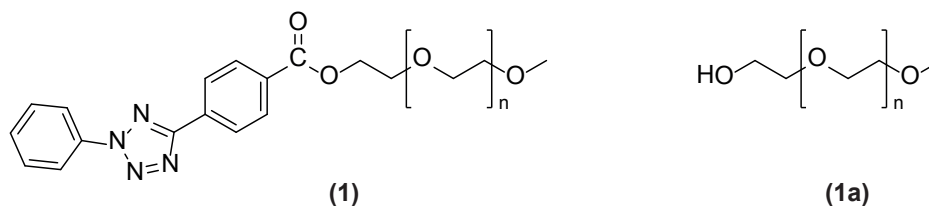


**Figure 4.12:** Structure of tetrazole functionalized PEG 1.

**Table 4.1:** Theoretical and measured  $m/z$  ratios of the tetrazole functionalized PEG 1 on the example of the species appearing in one repeat unit. It should be noted that the agreement between theoretical and experimental  $m/z$  ratios is equally satisfactory in other repeat units.

Structure	$[M + Na]^+$		
	$m/z^{\text{theo}}$	$m/z^{\text{exp}}$	$\Delta m/z$
<b>1</b>	1711.92	1711.77	0.15
<b>1a</b>	1728.01	1727.88	0.13

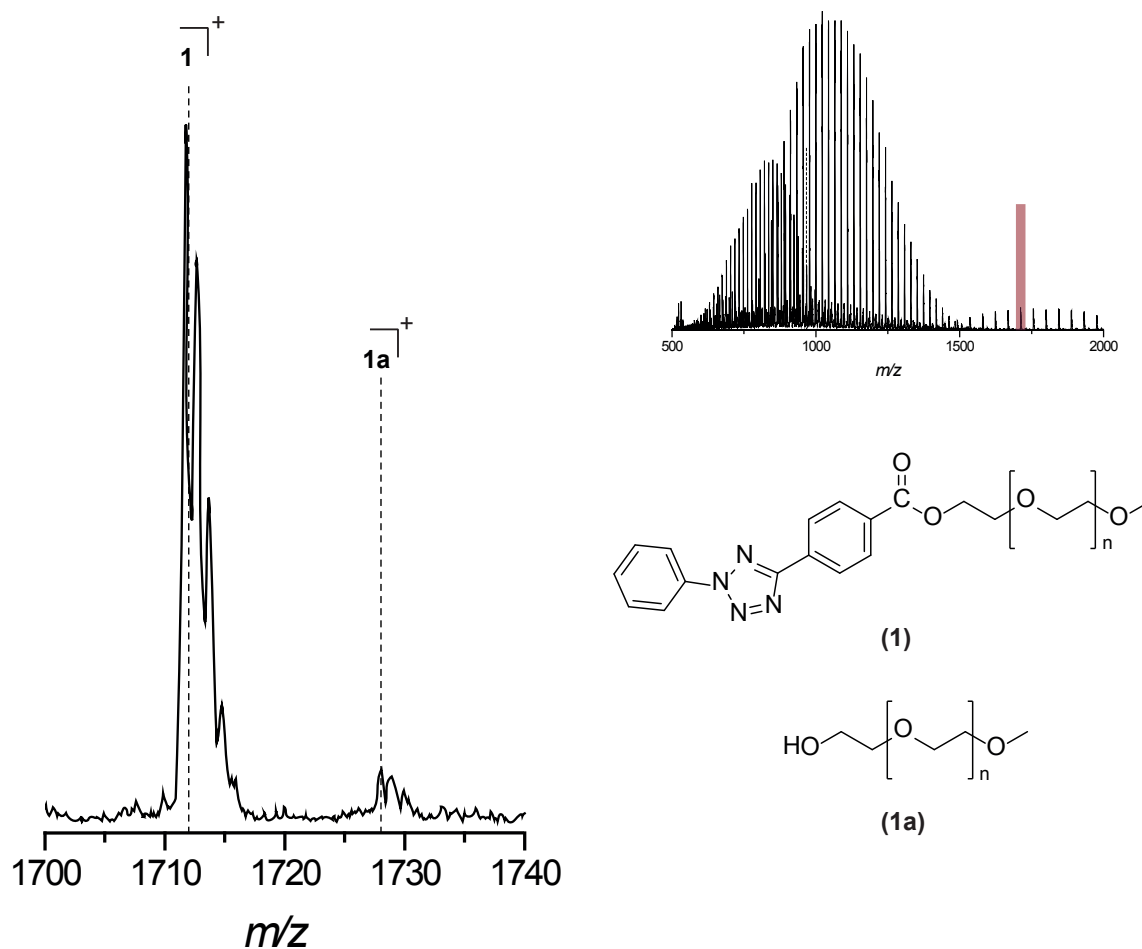


**Figure 4.13:** Electrospray ionization mass spectra of tetrazole functionalized PEG **1** in the charge state  $z = 1$  on the example of the species appearing in one repeat unit. It should be noted that the agreement between theoretical and experimental  $m/z$  ratios is equally satisfactory in other repeat units. The inset shows the overview of the spectrum.

## Maleimide functionalized PEG 2

The synthesis of the maleimide functionalized PEG was carried out according to Dag *et al.*<sup>277</sup>. The success of the reaction was confirmed by ESI-MS. The spectrum is shown in Figure 4.15 and depicts the product as well as a negligible amount of unidentified side product. The structure of **2** is depicted in Figure 4.14. Table 4.2 depicts the comparison of the theoretical and experimental  $m/z$  values of the tetrazole functionalized PEG.

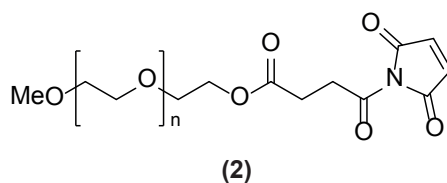


**Figure 4.14:** Structure of maleimide functionalized PEG **2**.

**Table 4.2:** Theoretical and measured  $m/z$  ratio of the maleimide functionalized PEG **2** on the example of the species appearing in one repeat unit. It should be noted that the agreement between theoretical and experimental  $m/z$  ratios is equally satisfactory in other repeat units.

Structure	$[M + Na]^+$		
	$m/z^{\text{theo}}$	$m/z^{\text{exp}}$	$\Delta m/z$
<b>2</b>	1730.93	1730.92	0.01

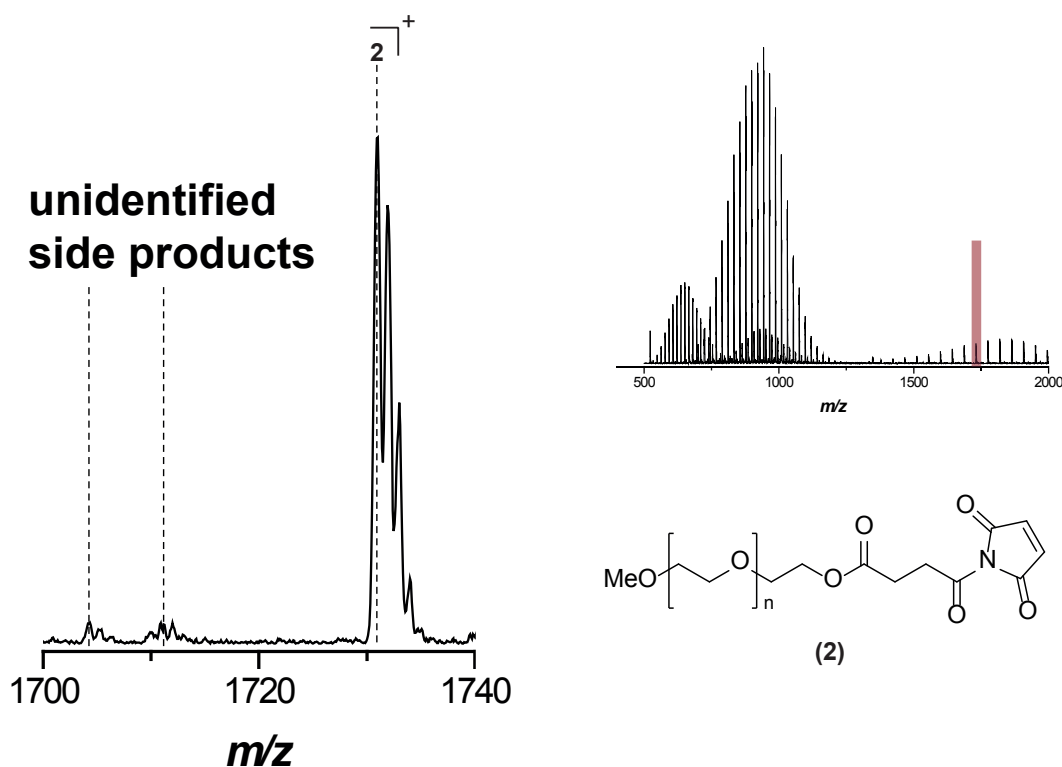


**Figure 4.15:** Electrospray ionization mass spectra of maleimide functionalized PEG **2** in the charge state  $z = 1$  on the example of the species appearing in one repeat unit. It should be noted that the agreement between theoretical and experimental  $m/z$  ratios is equally satisfactory in other repeat units. The inset shows the overview of the spectrum.

### Maleimide-pMMA **3**

The synthesis was carried out according to Mantovani *et al.*<sup>213</sup> MMA, Fur-Mal-ATRP,<sup>213</sup> CuBr, CuBr<sub>2</sub>, and 2,2'-bipyridine were added to a round-bottom flask in the ratio 100/1/0.105/0.0125/0.25. Acetone was subsequently added such that the resulting mixture contained 50 vol.-% acetone. The reaction mixture was purged with nitrogen for 30 min to remove residual oxygen. The mixture was sealed under nitrogen and placed in a thermostated oil bath set to 50 °C. After 2.5 h, the polymerization was stopped by cooling the mixture in an ice bath and exposure to oxygen. The mixture was subsequently passed through a short column of neutral alumina to remove the copper catalyst. Furan-protected maleimide-functionalized pMMA was isolated by 2-fold precipitation in cold *n*-hexane and after filtration the product was dried by employing reduced pressure. The crude product was redissolved in toluene followed by refluxing for 6 h. The polymer was precipitated in cold *n*-hexane and after filtration the maleimide functionalized pMMA **3** was dried employing reduced pressure (SEC:  $M_n = 2200 \text{ g mol}^{-1}$ ,  $PDI = 1.15$ ). Due to a loss of methylbromide and lactonization there appears a second product peak in the spectrum, which is shown in Figure 4.17. The two corresponding structures are

shown in Figure 4.16. Excellent agreement of the theoretical  $m/z$  and the measured  $m/z$  is observed. There is no influence of the applied reactivity of the two maleimide functionalized polymers as the lactonized end-group is stable under the reaction conditions. Table 4.3 shows the comparison of the theoretical and the experimental  $m/z$  values of the two maleimide functionalized pMMA products **3** and **3a**.

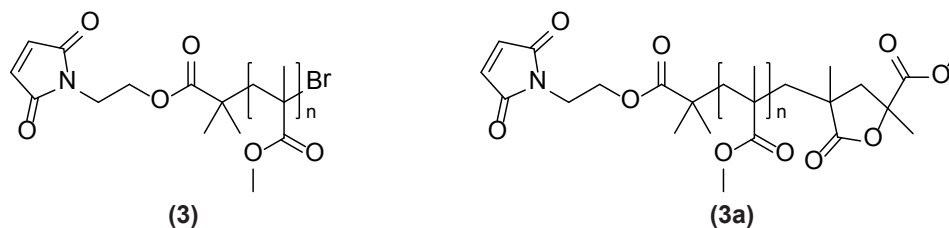


**Figure 4.16:** Structures of the maleimide functionalized pMMA products **3** and **3a** with two different end-groups (see text).

**Table 4.3:** Theoretical and measured  $m/z$  ratios of the maleimide functionalized pMMA **3** and **3a** on the example of the species appearing in one repeat unit. It should be noted that the agreement between theoretical and experimental  $m/z$  ratios is equally satisfactory in other repeat units.

Structure	[M + Na] <sup>+</sup>		
	$m/z^{\text{theo}}$	$m/z^{\text{exp}}$	$\Delta m/z$
<b>3</b>	1712.72	1712.33	0.39
<b>3a</b>	1718.75	1718.83	0.08

### 4.3.2 The TEMPO/Photoinitiator Conjugation Approach

#### 4-(2-(4-(2-Hydroxy-2-methylpropanoyl)phenoxy)ethoxy)-4-oxobutanoic acid **4**

*N,N*-diisopropylethylamine (9.26 mL, 53.16 mmol, 0.99 equiv.), succinic anhydride (6.18 g, 61.8 mmol, 1.15 equiv.) and Irgacure 2959<sup>TM</sup> (12.0 g, 53.55 mmol, 1.00 equiv.) were dissolved in 20 mL acetone, freed from oxygen (degassing with nitrogen) and stirred for 24 h at ambient temperature. The solvent was removed under reduced pressure resulting in the crude product as a light orange oil. The oil was purified employing chromatography over silica gel with pure diethylether as the eluent to afford the title compound (15.2 g, 46.8 mmol). The purity was confirmed by <sup>1</sup>H NMR (250 MHz, CDCl<sub>3</sub>, 25 °C):  $\delta$  1.55 (s, 6H, -(CH<sub>3</sub>)<sub>2</sub>-OH), 1.97 (s, 1H, -CH<sub>3</sub>-OH), 2.60 (s, 4H, -CH<sub>2</sub>-CH<sub>2</sub>-CO<sub>2</sub>H), 4.17 (t, <sup>3</sup>J<sub>HH</sub> = 5.05 Hz, 2H, -O-CH<sub>2</sub>-CH<sub>2</sub>-O-CO<sub>2</sub>-), 4.41 (t, <sup>3</sup>J<sub>HH</sub> = 4.29 Hz, 2H, -O-CH<sub>2</sub>-CH<sub>2</sub>-CO<sub>2</sub>-), 6.85-6.91 (d, <sup>3</sup>J<sub>HH</sub> = 8.81 Hz, 2H, -CH-CH-O-), 7.97- 8.01 ppm (d, <sup>3</sup>J<sub>HH</sub> = 8.67 Hz, 2H, -CH<sub>2</sub>-CH<sub>2</sub>-O-).

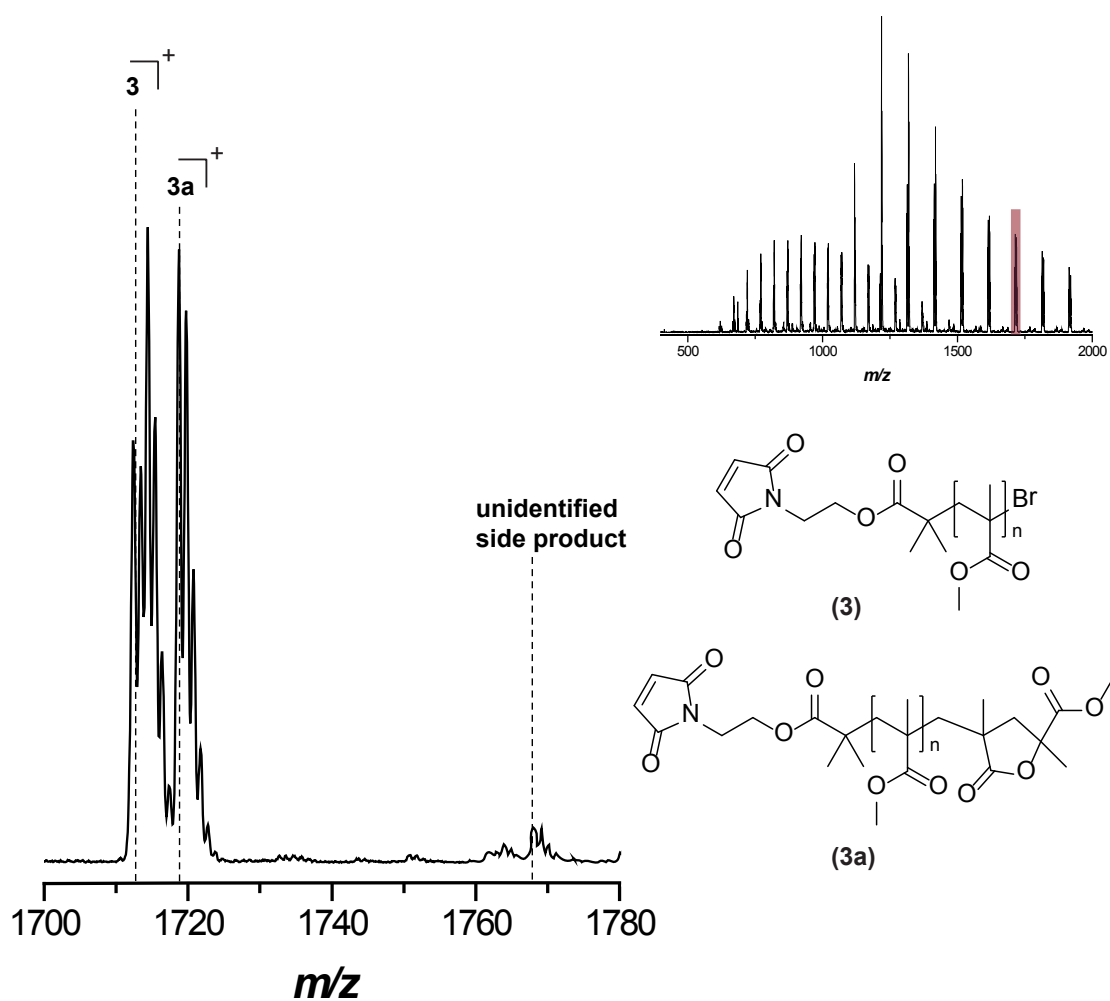


**Figure 4.17:** Electrospray ionization mass spectra of maleimide functionalized pMMA **3** and **3a** with two different end-groups in the charge state  $z = 1$  on the example of the species appearing in one repeat unit. It should be noted that the agreement between theoretical and experimental  $m/z$  ratios is equally satisfactory in other repeat units. The inset shows the overview of the spectrum.

### 2,2,6,6-Tetramethyl-4-piperidone-1-oxyl 5

2,2,6,6-Tetramethyl-4-piperidone (11.8 g, 76 mmol, 1.00 equiv.), sodium bicarbonate (5.1 g, 60.74 mmol, 0.80 equiv.) and sodium tungstate dihydrate (729 mg, 2.26 mmol, 0.03 equiv.) were dissolved in a mixture of 150 mL methanol and 10 mL acetonitrile (15:1). H<sub>2</sub>O<sub>2</sub> (27.70 mL, 0.81 mmol, 0.01 equiv.) was added and the solution was stirred for 48 h at ambient temperature. Finally, the reaction mixture was diluted with H<sub>2</sub>O and extracted three times with diethylether. The combined organic layers were subsequently washed with water and brine followed by the removal of the solvent under reduced pressure to result in the title product **5** as an orange oil, which crystallized in the freezer (-18 °C). Due to the paramagnetism of the product, it was not possible to confirm the purity of the product *via* <sup>1</sup>H NMR. The product was used without further characterization.

### 1-Oxyl-4-cyano-2,2,6,6-tetramethylpiperidine 6

2,2,6,6-Tetramethyl-4-piperidone-1-oxyl **5** (4.23 g, 24.85 mmol, 1.00 equiv), tosylmethyl isocyanide (5.0 g, 25.61 mmol, 1.03 equiv.) and 170 mL dimethoxyethane were placed in a 500 mL round bottom flask, freed from oxygen (degassing with nitrogen) and stirred at 0 °C. Potassium-*tert*-butoxide (5.8 g, 51.21 mmol, 2.00 equiv.) dissolved in 86 mL of a 1:1 mixture of dimethoxyethane and *tert*-butyl alcohol were added and the solution was stirred at 0 °C for 45 min. The temperature was allowed to reach 20 °C and the solution was stirred for an additional 1 h. 430 mL of water was added and the mixture was extracted five times using diethylether. Magnesium sulfate was added as a drying agent and the ether was removed under reduced pressure to afford red crystals. The crystals were dissolved in ethylacetate, after which cyclohexane was added in small portions, resulting in the precipitation of the orange-red title compound **6** (2.5 g, 55 %, 13.8 mmol). Due to the paramagnetism of the product, it was not possible to confirm the purity of the product *via* <sup>1</sup>H NMR. The success of the reaction was confirmed by melting point measurements as well as IR spectroscopy. Melting point 146-148 °C; IR 2238 cm<sup>-1</sup> (-CN). Lit.:<sup>278</sup> mp 146.5-147 °C; IR 2250 cm<sup>-1</sup> (-CN).

### 1-Oxyl-4-carboxyl-2,2,6,6-tetramethylpiperidine 7

Barium hydroxide (12.0 g, 63.37 mmol, 4.6 equiv) and sodium hydroxide (1.0 g, 25.00 mmol, 1.8 equiv) were dissolved in 200 mL distilled water and added to a solution of 1-oxyl-4-cyano-2,2,6,6-tetramethylpiperidine **6** (2.5 g, 13.8 mmol, 1.00 equiv.) in 50 mL methanol. The mixture was refluxed for 24 h, cooled to ambient temperature and extracted once with chloroform to remove unreacted starting material. The aqueous phase was acidified with 10 % hydrochloric acid and extracted four times with chloroform.

The combined organic phases were dried over magnesium sulfate and the solvent was removed under reduced pressure to result in 1.6 g of a peach colored powder **7** (1.6 g, 58 %, 8.0 mmol). Due to the paramagnetism of the product, it was not possible to confirm the purity of the product *via*  $^1\text{H}$  NMR. The success of the reaction was confirmed by melting point measurements as well as IR spectroscopy. Melting point 178-182 °C; IR 1686  $\text{cm}^{-1}$  (-C=O). Lit.:<sup>278</sup> Melting point: 171-172 °C, 1680 (-C=O), 3300-3100  $\text{cm}^{-1}$  broad (-OH).

### PEG-functionalized 1-oxyl-4-carboxyl-2,2,6,6-tetramethylpiperidine **8**

PEG (1.0 g, 0.5 mmol, 1.00 equiv.), 1-oxyl-4-carboxyl-2,2,6,6-tetramethylpiperidine **7** (0.2 g, 1 mmol, 2.00 equiv.) and DMAP (0.06 mg, 0.5 mmol) were dissolved in dry dichloromethane (7 mL) to give solution A. *N,N'*-dicyclohexylcarbodiimide (DCC) (0.31 g, 1.5 mmol) was dissolved in DCM (3 mL) and added to solution A at ambient temperature. After 15 h, the reaction mixture was filtered over a small amount of silica to remove the urea side product. The mixture was washed with saturated sodium bicarbonate solution and dried over magnesium sulfate before purification by precipitation in diethylether (two times) to result in the title compound **8** which is shown in Figure 4.18. Purity was confirmed by ESI-MS. Table 4.4 shows the comparison of the theoretical and experimental  $m/z$  values for the charge state  $z = 1$  for the product. A negligible amount of unidentified side product at  $m/z = 1927.17$  could not be identified. The spectrum is shown in Figure 4.19.

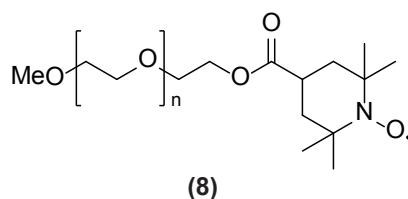


**Figure 4.18:** Structure of TEMPO functionalized PEG **8**.

**Table 4.4:** Theoretical and measured  $m/z$  ratios of the TEMPO-functionalized PEG **8** on the example of the species appearing in one repeat unit. It should be noted that the agreement between theoretical and experimental  $m/z$  ratios is equally satisfactory in other repeat units.

Structure	$[\text{M} + \text{Na}]^+$		
	$m/z^{\text{theo}}$	$m/z^{\text{exp}}$	$\Delta m/z$
<b>8</b>	1910.13	1909.85	0.28

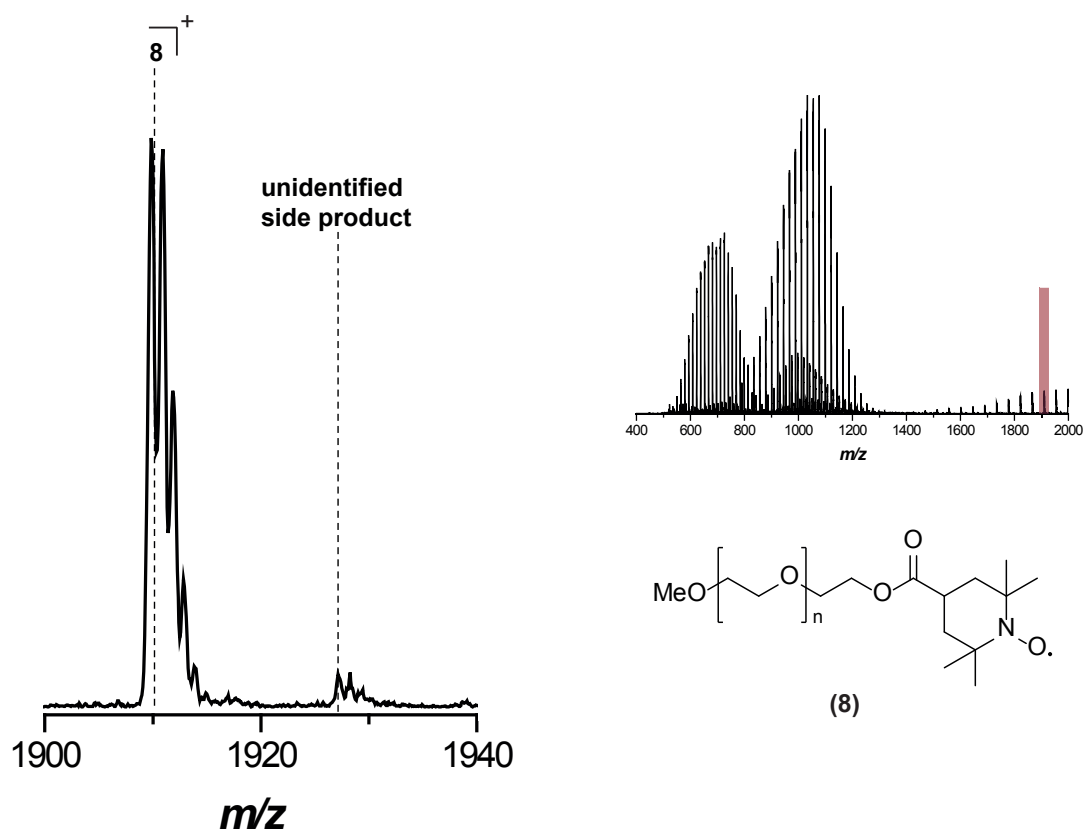


**Figure 4.19:** Electrospray ionization mass spectra of TEMPO functionalized PEG 8 in the charge state  $z = 1$  on the example of the species appearing in one repeat unit. It should be noted that the agreement between theoretical and experimental  $m/z$  ratios is equally satisfactory in other repeat units. The inset shows the overview of the spectrum.

### PEG functionalized with 4-(2-(4-(2-hydroxy-2-methylpropanoyl)phenoxy)ethoxy)-4-oxobutanoic acid **9**

The synthesis was identical as reported for **8** employing the following amounts of reagents: PEG (0.616 g, 0.3 mmol, 1.00 equiv.), 4-(2-(4-(2-hydroxy-2-methylpropanoyl)phenoxy)ethoxy)-4-oxobutanoic acid **4** (0.2 g, 0.6 mmol, 2.00 equiv.), DMAP (0.37 g, 0.3 mmol, 1.00 equiv.) and DCC (0.19 g, 0.9 mmol). The structure of the product is shown in 4.20. The success of the reaction was verified by ESI-MS, as shown in Figure 4.21 with the comparison of the theoretical and experimental  $m/z$  ratios for the charge state  $z = 1$  depicted in Table 4.5.

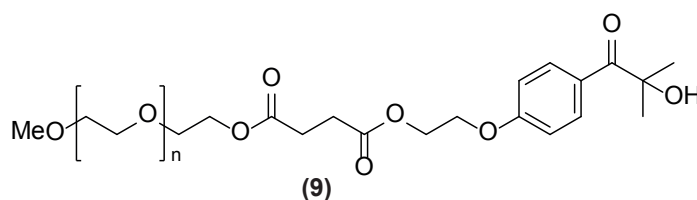


**Figure 4.20:** Structure of photoinitiator functionalized PEG **9**.

**Table 4.5:** Theoretical and measured  $m/z$  ratios of the photoinitiator functionalized PEG **9**. It should be noted that the agreement between theoretical and experimental  $m/z$  ratios is equally satisfactory in other repeat units. The inset shows the overview of the spectrum.

Structure	[M + Na] <sup>+</sup>		
	$m/z^{\text{theo}}$	$m/z^{\text{exp}}$	$\Delta m/z$
<b>9</b>	1902.05	1902.00	0.05

### Coupling reaction TEMPO functionalized PEG **8** and photoinitiator PEG **9** yielding an AA-type (block co)polymer **10**

TEMPO functionalized PEG **8** (7.0 mg, 0.0032 mmol) and photoinitiator functionalized PEG **9** (7.6 mg, 0.0033 mmol) were mixed in equimolar amounts in acetonitrile (2 mL). The reaction mixture was freed from oxygen by purging with nitrogen for five minutes. The reaction mixture was placed in front of a UV-lamp (36 W, max. emission at 311 nm) at a distance of 3 cm and mixed with a magnetic stir bar during the irradiation experiment. In addition to conducting block copolymer conjugation, test experiments were also conducted with functionalized PEG and small molecules. During the experiments the ratios of reactants were changed, yet the general applied procedure was the same as above (details are provided in the Results and Discussion section below).

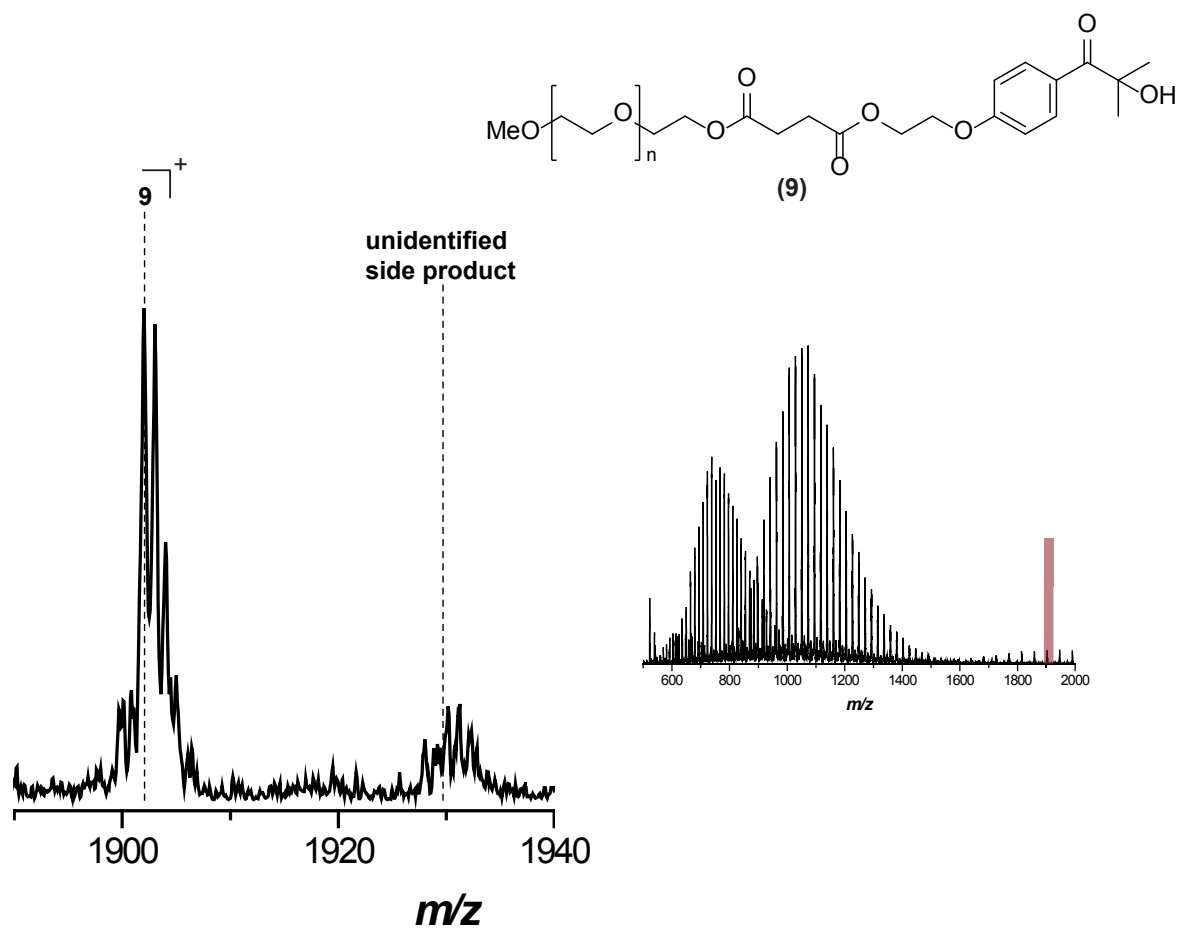


**Figure 4.21:** Electrospray ionization mass spectra of photoinitiator functionalized PEG 9 in the charge state  $z = 1$  on the example of the species appearing in one repeat unit. It should be noted that the agreement between theoretical and experimental  $m/z$  ratios is equally satisfactory in other repeat units. The inset shows the overview of the spectrum.

## 4.4 Results and Discussion

### 4.4.1 The Nitrile Imine-mediated 1,3-Dipolar Cycloaddition of Tetrazole and Ene Coupling (NITEC) Approach for Block Copolymer Formation

While the NITEC has been successfully applied for the conjugation of a number of small molecules with each other or small molecules to proteins as well as for PEGylation of proteins, the technique has never been applied to ligate two synthetic macromolecules. To evaluate this possibility, model conjugation experiments for the formation of AA- and AB-type block copolymers were conducted. Figure 4.22 depicts the synthetic pathway for the formation of diblock copolymers from tetrazole and maleimide end-functionalized polymers, respectively.

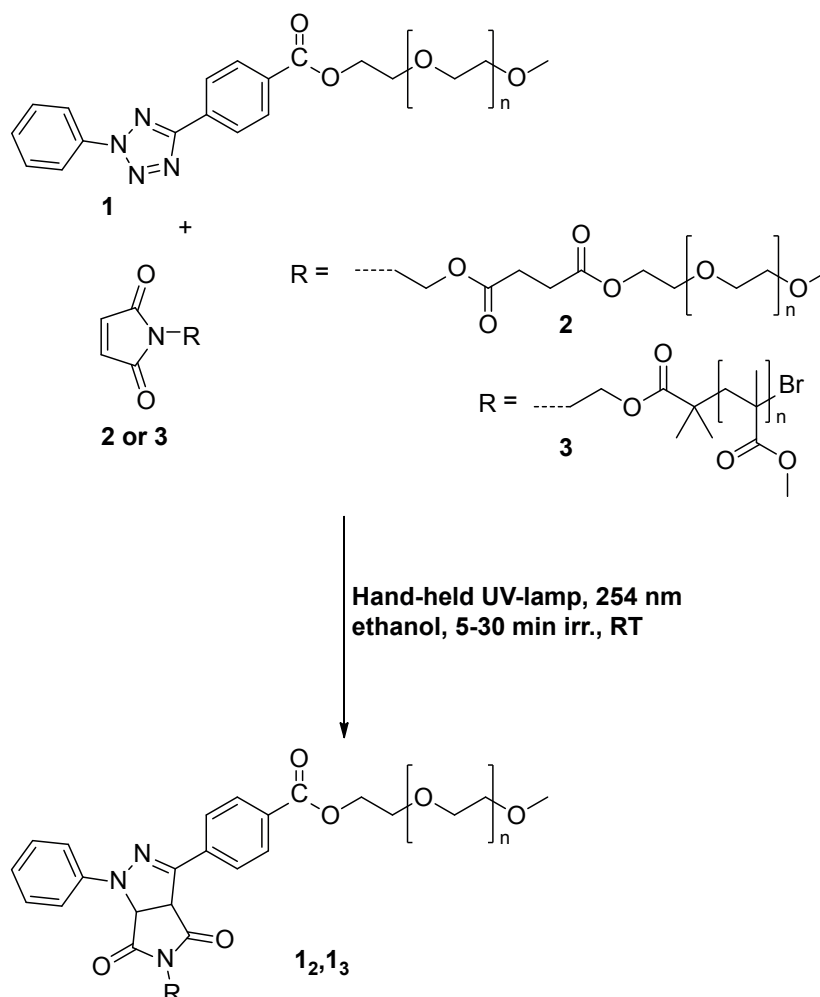


**Figure 4.22:** General reaction pathway between tetrazole functionalized PEG **1** and maleimide functionalized PEG **2** or maleimide functionalized pMMA **3**.

In the first part of the study, the tetrazole and the maleimide moieties were installed on low molecular weight ( $M_n = 2000 \text{ g mol}^{-1}$ ) poly(ethylene glycol) methyl ether (PEG)

by esterification. Employing DCC coupling, tetrazole-bearing PEG **1** and maleimide-terminated PEG **2** were synthesized with high end-group functionality confirmed employing ESI-MS. The end-group fidelity was determined by ESI-MS to >90 % for **1** and >83 % for **2** according to integration of the respective peak areas (see figures 4.13 and 4.17). Maleimide was chosen as the dipolarophile end-group as it has been shown to undergo rapid reactions with nitrile imine intermediates.<sup>275</sup> In addition to the post-polymerization approach, an ATRP functional initiator can be used to readily introduce a maleimide moiety on a wide range of polymers. This procedure was followed to produce an  $\alpha$ -maleimido poly(methyl methacrylate) (pMMA). To assess the conjugation efficiency of the NITEC, equimolar amounts of **1** and **2** were dissolved in ethanol and subsequently irradiated at 254 nm using a hand-held laboratory TLC lamp. Figure 4.23 depicts the size-exclusion chromatograms of samples withdrawn after pre-determined irradiation times (5-25 min) and left to react overnight for complete conversion. The success of the conjugation is evidenced by a distinct shift of the SEC traces to shorter retention times due to the formation of higher molecular weight polymers, which corresponds to the double molecular weight of the starting material. The intensity of the peak according to the starting materials decreases progressively with the increase of the intensity for the peak at higher molecular weights, which is typical for the formation of block copolymers starting from homopolymer precursors. Indeed, such an evolution differs completely from what can be observed when a block copolymer is produced by the extension of a reactive polymer with iterative addition of monomer, i.e., a progressive shift of the whole peak in the ideal case.<sup>71</sup> The final product exhibits a molecular weight of  $M_n = 4300 \text{ g mol}^{-1}$  (determined by SEC), which is (approximately) double of that of the starting compounds as expected in the case of a quantitative conjugation. The reaction was also investigated *via* SEC/ESI-MS. A closer look at the intermediate samples reveals that after only 5 minutes of UV-light irradiation half of the starting materials had already reacted, and about a fifth was only left after 10 min. No significant difference could be observed between samples taken after 15, 20, or 25 minutes. The remaining of starting material may be explained by a non-quantitative functionalization during the synthesis of tetrazole functionalized PEG **1** and maleimide functionalized PEG **2**. It is important to note that a perfectly equimolar solution of starting material is not easy to prepare when one works with macromolecules, owing to their (inherent) polydispersities. Non-exact equimolarities could thus be an explanation for the remaining low molecular weight starting material. Due to the employment of low molecular weight PEG as starting material, it was also possible to perform SEC ESI-MS measurements on the resulting block copolymer. Figure 4.24 depicts a zoom of the block copolymer region showing the molecular proof of the conjugation reaction. The experimental and theoretical  $m/z$  values for the PEG-*b*-PEG block copolymer are in good agreement and shown in Table 4.6. Due to the coupling, the molecular weight of the block copolymer doubled, therefore only peaks in the  $z = 2$  region can be observed and hence the

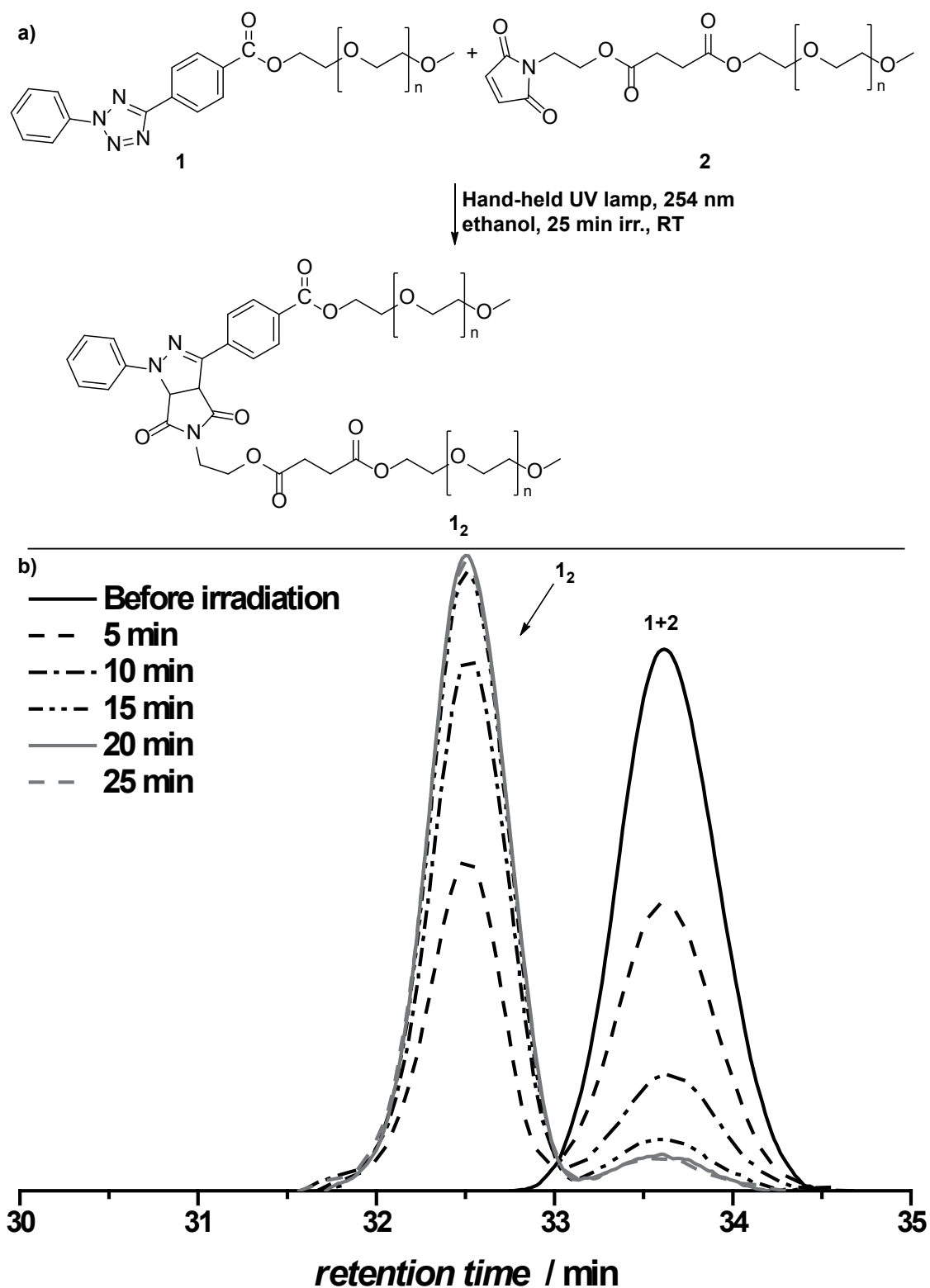


**Figure 4.23:** a) Reaction sequence of the UV-light activated conjugation between tetrazole functionalized PEG 1 and maleimide functionalized PEG 2 resulting in the AA-type block copolymer  $1_2$  b) SEC monitoring of the block copolymer formation *via* irradiation of an equimolar solution of tetrazole functionalized PEG 1 and maleimide functionalized PEG 2 in ethanol with a hand-held UV-lamp at a wavelength of 254 nm at ambient temperature resulting in the AA-type block copolymer  $1_2$ .

resolution as well as the signal to noise ratio of the peaks are lower compared to the peaks in the  $z = 1$  regime.

**Table 4.6:** Theoretical and measured  $m/z$  ratios of the PEG-*b*-PEG block copolymer **1<sub>2</sub>**. It should be noted that the agreement between theoretical and experimental  $m/z$  ratios is equally satisfactory in other repeat units. The inset shows the overview of the spectrum.

Structure	[M + 2Na] <sup>2+</sup>		
	$m/z^{\text{theo}}$	$m/z^{\text{exp}}$	$\Delta m/z$
<b>1<sub>2</sub></b>	1729.44	1729.83	0.39

After the successful formation of AA-type block copolymers the concept was extended to AB-type block copolymers. The formation of AB-type block copolymers between tetrazole functionalized PEG **1** and maleimide functionalized pMMA **1 3** was followed by SEC. Performing ESI-MS is not suitable for these AB-type block copolymers due to substantially increased complexity of the evaluation of such a spectrum. Although the block copolymer formation did proceed - as depicted in Figure 4.25 - the yield of the block copolymer was not as high yields as previously shown for AA-block copolymer formation with the PEG derivatives (see Figure 4.23). Explanations for the lower efficiency could be similar as already noted before, i.e., not exact equimolarities or non-quantitative polymer functionalization. It has to be further noted that some solvents might interfere with the conjugation reaction in a concurrent reaction. An example of such a solvent is THF. While ethanol was suitable as solvent for the conjugation reaction, even small amounts of THF did interfere during the coupling reaction resulting in a poor block copolymer formation. This interesting observation was investigated by ESI-MS after irradiation of maleimide functionalized pMMA **3** in a mixture of ethanol/THF (99/1) for 15 minutes at ambient temperature. The resulting electrospray ionization mass spectrum is depicted in Figure 4.26 and shows a decrease in starting material **3** and **3a** while unidentified side products rise in intensity. Thus, the choice of solvent is very important for the success of the conjugation reaction.

In the current section, the NITEC approach was evaluated for the employment in synthetic polymer chemistry. The results of this evaluation show the successful formation of AA-type and AB-type block copolymers after activation for up to one hour with a hand-held UV-lamp in an environmentally friendly solvent. The NITEC reaction does fulfill some criteria for *click*-type reactions for polymers,<sup>240</sup> such as equimolarity and fast reaction scale, but has to prove itself in further studies for large-scale purification techniques. Experience gained during the evaluation of the NITEC reaction as a conjugation technique will be employed in the following chapter, in which biofunctional materials are decorated with various polymer classes in order to change the surface characteristics. The next section is dedicated to the TEMPO/photoinitiator approach

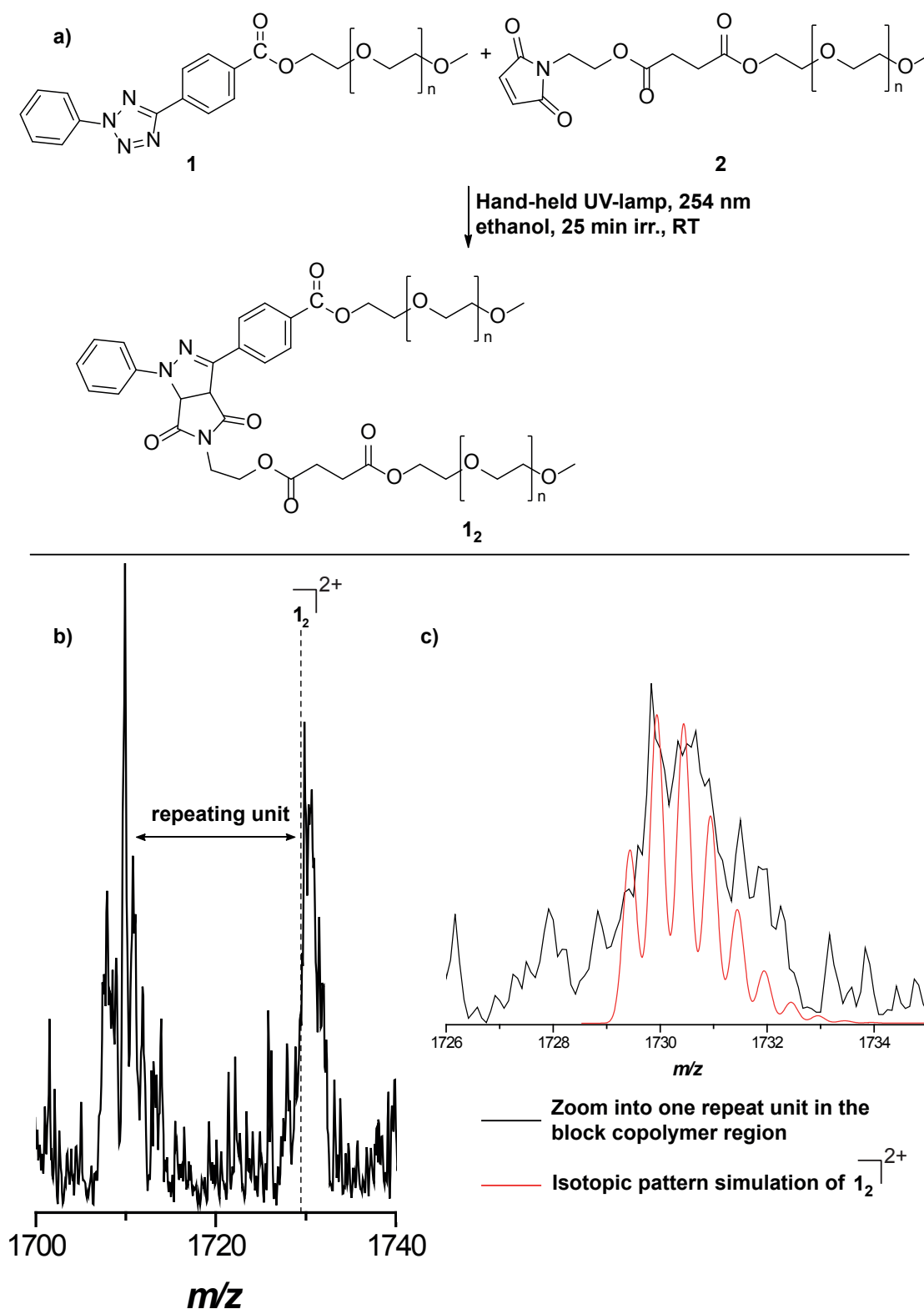


**Figure 4.24:** a) Reaction sequence of the UV-light activated conjugation between tetrazole functionalized PEG **1** and maleimide functionalized PEG **2** resulting in the AA-type block copolymer **1<sub>2</sub>** b) Electrospray ionization mass spectra of the PEG-*b*-PEG block copolymer region in the charge state  $z = 2$  showing the conjugation product **1<sub>2</sub>** on the example of the species appearing in two repeat units. It should be noted that the agreement between theoretical and experimental  $m/z$  ratios is equally satisfactory in other repeat units. c) Comparison of one repeat unit of the AA-type block copolymer with a simulated isotopic pattern for the specific repeat unit (Gaussian profile, resolution 0.3 Dalton, charge state  $z = 2$ ).

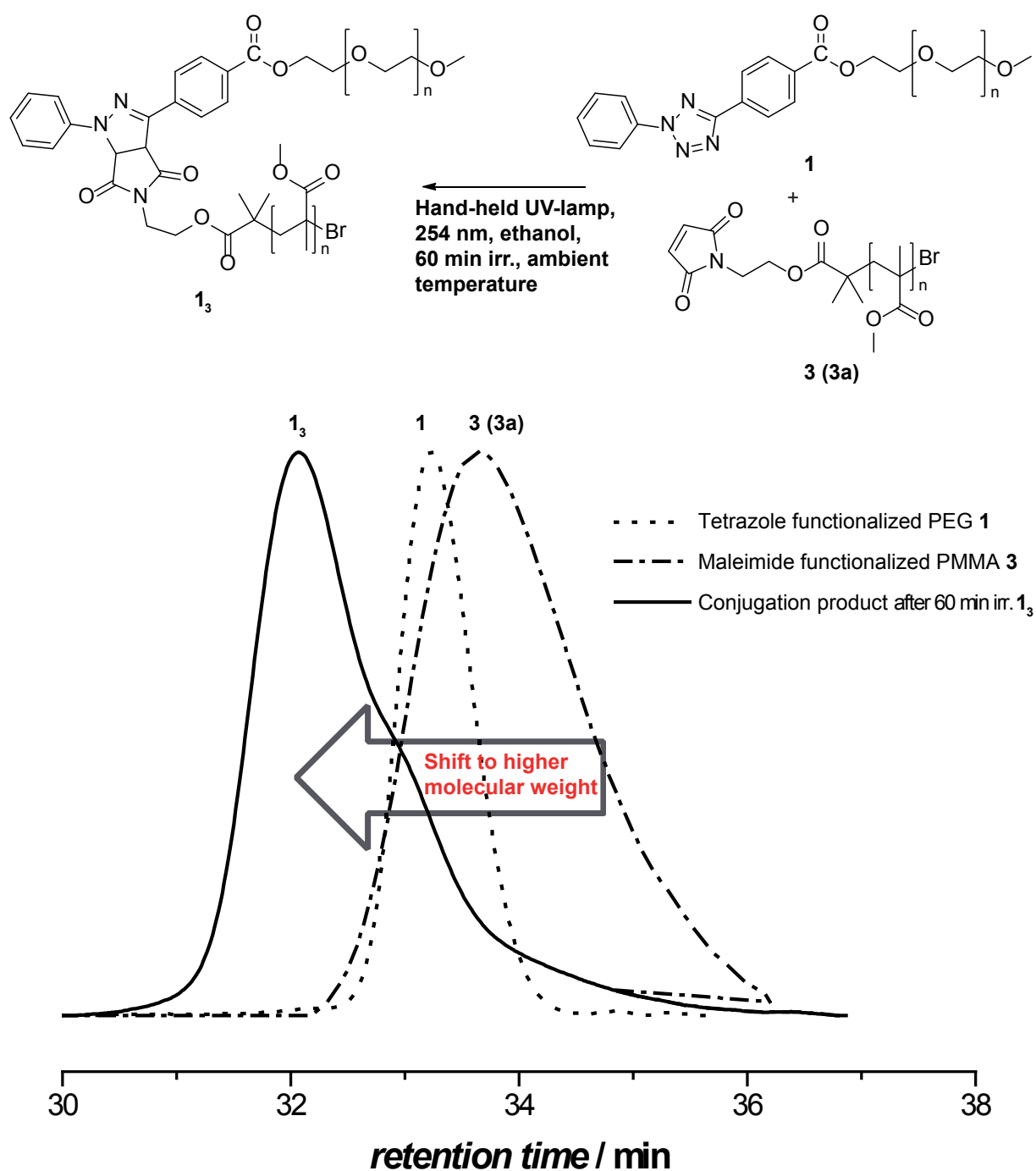


**Figure 4.25:** a) Reaction scheme of the UV-light activated conjugation between tetrazole functionalized PEG **1** and maleimide functionalized pMMA **3** resulting in the AB-type block copolymer **1<sub>3</sub>** (although only one version of the maleimide functionalized pMMA is shown **3**, it has to be kept in mind that also the maleimide functionalized but lactonized pMMA (**3a**) reacts in the same manner). b) SEC traces of the block copolymer formation of poly(ethylene glycol)-*block*-poly(methyl methacrylate) *via* irradiation of an equimolar solution of **1** and **3** for 60 minutes in ethanol with a hand-held UV-lamp at a wavelength of 254 nm at ambient temperature.

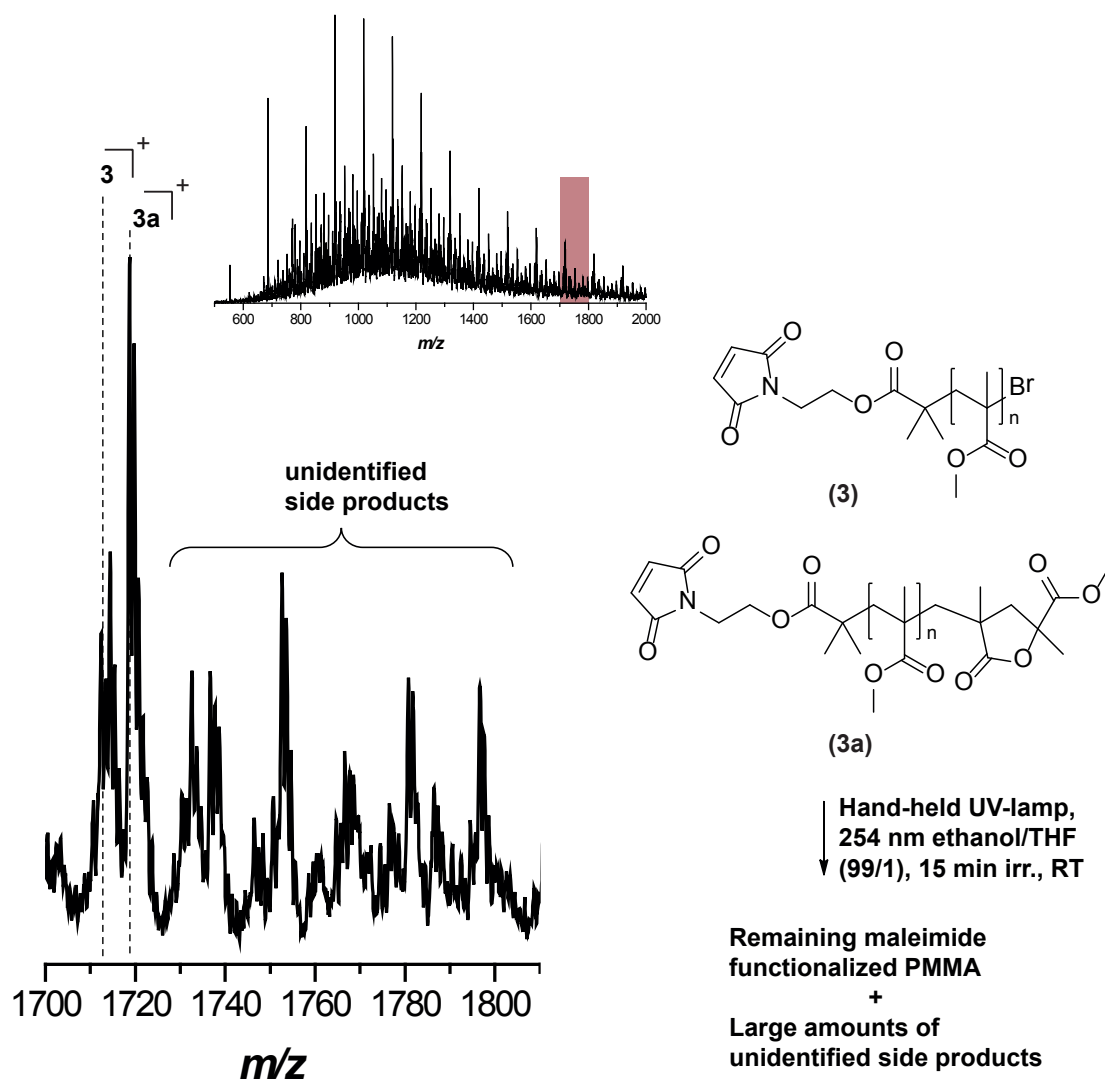


**Figure 4.26:** Electrospray ionization mass spectra of maleimide functionalized pMMA **3** and **3a** dissolved in a mixture of ethanol/THF (99/1) after an irradiation time of 15 minutes in the charge state  $z = 1$  showing the remaining starting material **3** and **3a** on the example of the species appearing in one repeat unit. It should be noted that the agreement between theoretical and experimental  $m/z$  ratios is equally satisfactory in other repeat units.

for macromolecular ligation.

As presented in the introduction of the current chapter, carbon-centered radicals have tendency to react with stable nitroxide radicals.<sup>273</sup> This reaction shall be exploited as a new conjugation technique and therefore the next section of the current chapter is dealing with the evaluation of the technique which is based on combining photochemistry with radical trapping. The test system consists out of stable nitroxide radicals employed to capture carbon-centered radicals yielding a covalent bond between both molecules. These carbon-centered radicals are generated by irradiation of a photoinitiator and its subsequent decay into such radicals while TEMPO derivatives are employed as the capturing nitroxide radicals.

#### 4.4.2 The TEMPO/Photoinitiator Conjugation Approach

The aim of the following section is to present an evaluation of an innovative coupling technique employing stable nitroxide radicals in conjunction with *in situ* generated carbon-centered radicals to form a covalent linkage. Figure 4.27 shows the general concept for the reaction. The first step is the synthesis of a photoinitiator bearing PEG as well as a nitroxide functionalized PEG. Both functional polymers were synthesized by a *Steglich* esterification of PEG and the carboxy functionalized photoinitiator Irgacure 2959<sup>TM</sup> or the carboxy-TEMPO, respectively. The end-group functionality was confirmed via ESI-MS. The end-group fidelity was determined by integration of the interested peak area of the mass spectral abundances to be >90 % for **8** and >63 % for **9**. It has to be noted that the end-group fidelity for the photoinitiator functionalized PEG **9** has to be handled with care because the rate of ionization is lower than the ionization rate of the TEMPO functionalized PEG **8**. Additionally, the signal to noise ratio of the photoinitiator functionalized PEG **9** is also significantly lower than for the TEMPO functionalized PEG **8**. Unless stated explicitly otherwise, all reactions were performed under nitrogen atmosphere. While the final aim was to assess the coupling of two macromolecules to generate an AA-type (block co)polymer, the first experiments were conducted with small molecule analogues of the photoinitiator and the nitroxide radical, respectively. Figure 4.29 shows the resulting ESI mass spectra after different time intervals for the reaction between the TEMPO functionalized PEG **8** and a 5-fold molar excess of Irgacure 2959<sup>TM</sup> in acetonitrile performed under ambient atmosphere. Figure 4.28 depicts the structure of the major product after irradiation. The green line shows the starting material at  $t = 0$  minutes. From the ESI mass spectrum it can be concluded that the formation of the coupling product **8a** does not increase after 30 minutes of irradiation although the amount of side product continues to accumulate (blue and purple line). The ratio of unreacted TEMPO functionalized PEG **8** and coupling product **8a** is approximately 1:1 which is the result one would expect based on the assumption that the photoinitiator releases two radicals but only one of them leads toward the desired product. The

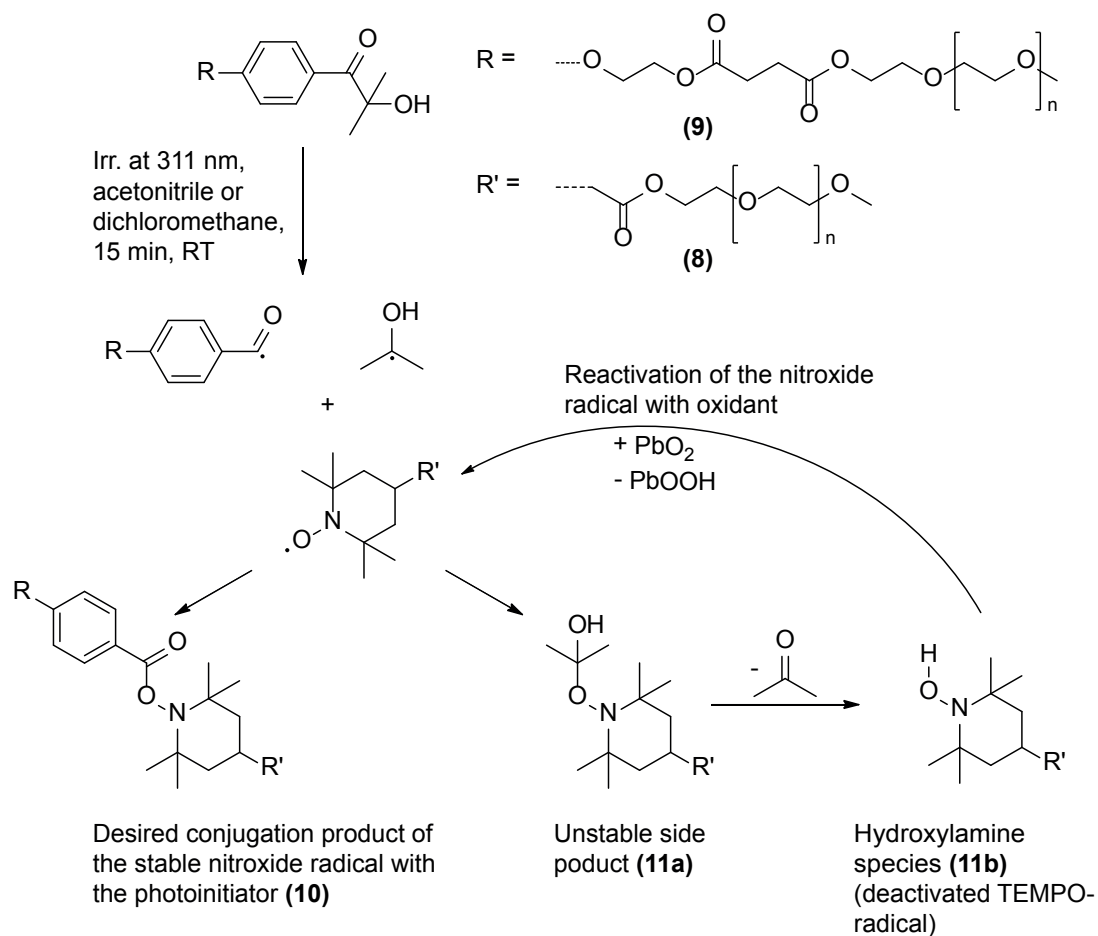


**Figure 4.27:** General reaction scheme for the reaction between a stable nitroxide radical and a carbon-centered radical resulting in a covalent linkage. Details of the depicted reaction sequences - including the oxidation sequence - are discussed in the text.

side reaction of the tertiary radical with the TEMPO functionalized PEG results in the unstable side product (**11a**). After the release of an acetone molecule, the before active TEMPO functionalized PEG is transformed into the hydroxylamine species **11b**, which can not participate any more in the desired radical coupling. Unfortunately, the signal according to the starting material **8** overlaps in the ESI mass spectrum with the side product **11b**. Therefore it is difficult at a first glance to distinguish between the TEMPO functionalized PEG **8** and the hydroxylamine species **11b**. The theoretical and experimental  $m/z$  ratios for the charge state  $z = 1$  are depicted in Table 4.7. It has to be noted that the radical coupling reaction worked surprisingly well with only small amounts of side products present even when the coupling reaction was carried out under ambient atmospheric conditions. Although the radical coupling did proceed, the ESI mass spectra shows much more noise and unidentified side products probably due to existence of oxygen in the reaction mixture. Therefore - and for a better reproducibility - the reactions should preferably be performed under a nitrogen atmosphere. Generally, the new established radical coupling has been successful, but the amount of hydroxylamine species **11b** would disqualify the reaction as a technique for macromolecular block formation due to difficult removal of the hydroxylamine polymer species. Fortunately, there are methods available to reoxidize the hydroxylamine species **11b** employing oxidants such as molecular oxygen,  $MnO_4$ ,  $AgO$  or  $PbO_2$  to regain the starting nitroxide radical **8**.<sup>279,280</sup>

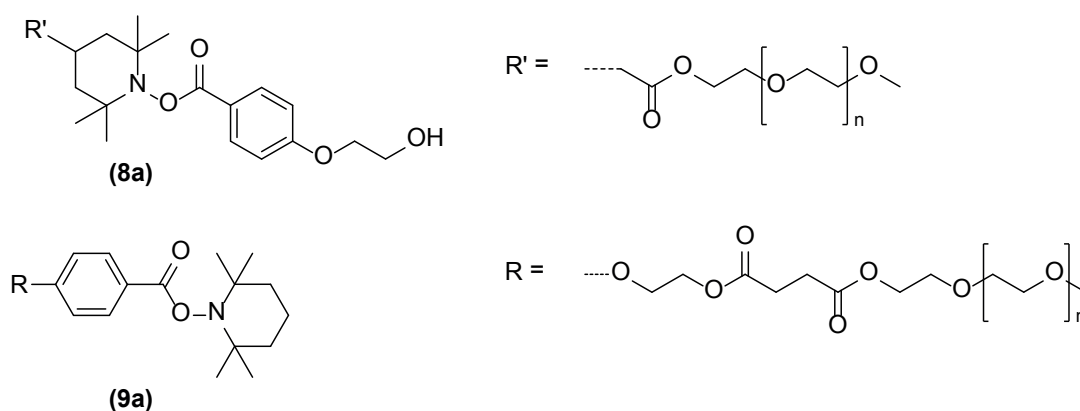


**Figure 4.28:** Desired products from the reaction between TEMPO functionalized PEG **8** with Irgacure 2959<sup>TM</sup> yielding **8a** and the reaction of photoinitiator functionalized PEG **9** with TEMPO yielding **9a** after irradiation at ambient temperature employing acetonitrile as solvent.

To assess the intended reoxidation reaction of the hydroxylamine **11b** - also in comparison with possible side reactions -  $PbO_2$  was introduced into the before mentioned TEMPO functionalized PEG and Irgacure 2959<sup>TM</sup> model system. Figure 4.30 shows the ESI mass spectra of the different reaction stages. The red line after 60 min of irradiation appears similar to the ones depicted in Figure 4.29 and evidences the reproducibility of the reaction. The irradiation was stopped and the reaction mixture was exposed to air at ambient temperature. After 18 h exposure to air, a 4.5-fold molar excess of  $PbO_2$ , with respect to the TEMPO functionalized PEG **8**, was added. The blue line depicts

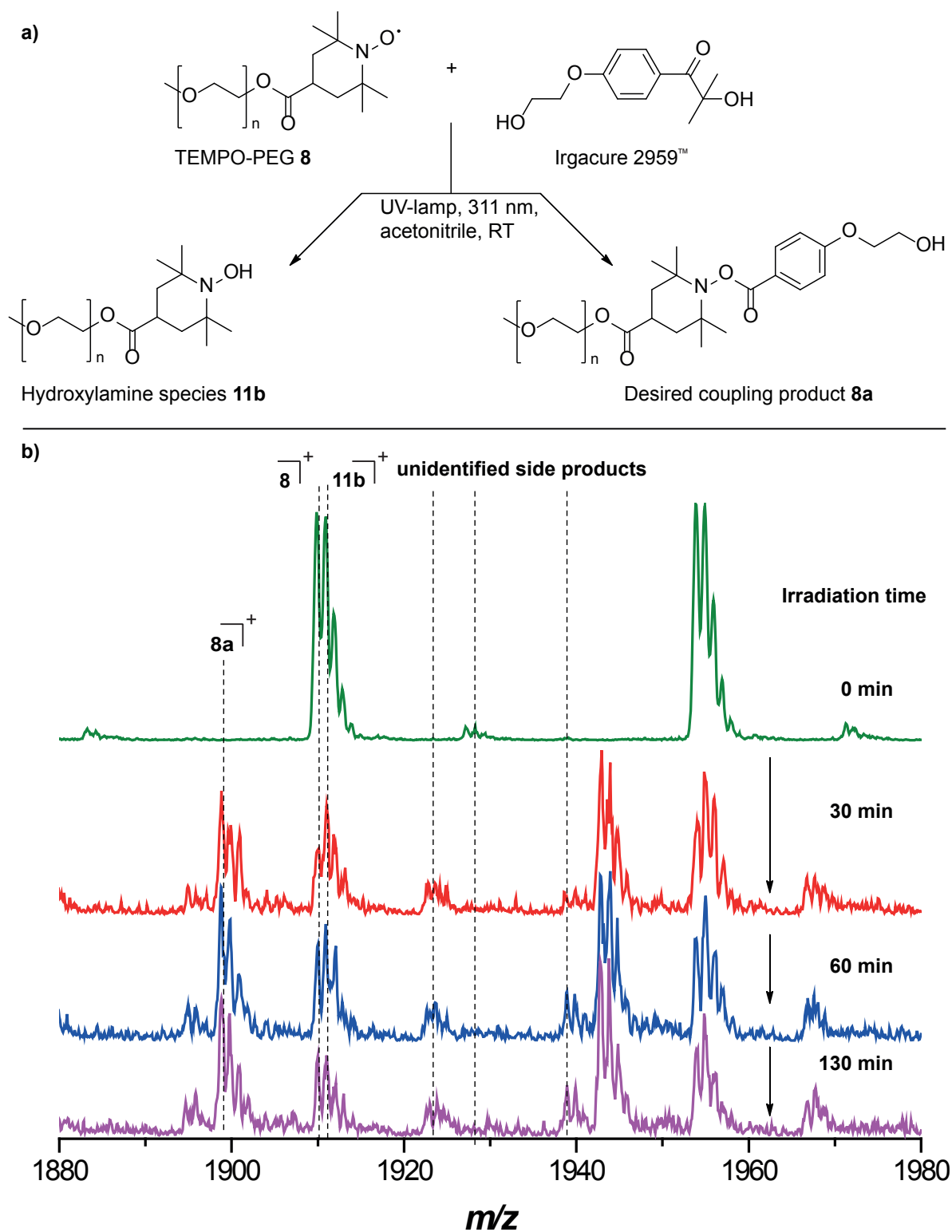


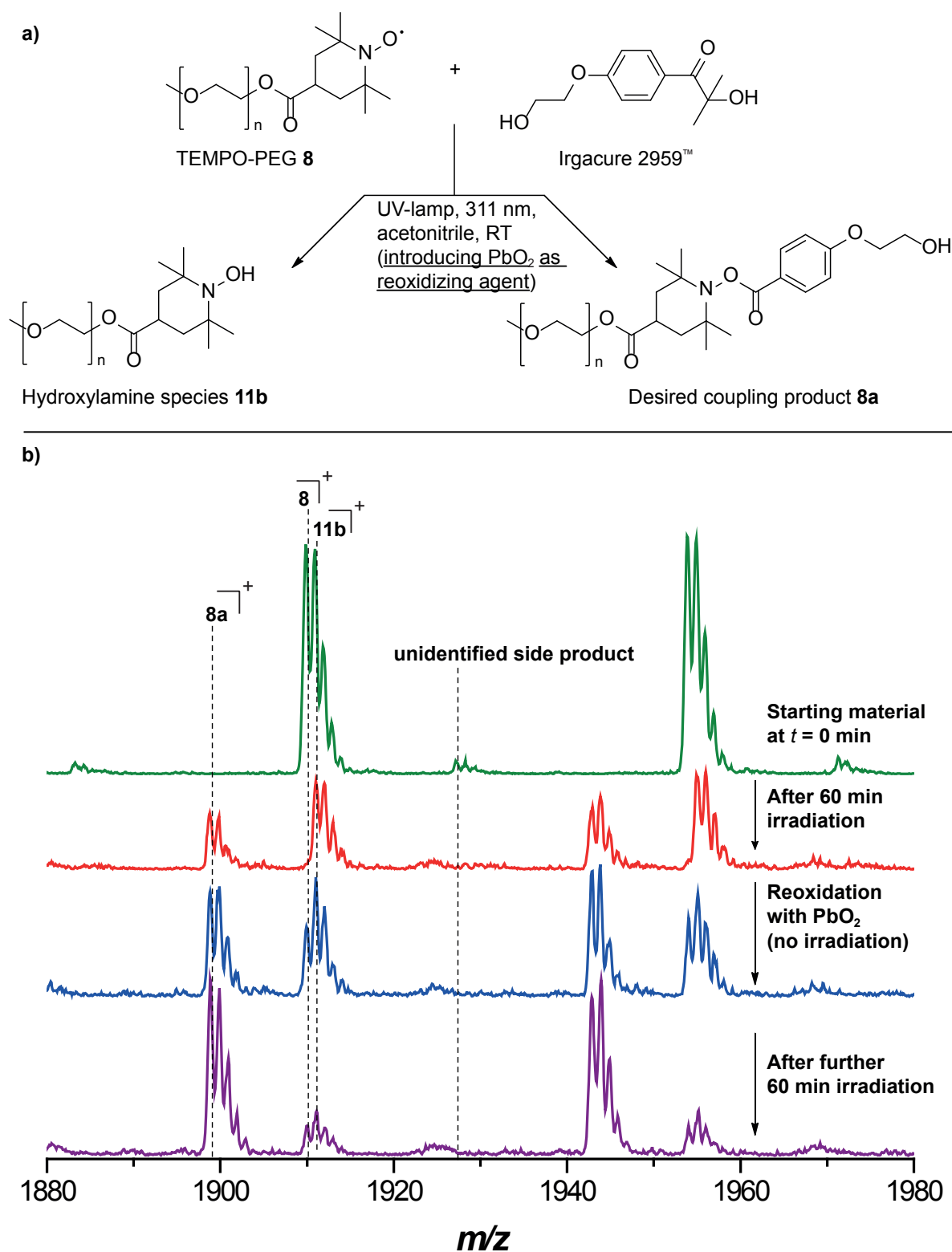
**Figure 4.29:** a) Reaction pathway of the UV-light activated reaction between TEMPO functionalized PEG **8** and Irgacure 2959<sup>TM</sup> yielding the desired coupling product **8a**, as well as in the hydroxylamine species **11b**. b) Electrospray ionization mass spectra in the charge state  $z = 1$  for the reaction between TEMPO functionalized PEG **8** with a 5-fold molar excess of Irgacure 2959<sup>TM</sup> in the charge state  $z = 1$  in acetonitrile at ambient temperature and atmosphere after pre-determined time intervals of irradiation with a 311 nm UV broadband lamp on the example of the species appearing in one repeat unit. It should be noted that the agreement between theoretical and experimental  $m/z$  ratios is equally satisfactory in other repeat units.

**Table 4.7:** Theoretical and measured  $m/z$  ratios of the PEG-TEMPO products after irradiation in the presence of Irgacure 2959<sup>TM</sup>. It should be noted that the agreement between theoretical and experimental  $m/z$  ratios is equally satisfactory in other repeat units. The inset shows the overview of the spectrum.

Structure	[M + Na] <sup>+</sup>		
	$m/z^{\text{theo}}$	$m/z^{\text{exp}}$	$\Delta m/z$
<b>8</b>	1910.13	1909.85	0.28
<b>8a</b>	1899.08	1898.75	0.33
<b>11b</b>	1911.14	1911.00	0.11

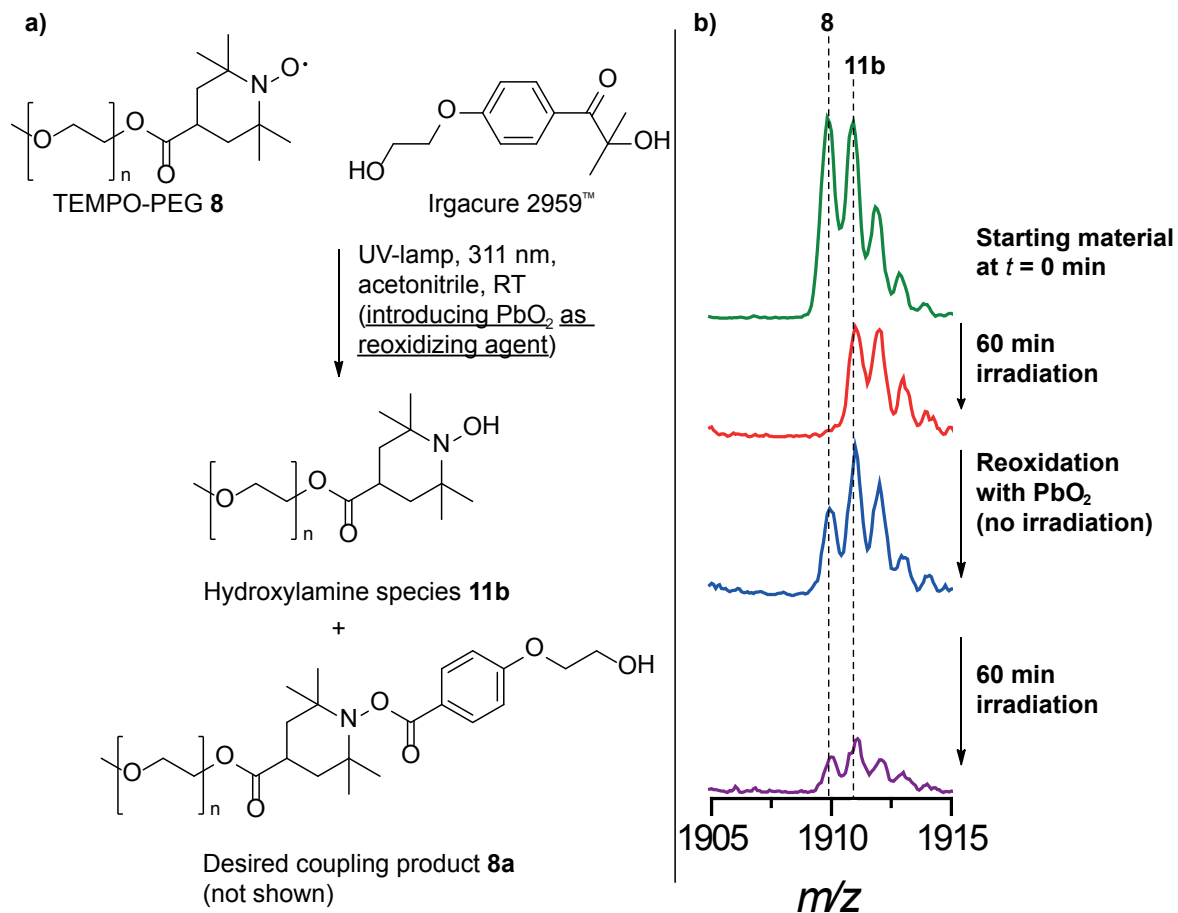
the ESI mass spectrum after the reoxidation of the hydroxylamine species and indeed shows the expected reoxidized TEMPO functionalized PEG **8**. The PbO<sub>2</sub> was removed by filtration and the residual solvent was freed from oxygen and irradiated for additional 60 minutes. The purple line shows the ESI mass spectrum after the additional 60 minutes of irradiation. It can clearly be stated that the ratio of coupling product **8a** and the TEMPO functionalized PEG **8** increased significantly. Furthermore, the intensity and thus the amount of the hydroxylamine species **11b** is reduced, which can be concluded by comparing the red line after 60 minutes irradiation and the purple line after subsequent reoxidation and a further 60 minutes irradiation. The introduction of PbO<sub>2</sub> as an oxidizing agent for the hydroxylamine species leads to a higher efficiency of the coupling reaction.

Figure 4.31 depicts a zoomed region of the electrospray ionization mass spectra in the charge state  $z = 1$  shown in Figure 4.30 for the reaction between TEMPO functionalized PEG **8** and Irgacure 2959<sup>TM</sup> to highlight the reappearance of the TEMPO functionalized PEG **8** after reoxidation with PbO<sub>2</sub>. The first peak in the isotopic pattern of the ESI mass spectrum at  $t = 0$  can be assigned to the TEMPO functionalized PEG **8**. After 60 minutes of irradiation the peak has almost disappeared, inducing the formation of the hydroxylamine species **11b** (red line) and coupling product **8a** (not shown). The oxidation of the hydroxylamine **11b** species with oxygen and PbO<sub>2</sub> leads to a reappearance of the peak of the initial TEMPO functionalized PEG **8** (blue line). Inspection of the purple line, which corresponds to additional 60 minutes irradiation after reoxidation with PbO<sub>2</sub>, it can be noted that the intensity of the peak decreased substantially in relation to the spectra before, which evidences that the reappeared TEMPO functionalized PEG **8** reacts further to give the desired coupling product **8a** (not shown) but does not completely disappear. Complete disappearance is probably not observed because there are no photoinitiator molecules of Irgacure 2959<sup>TM</sup> left in the reaction mixture. The decreasing intensity of the TEMPO functionalized PEG **8** in conjunction with the increasing intensity of the



**Figure 4.30:** a) Reaction pathway of the UV-light activated reaction between TEMPO functionalized PEG **8** and Irgacure 2959<sup>TM</sup> yielding the desired coupling product **8a** and the hydroxylamine species **11b**. b) ESI mass spectra in the charge state  $z = 1$  for the above described reaction employing a 5-fold molar excess of Irgacure 2959<sup>TM</sup> in acetonitrile at ambient temperature at  $t = 0$  (green line), after irradiation with a 311 nm UV broadband lamp for 60 minutes (red line), exposure to oxygen for 18 h and further 3 h exposure to 4.5 equivalents of PbO<sub>2</sub> (with respect to **8**) (blue line) and additional irradiation for 60 minutes of the reaction mixture after filtration of PbO<sub>2</sub>. It should be noted that the agreement between theoretical and experimental  $m/z$  ratios is equally satisfactory in other repeat units.

radical coupling product **8a** evidences the successful approach of the addition of  $\text{PbO}_2$  as (re)oxidizing agent.



**Figure 4.31:** a) Reaction pathway of the UV-light activated reaction between TEMPO functionalized PEG **8** and Irgacure 2959<sup>TM</sup> yielding the desired coupling product **8a** and the hydroxylamine species **11b**. b) Electro spray ionization mass spectra in the charge state  $z = 1$  for the reaction between TEMPO functionalized PEG **8** and a 5-fold molar excess of Irgacure 2959<sup>TM</sup> in acetonitrile at ambient temperature at  $t = 0$  (green line), after irradiation with a 311 nm UV broadband lamp for 60 minutes (red line), exposure to oxygen for 18 h and further 3 h exposure to 4.5 equivalents of  $\text{PbO}_2$  (with respect to TEMPO functionalized PEG **8**) (blue line) and additional irradiation for 60 minutes of the reaction mixture after filtration of the  $\text{PbO}_2$  depicting the zoom into one repeat unit. It should be noted that the agreement between theoretical and experimental  $m/z$  ratios is equally satisfactory in other repeat units.

The radical coupling reaction is considerably improved by employing the reoxidation of the hydroxylamine species **11b** with  $\text{PbO}_2$ ; furthermore the absence of additional side products is an extra advantage. Therefore, the model coupling reaction between TEMPO functionalized PEG **8** and Irgacure 2959<sup>TM</sup> was tested employing the same reaction conditions as before, yet with the oxidant  $\text{PbO}_2$  present in the solution evaluating the feasibility of *in situ* reoxidation of the hydroxylamine species **11b** toward the active starting material **8**. Figure 4.32 shows the - so far - most optimized version of the rad-

ical coupling of the TEMPO functionalized PEG **6** and Irgacure 2959<sup>TM</sup>. The irradiation time was reduced to 30 minutes, the excess of Irgacure 2959<sup>TM</sup> was reduced to a 3-fold molar excess and the PbO<sub>2</sub> was reduced to a 2-fold molar excess with respect to the TEMPO functionalized PEG **8**. Although, all reaction parameters were reduced, it can be noted that the radical coupling proceeds to a 100 % conversion with respect to the TEMPO functionalized PEG **8** and only a negligible amount of unidentified side product is formed. Performing the radical coupling with PbO<sub>2</sub> as an *in situ* (re)oxidizing agent dramatically improved the yield of the desired coupling product **8a**.

Due to toxicity of PbO<sub>2</sub>, a less toxic oxidizing agent - MnO<sub>4</sub> - was employed to test the *in situ* reoxidation of the hydroxylamine species **11b** toward the active TEMPO functionalized PEG **8**. Not only is MnO<sub>2</sub> less toxic, but also less active as an oxidizing agent than PbO<sub>2</sub>. Figure 4.33 depicts the ESI mass spectra of the reaction products after pre-determined irradiation times with the 311 nm UV lamp (green, red and blue line) and one ESI mass spectrum after 18 h exposure of the reaction mixture to air and MnO<sub>4</sub> (purple line). The coupling reaction did proceed (see red line), yet the coupling product **8a** appears to be prone to reoxidation to the starting material **8**, which reappears after 30 minutes to a significant amount (see blue line). The reoxidation seemed to proceed relatively fast, as 30 minutes after the addition of the oxidizing agent the starting material increases again (blue line). With exposure to air and MnO<sub>2</sub> for 18 h the degradation continued, as can be concluded by the increase of the peak intensity of the starting material (purple line).

Although, the effect of MnO<sub>4</sub> reoxidizing the coupling product **8a**, yet giving relatively pure conversion after 15 minutes, was interesting, it was not further investigated as the PbO<sub>2</sub> appeared to be more robust due to its overall very clean reoxidation reaction. Therefore, PbO<sub>2</sub> was employed as oxidizing agent of choice for polymer-polymer conjugation reactions between TEMPO functionalized PEG **8** and photoinitiator functionalized PEG **9**.

Before performing the polymer-polymer conjugations it appeared mandatory to assess whether the reverse process, i.e., equipping a polymer strand with a photoinitiating moiety and reacting it with a TEMPO species, would give the same result. Thus, the radical coupling reaction was also carried out employing the reaction between the photoinitiator functionalized PEG **9** and TEMPO molecules for investigating the inverted process. The photoinitiator functionalized PEG **9** was mixed with a 4-fold molar excess of TEMPO and after removing residual oxygen by four freeze-pump-thaw cycles, the reaction mixture was irradiated for pre-determined time intervals (40, 70, 240 minutes). Figure 4.34 depicts the resulting ESI mass spectra of the desired coupling product **9a** as well as unidentified side products. The green line shows the unreacted photoinitiator functionalized PEG **5** starting material at  $t = 0$ . Forty minutes later the starting material decreased to around 50 % of the starting amount as can be depicted from the red line in the Figure 4.34. Between 70 and 240 minutes the starting material disappeared

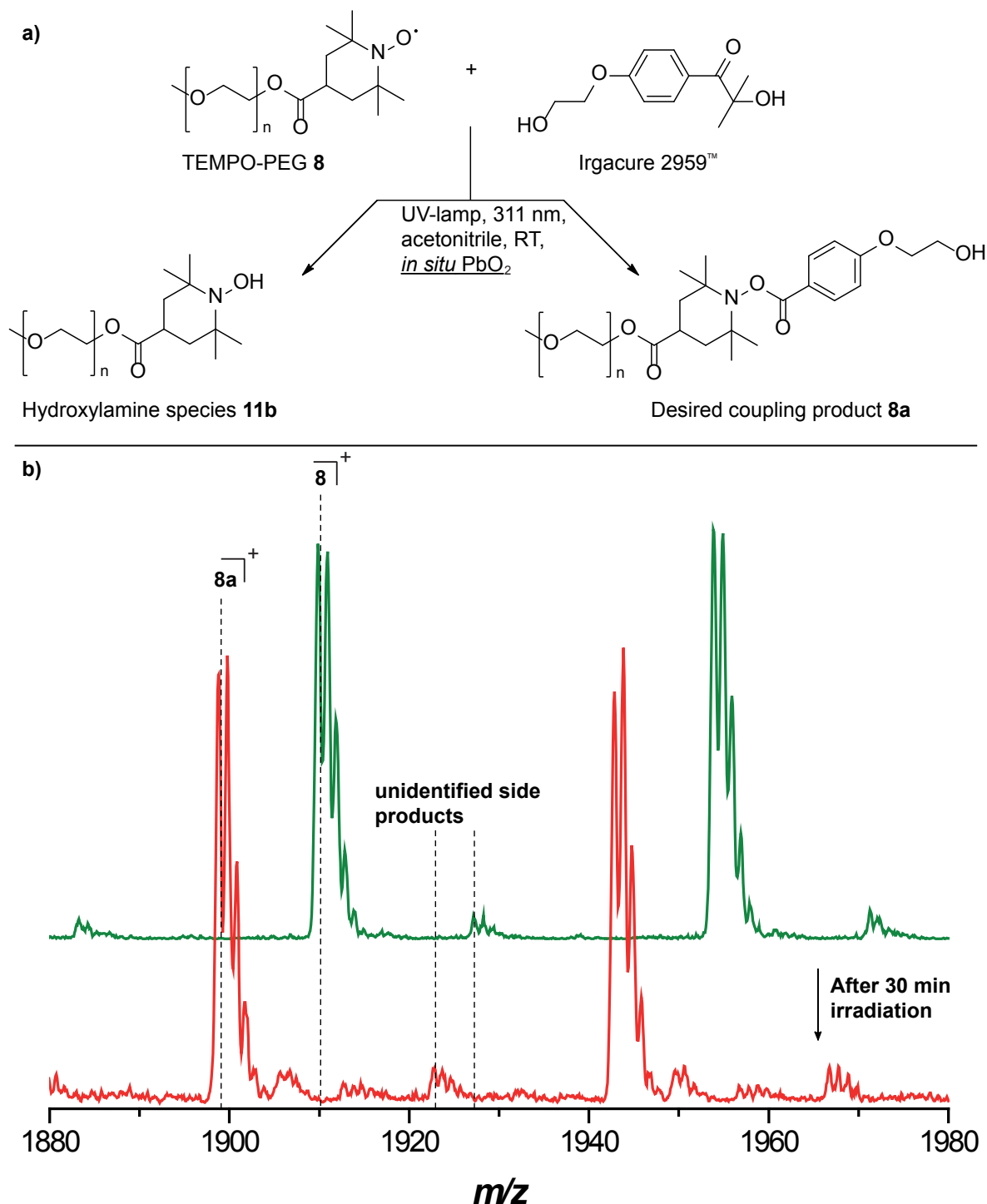


**Figure 4.32:** a) Reaction pathway of the UV-light activated reaction between TEMPO functionalized PEG **8** and Irgacure 2959<sup>TM</sup> yielding the desired coupling product **8a**. b) Electrospray ionization mass spectra in the charge state  $z = 1$  for the reaction between **8** and a 3-fold molar excess of Irgacure 2959<sup>TM</sup> and a 2-fold molar excess of PbO<sub>2</sub> in acetonitrile at ambient temperature after 30 minutes of irradiation with a 311 nm UV broadband lamp. It should be noted that the agreement between theoretical and experimental  $m/z$  ratios is equally satisfactory in other repeat units.

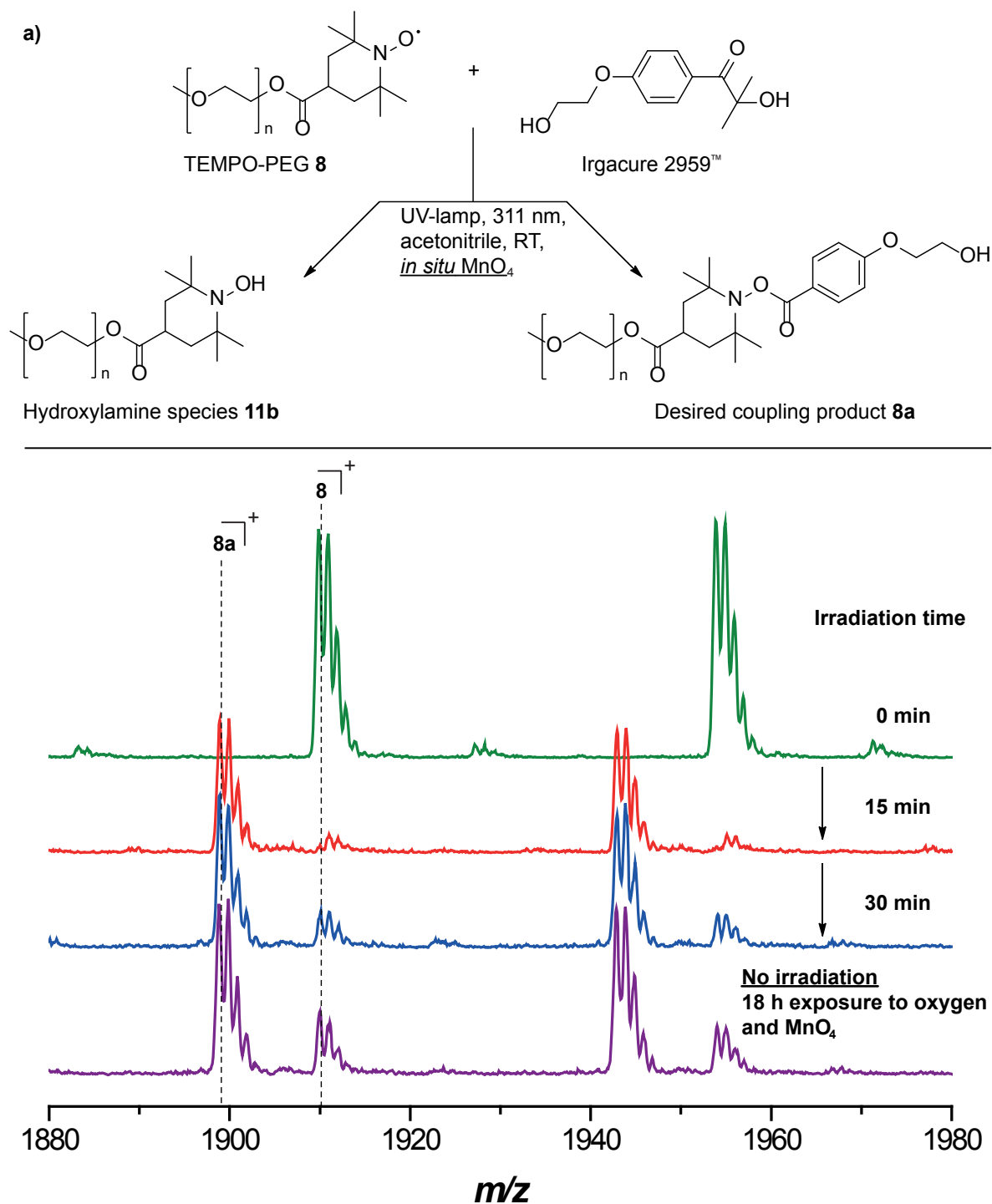


**Figure 4.33:** a) Reaction pathway of the UV-light activated reaction between TEMPO functionalized PEG **8** and Irgacure 2959™ yielding the desired coupling product **8a**. b) ESI mass spectra in the charge state  $z = 1$  for the reaction of the reaction between **8**, a 3.2-fold molar excess of Irgacure 2959™ and a 20-fold molar excess of MnO<sub>2</sub> in acetonitrile at ambient temperature after pre-determined irradiation intervals (15 and 30 min) with a 311 nm UV broadband lamp. It should be noted that the agreement between theoretical and experimental  $m/z$  ratios is equally satisfactory in other repeat units.

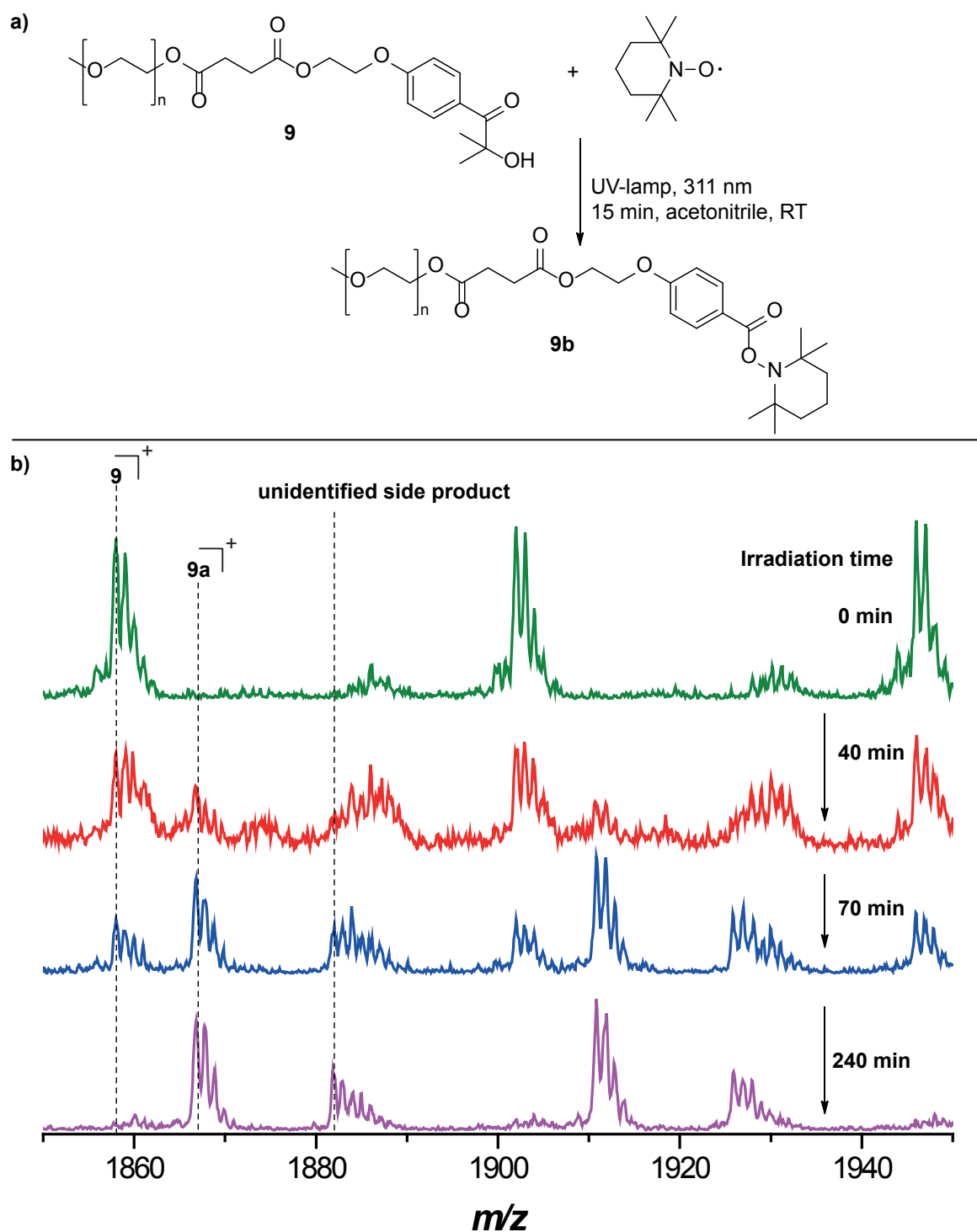
completely and beside the expected coupling product **9a** another unidentified product formed in quite large amounts. The comparison of the theoretical and experimental  $m/z$  values are depicted in Table 4.8.

**Table 4.8:** Theoretical and measured  $m/z$  ratios of the photoinitiator functionalized PEG products after irradiation in presence of TEMPO. It should be noted that the agreement between theoretical and experimental  $m/z$  ratios is equally satisfactory in other repeat units. The inset shows the overview of the spectrum.

Structure	[M + Na] <sup>+</sup>		
	$m/z^{\text{theo}}$	$m/z^{\text{exp}}$	$\Delta m/z$
<b>9</b>	1858.02	1858.00	0.02
<b>9a</b>	1867.02	1866.83	0.21
<b>unident.side product</b>	-	1881.80	-

Although a side product appeared in the coupling reaction of the photoinitiator functionalized PEG **9** with TEMPO, the reaction seemed to be promising for coupling reactions between two macromolecules. Hence, the next step was the coupling of TEMPO functionalized PEG **8** and photoinitiator functionalized PEG **9** with the aim to synthesize an AA-type block copolymer. A mixture of equimolar amounts of the two starting polymers **8** and **9** was prepared with a 3-fold molar excess of PbO<sub>2</sub>. The mixture was irradiated for pre-determined time intervals (15-45 minutes) and investigated with size exclusion chromatography coupled electrospray ionization mass spectrometry. Figure 4.35 depicts the time resolved ESI mass spectrum in the SEC region of the starting materials region as well as the SEC traces of the investigated materials.

On initial inspection of the spectrum in Figure 4.35 at  $t = 0$  (green line) there appears to be a discrepancy between the amount of starting materials, although equimolar amounts were employed. The discrepancy appears because the starting materials (**8** and **9**) are ionized with different efficiencies by the ESI source. Due to the higher polarity of the TEMPO functionalized PEG **8** the ionization is much better in comparison to the photoinitiator functionalized PEG **9** resulting in the different peaks heights. Unfortunately, there was always a small amount of unreacted TEMPO functionalized polymer visible in the ESI mass spectra, which could be due to the facts mentioned before in the NITEC coupling approach, i.e., end-group fidelity, non-equimolarity of the starting polymers and side reactions. Although starting material seems to be apparent in the SEC trace after the reaction, the radical coupling did proceed with high efficiency as can be gleaned from the blue SEC trace, which shows the situation of the block copolymer formation after 30 minutes irradiation time. There is only a small peak left in the starting material region, while most of the polymer chains underwent radical coupling. Thanks to employment of low molecular weight PEG ( $M_n = 2000 \text{ g mol}^{-1}$ ) as starting



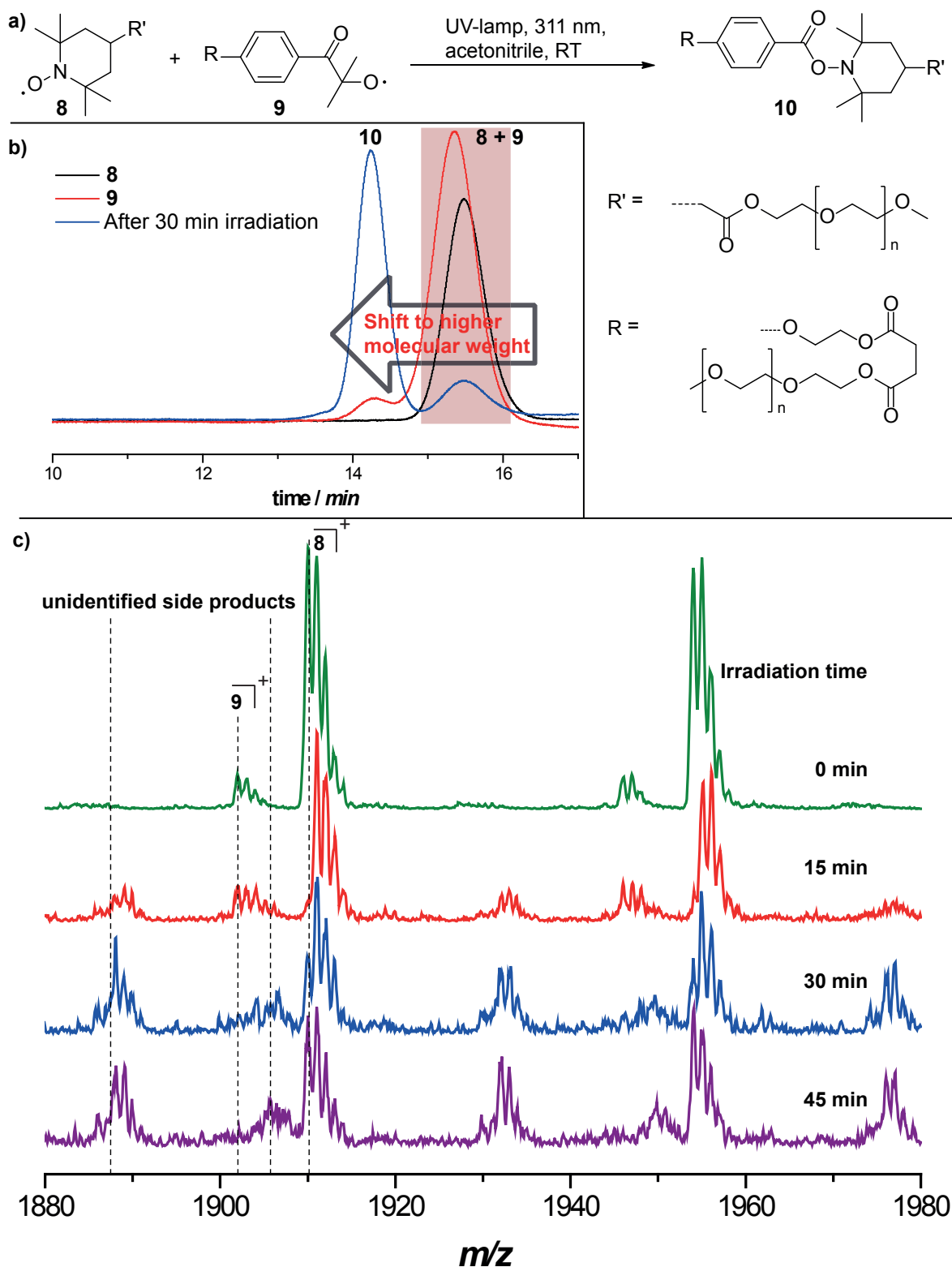


**Figure 4.35:** a) Reaction pathway of the UV-light activated reaction between TEMPO functionalized PEG **8** and Irgacure 2959<sup>TM</sup> functionalized PEG **9** yielding the desired coupling product **10**. b) SEC traces of the above mentioned reaction for  $t = 0$  and 30 min. c) Electrospray ionization mass spectra of the red highlighted starting materials SEC region (after pre-determined time intervals) in the charge state  $z = 1$  for the reaction between **8** and an equimolar amount **9** in acetonitrile at ambient temperature at pre-determined irradiation intervals with a 311 nm UV broadband lamp. It should be noted that the agreement between theoretical and experimental  $m/z$  ratios is equally satisfactory in other repeat units.

material, it was possible to gain a better insight on the molecular level and therefore the block copolymer region was investigated by SEC/ESI-MS. Figure 4.36 depicts the ESI-MS spectrum of the block copolymer region and SEC/ESI-MS shows also a comparison of the isotopic pattern of the radical coupling product **10** with a simulation of the isotopic pattern of **10**. There is a good agreement between the theoretical and experimental  $m/z$  ratios which underpins the proposed mechanism depicted in Figure 4.27. The comparison of the theoretical and experimental  $m/z$  values are depicted in Table 4.9.

**Table 4.9:** Theoretical and measured  $m/z$  ratios of the radical coupling product between the TEMPO functionalized PEG **8** and the photoinitiator functionalized PEG **9** after irradiation in presence of three-fold molar excess of  $\text{PbO}_2$ . It should be noted that the agreement between theoretical and experimental  $m/z$  ratios is equally satisfactory in other repeat units. The inset shows the overview of the spectrum.

Structure	$[\text{M} + 2 \text{Na}]^{2+}$		
	$m/z^{\text{theo}}$	$m/z^{\text{exp}}$	$\Delta m/z$
<b>10</b>	1920.59	1920.50	0.09

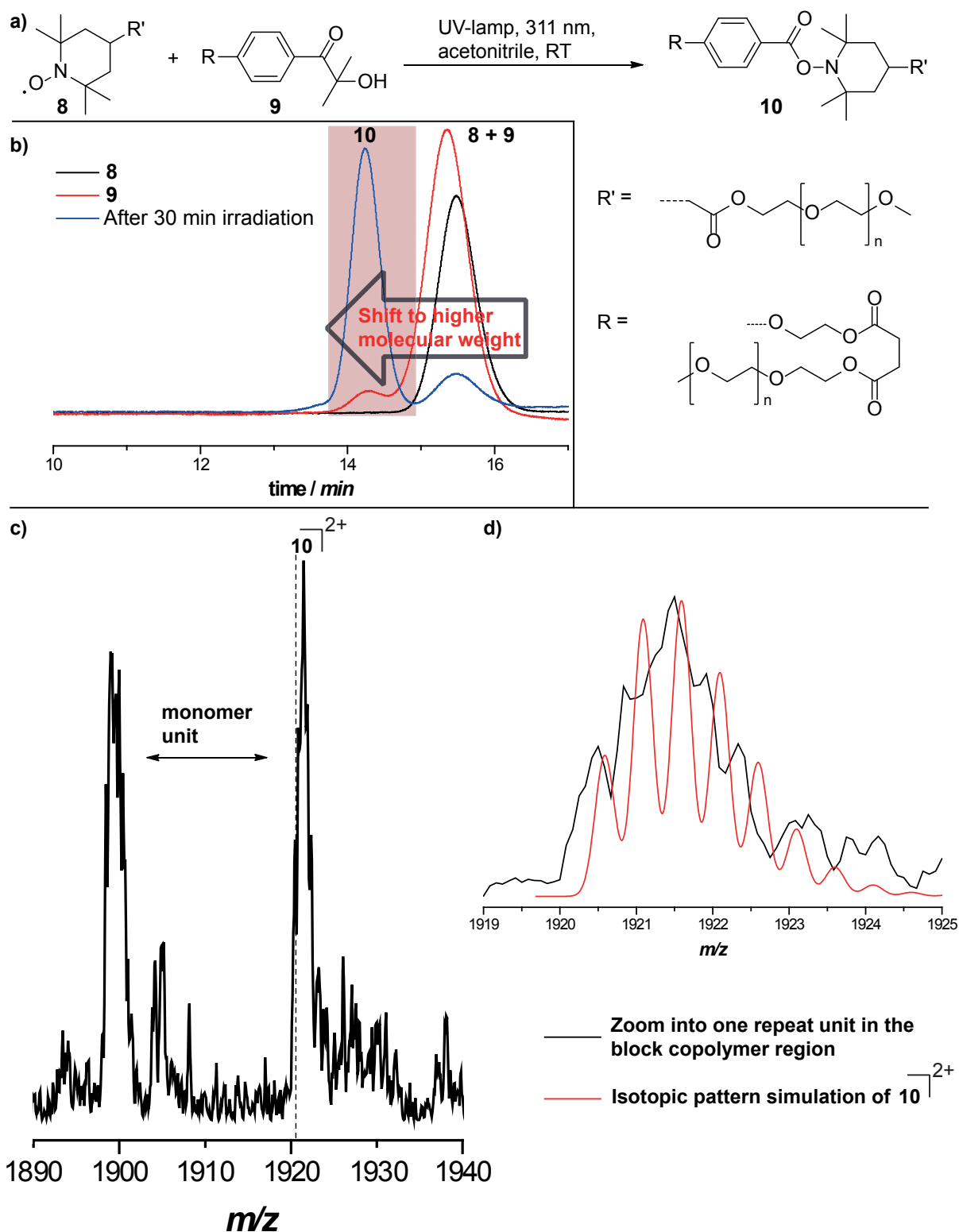


**Figure 4.36:** a) Reaction pathway of the UV-light activated reaction between TEMPO functionalized PEG **8** and Irgacure 2959<sup>TM</sup> functionalized PEG **9** yielding the desired coupling product **10**. b) SEC traces of the above mentioned reaction for  $t = 0$  and 30 min. c) ESI mass spectrum of the red highlighted block copolymer SEC region in the charge state  $z = 2$  for the reaction between **8** and an equimolar amount **9** in acetonitrile at ambient temperature after 30 minutes irradiation time with a 311 nm UV broadband lamp. It should be noted that the agreement between theoretical and experimental  $m/z$  ratios is equally satisfactory in other repeat units. d) Comparison of one repeat unit of the AA-type block copolymer with a simulated isotopic pattern for the specific repeat unit (Gaussian profile, resolution 0.3 Dalton, charge state  $z = 2$ ).

## 4.5 Conclusions and Outlook

In the current chapter, two different, yet both UV-light activated, conjugation systems were presented, i.e., the NITEC approach and the TEMPO/photoinitiator approach in an evaluation of their possibilities to be employed in synthetic polymer architecture design. Although both systems are UV-light activated, they differ in their chemical nature of conjugation. While the NITEC is driven by a 1,3-dipolar cycloaddition, the TEMPO/photoinitiator system operates *via* radical addition of a stabilized TEMPO radical toward an *in situ* generated carbon-centered radical. Both methods have been proven to work in the area of macromolecular coupling of small molecules as well as polymer conjugation for the synthesis of block copolymers. Yet, the herein presented coupling reactions are not fully optimized and there is potential for further optimization in yield as well as in reaction time. The great advantage of the tetrazole approach is the absence of a metal catalyst which makes it more attractive for biological systems than the TEMPO/photoinitiator approach which employs  $\text{PbO}_2$  as reagent. The conclusion of the herein presented coupling techniques are explained separately in detail in the following section.

### 4.5.1 The Nitrile Imine-mediated 1,3-Dipolar Cycloaddition of Tetrazole and Ene Coupling (NITEC) Approach for Block Copolymer Formation

One aim of the current chapter was the evaluation of the NITEC approach for applications, such as block copolymer formation in synthetic macromolecular chemistry. The model system consisted of a tetrazole functionalized PEG and a maleimide functionalized PEG which has been irradiated for different time intervals (5-25 min). The formation of the PEG-*b*-PEG block copolymer has been followed by size exclusion chromatography. After 25 minutes the formation of the block-copolymer was complete and only a small shoulder of low molecular weight PEG was visible in the SEC trace, which may be due to various effects, such as side reactions, non-perfect end-group fidelity, difficulties in preparing equimolar polymer solutions. The next step was the synthesis of an AB-type block copolymer which consisted of tetrazole functionalized PEG and maleimide functionalized pMMA. Although the block formation did not proceed in such a clean fashion as the AA-type block copolymer, the coupling reaction was overall successful with a small shoulder of unreacted starting material present in the reaction mixture. The reasons for the shoulder are the same as mentioned before for the AA-type block copolymer. It can be concluded that the NITEC approach shows great potential for more advanced applications in synthetic polymer architecture design. Further advantages of the presented conjugation reaction include its lack of metal catalysts, the fast reaction

time scale of the coupling, as well as the possibility of employing spatial resolution on surfaces due to the UV-light triggered initiation of the conjugation reaction. It has to be mentioned that the solvent in which such conjugations take place has to be chosen carefully. While the conjugation took place with high yields, the employment of small amounts ( $\leq 1$  vol.-%) of additional THF decreased the yield of the coupling product significantly. In order to reveal further potential of the herein presented NITEC, the next chapter combines the NITEC approach with heterogenous system grafting. Specifically, silicon wafers and biosurfaces are decorated with tetrazole moieties, which were subsequently irradiated in presence of functional polymers, such as pMMA or poly(2-(dimethylamino)ethyl methacrylate) (PDMAEMA), in order to alter the mechanical and chemical properties of the surface while leaving the bulk properties of the surface untouched. It has to be generally noted that, although the time scale of the NITEC is quite fast (overnight), the term *click*-type reaction should not be used unless further investigations and optimizations have been carried out.

#### 4.5.2 The TEMPO/Photoinitiator Conjugation Approach

The TEMPO/photoinitiator-approach is a new and innovative way in combining photografting and radical coupling into one method. The model system consisted of PEG functionalized with either a photoinitiator group or a stable TEMPO radical which were attached *via* esterification. The first coupling reactions were carried out between a polymer and a small molecule analogue to evaluate the coupling efficiency in detail and gain information about the reaction time scale and side products. A very important observation was the introduction of an oxidizing agent, which was found to increase the yield of the coupling product between the TEMPO functionalized PEG and the photoinitiator Irgacure 2959<sup>TM</sup>. The inverse system, consisting of a photoinitiator functionalized PEG and TEMPO molecules, generated potentially more side products, but generally the coupling reactions were also successful. Therefore, polymer-polymer conjugations were performed on the model system of TEMPO functionalized PEG and Irgacure 2959<sup>TM</sup> functionalized PEG resulting in AA-type (block co)polymers. Thanks to the experience in the TEMPO functionalized PEG and Irgacure 2959<sup>TM</sup> system, PbO<sub>2</sub> was employed as a oxidizing agent for the hydroxylamine species which is formed as a side product during the coupling reaction. The oxidizing agent ensured the reformation of the active TEMPO coupling species from its hydroxylamine species (see Figure 4.27 for details). Employing PbO<sub>2</sub>, a toxic substance, disqualifies the radical coupling from being a *click*-type reaction as well as for most biological applications. Although these drawbacks exist, the radical coupling reaction is innovative and affords the desired AA-type (block co)polymers. As the coupling reaction is at the beginning of its investigations, the conditions have to be optimized and future improvements may overcome the drawback of using a toxic oxidizing agent. Nevertheless, the TEMPO/photoinitiator approach

seemed to be promising for further investigations on surfaces. The following chapter makes use of the method established in the current chapter and exploits the presented technique forward to more advanced applications, such as grafting of functional polymers onto biosurfaces. Consequently, a biosurface (cellulose) was decorated with a photoinitiator and irradiated in presence of a TEMPO functionalized polymer with the aim to change the mechanical and chemical properties of the surface, while keeping the bulk properties unaffected.



# 5

## Tailored Modification of Biosurfaces

### 5.1 Introduction

Based on the results of the previous chapter which showed the successful polymer-polymer ligation by new conjugation techniques, namely the NITEC and the TEMPO/photoinitiator approach, these coupling reactions are now evaluated in the context of polymer grafting onto surfaces. Both techniques proved themselves as fast and atom-efficient reactions. The aim of the current chapter is the evaluation of both techniques for grafting polymer chains in heterogeneous media, specifically on biosurfaces. In order to change the surface properties of a bulk material, a viable technique is the application of a covalent polymer coating. A covalent coating is desirable to prevent its dissolution into any solvent the material could come in contact with. Polymer brushes<sup>281</sup> are a particular class of covalent coatings since they consist of chains individually linked to the substrate *via* only one chemical bond. To covalently graft polymers to a surface, material scientists have two options. They can either grow the macromolecules from the surface (*grafting from*), or synthesize the polymer beforehand and subsequently attach it *via* a chemical linkage (*grafting to*).<sup>170</sup> Both techniques have been explained in more detail in chapter 1. The first option has the advantage of being able to reach a high grafting density since steric hindrance is rather low (only small monomeric molecules are added). However, the second technique has the advantage of giving access to a full characterization of the polymer before its coating. In addition,

grafting-to processes can be more readily implemented in an industrial production setting. Potentially, the optimization of the chemical attachment of the polymer onto the surface (fast reaction time, high yield) can lead to a more efficient coverage of the surface. Several techniques have been established in the field of macromolecular science to fulfill such requirements. The combination of controlled/living radical polymerization (CRP)<sup>282</sup> and highly orthogonal and efficient conjugation reactions is a state-of-the-art example of precision chemistry giving control over material properties. In terms of CRP, nowadays the three main techniques consist of nitroxide-mediated polymerization (NMP),<sup>56</sup> atom-transfer radical polymerization (ATRP)<sup>15,19</sup> and the reversible addition-fragmentation transfer (RAFT) process<sup>224</sup> which are explained in detail in the introduction chapter 1. All these methods have been applied synergistically with the concepts of *click*-type reactions<sup>132</sup> to produce a powerful toolbox for synthesizing materials with tailored macromolecular architectures.<sup>136,144,198,283,284</sup> Numerous *click*-type reactions have already been applied to polymer chemistry and surface grafting.<sup>133,146,285-287</sup> A considerable fraction of the reported studies involves the use of a metal catalyst (copper or zinc). When working with biological systems, the use of these metal catalysts is predominantly prohibited due to their potential cytotoxicity.<sup>288-290</sup> Yet, some *click*-type reactions feature a light-triggered activation process, e.g., thiol-ene and thiol-yne radical additions when performed in the presence of a photoinitiator<sup>255,291</sup> or the recently reported UV-light triggered Diels-Alder reaction between 2,5-dimethylbenzophenone derivatives and maleimides.<sup>292,293</sup>

Recently, a new *click*-type reaction for selective functionalization of proteins, employing the NITEC was demonstrated by Lin *et al.* Starting with a tetrazole-containing compound, the reaction is initiated by UV-light irradiation.<sup>275</sup> Upon UV-light exposure, nitrogen is released from the molecule and a reactive nitrile imine moiety is formed *in situ* (see Figure 4.11 in chapter 4). Nitrile imines have been shown to readily undergo reactions with various electron-deficient and unactivated terminal alkenes and alkynes to form a stable pyrazoline-based covalent linkage.<sup>275,294,295</sup> The advantage of this method over other more established *click*-type reactions is the absence of metal catalyst, the fast reaction times and its bio-orthogonality. For instance, it was possible to modify a genetically engineered protein directly in *E. coli*.<sup>212</sup> or - even more impressively - stabilize the helical structure of a peptide by intramolecular NITEC-stapling.<sup>296</sup> For more in depth information about the NITEC see chapter 4. It is interesting to note that one of the latest additions to the variety of conjugation techniques was shown by Hansell *et al.*<sup>297</sup> The authors are employing tetrazines which can be coupled to norbornenes upon thermal activation standing as an example of the great importance of coupling techniques employing heterocycles as handles for macromolecular architecture design. Furthermore, the TEMPO/photoinitiator technique is evaluated within the current chapter. The general principle is shown in Figure 4.27 of chapter 4. The coupling reaction is initiated by UV-light irradiation to *in situ* generate carbon-centered radicals.

TEMPO functionalized polystyrene in the reaction mixture captures the free carbon-centered radical building a covalent bond between the photoinitiator and the TEMPO moiety.

The first part of the subsequent section covers the NITEC approach while the second part evaluates the TEMPO/photoinitiator approach for surface grafting.

## 5.2 Experimental

### 5.2.1 The Nitrile Imine-mediated 1,3-Dipolar Cycloaddition of Tetrazole and Ene Coupling (NITEC) Approach

#### Tetrazole functionalized silane 1

In a 10 mL round-bottom flask, carboxy-functionalized tetrazole (synthesis described in chapter 4) (100 mg, 39  $\mu\text{mol}$ ), APTS (85 mg, 385  $\mu\text{mol}$ ), and DMAP (6 mg, 49  $\mu\text{mol}$ ) were dissolved in dry DCM (3 mL) to give solution A. A solution of DCC (95.3 mg, 462  $\mu\text{mol}$ ) in dry DCM (2 mL) was added dropwise to solution A. The reaction mixture was stirred for 18 h at ambient temperature. Urea was removed *via* filtration and the solvent removed under reduced pressure. The raw product was purified by column chromatography with cyclohexane and ethyl acetate as mobile phase (1:1) to give the tetrazole-functionalized silane as a red solid (65 mg, 35 %). The  $^1\text{H}$  NMR spectrum is shown in Figure 5.1.  $^1\text{H}$  NMR (400 MHz,  $\text{CDCl}_3$ , 25  $^\circ\text{C}$ ):  $\delta$  0.74 (t, 2H,  $J = 7.5$  Hz, - $\text{CH}_2\text{-Si}$ ), 1.23 (t, 9H,  $J = 7.0$  Hz, - $\text{CH}_3$ ), 1.76-1.83 (m, 2H, - $\text{CH}_2\text{-CH}_2\text{-CH}_2$ ), 3.51 (m, 2H, - $\text{NH-CH}_2$ ), 3.84 (q, 2H,  $J = 7.0$  Hz, - $\text{CH}_2\text{-CH}_3$ ), 6.69 (t, 1H,  $J = 5.4$  Hz, - $\text{NH}$ ), 7.52 (m, 1H, - $\text{CH-CH-CH-CN-}$ ), 7.59 (m, 2H, - $\text{CH-CH-CH-CN-}$ ), 7.94 (m, 2H, - $\text{CH-CH-CH-CN-}$ ), 8.21 (m, 2H, - $\text{C-CH-CH-CO-}$ ), 8.33 (m, 2H, - $\text{C-CH-CH-CO-}$ ).

#### Maleimide-pMMA 2

The synthesis has been described in chapter 4.

#### Maleimide functionalized poly((2-dimethylamino)ethyl methacrylate) (PDMAEMA) 3

In a 25 mL round-bottom flask, DMAEMA (3.722 g, 23.7 mmol), Fur-Mal-ATRP (0.207 g, 0.6 mmol), and bpy (0.183 g, 1.2 mmol) were dissolved in toluene (4.83 g). The mixture was deoxygenated by purging with nitrogen for a period of 40 min and added *via* cannula to a Schlenk tube containing CuBr (0.0852 g, 1.27 mmol) which had previously

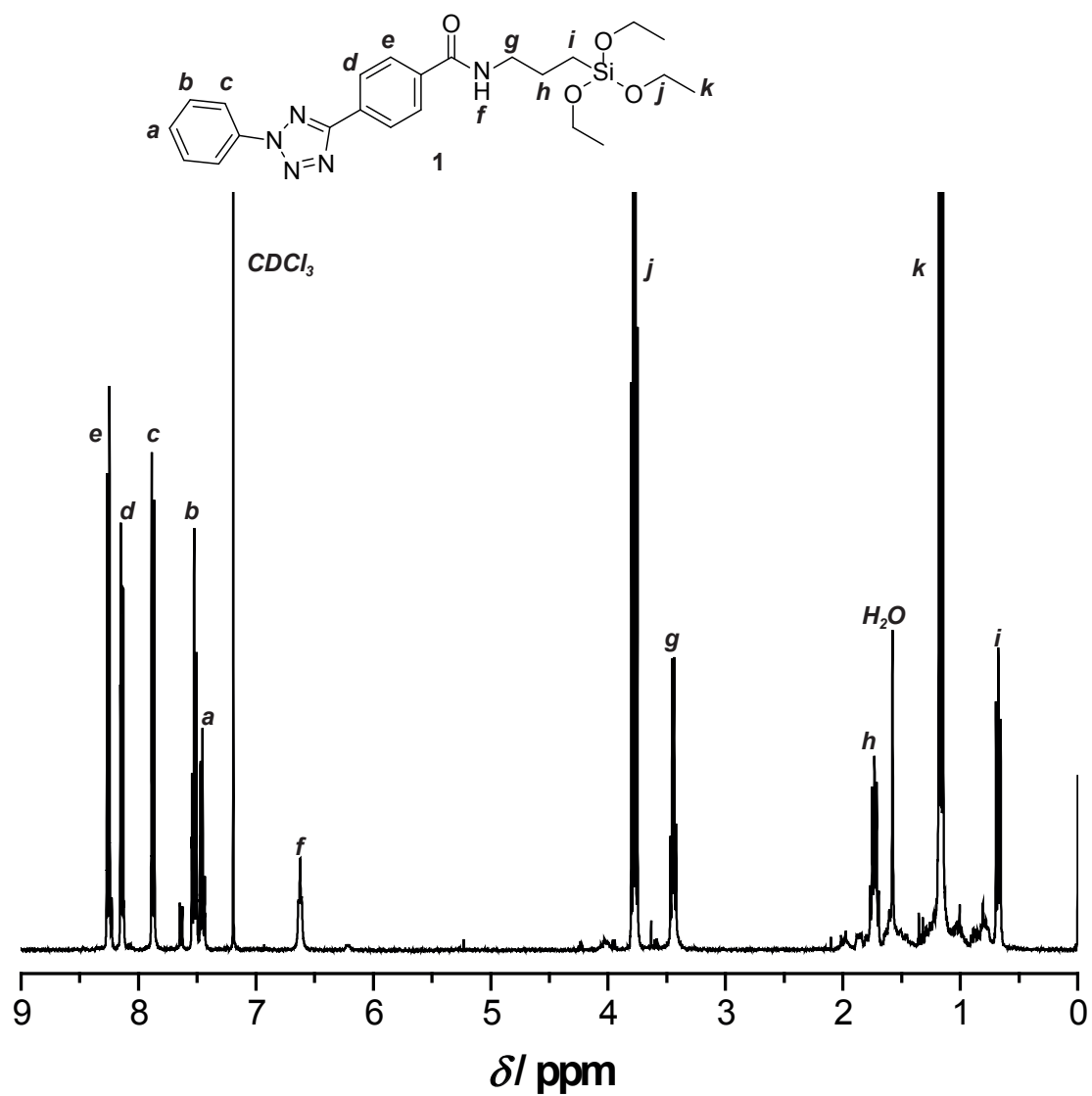
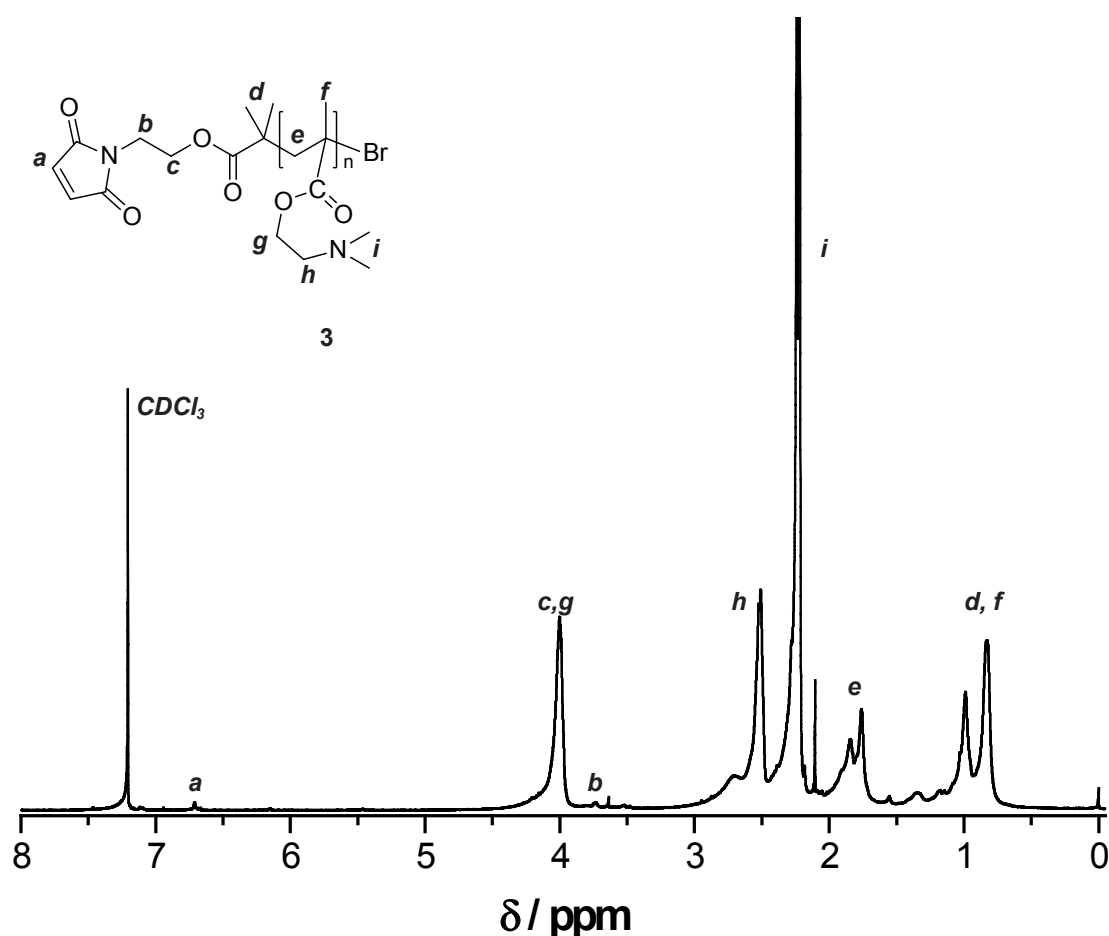


Figure 5.1: 400 MHz <sup>1</sup>H NMR spectrum of the tetrazole-functionalized silane 1 in dms0-d6.

been evacuated and backfilled with nitrogen three times. The tube was immediately immersed into an oil bath pre-heated to 70 °C. After 130 min, the polymerization was stopped by cooling to ambient temperature and exposure to air (36 % conversion). The monomer/polymer mixture was passed through a short plug of basic alumina to remove the copper catalyst (flush with THF). The solution was concentrated under vacuum and the polymer recovered by precipitation in *n*-hexane (1.259 g, SEC/DMAc:  $M_n = 6100 \text{ g mol}^{-1}$ ,  $PDI = 1.4$ ). The maleimide end-group was deprotected by refluxing the polymer in toluene ( $0.1 \text{ g L}^{-1}$ ) at 120 °C during 12 h. After evaporation of the solvent, the product was redissolved in a minimal amount of acetone. The maleimide functionalized **3** was obtained as a viscous orange oil after precipitation in *n*-hexane (1.019g). The  $^1\text{H}$  NMR spectrum is shown in Figure 5.2.



**Figure 5.2:** 400 MHz  $^1\text{H}$  NMR spectrum of maleimide functionalized PDMAEMA **3** in  $\text{CDCl}_3$ .

#### Quaternized maleimide functionalized poly((2-dimethylamino)ethyl methacrylate) (PDMAEMA) **4**

In a 50 mL round-bottom flask, **3** (0.599 g, 0.10 mmol) was dissolved in ethanol (12 mL) and bromoethane (0.32 mL, 4.29 mmol) was added. The mixture was stirred for 2

days at 40 °C. Residual bromoethane and ethanol were removed under reduced pressure. The quaternized polymer **4** was obtained as an orange-pink powder (0.769 g). The  $^1\text{H}$  NMR spectrum is shown in Figure 5.3.

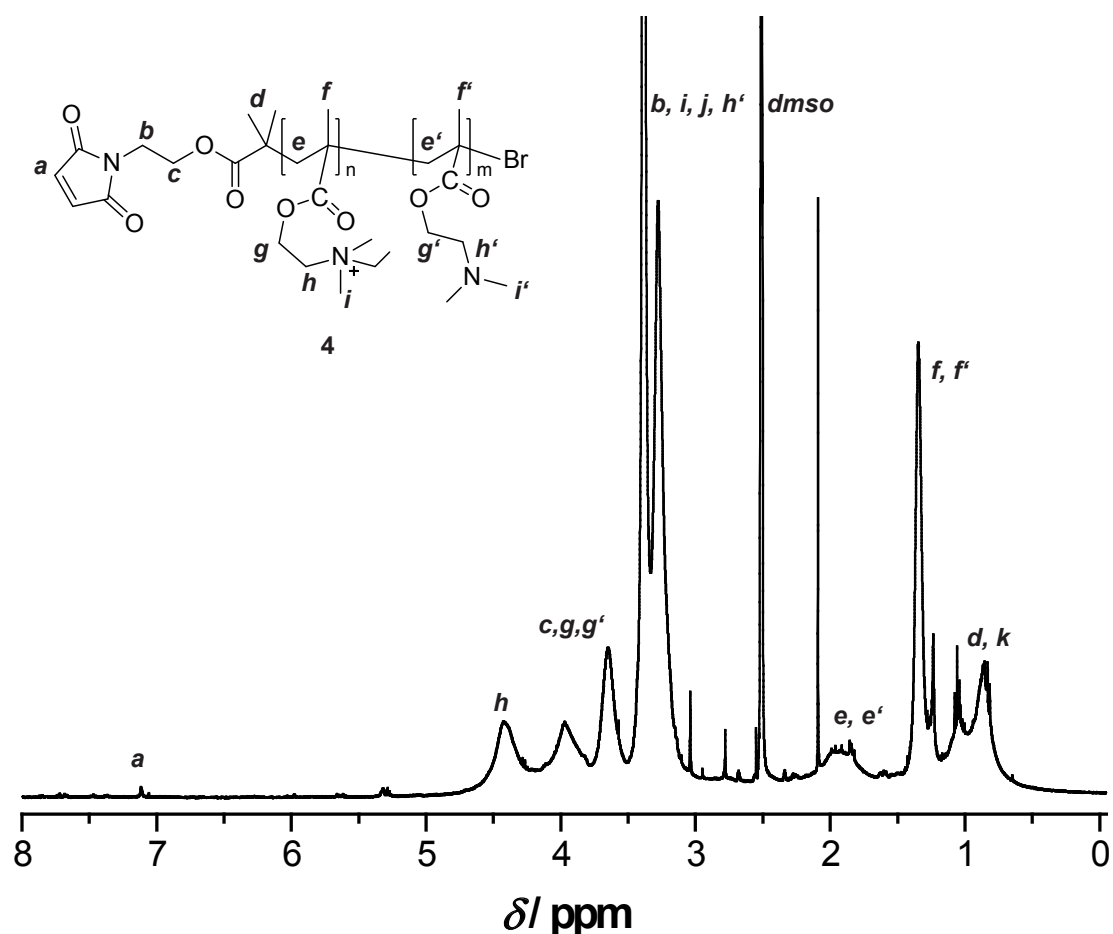


**Figure 5.3:** 400 MHz  $^1\text{H}$  NMR spectrum of quaternized maleimide functionalized PDMAEMA **4** in  $\text{CDCl}_3$ .

### Functionalization of silicon wafers with tetrazole **7**

Prior to surface functionalization, the silicon wafers (p-type, boron doped (100) from Siltron INS Korea) were activated by immersion in piranha solution ( $\text{H}_2\text{SO}_4$  95 %/ $\text{H}_2\text{O}_2$  35 % 2:1 vol/vol) at 100 °C for one hour. Caution: **piranha solution is an extremely strong oxidant and should be handled very carefully!**

After extensive rinsing with deionized water, the wafers were dried under a stream of nitrogen. Three activated wafers ( $0.8 \times 0.8$  cm) were subsequently placed in a 10 mL round-bottom flask containing a solution of silane functionalized tetrazole in dry toluene (10 mg in 2 mL). The flask was heated to 50 °C for 2 h and subsequently at ambient temperature for a further 15 h, after which the wafers were rinsed thoroughly with fresh toluene and sonicated for 15 min in toluene and an additional 5 min in acetone.

The wafers were finally dried in a stream of nitrogen. The characterization is shown in the results and discussion section.

### Functionalization of silicon wafers with pMMA 8

The wafers were introduced into separate quartz cuvettes containing a solution of **2** (25 mg) in ethanol (1 mL) and placed directly in front of a hand-held UV-lamp (254 nm with 8 W output). The wafers were irradiated for 15 min and left in the reaction mixture for further 60 min to obtain full conversion (see chapter 4). Before analysis, the pMMA functionalized silicon wafers were extensively rinsed with fresh ethanol and acetone. For the control experiments, either no polymer was present or no irradiation was performed. The characterization is shown in the results and discussion section.

### Functionalization of cellulose with tetrazole 9

Cellulose consists of D-glucose units joined together by  $\beta$ -1,4-linkages. In their native state, cellulose chains feature strong intermolecular hydrogen bonding due to the hydroxyl groups on the main chain. Prior to surface modification, cellulose substrates were thus subjected to a pretreatment: The cellulose sheets were immersed in an aqueous solution of 10 wt-% NaOH to break down the extensive hydrogen bonding between the OH groups and to open up the ordered regions so that the reagents can penetrate more readily into the cellulose substrate and render it accessible for further modification. The cellulose sheets were subsequently washed thoroughly with ethanol, DCM, and finally with dry DCM. Prior to the reaction with cellulose, the carboxy-functionalized tetrazole was turned into its more reactive acyl chloride counterpart: Carboxy-functionalized tetrazole (110 mg, 0.41 mmol) was dissolved in dry DCM (10 mL) with a catalytic amount of dry DMF, oxalyl chloride (140  $\mu$ L, 1.63 mmol) was added dropwise and reacted overnight. After the reaction the excess of oxalyl chloride was removed employing reduced pressure. The acid chloride-functionalized tetrazole was redissolved in dry DCM (2 mL) and added dropwise to a suspension of freshly NaOH-treated cellulose (3 pieces, 0.8  $\times$  1.5 cm each) in dry DCM (5 mL) containing DMAP (26 mg, 0.21 mmol) and DIPEA (0.7 mL, 4.02 mmol). After overnight reaction, the functionalized cellulose was washed extensively with ethanol, acetone and DCM and finally stored in pure ethanol under exclusion of light.

### Functionalization of cellulose with polymer 10

The pieces of cellulose were placed into separate quartz cuvettes containing a solution of **2**, **3**, or **4** (20 mg) in ethanol (1 mL). The samples were irradiated for 10 min (hand-held UV-lamp (254 nm with 8 W output)) on each side of the cellulose sheets and left to

stand in the solution for another 50 min for achieving complete conversion (see chapter 4). Eventually the cellulose samples were rinsed extensively with ethanol, acetone and water before being dried overnight in a vacuum oven at 40 °C. For the control experiments, either no polymer was present or part of the samples were protected from irradiation (masking technique).

## 5.2.2 The TEMPO/Photoinitiator Conjugation Approach

### Hydroxyl functionalized polystyrene *via* ATRP mediated polymerization 11

The synthesis of the hydroxyl functionalized polystyrene was carried out according to a modified procedure published by Wolf *et al.*<sup>215</sup> The polymerization was carried out using HBMP (267 mg, 1.26 mmol), PMDETA (203 mg, 1.17 mmol), styrene (10 g, 100 mmol) and CuBr (168 mg, 1.17 mmol). The mixture was heated to 80 °C for 2 h. The polymerization was stopped by exposure to air and cooling to ambient temperature. After passing through a short column of alumina, the hydroxyl functional polymer was purified by precipitation in cold methanol (SEC/THF:  $M_n = 3900 \text{ g mol}^{-1}$ ,  $PDI = 1.09$ ).

### TEMPO functionalized polystyrene (PS) 12

Hydroxyl functionalized polystyrene **8** (750 mg, 0.19 mmol), 1-oxyl-4-carboxyl-2,2,6,6-tetramethylpiperidine (see chapter 4 for synthesis) (150 mg, 0.75 mmol) and DMAP (62 mg, 0.5 mmol) were dissolved in dry DCM (5 mL) to give solution A. DCC (235 mg, 1.13 mmol) dissolved in dry DCM (2 mL) was added dropwise to solution A at ambient temperature. The urea was removed by filtration and the TEMPO functionalized PS **8** was purified by precipitation in cold methanol (two times) (SEC/THF:  $M_n = 3800 \text{ g mol}^{-1}$ ,  $PDI = 1.09$ ). It has to be noted that in general GPC values exhibit typically an error of  $\pm 10 \%$ , explaining the discrepancy of polymer **12** being smaller than polymer **11**. The success of the reaction was evidenced by  $^1\text{H}$  NMR spectroscopy. Due to paramagnetism of the free nitroxide radical, direct analysis is not possible due to line widening of the individual peaks. To overcome this problem, phenylhydrazine was added (50  $\mu\text{L}$  for 20 mg of **12**) to reduce the free nitroxide *in situ* into the hydroxyl amine species (see Figure 5.4. The molecular weight calculated *via*  $^1\text{H}$  NMR end-group analysis - with reference to peak *d* - was determined to be  $3300 \text{ g mol}^{-1}$ , which is in reasonable agreement with the before reported SEC analysis ( $3900 \text{ g mol}^{-1}$ ).

### Functionalization of cellulose with photoinitiator 13

Pretreatment of cellulose has been performed in the same fashion as explained for the functionalization of cellulose with tetrazole **9**. The esterification of cellulose with

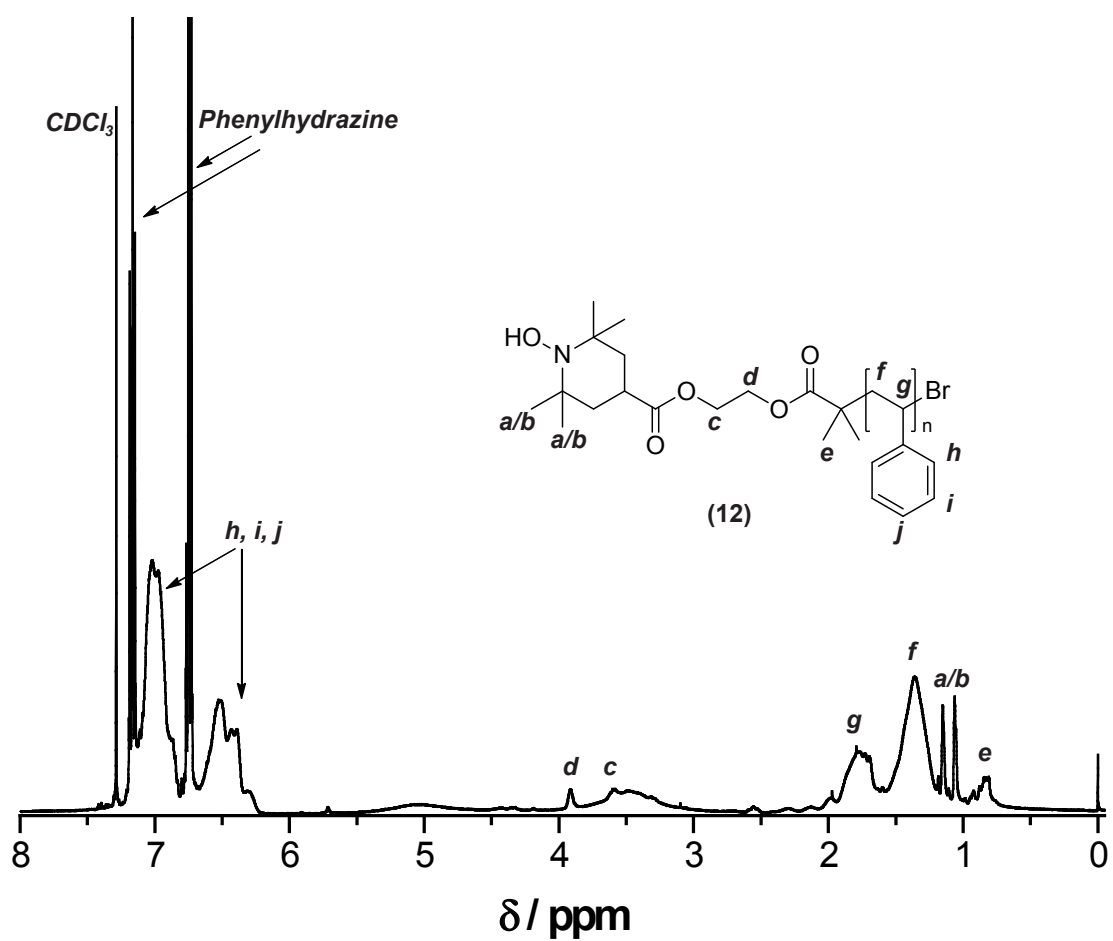


Figure 5.4: 400 MHz  $^1\text{H}$  NMR spectrum of TEMPO functionalized polystyrene **12** in  $\text{CDCl}_3$ .

the carboxy modified photoinitiator Irgarcure 2959<sup>TM</sup> (see compound No. 4 in chapter 4) was performed employing *Steglich* esterification conditions. Cellulose pieces (3 pieces, 0.8 × 1.5 cm each), DMAP (130 mg, 1.06 mmol) and 4-(2-(4-(2-hydroxy-2-methylpropanoyl)phenoxy)ethoxy)-4-oxobutanoic acid (430 mg, 1.27 mmol) (synthesis described in chapter 4) were dispersed in dry DCM (5 mL). DCC (500 mg, 2.42 mmol) was dissolved in dry DCM (5 mL) and added dropwise to the dispersed cellulose at ambient temperature. The reaction was stopped after 12 h and the cellulose was thoroughly rinsed with DCM, acetone and finally washed with toluene and stored in toluene under the exclusion of light at ambient temperature.

### Functionalization of cellulose with polymer 14

The photoinitiator functionalized cellulose **13** was put upright in a glass vial and completely covered by a solution of **12** (46 mg, 0.012 mmol) in toluene (10 mL) and placed in front of the UV-lamp (maximum emission between 300-320 nm and 36 W output) at a distance of 3 cm.

## 5.3 Results and Discussion

The results and discussion section is divided according to the employed techniques for better clarity.

### 5.3.1 The Nitrile Imine-mediated 1,3-Dipolar Cycloaddition of Tetrazole and Ene Coupling (NITEC) Approach

#### Grafting polymers onto silicon wafers

After the successful coupling of two telechelic polymer chains, the grafting of functional polymers onto surfaces was examined. Initially, silicon wafers were chosen as the substrate due to their ease of characterization with techniques such as X-ray photoelectron spectroscopy (XPS). In achieving the functionalization of a surface, a tetrazole functionalized silane was synthesized in view of a covalent attachment to the surface of the wafers (see Figure 5.5).

The functionalization was realized by heating a cleaned and activated silicon wafer in a tetrazole functionalized silane solution, yielding a polysiloxane multilayer coating with covalently bound tetrazole moieties. The tetrazole functionalized silicon wafer **7** was cleaned extensively after the reaction by rinsing with fresh solvent and ultrasonification to remove any physisorbed tetrazole functionalized silane from the surface. Figure

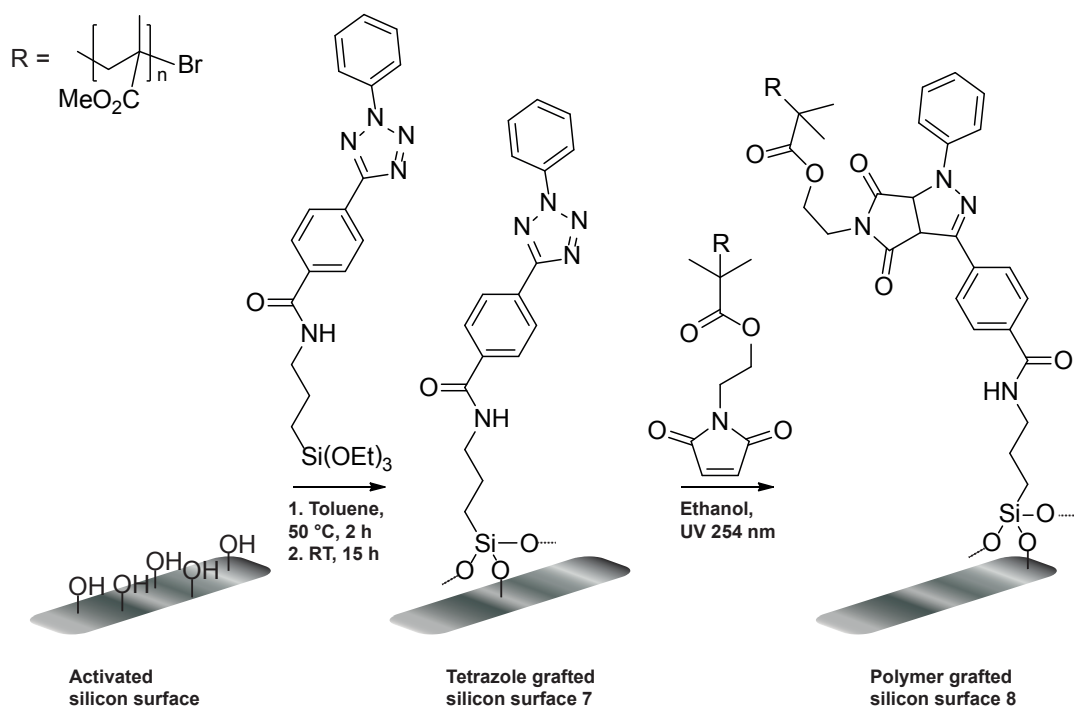


**Figure 5.5:** Synthetic route for the formation of polymer-grafted silicon wafers *via* the NITEC approach.

5.6a displays the C 1s and N 1s regions of the XPS spectra of the silicon wafer after tetrazole functionalization. The spectra were normalized to the peak with the highest intensity. The main peak in the C 1s spectrum at 285.0 eV is assigned to saturated carbon atoms (C-C, C-H) and is employed as a reference to compare the evolution of the different carbon species present on the surface. The peak at 286.7 eV is assigned to carbon atoms involved in various single bonds with oxygen and nitrogen (C-O, C-N), while the peak at 288.6 eV is assigned to the carboxyl group (-O-C=O).<sup>298,299</sup> The N 1s spectrum shows a strong peak at 400.4 eV which can be assigned to the tetrazole species (-N=N-)<sup>300</sup> while the additional weak N 1s component at 402.4 eV (probably positively charged nitrogen) cannot be assigned unambiguously.<sup>301</sup> The assignments are valid for all investigated silicon wafer samples. Moreover, well-defined peaks in the C 1s region reveal the presence of carbonyl-containing moieties on the surface. Figure 5.7 depicts a comparison between the theoretical atomic concentrations of tetrazole functionalized silicon wafers with experimental XPS data extracted from the spectrum shown in Figure 5.6a, which are in good agreement. It has to be noted that wet analysis compared to surface analysis is far more difficult and more prone to contaminations due to the sensitivity of the surface analysis technique, i.e., XPS. Nitrile imines have mostly been considered as transient intermediates and are not easy to observe.<sup>302-304</sup> It has already been shown that a nitrile imine very similar in structure to the one generated in the present study can be trapped by nucleophilic addition of ethanol or water to form a hydrazone or a hydrazide, respectively.<sup>305,306</sup> To assess the possibility of this side reaction,

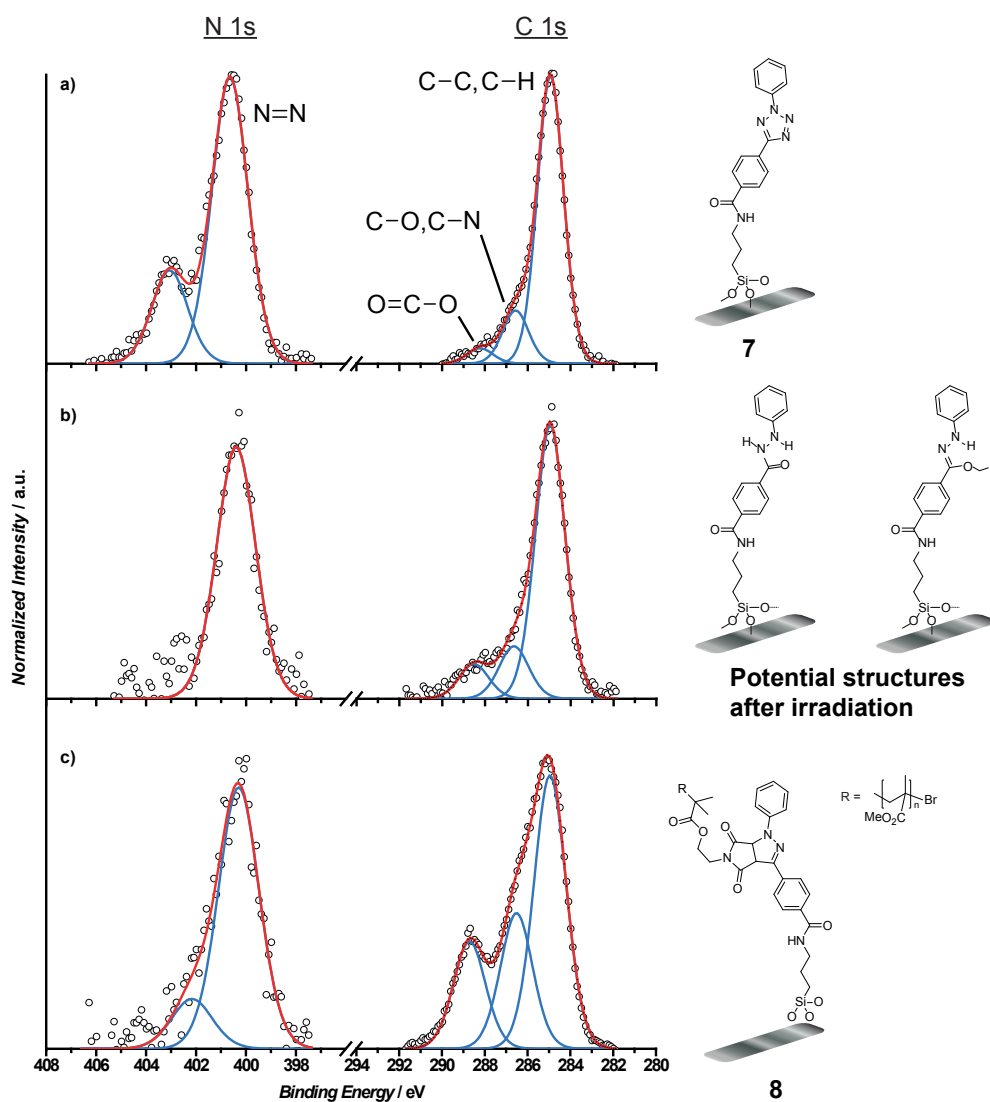
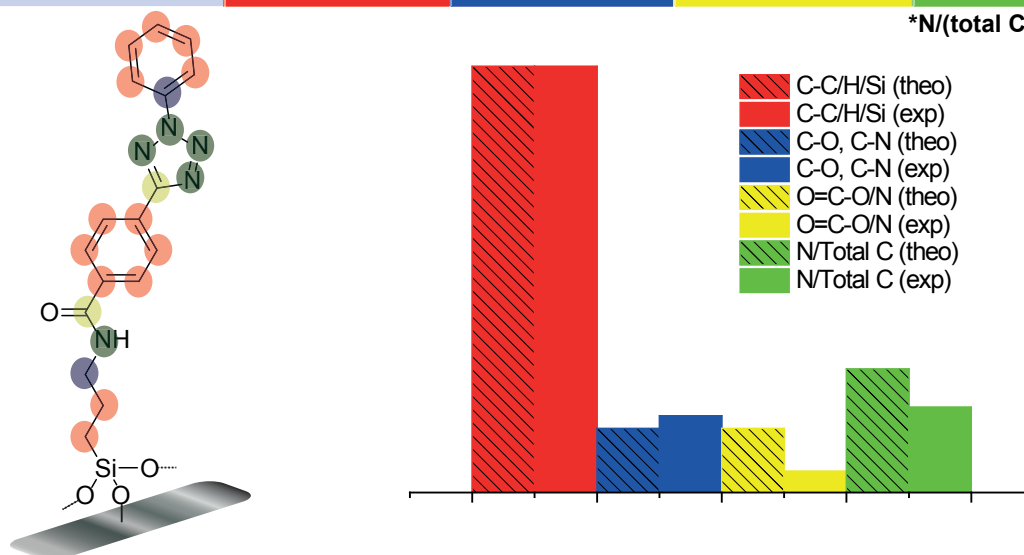


**Figure 5.6:** Comparison of the C 1s (280-294 eV) and N 1s (396-408 eV) normalized peaks in the XPS spectra of 7 (a), 7 irradiated for 15 min at 254 nm in ethanol (b) and 8 (c). All spectra are normalized to maximum intensity.

	C-C/H/Si	C-O, C-N	O=C-O/N	N1s
Tet. funct. Wafer 7 theor.	13	2	2	5
Tet. funct. Wafer 7 theor. normalized	1.00	0.15	0.15	0.29*
Tet. funct. Wafer 7 exp.	1.00	0.18	0.05	0.20*

\*N/(total C)



**Tetrazole functionalized silicon wafer 7**

**Figure 5.7:** Comparison of theoretical atomic concentrations of tetrazole functionalized silicon surface with experimental XPS data extracted from Figure 5.6a. The spectra were normalized to C-C/H/Si (285.0 eV). The bar chart is a visualization of the above shown table.

7 was irradiated in ethanol in absence of any dipolarophile (see Figure 5.6b). The XPS results are in rather good agreement with the assumption that these reactions do occur as can be depicted from Figure 5.8 and Figure 5.9 which show a theoretical comparison between the assumed structures and the experimental XPS data extracted from Figure 5.6b. For a constant carbon concentration, the nitrogen content is more than halved while the concentration of heteroatom-bound carbon slightly increases after irradiation of 7 in ethanol.

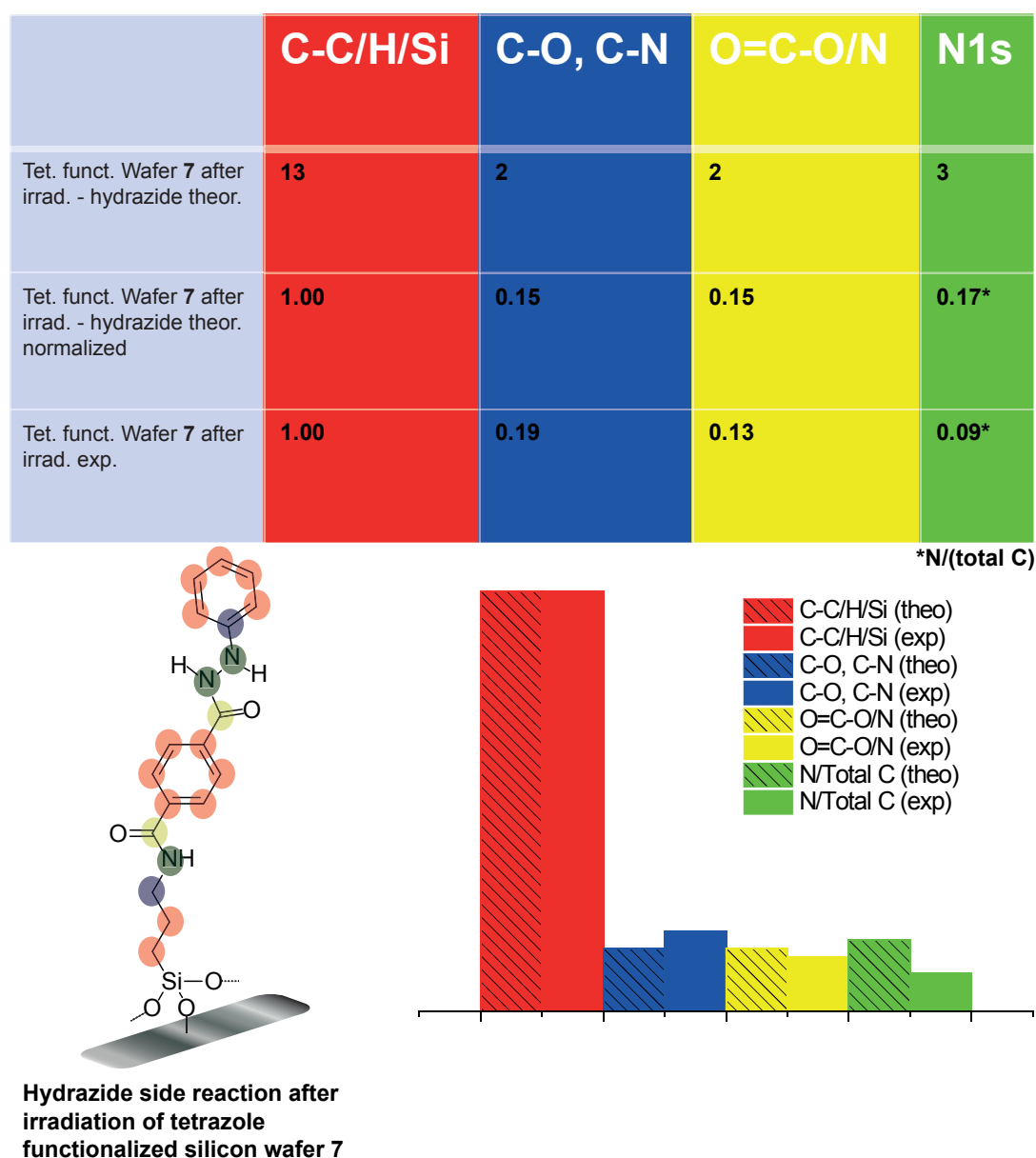
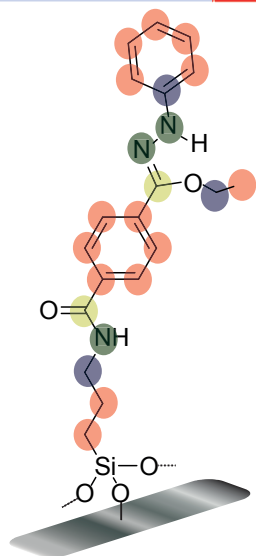


**Figure 5.8:** Comparison of theoretical atomic concentrations of tetrazole functionalized silicon surface transferred into a hydrazide species with experimental XPS data extracted from Figure 5.6b. The spectra were normalized to C-C/H/Si (285.0 eV). The bar chart is a visualization of the above shown table.

To graft a maleimide-functionalized polymer, a similar methodology as described before for the block copolymer formation (see chapter 4) was employed for the NITEC

	C-C/H/Si	C-O, C-N	O=C-O/N	N1s
Tet. funct. Wafer 7 after irradi. - hydrazone theor.	14	3	2	3
Tet. funct. Wafer 7 after irradi. - hydrazone theor. normalized	1.00	0.21	0.14	0.21*
Tet. funct. Wafer 7 after irradi. exp.	1.00	0.19	0.13	0.09*

\*N/(total C)



**Hydrazone side reaction after irradiation of tetrazole functionalized silicon wafer 7**

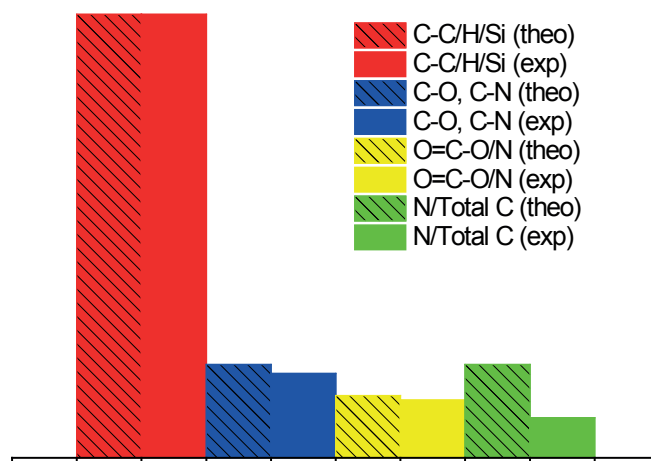


**Figure 5.9:** Comparison of theoretical atomic concentrations of a hydrazone species deriving from tetrazole functionalized silicon surface with experimental XPS data extracted from Figure 5.6b. The spectra were normalized to C-C/H/Si (285.0 eV). The bar chart is a visualization of the above shown table.

reaction on the silicon surface. A tetrazole functionalized silicon wafer **7** was placed in a solution of **2** in ethanol, irradiated for 15 min and left to stand in the polymer solution for a further 45 min for achieving complete conversion (see chapter 4). The sample was investigated by XPS after extensive rinsing with fresh solvent (see Figure 5.6c). In comparison with the unreacted tetrazole-containing wafer **7** (Figure 5.6a), **8** contains 2.8-fold saturated and unsaturated carbon atoms and 7.8-fold greater amounts of carbons atoms bound to a nitrogen or an oxygen atom. The result of this investigation evidences the presence of the methacrylic polymer **2** on the surface. The magnitude of the increase for these particular XPS signals is in the range expected for a close to quantitative grafting. Figure 5.10 depicts a comparison between theoretical atomic concentrations of pMMA grafted silicon wafers with experimental XPS data extracted from the spectrum shown in Figure 5.6c, which are in good agreement. However, the expected bromine content is below the detection limit of XPS and it is impossible to distinguish between nitrogen attributed to tetrazole and imide/amide, respectively.<sup>307</sup>

Compared to unmodified silicon wafers or control experiments where either the tetrazole or the polymer was missing, the overall spectrum shows a decrease in surface silicon content (divided by 4) due to the formation of a thicker hydrocarbon layer on the surface and corroborates the success of the surface functionalization (not shown). The results, although no quantification of the grafting density can be given, strongly evidence the successful grafting of pMMA onto tetrazole functionalized silicon wafers.

### Grafting of polymers onto cellulose

Due to the successful grafting of pMMA onto silicon wafers, further investigation of the presented functionalization technique was performed on a more complex system. Cellulose was chosen as a wide-range-application biosubstrate. Cellulose membranes were immersed in a 10 wt-% sodium hydroxide solution to break down the extensive hydrogen bonding due to the numerous hydroxyl groups and to open any crystalline regions in order to increase the availability of these free hydroxyl groups at the surface (Cel-OH). The carboxy-containing tetrazole previously used for the synthesis of **1** was covalently bound to the cellulose *via* esterification of the primary alcohol present on the repeating sugar unit to give tetrazole functionalized cellulose **9** (see Figure 5.11). After thorough rinsing, the tetrazole functionalized cellulose **9** was analyzed by XPS (see Figure 5.12).

Contrary to silicon wafers, cellulose is a fibrous material and is thus intrinsically heterogeneous. Consequently, when the surface modification consists in the grafting of a small molecule, it is challenging to draw conclusive interpretation and close to impossible to predict theoretical values of atomic contents. However, observation of the evolution of the different species can still be useful. Indeed, while no signal was detected in the N 1s

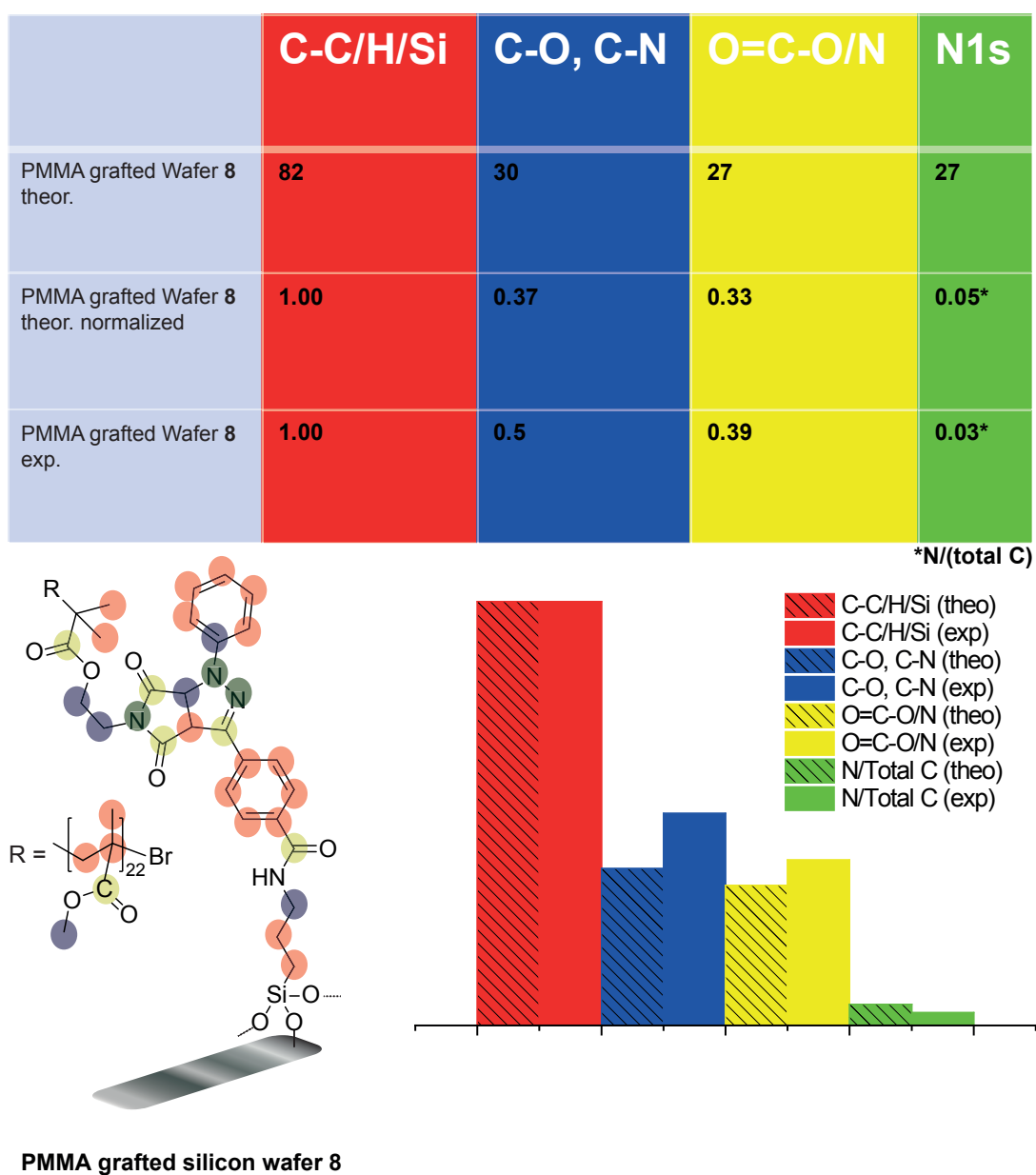


**Figure 5.10:** Comparison of theoretical atomic concentrations of pMMA grafted silicon surface with experimental XPS data extracted from Figure 5.6b. The spectra were normalized to C-C/H/Si (285.0 eV). The bar chart is a visualization of the above shown table.

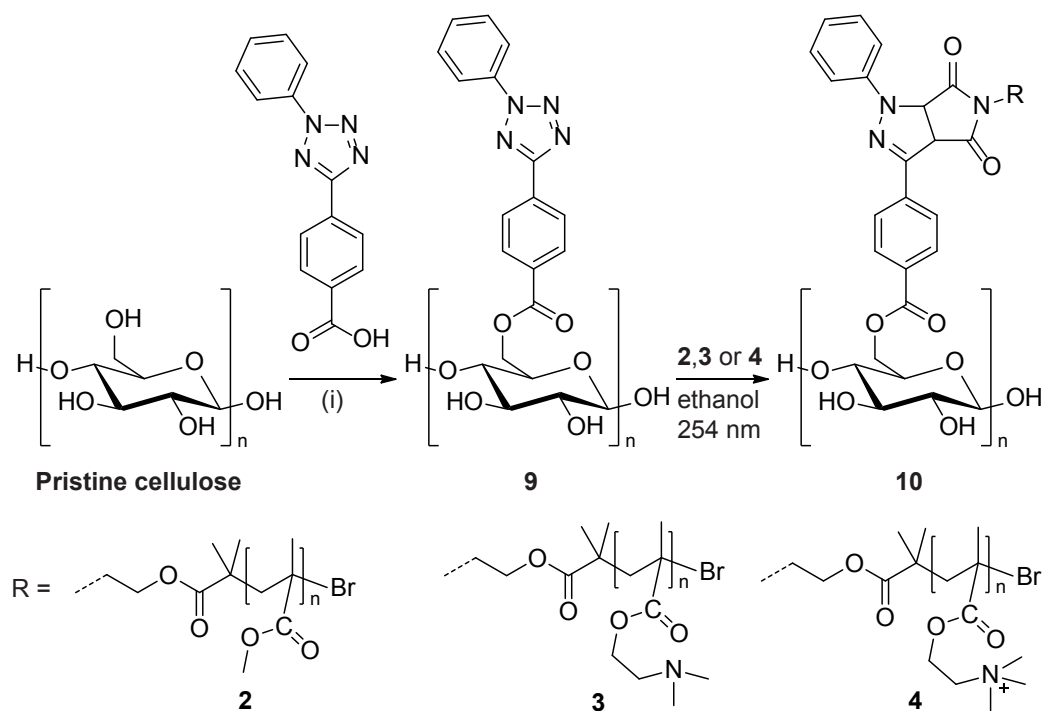


**Figure 5.11:** Strategy for surface modification of cellulose *via* NITEC employing different classes of polymers (2, 3 or 4). (i) oxalyl chloride, DMF, DCM then DMAP, DIPEA, DCM.

region of the XPS spectrum of pristine cellulose (see Figure 5.12a), a low-intensity peak could be observed on tetrazole functionalized cellulose **9** at 400.4 eV (see figure 5.12b), which indicates the presence of the nitrogen-containing tetrazole. On the contrary, it is not possible to use the C 1s region since the cellulose signals are very strong in this region and prevent any accurate detection of a contribution - which would be very low - from the tetrazole handle. While the weak contribution at 285.0 eV (C-C, C-H) is caused by hydrocarbon contamination, it must be noted that carbonyl groups can be detected in pristine cellulose and originate from oxidation that can readily occur on natural fibers such as cellulose.<sup>308</sup> The tetrazole-functionalized cellulose was subsequently immersed in a solution of **2** in ethanol and irradiated at 254 nm at ambient temperature for 10 min on each side and left to stand in the polymer solution for a further 50 min to achieve complete conversion (see chapter 4) before washing with different solvents and dried under reduced pressure. XPS data supports the formation of a grafted (meth)acrylic polymer layer as shown in Figure 5.12c. Indeed, in comparison to the cellulose characteristic peaks, a clear increase of the C-C/C-H signal (285.0 eV) as well as of the O=C-O signal (288.6 eV) is observed. As a complementary surface characterization technique high resolution FT-IR microscopy was employed, which allows a spatial chemical mapping. It was already shown in our group that spatial resolution FT-IR microscopy is efficient to prove the grafting of polymer chains onto cellulose *via* an acid-catalyzed hetero-Diels-Alder *click* reaction.<sup>148</sup> Figure 5.13 depicts the false-color, high-resolution FT-IR microscope images of the pMMA-grafted cellulose and of the control sample in

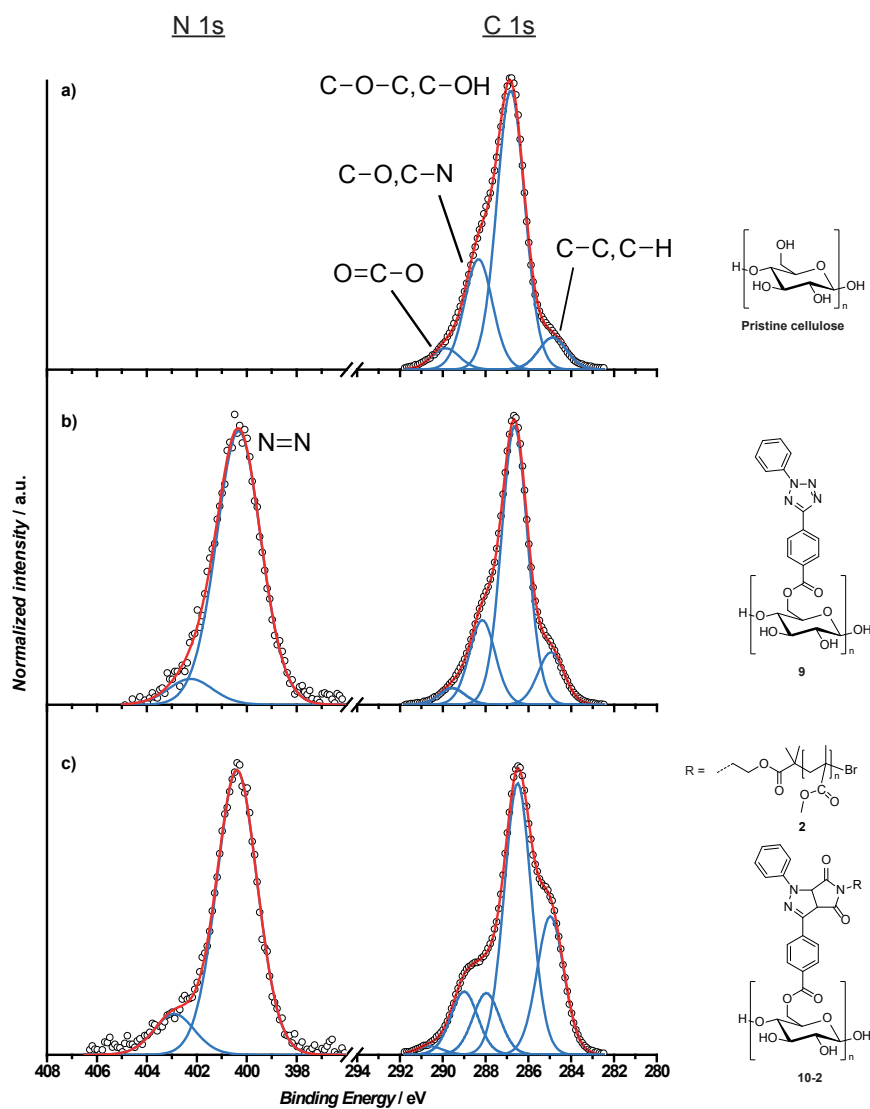


**Figure 5.12:** Comparison of the C 1s (280-294 eV) and N 1s (396-408 eV) normalized peaks in the XPS spectra of pristine cellulose (a), tetrazole functionalized cellulose **9** (b) and pMMA functionalized cellulose after the coupling reaction **10** (c).

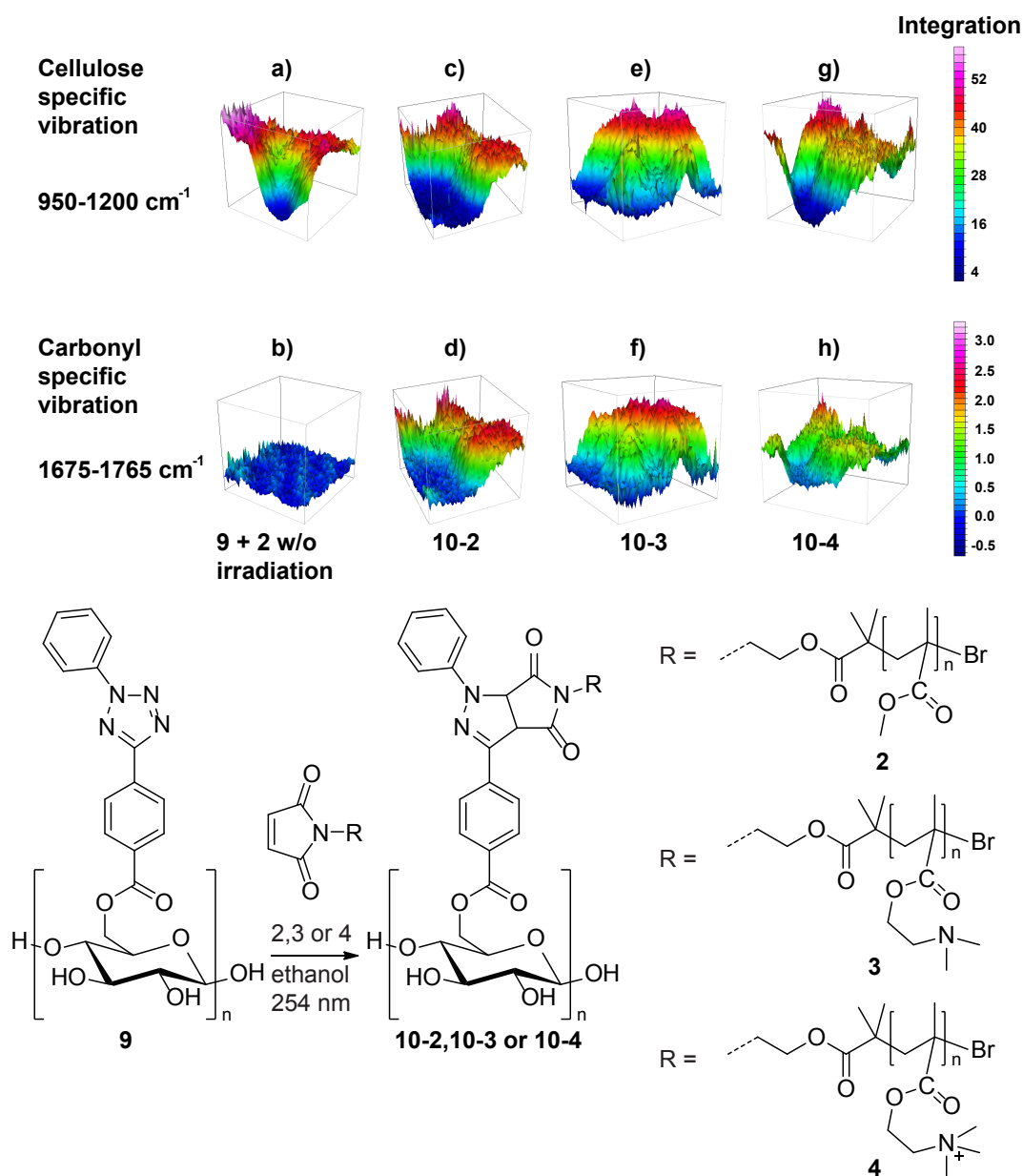
which tetrazole functionalized cellulose was immersed in a solution of **2** but not irradiated.

Figure 5.13a and 5.13c show the integration range corresponding to the characteristic cellulose signals of the C-O stretching vibration ( $950\text{-}1200\text{ cm}^{-1}$ ) and therefore represent a cellulose fiber. Figure 5.13b and 5.13d show the carbonyl spectral region ( $1675\text{-}1765\text{ cm}^{-1}$ ), present in the pMMA lateral ester groups. The sample obtained from the reaction of maleimide functionalized pMMA **2** with the tetrazole functionalized cellulose **9** is much richer in carbonyl groups (see Figure 5.13b) than the control sample, where no distinguishable peak is visible (see Figure 5.13d). Although a carbonyl bond is introduced on the cellulose after the tetrazole functionalization, it is not visible as its amount is too low to be detected with the focal plane array detector. This result corroborates the attribution of the carbonyl bonds observed in Figure 5.13b to the presence of the polymer on the surface of the cellulose fibers and proves that no polymer is physically adsorbed on the surface after the washing procedure.

It is interesting to note that during and after the successful coupling a strong fluorescence can be observed. This fluorescence arises from the newly formed diaryl- $\Delta^2$ -pyrazoline which, although it does not present any continuous conjugation in its classical form, possesses two mesomeric canonic forms allowing the two aromatic rings to interact.<sup>309</sup> The fluorescence is thus only observed in samples where successful coupling has occurred. When the tetrazole was irradiated for long periods in the absence of a dipolarophile, no fluorescence was observed. Indeed all the samples which were successfully functionalized as XPS and FT-IR data shows fluorescence. To demonstrate that the light-triggered nature of the presented method could be used to precisely pattern surfaces, the same reaction as above was performed but a partly masked tetrazole-functionalized cellulose membrane **9** was subjected to irradiation in presence of a maleimide functionalized pMMA **2**. Actually, a simple wrapping procedure of one part of a cellulose band with aluminium foil was sufficient, which demonstrates the ease of manipulation of the NITEC.

The clear difference in behavior under a 366-nm light between the irradiated and the masked parts is evidenced in Figure 5.14a. Submitting this piece of cellulose to XPS showed that the masked and the irradiated parts had spectra comparable to that of the initial tetrazole-functionalized cellulose **9** and the pMMA-grafted cellulose **10-2**, respectively (not shown).

An additional proof that polymer grafting occurred only on the non-masked part can be seen in the change of physical properties due to the presence of a hydrophobic polymer such as pMMA on the surface. Figure 5.14b depicts the partly irradiated cellulose samples where a water droplet had been placed on each region, either irradiated or not. While the droplet remained unchanged on the irradiated region for several tens of minutes without any drastic change, the one on the masked part was instantaneously



**Figure 5.13:** False-color high-resolution FT-IR microscope images ( $4 \text{ cm}^{-1}$  spectral resolution with a  $0.25 \mu\text{m}^2$  spatial pixel resolution and an optical resolution of close to  $1 \mu\text{m}$ ) of the different cellulose samples. Top row: Integration in the  $950\text{-}1200 \text{ cm}^{-1}$ . Bottom row: Integration in the  $1675\text{-}1765 \text{ cm}^{-1}$ . a) and b) tetrazole functionalized cellulose **9** immersed in a solution of maleimide functionalized pMMA **2** without being irradiated; c) and d) **9** after irradiation with maleimide functionalized pMMA **2**; (e) and (f) maleimide functionalized PDMAEMA **3**; (g) and (h) maleimide functionalized quaternized PDMAEMA **4**. Cellulose regions with green to pink colors correspond to an increasing degree of functionalization within the particular integrated wavelength region.

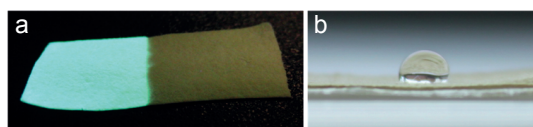


**Figure 5.14:** Tetrazole functionalized cellulose **9** after irradiation of the left half with maleimide functionalized pMMA **2** exhibiting a strong fluorescence when irradiated with a hand-held UV-lamp at 366 nm (**10-2**) (a). Photograph of a water droplet 10 minutes after its deposition on a piece of pMMA grafted cellulose **10-2** (b).

absorbed. Furthermore, water contact angle measurement were conducted. Due to the inherent roughness and absorbing nature of the cellulose surface, this measurement is not straightforward. Indeed it is generally impossible to obtain a value for the pristine cellulose due to the aforementioned fast absorption. However, in the present case, the control sample is not pristine cellulose but tetrazole functionalized cellulose **9**. This result is rather interesting since it shows that before the polymer grafting, the sample properties are not drastically altered by the tetrazole functionalization. On the contrary, the region which had been irradiated in presence of maleimide functionalized pMMA **2** became very hydrophobic exhibiting a water contact angle of  $126^\circ$  (see Figure 5.14c). In addition to the grafting of a hydrophobic polymer and to demonstrate the power of the combination of modern polymer chemistry and NITEC to yield functional materials, by grafting the thermo- and pH-sensitive polymer PDMAEMA **3** and the antibacterial polymer **4**. FT-IR microscopy data (see Figure 5.13e and 5.13f, and 5.13g and 5.13h, respectively) and simple fluorescence observations (see Figure 5.15a and 5.15b, respectively) proved the success of the grafting. Finally the patterning ability offered by the NITEC was evidenced by the use of a slightly more complicated mask representing the KIT logo presented in Figure 5.15c.



**Figure 5.15:** Photographs of pieces of cellulose under irradiation of light (366 nm) after the NITEC coupling, on their right-hand half in ethanol solutions containing maleimide functionalized PDMAEMA **3** (a), quaternized maleimide functionalized PDMAEMA **4** (b) and using a hand-made aluminum foil KIT mask in an ethanol solution containing maleimide functionalized pMMA **2** (c).

### 5.3.2 The TEMPO/Photoinitiator Conjugation Approach

The successful formation of block copolymers employing the radical capturing of *in situ* generated carbon-centered radicals by stable nitroxide radicals was shown in chapter

4. Based on the results obtained on the formation of such block copolymers, the final aim of this section is the decoration of cellulose with polystyrene using the aforementioned TEMPO/photoinitiator technique, in order to change the surface characteristics of cellulose. The synthetic pathway for achieving this goal is shown in Figure 5.16.

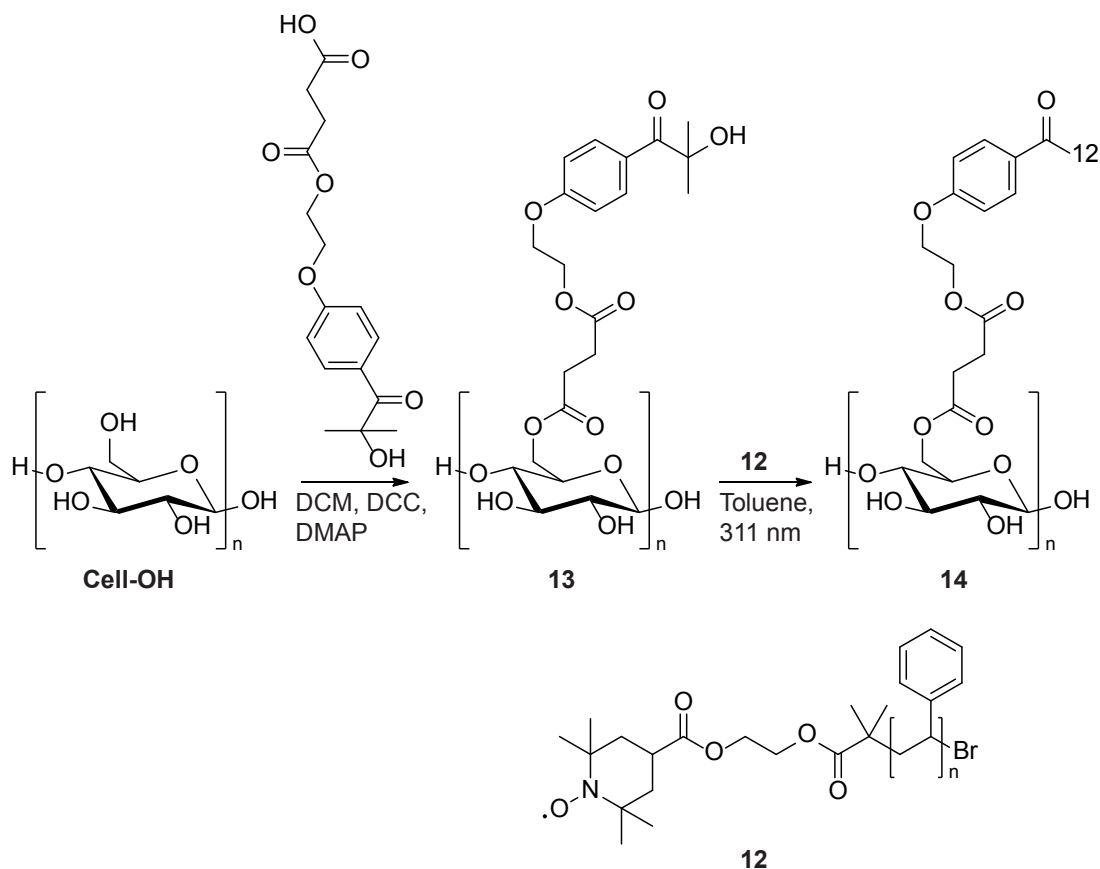


**Figure 5.16:** Strategy for surface modification of photoinitiator functionalized cellulose **13** via UV-light irradiation in the presence of TEMPO functionalized polystyrene **12** yielding polystyrene grafted cellulose **14**.

The first step was the esterification of pretreated cellulose with a carboxy functionalized photoinitiator which was already employed in the polymer conjugation system (see chapter 4 for details). Polystyrene bearing a hydroxyl group **11** was esterified with 1-oxyl-4-carboxyl-2,2,6,6-tetramethylpiperidine yielding TEMPO functionalized polystyrene **12**. Sodium hydroxide pre-treated cellulose was esterified with the carboxy modified photoinitiator Irgarcure 2959<sup>TM</sup> to yield the photoinitiator functionalized cellulose **13**. The polymer grafting reaction was prepared by dissolving TEMPO functionalized polystyrene **12** in toluene followed by dispersing a photoinitiator functionalized cellulose sheet **13** in the polymer solution. After purging the reaction mixture for 5 min with nitrogen, the cellulose sheet was irradiated with an UV-lamp at 311 nm for 10 min on each side (3 cm distance to lamp). It has to be noted that the surface grafting reaction was carried out without the use of an oxidant, as it was the case for the polymer conjugation. Currently only PbO<sub>2</sub> is known as oxidant for the

presented TEMPO/photoinitiator system.  $\text{PbO}_2$  however, is very toxic and therefore unsuitable for bioconjugations. Generated hydroxyl amine species from side reactions will be washed of the cellulose sheet because there is no covalent bond between such polymers and the cellulose surface. After thoroughly washing of the grafted cellulose sheet **14** with acetone and dichloromethane the cellulose was dried in a vacuum oven at ambient temperature and analyzed employing XPS. Figure 5.17 depicts the XPS spectra of photoinitiator functionalized cellulose **13** and polystyrene grafted cellulose after the coupling reaction **14**. Due to the afore mentioned fact that cellulose is a fibrous material with intrinsic heterogeneity, the same challenges in interpretation of XPS analysis results apply here. Yet, it is possible to follow the evolution of different species. Compared to pristine cellulose (see Figure 5.17a), the intensity of the peak in the 285 eV region (C-C, C-H) increased significantly in the photoinitiator functionalized cellulose. However, the main peak in this distribution has a contribution from pristine cellulose, as can be concluded from the high intensity of the 287 eV region (C-O-C, C-OH). Once the polymer is grafted on the cellulose, a drastic change in the peak distribution of the C 1s region can be observed (see Figure 5.17c). The intensity of the peak region at 285 eV (C-C, C-H) increased by a large amount showing the decreasing influence of the cellulosic bulk material onto the surface. The increase of the peak region at 285 eV (C-C, C-H) can be explained by polystyrene chains which are grafted on the surface. Furthermore, an additional peak appears in the 292 eV region which can be assigned to a  $\pi$ - $\pi^*$ -transition.<sup>310</sup> The  $\pi$ - $\pi^*$ -transition is a weak signal and is characteristic for aromatic systems. Although the photoinitiator grafted cellulose **13** exhibits such groups, they were not detected due to their low concentration. The result of the  $\pi$ - $\pi^*$ -transition is very important as it supports the successful grafting of the polystyrene onto the cellulose surface. Contact angle measurements were performed on the polymer grafted cellulose surface to investigate the physical changes accompanied by the polymer grafting. Since polystyrene is a hydrophobic polymer, the contact angle for a water drop on the surface should increase compared to pristine cellulose, which can indeed be observed ( $86^\circ$ ). Control studies using the same reaction conditions as in the grafting reaction, employing pre-treated cellulose irradiated in the presence of TEMPO functionalized polystyrene **12** sheets were performed. No contact angle could be measured due to high hydrophilicity of the cellulose. Consequently, there was no grafting of polymer onto the surface which corroborates the mechanistic scheme in figure 5.16. Although the contact angle is smaller than in previous studies with grafted polystyrene on cellulose shown by Barsbay *et al.*,<sup>200</sup> the effect of the herein presented polymer grafting - change of physical properties on the surface - is still significant and therefore the grafting reaction appeared to be successful.

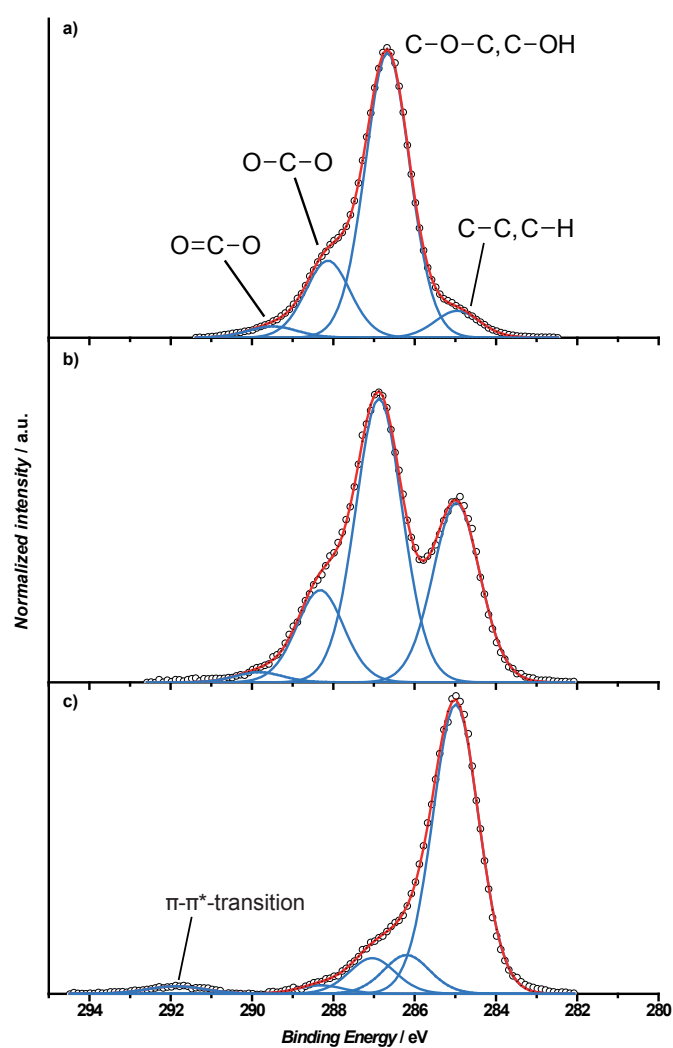


**Figure 5.17:** Comparison of the C 1s (280-294 eV) normalized peaks in the XPS spectra of pristine cellulose (a), photoinitiator functionalized cellulose **13** (b) and polystyrene functionalized cellulose after the grafting reaction **14** (c).

## 5.4 Conclusion and Outlook

### 5.4.1 The Nitrile Imine-mediated 1,3-Dipolar Cycloaddition of Tetrazole and Ene Coupling (NITEC) Employed for Polymer Grafting on Surfaces

In summary the UV-light induced formation of nitrile imines from tetrazoles and its subsequent 1,3-dipolar cycloaddition with maleimides was successfully employed for the grafting of polymer chains onto surfaces like silicon or - even more demanding in analysis - cellulose. The efficient coupling has been demonstrated for the coupling of polymers yielding in block copolymers in chapter 4. As the reaction requires irradiation by UV-light for initiation of the reaction, a spatially defined polymer grafting can be achieved. The reaction works simply and very rapidly under non-demanding conditions, and could be applied to a number of polymers thanks to the ease of introduction of alkene end-groups on macromolecules, but also to many different surfaces provided that the tetrazole moiety can be anchored. The other exceptional advantages of this technique are the absence of necessary purification (the only by-product is molecular nitrogen), its high fluorescent character after coupling allowing a rapid assessment of the successful grafting, and its already-proven bioorthogonality. Compared to other more established click reactions, the NITEC seems to have a much greater potential. Efforts in our lab are currently directed to the application of this technique in nanobiotechnology.

### 5.4.2 The TEMPO/Photoinitiator Employed for Polymer Grafting on Surfaces

The TEMPO/photoinitiator approach has been applied on cellulose in order to change the physical properties of the surface while keeping the bulk properties unchanged. The results of the TEMPO/photoinitiator approach exhibit strong evidence for the successful grafting of TEMPO functionalized polymers onto photoinitiator functionalized cellulose surfaces. The grafting was confirmed by XPS spectroscopy and contact angle measurements. The concept of the TEMPO/photoinitiator approach is therefore applicable on surfaces yet there is still room for improvements of the newly invented method, such as employing different polymer classes as well as employing the concept of a (re)oxidizing agent for the hydroxyl amine species - as explained in chapter 4.

# References

- [1] <http://www.plasticseurope.org/cust/documentrequest.aspx?DocID=46728> .
- [2] G. Odian, *Principles of polymerization*, 4. ed. Edition, Wiley-Interscience, Hoboken, NJ, **2004**.
- [3] D. Braun, *International Journal of Polymer Science* **2009**.
- [4] H. Fischer, L. Radom, *Angew. Chem., Int. Ed.* **2001**, 40(8), 1340–1371.
- [5] M. Buback, R. G. Gilbert, R. A. Hutchinson, B. Klumperman, F.-D. Kuchta, B. G. Manders, K. F. O'Driscoll, G. T. Russell, J. Schweer, *Macromol. Chem. Phys.* **1995**, 196(10), 3267–3280.
- [6] S. Beuermann, M. Buback, T. P. Davis, R. G. Gilbert, R. A. Hutchinson, O. F. Olaj, G. T. Russell, J. Schweer, A. M. van Herk, *Macromol. Chem. Phys.* **1997**, 198(5), 1545–1560.
- [7] S. Beuermann, M. Buback, T. P. Davis, R. G. Gilbert, R. A. Hutchinson, A. Kajiwara, B. Klumperman, G. T. Russell, *Macromol. Chem. Phys.* **2000**, 201(12), 1355–1364.
- [8] S. Beuermann, M. Buback, T. P. Davis, N. García, R. G. Gilbert, R. A. Hutchinson, A. Kajiwara, M. Kamachi, I. Lacić, G. T. Russell, *Macromol. Chem. Phys.* **2003**, 204(10), 1338–1350.
- [9] J. M. Asua, S. Beuermann, M. Buback, P. Castignolles, B. Charleux, R. G. Gilbert, R. A. Hutchinson, J. R. Leiza, A. N. Nikitin, J.-P. Vairon, A. M. van Herk, *Macromol. Chem. Phys.* **2004**, 205(16), 2151–2160.
- [10] D. R. Taylor, K. Y. van Berkel, M. M. Alghamdi, G. T. Russell, *Macromol. Chem. Phys.* **2010**, 211(5), 563–579.
- [11] C. Barner-Kowollik, G. T. Russell, *Prog. Polym. Sci.* **2009**, 34(11), 1211–1259.
- [12] A. M. North, *The Influence of Chain Structure on the Free Radical Termination Reaction*, (Editor: A. Jenkins, A. Ledwith), Wiley- Interscience, New York, **1974**.
- [13] M. Szwarc, *Nature* **1956**, 178(4543), 1168–1169.

- [14] A. D. Jenkins, R. G. Jones, G. Moad, *Polymer* **2010**, *82*(2), 483–491.
- [15] M. Kato, M. Kamigaito, M. Sawamoto, T. Higashimura, *Macromolecules* **1995**, *28*(5), 1721–1723.
- [16] J.-S. Wang, K. Matyjaszewski, *J. Am. Chem. Soc.* **1995**, *117*(20), 5614–5615.
- [17] K. Matyjaszewski, J. Xia, *Chem. Rev.* **2001**, *101*(9), 2921–2990.
- [18] W. Tang, N. V. Tsarevsky, K. Matyjaszewski, *J. Am. Chem. Soc.* **2006**, *128*(5), 1598–1604.
- [19] J.-S. Wang, K. Matyjaszewski, *Macromolecules* **1995**, *28*(22), 7572–7573.
- [20] W. Jakubowski, K. Matyjaszewski, *Macromolecules* **2005**, *38*(10), 4139–4146.
- [21] K. Min, H. Gao, K. Matyjaszewski, *J. Am. Chem. Soc.* **2005**, *127*(11), 3825–3830.
- [22] J. K. Oh, C. Tang, H. Gao, N. V. Tsarevsky, K. Matyjaszewski, *J. Am. Chem. Soc.* **2006**, *128*(16), 5578–5584.
- [23] J. K. Oh, H. Dong, R. Zhang, K. Matyjaszewski, H. Schlaad, *J. Polym. Sci., Part A: Polym. Chem.* **2007**, *45*(21), 4764–4772.
- [24] W. Jakubowski, K. Matyjaszewski, *Angew. Chem., Int. Ed.* **2006**, *45*(27), 4482–4486.
- [25] K. Min, H. Gao, K. Matyjaszewski, *Macromolecules* **2007**, *40*(6), 1789–1791.
- [26] K. Matyjaszewski, W. Jakubowski, K. Min, W. Tang, J. Huang, W. A. Braunecker, N. V. Tsarevsky, *Proc. Natl. Acad. Sci. USA* **2006**, *103*(42), 15309–15314.
- [27] F. di Lena, K. Matyjaszewski, *Prog. Polym. Sci.* **2010**, *35*(8), 959–1021.
- [28] T. Pintauer, K. Matyjaszewski, *Chem. Soc. Rev.* **2008**, *37*(6), 1087–1097.
- [29] J. Chiefari, Y. K. B. Chong, F. Ercole, J. Krstina, J. Jeffery, T. P. T. Le, R. T. A. Mayadunne, G. F. Meijs, C. L. Moad, G. Moad, E. Rizzardo, S. H. Thang, *Macromolecules* **1998**, *31*(16), 5559–5562.
- [30] Y. K. Chong, T. P. T. Le, G. Moad, E. Rizzardo, S. H. Thang, *Macromolecules* **1999**, *32*(6), 2071–2074.
- [31] P. Corpart, D. Charmot, T. Biadatti, S. Zard, D. Michelet **1998**, (PCT Int. Appl. WO 9858974 A1 19981230).
- [32] M. Destarac, W. Bzducha, D. Taton, I. Gauthier-Gillaizeau, S. Z. Zard, *Macromol. Rapid Commun.* **2002**, *23*(17), 1049–1054.
- [33] R. W. Simms, T. P. Davis, M. F. Cunningham, *Macromol. Rapid Commun.* **2005**, *26*(8), 592–596.

- [34] J. Bernard, A. Favier, L. Zhang, A. Nilasaroya, T. P. Davis, C. Barner-Kowollik, M. H. Stenzel, *Macromolecules* **2005**, 38(13), 5475–5484.
- [35] B. Dervaux, T. Junkers, M. Schneider-Baumann, F. E. Du Prez, C. Barner-Kowollik, *J. Polym. Sci., Part A: Polym. Chem.* **2009**, 47(23), 6641–6654.
- [36] R. T. A. Mayadunne, E. Rizzardo, J. Chiefari, Y. K. Chong, G. Moad, S. H. Thang, *Macromolecules* **1999**, 32(21), 6977–6980.
- [37] D. Hua, R. Bai, W. Lu, C. Pan, *J. Polym. Sci., Part A: Polym. Chem.* **2004**, 42(22), 5670–5677.
- [38] R. Bussels, C. Bergman-Göttgens, J. Meuldijk, C. Koning, *Macromolecules* **2004**, 37(25), 9299–9301.
- [39] R. Bussels, C. Bergman-Göttgens, J. Meuldijk, C. Koning, *Polymer* **2005**, 46(19), 8546 – 8554.
- [40] S. H. Thang, B. K. Chong, R. T. A. Mayadunne, G. Moad, E. Rizzardo, *Tetrahedron Lett.* **1999**, 40(12), 2435 – 2438.
- [41] Z. Szablan, A. A. Toy, T. P. Davis, X. Hao, M. H. Stenzel, C. Barner-Kowollik, *J. Polym. Sci., Part A: Polym. Chem.* **2004**, 42(10), 2432–2443.
- [42] C. Barner-Kowollik, S. Perrier, *J. Polym. Sci., Part A: Polym. Chem.* **2008**, 46(17), 5715–5723.
- [43] A. Favier, M.-T. Charreyre, *Macromol. Rapid Commun.* **2006**, 27(9), 653–692.
- [44] G. Moad, E. Rizzardo, S. H. Thang, *Aust. J. Chem.* **2005**, 58(6), 379–410.
- [45] S. Perrier, P. Takolpuckdee, *J. Polym. Sci., Part A: Polym. Chem.* **2005**, 43(22), 5347–5393.
- [46] A. M. Bivigou-Koumba, J. Kristen, A. Laschewsky, P. Mueller-Buschbaum, C. M. Papadakis, *Macromol. Chem. Phys.* **2009**, 210(7), 565–578.
- [47] J. F. Quinn, R. P. Chaplin, T. P. Davis, *J. Polym. Sci., Part A: Polym. Chem.* **2002**, 40(17), 2956–2966.
- [48] J. Xu, L. Tao, J. Liu, V. Bulmus, T. P. Davis, *Macromolecules* **2009**, 42(18), 6893–6901.
- [49] J. Bernard, F. Lortie, B. Fenet, *Macromol. Rapid Commun.* **2009**, 30(2), 83–88.
- [50] M. H. Stenzel, *Macromol. Rapid Commun.* **2009**, 30(19), 1603–1624.
- [51] M. H. Stenzel, *Chem. Commun.* **2008**, (30), 3486–3503.
- [52] J. Skey, R. K. O'Reilly, *Chem. Commun.* **2008**, (35), 4183–4185.
- [53] M. R. Wood, D. J. Duncalf, S. P. Rannard, S. Perrier, *Org. Lett.* **2006**, 8(4), 553–556.

- [54] D. J. Coady, B. C. Norris, V. M. Lynch, C. W. Bielawski, *Macromolecules* **2008**, *41*(11), 3775–3778.
- [55] V. Coessens, T. Pintauer, K. Matyjaszewski, *Prog. Polym. Sci.* **2001**, *26*(3), 337 – 377.
- [56] C. J. Hawker, A. W. Bosman, E. Harth, *Chem. Rev.* **2001**, *101*(12), 3661–3688.
- [57] J. Hentschel, K. Bleek, O. Ernst, J.-F. Lutz, H. G. Börner, *Macromolecules* **2008**, *41*(4), 1073–1075.
- [58] M. Bathfield, D. Daviot, F. D’Agosto, R. Spitz, C. Ladavière, M.-T. Charreyre, T. Delair, *Macromolecules* **2008**, *41*(22), 8346–8353.
- [59] J. Liu, V. Bulmus, D. L. Herlambang, C. Barner-Kowollik, M. H. Stenzel, T. P. Davis, *Angew. Chem., Int. Ed.* **2007**, *46*(17), 3099–3103.
- [60] G. Zhou, I. I. Harruna, *Macromolecules* **2005**, *38*(10), 4114–4123.
- [61] A. Samakande, R. Chaghi, G. Derrien, C. Charnay, P. C. Hartmann, *J. Colloid Interface Sci.* **2008**, *320*(1), 315 – 320.
- [62] P. De, M. Li, S. R. Gondi, B. S. Sumerlin, *J. Am. Chem. Soc.* **2008**, *130*(34), 11288–11289.
- [63] Y. K. Chong, G. Moad, E. Rizzardo, S. H. Thang, *Macromolecules* **2003**, *40*(13), 4446–4455.
- [64] G. Moad, Y. Chong, A. Postma, E. Rizzardo, S. H. Thang, *Polymer* **2005**, *46*(19), 8458 – 8468.
- [65] A. J. Inglis, M. H. Stenzel, C. Barner-Kowollik, *Macromol. Rapid Commun.* **2009**, *30*(21), 1792–1798.
- [66] S. Sinnwell, A. J. Inglis, M. H. Stenzel, C. Barner-Kowollik, *Blocks, Stars and Combs: Complex Macromolecular Architecture Polymers via Click Chemistry*, Click Chemistry for Biotechnology and Materials Science, John Wiley & Sons, Ltd, **2009**, p. 89–117.
- [67] G. Moad, E. Rizzardo, S. H. Thang, *Polymer* **2008**, *49*(5), 1079 – 1131.
- [68] A. B. Lowe, C. L. McCormick, *Prog. Polym. Sci.* **2007**, *32*(3), 283 – 351.
- [69] D. Crich, L. Quintero, *Chem. Rev.* **1989**, *89*(7), 1413–1432.
- [70] X. P. Chen, K. Y. Qiu, G. Swift, D. G. Westmoreland, S. Wu, *Eur. Polym. J.* **2000**, *36*(8), 1547 – 1554.
- [71] P. Li, S.-H. Qin, D.-Q. Qin, K.-Y. Qiu, *Polym. Int.* **2004**, *53*(6), 756–765.
- [72] P. Li, K.-Y. Qiu, *Macromol. Rapid Commun.* **2002**, *23*(18), 1124–1129.
- [73] A. Favier, B. Luneau, J. Vinas, N. Laissaoui, D. Gigmes, D. Bertin, *Macromolecules* **2009**, *42*(16), 5953–5964.

- [74] Y. Ao, J. He, X. Han, Y. Liu, X. Wang, D. Fan, J. Xu, Y. Yang, *J. Polym. Sci., Part A: Polym. Chem.* **2007**, *45*(3), 374–387.
- [75] R. T. A. Mayadunne, J. Jeffery, G. Moad, E. Rizzardo, *Macromolecules* **2003**, *36*(5), 1505–1513.
- [76] R. T. A. Mayadunne, E. Rizzardo, J. Chiefari, J. Krstina, G. Moad, A. Postma, S. H. Thang, *Macromolecules* **2000**, *33*(2), 243–245.
- [77] R. Plummer, D. J. T. Hill, A. K. Whittaker, *Macromolecules* **2006**, *39*(24), 8379–8388.
- [78] Z. Wang, J. He, Y. Tao, L. Yang, H. Jiang, Y. Yang, *Macromolecules* **2003**, *36*(20), 7446–7452.
- [79] A. Favier, C. Ladavière, M.-T. Charreyre, C. Pichot, *Macromolecules* **2004**, *37*(6), 2026–2034.
- [80] D. B. Thomas, A. J. Convertine, R. D. Hester, A. B. Lowe, C. L. McCormick, *Macromolecules* **2004**, *37*(5), 1735–1741.
- [81] D. L. Patton, M. Mullings, T. Fulghum, R. C. Advincula, *Macromolecules* **2005**, *38*(20), 8597–8602.
- [82] S. Harrisson, *Macromolecules* **2009**, *42*(4), 897–898.
- [83] B. Yu, J. W. Chan, C. E. Hoyle, A. B. Lowe, *J. Polym. Sci., Part A: Polym. Chem.* **2009**, *47*(14), 3544–3557.
- [84] C. W. Scales, A. J. Convertine, C. L. McCormick, *Biomacromolecules* **2006**, *7*(5), 1389–1392, PMID: 16677018.
- [85] C. L. McCormick, A. B. Lowe, *Acc. Chem. Res.* **2004**, *37*(5), 312–325.
- [86] B. S. Sumerlin, A. B. Lowe, P. A. Stroud, P. Zhang, M. W. Urban, C. L. McCormick, *Langmuir* **2003**, *19*(14), 5559–5562.
- [87] Y. Kabachii, S. Kochev, *Polymer Science Series A* **2006**, *48*, 717–722.
- [88] M.-Q. Zhu, L.-Q. Wang, G. J. Exarhos, A. D. Q. Li, *J. Am. Chem. Soc.* **2004**, *126*(9), 2656–2657.
- [89] A. S. Goldmann, A. Walther, L. Nebhani, R. Joso, D. Ernst, K. Loos, C. Barner-Kowollik, L. Barner, A. H. E. Müller, *Macromolecules* **2009**, *42*(11), 3707–3714.
- [90] A. N. Zelikin, G. K. Such, A. Postma, F. Caruso, *Biomacromolecules* **2007**, *8*(9), 2950–2953.
- [91] V. Lima, X. Jiang, J. Brokken-Zijp, P. J. Schoenmakers, B. Klumperman, R. Van Der Linde, *J. Polym. Sci., Part A: Polym. Chem.* **2005**, *43*(5), 959–973.
- [92] D. L. Patton, R. C. Advincula, *Macromolecules* **2006**, *39*(25), 8674–8683.

- [93] F. Segui, X.-P. Qiu, F. M. Winnik, *J. Polym. Sci., Part A: Polym. Chem.* **2008**, 46(1), 314–326.
- [94] X.-P. Qiu, F. M. Winnik, *Macromolecules* **2007**, 40(4), 872–878.
- [95] W. Shen, Q. Qiu, Y. Wang, M. Miao, B. Li, T. Zhang, A. Cao, Z. An, *Macromol. Rapid Commun.* **2010**, 31(16), 1444–1448.
- [96] L. Feng, K. Cavicchi, *PMSE Prepr.* **2010**, 102.
- [97] G. Moad, E. Rizzardo, S. H. Thang, *Polym. Int.* **2011**, 60(1), 9–25.
- [98] M. Chen, K. P. Ghiggino, E. Rizzardo, S. H. Thang, G. J. Wilson, *Chem. Commun.* **2008**, (9), 1112–1114.
- [99] D. Mathias, K. Chakib, W. Agnieszka, P. Laurence, V. G. Eric, Z. S. Z., *Various Strategies for the Chemical Transformation of Xanthate-Functional Chain Termini in MADIX Copolymers*, Chapter 39, p. 564–577.
- [100] Y.-Y. Tong, Y.-Q. Dong, F.-S. Du, Z.-C. Li, *J. Polym. Sci., Part A: Polym. Chem.* **2009**, 47(7), 1901–1910.
- [101] D. H. R. Barton, S. W. McCombie, *J. Chem. Soc., Perkin Trans. 1* **1975**, (16), 1574–1585.
- [102] M. J. Robins, J. S. Wilson, F. Hansske, *J. Am. Chem. Soc.* **1983**, 105(12), 4059–4065.
- [103] A. Studer, S. Amrein, *Synthesis* **2002**, 7, 835–849.
- [104] W. B. Farnham, M. Fryd, G. Moad, S. H. Thang, E. Rizzardo, Removing sulfur-containing end-groups from vinyl polymer without changing solvent Patent No. WO2005113612A1, **2005**.
- [105] A. Gridnev, *J. Polym. Sci., Part A: Polym. Chem.* **2000**, 38(10), 1753–1766.
- [106] A. H. Soeriyadi, C. Boyer, J. Burns, C. R. Becer, M. R. Whittaker, D. M. Haddleton, T. P. Davis, *Chem. Commun.* **2010**, 46(34), 6338–6340.
- [107] S. Perrier, P. Takolpuckdee, C. A. Mars, *Macromolecules* **2005**, 38(6), 2033–2036.
- [108] P. J. Roth, K. T. Wiss, R. Zentel, P. Theato, *Macromolecules* **2008**, 41(22), 8513–8519.
- [109] A. Postma, T. P. Davis, R. A. Evans, G. Li, G. Moad, M. S. O’Shea, *Macromolecules* **2006**, 39(16), 5293–5306.
- [110] B. J. Kim, S. Given-Beck, J. Bang, C. J. Hawker, E. J. Kramer, *Macromolecules* **2007**, 40(6), 1796–1798.
- [111] X. Zhang, J. Li, W. Li, A. Zhang, *Biomacromolecules* **2007**, 8(11), 3557–3567.
- [112] M. Chen, G. Moad, E. Rizzardo, *Polymer* **2009**, 6704–6714.

- [113] Y. Kwak, K. Matyjaszewski, *Macromolecules* **2008**, *41*(18), 6627–6635.
- [114] Y. Kwak, R. Nicolaÿ, K. Matyjaszewski, *Aust. J. Chem.* **2009**, *62*(11), 1384–1401.
- [115] Y. Kwak, R. Nicolaÿ, K. Matyjaszewski, *Macromolecules* **2008**, *41*(18), 6602–6604.
- [116] X. Xue, W. E. I. Zhang, Z. Cheng, J. Zhu, X. Zhu, *Polymer* **2008**, *46*(16), 5626–5637.
- [117] W. Zhang, W. Zhang, Z. Cheng, N. Zhou, X. Zhu, *J. Macromol. Sci., Part A: Pure Appl. Chem.* **2011**, *45*(10), 850–856.
- [118] S. Harihara Subramanian, R. Prakash Babu, R. Dhamodharan, *Macromolecules* **2008**, *41*(1), 262–265.
- [119] Z. Zhang, W. Wang, H. Xia, J. Zhu, W. Zhang, X. Zhu, *Macromolecules* **2009**, *42*(19), 7360–7366.
- [120] Z. Zhang, W. Zhang, X. Zhu, Z. Cheng, J. Zhu, *J. Polym. Sci., Part A: Polym. Chem.* **2007**, *45*(24), 5722–5730.
- [121] J. Chiefari, R. T. A. Mayadunne, C. L. Moad, G. Moad, E. Rizzardo, A. Postma, , S. H. Thang, *Macromolecules* **2003**, *36*(7), 2273–2283.
- [122] M. Benaglia, J. Chiefari, Y. K. Chong, G. Moad, E. Rizzardo, S. H. Thang, *J. Am. Chem. Soc.* **2009**, *131*(20), 6914–6915.
- [123] A. Postma, T. P. Davis, G. Li, G. Moad, M. S. O’Shea, *Macromolecules* **2006**, *39*(16), 5307–5318.
- [124] A. Postma, T. P. Davis, G. Moad, M. S. O’Shea, *Macromolecules* **2005**, *38*(13), 5371–5374.
- [125] B. Chong, G. Moad, E. Rizzardo, M. Skidmore, S. H. Thang, *Aust. J. Chem.* **2006**, *59*(10), 755–762.
- [126] R. S. Lehrle, E. J. Place, *Polym. Degrad. Stab.* **1997**, *56*(2), 215 – 219.
- [127] R. S. Lehrle, E. J. Place, *Polym. Degrad. Stab.* **1997**, *56*(2), 221 – 226.
- [128] L. Tschugaeff, *Ber.* **1899**, *32*(3), 3332–3335.
- [129] C. H. DePuy, R. W. King, *Chem. Rev.* **1960**, *60*(5), 431–457.
- [130] J. Xu, J. He, D. Fan, W. Tang, Y. Yang, *Macromolecules* **2006**, *39*(11), 3753–3759.
- [131] M. Destarac, C. Kalai, A. Wilczewska, G. Mignani, S. Zard, *Polym. Prepr. (Am. Chem. Soc., Div. Polym. Chem.)* **2005**, *46*, 213–214.
- [132] H. C. Kolb, M. G. Finn, K. B. Sharpless, *Angew. Chem., Int. Ed.* **2001**, *40*(11), 2004–2021.
- [133] R. A. Evans, *Aust. J. Chem.* **2007**, *60*(6), 384–395.

- [134] J. A. Johnson, M. G. Finn, J. T. Koberstein, N. J. Turro, *Macromol. Rapid Commun.* **2008**, 29(12-13), 1052–1072.
- [135] W. H. Binder, R. Sachsenhofer, *Macromol. Rapid Commun.* **2007**, 28(1), 15–54.
- [136] W. H. Binder, R. Sachsenhofer, *Macromol. Rapid Commun.* **2008**, 29(12-13), 952–981.
- [137] A. J. Inglis, C. Barner-Kowollik, *Macromol. Rapid Commun.* **2010**, 31(14), 1247–1266.
- [138] M. A. Harvison, A. B. Lowe, *Macromol. Rapid Commun.* **2011**, 32(11), 779–800.
- [139] C. Boyer, V. Bulmus, T. P. Davis, V. Ladmiral, J. Liu, S. Perrier, *Chem. Rev.* **2009**, 109(11), 5402–5436.
- [140] G. Moad, M. Chen, M. Haussler, A. Postma, E. Rizzardo, S. H. Thang, *Polym. Chem.* **2011**, 2(3), 492–519.
- [141] B. Heuzé, R. Gasparova, M. Heras, S. Masson, *Tetrahedron Lett.* **2000**, 41(38), 7327–7331.
- [142] P. Metzner, *Thiocarbonyl Compounds as Specific Tools for Organic Synthesis*, Vol. 204 von *Topics in Current Chemistry*, (Editor: P. Page), Springer Berlin / Heidelberg, **1999**, p. 127–181.
- [143] S. Sinnwell, A. J. Inglis, T. P. Davis, M. H. Stenzel, C. Barner-Kowollik, *Chem. Commun.* **2008**, (17), 2052–2054.
- [144] A. J. Inglis, S. Sinnwell, M. H. Stenzel, C. Barner-Kowollik, *Angew. Chem., Int. Ed.* **2009**, 48(13), 2411–2414.
- [145] A. J. Inglis, S. Sinnwell, T. P. Davis, C. Barner-Kowollik, M. H. Stenzel, *Macromolecules* **2008**, 41(12), 4120–4126.
- [146] L. Nebhani, S. Sinnwell, A. J. Inglis, M. H. Stenzel, C. Barner-Kowollik, L. Barner, *Macromol. Rapid Commun.* **2008**, 29(17), 1431–1437.
- [147] L. Nebhani, P. Gerstel, P. Atanasova, M. Bruns, C. Barner-Kowollik, *J. Polym. Sci., Part A: Polym. Chem.* **2009**, 47(24), 7090–7095.
- [148] A. S. Goldmann, T. Tischer, L. Barner, M. Bruns, C. Barner-Kowollik, *Biomacromolecules* **2011**, 12(4), 1137–1145.
- [149] S. Zard, B. Sire, P. Jost, Method for partial or total oxidation of one or several thiocarbonylthio ends of a polymer obtained by radical polymerisation controlled by reversible addition-fragmentation, **2009**.
- [150] S. Z. Quiclet-Sire, Beatrice ; Zard, *Bull. Korean Chem. Soc.* **2010**, 31.
- [151] P. Vana, L. Albertin, L. Barner, T. P. Davis, C. Barner-Kowollik, *J. Polym. Sci., Part A: Polym. Chem.* **2002**, 40(22), 4032–4037.

- [152] P. G. Pfukwa R., K. B., *Polym. Prepr. (Am. Chem. Soc., Div. Polym. Chem.)* **2008**, *49*, 117–118.
- [153] T. Gründling, R. Pickford, M. Guilhaus, C. Barner-Kowollik, *J. Polym. Sci., Part A: Polym. Chem.* **2008**, *46*(22), 7447–7461.
- [154] F. Cerreta, A. M. Lenoher, C. Leriverend, P. Metzner, T. N. Pham, *Bull. Soc. Chim. France* **1995**, *132*, 67–74.
- [155] H. De Brouwer, M. A. J. Schellekens, B. Klumperman, M. J. Monteiro, A. L. German, *J. Polym. Sci., Part A: Polym. Chem.* **2000**, *38*(19), 3596–3603.
- [156] J. F. Quinn, L. Barner, C. Barner-Kowollik, E. Rizzardo, T. P. Davis, *Macromolecules* **2002**, *35*(20), 7620–7627.
- [157] P. Metzner, *Pure Appl. Chem.* **1996**, *68*(4), 863–868.
- [158] M. J. Rogers, S. Semaw, *From Nothing to Something: The Appearance and Context of the Earliest Archaeological Record*, (Editor: M. Camps, P. Chauhan), Springer New York, **2009**, p. 155–171.
- [159] I. J. Lin, S. Nadiv, *Mater. Sci. and Eng.* **1979**, *39*(2), 193–209.
- [160] P. G. Fox, *J. Mater. Sci.* **1975**, *10*, 340–360.
- [161] D. M. Kolb, *Angew. Chem., Int. Ed.* **2001**, *40*(7), 1162–1181.
- [162] J. E. Gray, B. Luan, *J. Alloys Compd.* **2002**, *336*(1-2), 88–113.
- [163] W. Schwarz, H. Kretzdorn, *Angew. Bot.* **1931**, *13*, 122–137.
- [164] R. R. Netz, D. Andelman, *Phys. Rep.* **2003**, *380*(1-2), 1–95.
- [165] S. T. Milner, *Science* **1991**, *251*(4996), 905–914.
- [166] C. Marques, J. F. Joanny, L. Leibler, *Macromolecules* **1988**, *21*(4), 1051–1059.
- [167] Z. Qingye, N. Yo, I. Seiji, P. Mi-kyoung, W. Yingfan, F. Xiaowu, M. Jimmy, A. Rigoberto, *Surface-Initiated Anionic Polymerization: Tethered Polymer Brushes on Silicate Flat Surfaces*, Chapter 6, p. 39–55.
- [168] R. Advincula, in *Surface-Initiated Polymerization I*, Vol. 197 von *Advances in Polymer Science*, (Published by R. Jordan), Springer Berlin / Heidelberg, **2006**, p. 107–136.
- [169] J. Pyun, T. Kowalewski, K. Matyjaszewski, *Macromol. Rapid Commun.* **2003**, *24*(18), 1043–1059.
- [170] B. Zhao, W. J. Brittain, *Prog. Polym. Sci.* **2000**, *25*(5), 677–710.
- [171] S. Edmondson, V. L. Osborne, W. T. S. Huck, *Chem. Soc. Rev.* **2004**, *33*, 14–22.

- [172] B. S. Sumerlin, D. Neugebauer, K. Matyjaszewski, *Macromolecules* **2005**, *38*(3), 702–708.
- [173] B. Zdyrko, I. Luzinov, *Macromol. Rapid Commun.* **2011**, *32*(12), 859–869.
- [174] K. S. Iyer, B. Zdyrko, H. Malz, J. Pionteck, I. Luzinov, *Macromolecules* **2003**, *36*(17), 6519–6526.
- [175] H.-S. Lee, L. S. Penn, *Macromolecules* **2010**, *43*(1), 565–567.
- [176] S. Michielsen, H. J. Lee, *Langmuir* **2007**, *23*(11), 6004–6010.
- [177] V. Tsyalkovsky, V. Klep, K. Ramaratnam, R. Lupitsky, S. Minko, I. Luzinov, *Chem. Mater.* **2008**, *20*(1), 317–325.
- [178] M. Eastwood, D. Kritchevsky, *Annu. Rev. Nutr.* **2005**, *25*(1), 1–8.
- [179] L. Shen, J. Haufe, M. K. Patel, *Group Science, Technology and Society, Copernicus Institute* **2009**, 1–245.
- [180] V. Kumar, G. S. Banker, *Drug Dev. Ind. Pharm.* **1993**, *19*(1-2), 1–31.
- [181] V. Stannett, *Some Challenges in Grafting to Cellulose and Cellulose Derivatives*, Chapter 2, p. 3–20.
- [182] V. Raus, M. Štěpánek, M. Uchman, M. Šlouf, P. Látalová, E. Čadová, v. Netopilík, J. Kříž, J. Dybal, P. Vlček, *J. Polym. Sci., Part A: Polym. Chem.* **2011**.
- [183] M. Gericke, T. Liebert, O. A. E. Seoud, T. Heinze, *Macromol. Mater. Eng.* **2011**, *296*(6), 483–493.
- [184] L. Yan, K. Ishihara, *J. Polym. Sci., Part A: Polym. Chem.* **2008**, *46*(10), 3306–3313.
- [185] F. Chang, K. Yamabuki, K. Onimura, T. Oishi, *Polym. J* **2008**, *40*(12), 1170–1179.
- [186] T. Meng, X. Gao, J. Zhang, J. Yuan, Y. Zhang, J. He, *Polymer* **2009**, *50*(2), 447–454.
- [187] L. Chun-xiang, Z. Huai-yu, L. Ming-hua, F. Shi-yu, Z. Jia-jun, *Carbohydr. Polym.* **2009**, *78*(3), 432–438.
- [188] X. Sui, J. Yuan, M. Zhou, J. Zhang, H. Yang, W. Yuan, Y. Wei, C. Pan, *Biomacromolecules* **2008**, *9*(10), 2615–2620.
- [189] D. Roy, M. Semsarilar, J. T. Guthrie, S. Perrier, *Chem. Soc. Rev.* **2009**, *38*(7), 2046–2064.
- [190] M. Tizzotti, A. Charlot, E. Fleury, M. Stenzel, J. Bernard, *Macromol. Rapid Commun.* **2010**, *31*(20), 1751–1772.
- [191] T. Heinze, K. Petzold, in *Monomers, Polymers and Composites from Renewable Resources*, (Published by M. N. Belgacem, A. Gandini), Elsevier, Amsterdam, **2008**, p. 343–368.

- [192] T. Heinze, T. Liebert, *Prog. Polym. Sci.* **2001**, *26*(9), 1689–1762.
- [193] G. S. Chauhan, L. K. Guleria, B. Misra, I. Kaur, *J. Polym. Sci., Part A: Polym. Chem.* **1999**, *37*(12), 1763–1769.
- [194] R. Narayan, *Appl. Biochem. Biotechnol.* **1988**, *17*, 7–22.
- [195] V. Castelvetro, M. Geppi, S. Giaiacopi, G. Mollica, *Biomacromolecules* **2007**, *8*(2), 498–508.
- [196] A. Carlmark, E. E. Malmström, *Biomacromolecules* **2003**, *4*(6), 1740–1745.
- [197] Q. Zhou, L. Greffe, M. J. Baumann, E. E. Malmström, T. T. Teeri, H. Brumer, *Macromolecules* **2005**, *38*(9), 3547–3549.
- [198] D. Nyström, J. Lindqvist, E. Östmark, A. Hult, E. E. Malmström, *Chem. Commun.* **2006**, (34), 3594–3596.
- [199] S. B. Lee, R. R. Koepsel, S. W. Morley, K. Matyjaszewski, Y. Sun, A. J. Russell, *Biomacromolecules* **2004**, *5*(3), 877–882.
- [200] M. Barsbay, O. Güven, M. H. Stenzel, T. P. Davis, C. Barner-Kowollik, L. Barner, *Macromolecules* **2007**, *40*(20), 7140–7147.
- [201] R. Bongiovanni, E. Zeno, A. Pollicino, P. Serafini, C. Tonelli, *Cellulose* **2011**, *18*, 117–126.
- [202] L. Nebhani, C. Barner-Kowollik, *Adv. Mater.* **2009**, *21*(34), 3442–3468.
- [203] J.-F. Lutz, *Angew. Chem., Int. Ed.* **2007**, *46*(7), 1018–1025.
- [204] L. Nebhani, D. Schmiedl, L. Barner, C. Barner-Kowollik, *Adv. Funct. Mater.* **2010**, *20*(12), 2010–2020.
- [205] G.-L. Zhao, J. Háfren, L. Deiana, A. Córdova, *Macromol. Rapid Commun.* **2010**, *31*(8), 740–744.
- [206] T. Liebert, C. Hänsch, T. Heinze, *Macromol. Rapid Commun.* **2006**, *27*(3), 208–213.
- [207] M. Krouit, J. Bras, M. N. Belgacem, *Eur. Polym. J.* **2008**, *44*(12), 4074–4081.
- [208] S. Perrier, C. Barner-Kowollik, J. F. Quinn, P. Vana, T. P. Davis, *Macromolecules* **2002**, *35*(22), 8300–8306.
- [209] C. Barner-Kowollik, J. F. Quinn, T. L. U. Nguyen, J. P. A. Heuts, T. P. Davis, *Macromolecules* **2001**, *34*(22), 7849–7857.
- [210] N. Aoyagi, T. Endo, *J. Polym. Sci., Part A: Polym. Chem.* **2009**, *47*(14), 3702–3709.
- [211] S. Ito, Y. Tanaka, A. Kakehi, K. Kondo, *Bull. Chem. Soc. Jpn.* **1976**, *49*, 1920–1923.

- [212] W. Song, Y. Wang, J. Qu, M. M. Madden, Q. Lin, *Angew. Chem., Int. Ed.* **2008**, *47*(15), 2832–2835.
- [213] G. Mantovani, F. Lecolley, L. Tao, D. M. Haddleton, J. Clerx, J. J. L. M. Cornelissen, K. Velonia, *J. Am. Chem. Soc.* **2005**, *127*(9), 2966–2973.
- [214] H. Durmaz, F. Karatas, U. Tunca, G. Hizal, *J. Polym. Sci., Part A: Polym. Chem.* **2006**, *44*(13), 3947–3957.
- [215] F. F. Wolf, N. Friedemann, H. Frey, *Macromolecules* **2009**, *42*(15), 5622–5628.
- [216] T. Gründling, M. Guilhaus, C. Barner-Kowollik, *Anal. Chem.* **2008**, *80*(18), 6915–6927.
- [217] M. Buback, C. H. Kurz, C. Schmaltz, *Macromol. Chem. Phys.* **1998**, *199*(8), 1721–1727.
- [218] S. Beuermann, D. A. Paquet, J. H. McMinn, R. A. Hutchinson, *Macromolecules* **1996**, *29*(12), 4206–4215.
- [219] C. Strazielle, H. Benoit, O. Vogl, *Eur. Polym. J.* **1978**, *14*(5), 331–334.
- [220] K. L. Parry, A. G. Shard, R. D. Short, R. G. White, J. D. Whittle, A. Wright, *Surf. Interface Anal.* **2006**, *38*(11), 1497–1504.
- [221] J. H. Scofield, *J. Electron Spectrosc. Relat. Phenom.* **1976**, *8*(2), 129–137.
- [222] S. Tanuma, C. J. Powell, D. R. Penn, *Surf. Interface Anal.* **1994**, *21*(3), 165–176.
- [223] L. Barner, T. P. Davis, M. H. Stenzel, C. Barner-Kowollik, *Macromol. Rapid Commun.* **2007**, *28*(5), 539–559.
- [224] C. Barner-Kowollik, *Handbook of RAFT Polymerization*, 1st edn. Edition, (Editor: C. Barner-Kowollik), Wiley-VCH, **2008**.
- [225] M. D. Rowe, B. A. G. Hammer, S. G. Boyes, *Macromolecules* **2008**, *41*(12), 4147–4157.
- [226] C. L. Duvall, A. J. Convertine, D. S. W. Benoit, A. S. Hoffman, P. S. Stayton, *Mol. Pharm.* **2010**, *7*(2), 468–476.
- [227] S. R. S. Ting, A. M. Gregory, M. H. Stenzel, *Biomacromolecules* **2009**, *10*(2), 342–352.
- [228] T. Gründling, M. Dietrich, C. Barner-Kowollik, *Aust. J. Chem.* **2009**, *62*(8), 806–812.
- [229] M. Dietrich, M. Glassner, T. Gründling, C. Schmid, J. Falkenhagen, C. Barner-Kowollik, *Polymer Chemistry* **2010**, *1*(5), 634–644.
- [230] J. A. Howard, K. U. Ingold, *Can. J. Chem.* **1970**, *48*(6), 873–880.
- [231] J. A. Howard, K. U. Ingold, *Can. J. Chem.* **1969**, *47*(20), 3809–3815.

- [232] B. Maillard, K. U. Ingold, J. C. Scaiano, *J. Am. Chem. Soc.* **1983**, *105*(15), 5095–5099.
- [233] T. Gründling, G. Hart-Smith, T. P. Davis, M. H. Stenzel, C. Barner-Kowollik, *Macromolecules* **2008**, *41*(6), 1966–1971.
- [234] L. Serra, J. Doménech, N. A. Peppas, *European Journal of Pharmaceutics and Biopharmaceutics* **2009**, *71*(3), 519 – 528.
- [235] J. R. Husman, J. N. Kellen, R. E. McCluney, M. L. Tumeay, Acrylate copolymer pressure-sensitive adhesive composition and sheet materials coated therewith (Patent No. 06/719974), **1985**.
- [236] C. Schmid, J. Falkenhagen, C. Barner-Kowollik, *J. Polym. Sci., Part A: Polym. Chem.* **2011**, *49*(1), 1–10.
- [237] C. Barner-Kowollik, A. J. Inglis, *Macromol. Chem. Phys.* **2009**, *210*(12), 987–992.
- [238] G. Riess, *Prog. Polym. Sci.* **2003**, *28*(7), 1107–1170.
- [239] B. S. Sumerlin, A. P. Vogt, *Macromolecules* **2010**, *43*(1), 1–13.
- [240] C. Barner-Kowollik, F. E. Du Prez, P. Espeel, C. J. Hawker, T. Junkers, H. Schlaad, W. Van Camp, *Angew. Chem., Int. Ed.* **2011**, *50*(1), 60–62.
- [241] L. I. Smith, *Chem. Rev.* **1938**, *23*(2), 193–285.
- [242] R. Huisgen, *Angew. Chem., Int. Ed.* **1963**, *2*(10), 565–598.
- [243] V. V. Rostovtsev, L. G. Green, V. V. Fokin, K. B. Sharpless, *Angew. Chem., Int. Ed.* **2002**, *41*(14), 2596–2599.
- [244] J. E. Moses, A. D. Moorhouse, *Chem. Soc. Rev.* **2007**, *36*(8), 1249–1262.
- [245] C. J. Hawker, V. V. Fokin, M. G. Finn, K. B. Sharpless, *Aust. J. Chem.* **2007**, *60*(6), 381–383.
- [246] G. Wittig, A. Krebs, *Ber.* **1961**, *94*(12), 3260–3275.
- [247] N. J. Agard, J. A. Prescher, C. R. Bertozzi, *J. Am. Chem. Soc.* **2004**, *126*(46), 15046–15047.
- [248] J. M. Baskin, J. A. Prescher, S. T. Laughlin, N. J. Agard, P. V. Chang, I. A. Miller, A. Lo, J. A. Codelli, C. R. Bertozzi, *Proc. Natl. Acad. Sci. U. S. A.* **2007**, *104*(43), 16793–16797.
- [249] J. A. Codelli, J. M. Baskin, N. J. Agard, C. R. Bertozzi, *J. Am. Chem. Soc.* **2008**, *130*(34), 11486–11493.
- [250] T. Posner, *Ber.* **1905**, *38*(1), 646–657.
- [251] A. Michael, *Am. Chem. J.* **1887**, *9*, 115.

- [252] R. J. Pounder, M. J. Stanford, P. Brooks, S. P. Richards, A. P. Dove, *Chem. Commun.* **2008**, (41), 5158–5160.
- [253] J. W. Chan, B. Yu, C. E. Hoyle, A. B. Lowe, *Chem. Commun.* **2008**, (40), 4959–4961.
- [254] J. W. Chan, B. Yu, C. E. Hoyle, A. B. Lowe, *Polymer* **2009**, 50(14), 3158–3168.
- [255] C. E. Hoyle, C. N. Bowman, *Angew. Chem., Int. Ed.* **2010**, 49(9), 1540–1573.
- [256] S. P. S. Koo, M. M. Stamenovic, R. A. Prasath, A. J. Inglis, F. E. Du Prez, C. Barner-Kowollik, W. Van Camp, T. Junkers, *J. Polym. Sci., Part A: Polym. Chem.* **2010**, 48(8), 1699–1713.
- [257] J. W. Chan, C. E. Hoyle, A. B. Lowe, *J. Am. Chem. Soc.* **2009**, 131(16), 5751–5753.
- [258] D. Konkolewicz, A. Gray-Weale, S. Perrier, *J. Am. Chem. Soc.* **2009**, 131(50), 18075–18077.
- [259] E. Klemm, C. Stöckl, *Makromol. Chem.* **1991**, 192(1), 153–158.
- [260] B. M. Rosen, G. Lligadas, C. Hahn, V. Percec, *J. Polym. Sci., Part A: Polym. Chem.* **2009**, 47(15), 3931–3939.
- [261] M. L. Blackman, M. Royzen, J. M. Fox, *J. Am. Chem. Soc.* **2008**, 130(41), 13518–13519.
- [262] K. Gutmiedl, C. T. Wirges, V. Ehmke, T. Carell, *Org. Lett.* **2009**, 11(11), 2405–2408.
- [263] I. Singh, Z. Zarafshani, J.-F. Lutz, F. Heaney, *Macromolecules* **2009**, 42(15), 5411–5413.
- [264] A. Meyer, G. Pourceau, J.-J. Vasseur, F. Morvan, *J. Org. Chem.* **2010**, 75(19), 6689–6692.
- [265] A. Qin, J. W. Y. Lam, B. Z. Tang, *Macromolecules* **2010**, 43(21), 8693–8702.
- [266] K. L. Heredia, Z. P. Tolstyka, H. D. Maynard, *Macromolecules* **2007**, 40(14), 4772–4779.
- [267] H. Shao, M. M. Crnogorac, T. Kong, S.-Y. Chen, J. M. Williams, J. M. Tack, V. Gueriguian, E. N. Cagle, M. Carnevali, D. Tumelty, X. Paliard, L. P. Miranda, J. A. Bradburne, G. G. Kochendoerfer, *J. Am. Chem. Soc.* **2005**, 127(5), 1350–1351.
- [268] E. Beckmann, *Ber.* **1886**, 19(1), 988–993.
- [269] H. Otsuka, K. Aotani, Y. Higaki, A. Takahara, *Chem. Commun.* **2002**, (23), 2838–2839.
- [270] H. Otsuka, K. Aotani, Y. Higaki, A. Takahara, *J. Am. Chem. Soc.* **2003**, 125(14), 4064–4065.

- [271] Y. Higaki, H. Otsuka, A. Takahara, *Macromolecules* **2004**, 37(5), 1696–1701.
- [272] R. Nicolaÿ, L. Marx, P. Hémerly, K. Matyjaszewski, *Macromolecules* **2007**, 40(26), 9217–9223.
- [273] J. Kulis, C. A. Bell, A. S. Micallef, Z. Jia, M. J. Monteiro, *Macromolecules* **2009**, 42(21), 8218–8227.
- [274] W. Song, Y. Wang, J. Qu, Q. Lin, *J. Am. Chem. Soc.* **2008**, 130(30), 9654–9655.
- [275] Y. Wang, C. I. Rivera Vera, Q. Lin, *Org. Lett.* **2007**, 9(21), 4155–4158.
- [276] Y. Wang, W. Song, W. Hu, Q. Lin, *Angew. Chem., Int. Ed.* **2009**, 48(29), 5330–5333.
- [277] A. Dag, H. Durmaz, G. Hizal, U. Tunca, *J. Polym. Sci., Part A: Polym. Chem.* **2008**, 46(1), 302–313.
- [278] R. T. Borchardt, J. A. Huber, Y. S. Wu, *J. Org. Chem.* **1976**, 41(3), 565–567.
- [279] Z. Rappoport, J. Liebman, *The chemistry of hydroxylamines, oximes and hydroxamic acids*, John Wiley & Sons, **2009**.
- [280] J. P. Blinco, J. L. Hodgson, B. J. Morrow, J. R. Walker, G. D. Will, M. L. Coote, S. E. Bottle, *The Journal of Organic Chemistry* **2008**, 73(17), 6763–6771.
- [281] J. Rühe, A. M. Granville, W. J. Brittain, *Polymer Brushes: Synthesis, Characterization, Applications*, (Editor: R. C. Advincula, W. J. Brittain, K. C. Caster, J. Rühe), Wiley-VCH, **2004**.
- [282] W. A. Braunecker, K. Matyjaszewski, *Prog. Polym. Sci.* **2007**, 32, 93–146.
- [283] C. J. Hawker, K. L. Wooley, *Science* **2005**, 309, 1200–1205.
- [284] P. L. Golas, K. Matyjaszewski, *Chem. Soc. Rev.* **2010**, 39, 1338–1354.
- [285] S. Sinnwell, A. J. Inglis, M. H. Stenzel, C. Barner-Kowollik, *Click Chemistry for Biotechnology and Materials Science*, (Editor: J. Lahann), John Wiley & Sons, Ltd., Chichester, UK, **2009**.
- [286] H. Nandivada, J. Lahann, *Click Chemistry for Biotechnology and Materials Science*, (Editor: J. Lahann), John Wiley & Sons, Ltd., Chichester, UK, **2009**.
- [287] U. Mansfeld, C. Pietsch, R. Hoogenboom, C. R. Becer, U. S. Schubert, *Polym. Chem.* **2010**, 1, 1560–1598.
- [288] S. Luza, H. Speisky, *Am. J. Clin. Nutr.* **1996**, 63, 812–820.
- [289] F. Wolbers, P. ter Braak, S. L. Gac, R. Luttge, H. Andersson, I. Vermes, A. van den Berg, *Electrophoresis* **2006**, 27, 5073–5080.
- [290] E. M. Sletten, C. R. Bertozzi, *Angew. Chem. Int. Ed.* **2009**, 48, 6974–6998.

- [291] R. Hoogenboom, *Angew. Chem. Int. Ed.* **2010**, *49*, 3415–3417.
- [292] T. Gründling, K. K. Öhlenschlaeger, E. Frick, M. Glassner, C. Schmid, C. Barner-Kowollik, *Macromol. Rapid Commun.* **2011**, *32*, 807–812.
- [293] M. Glassner, K. K. Öhlenschlaeger, T. Gründling, C. Barner-Kowollik, *Macromolecules* **2011**, *44*, 4681–4689.
- [294] G. Bertrand, C. Wentrup, *Angew. Chem. Int. Ed.* **1994**, *33*, 527545.
- [295] D. Moderhack, *J. Prakt. Chem.* **1998**, *340*, 687.
- [296] M. M. Madden, C. I. Rivera Vera, W. Song, Q. Lin, *Chem. Commun.* **2009**, (37), 5588–5590.
- [297] C. F. Hansell, P. Espeel, M. M. Stamenovic, I. A. Barker, A. P. Dove, F. E. Du Prez, R. K. O'Reilly, *J. Am. Chem. Soc.* **2011**, *133*(35), 13828–13831.
- [298] E. H. Lock, D. Y. Petrovykh, P. Mack, T. Carney, R. G. White, S. G. Walton, R. F. Fernsler, *Langmuir* **2010**, *26*, 8857–8868.
- [299] C. D. Marco, S. M. Eaton, R. Suriano, S. Turri, M. Levi, R. Ramponi, G. Cerullo, R. Osellame, *ACS Appl. Mater. Interfaces* **2010**, *2*, 2377–2384.
- [300] E. Szócs, I. Bakó, T. Kosztolányi, I. Bertóti, E. Kálmán, *Electrochim. Acta* **2004**, *49*, 1371–1378.
- [301] P. G. Rouxhet, A. M. Misselyn-Bauduin, F. Ahimou, M. J. Genet, Y. Adriaensen, T. Desille, P. Bodson, C. Deroanne, *Surf. Interface Anal.* **2008**, *40*, 718–724.
- [302] H. Meier, H. Heimgartner, *Helv. Chim. Acta* **1985**, *68*(5), 1283–1300.
- [303] V. Lohse, P. Leihkauf, C. Csongar, G. Tomaschewski, *J. Prakt. Chem.* **1988**, *330*(3), 406–414.
- [304] R. Darkow, M. Yoshikawa, T. Kitao, G. Tomaschewski, J. Schellenberg, *J. Polym. Sci., Part A: Polym. Chem.* **1994**, *32*(9), 1657–1664.
- [305] H. Meier, W. Heinzelmann, H. Heimgartner, *Chimia* **1980**, *34*, 506–508.
- [306] S.-L. Zheng, Y. Wang, Z. Yu, Q. Lin, P. Coppens, *J. Am. Chem. Soc.* **2009**, *131*(50), 18036–18037.
- [307] D. Leonard, Y. Chevolut, O. Bucher, H. Sigrüst, H. Mathieu, *SIA, Surf. Interface Anal.* **1998**, *26*(11), 783–792.
- [308] J. S. Stevens, S. L. M. Schroeder, *Surf. Interface Anal.* **2009**, *41*(6), 453–462.
- [309] A. Wagner, C.-W. Schellhammer, S. Petersen, *Angew. Chem., Int. Ed.* **1966**, *5*(8), 699–704.
- [310] H. R. Thomas, J. J. O'Malley, *Macromolecules* **1979**, *12*(2), 323–329.

# Curriculum Vitae

Date of Birth: 07 November 1981  
Place of Birth: Herbolzheim, Germany  
Nationality: German

## Education

2008 - 09/2011 **Doctoral Studies in Chemistry**  
under the supervision of Prof. Dr. Christopher Barner-Kowollik  
Karlsruhe Institute of Technology, Germany

2007-2008 **Scientific Co-worker**  
in the group of Prof. Eckhard Bartsch  
University of Freiburg

2006-2007 **Diploma Thesis**  
*Calculation of static structure factors and their comparison with experiments*  
Supervisor: Prof. Eckhard Bartsch  
University of Freiburg  
Grade: 1.0

2001-2007 **University of Freiburg**  
Diploma in Chemistry  
Freiburg, Germany

1998-2001 **High School**  
Wirtschaftsgymnasium St. Landulin,  
Ettenheim, Germany  
Overall grade: 2.3

1992-1998 **High School**  
Naturwissenschaftliches Gymnasium  
Kenzingen, Germany

## Employment History

Mai 2011 - present

**Research group of Prof. Barner-Kowollik**

Institut für Technische Chemie und Polymer Chemie

Karlsruhe Institute of Technology, Karlsruhe, Germany

Scientific Co-worker

May 2008 - May 2011

**Fraunhofer Institute of Technology**

Pfinzthal, Germany

Scientific Co-worker

April 2007 - April 2008

**Research group of Prof. Bartsch**

Institute of Macromolecular Chemistry

University of Freiburg

Scientific Co-worker

# List of Publications and Conference Contributions

## Refereed Journal Publications

- [01] A Novel One-Pot Procedure for the Fast and Efficient Conversion of RAFT Polymers into Hydroxy-Functional Polymers  
T. Gruending, M. Dietrich, C. Barner-Kowollik *Aust. J. Chem.* **2009**, *62*, 806-812.
- [02] Facile conversion of RAFT polymers into hydroxyl functional polymers: A detailed investigation of variable monomer and RAFT agent combinations  
M. Dietrich, M. Glassner, T. Gruending, C. Schmid, J. Falkenhagen, C. Barner-Kowollik *Polym. Chem.* **2010**, *1*, 634-644.

## Submitted Publications

- [03] Photoclickable Surfaces for Profluorescent Covalent Polymer Coatings  
M. Dietrich; G. Delaittre, J. P. Blinco, A. J. Inglis, M. Bruns, C. Barner-Kowollik  
*Advanced Functional Materials*

## Conference Contributions

- [04] Facile conversion of RAFT polymers into hydroxyl functional polymers: a detailed investigation of variable monomer and RAFT agent combinations  
M. Dietrich, M. Glassner, T. Gruending, C. Schmid, J. Falkenhagen, C. Barner-Kowollik

*Controlled/Living Radical Polymerizations: Latest Trends in Synthesis, Characterization and Industrial Applications; Belgian/German Binational Conference, Houffalize, Belgium 2009*

Ich erkläre hiermit, dass ich die vorliegende Doktorarbeit im Rahmen der Betreuung durch Prof. Dr. Christopher Barner-Kowollik, selbständig verfasst und keine anderen als die angegebenen Quellen und Hilfsmittel verwendet habe. Hiermit erkläre ich, dass ich mich derzeit in keinem laufenden Promotionsverfahren befinde, und auch keine vorausgegangenen Promotionsversuche unternommen habe.

Karlsruhe, den 12.09.2011



# 6

## Acknowledgements

The work of the last 3 years was conducted in the *macroarc* group at the Karlsruhe Institute of Technology (KIT) with financial support from the Fraunhofer Gesellschaft. I would like to thank all the people who helped and guided me while going the long way to the 'Doktor'.

At first, I would like to thank Prof. Dr. Christopher Barner-Kowollik who offered me the great possibility to work on exciting topics in the field of polymer chemistry and surface grafting. His ideas and motivation had a great account for my work as well as his constant support during the whole time. His enthusiasm for science is contagious and motivated me during the 'hard times' every scientist experiences during research.

Many thanks go to Dr. Andrew Inglis, Dr. James Blinco and Dr. Guillaume Delaittre for essential hints and fruitful discussions during my first steps towards polymer coupling as well as just having a good time whether in the lab or in the office or in the pub.

Furthermore I would like to thank Dr. Till Gründling for his constant help, teaching me SEC/ESI-MS and his open mind for new ideas.

I would also like to thank Mathias Glassner for the hard work conducted during his diploma thesis under my supervision resulting in significant contributions to chapter 3.

Many thanks also to my 'Vertiefer'-student Astrid Hirschbiel who performed extraordinarily during her studies.

I have to thank my co-workers in the office, there's always a joke and an amazing atmosphere to find. It was a pleasure having you as colleagues.

For the tremendous help with XPS measurement and their evaluation I would like to thank Dr. Michal Bruns.

Thanks to Dr. Andrew Vogt for fruitful discussions and great pictures as well as Ruben Porter for the contact angle measurements.

I thank the people of the Fraunhofer ICT for their continues support and warm welcome in their team and especially Schweppe for his extraordinary effort so that I could concentrate on research. Many thanks to Ute Laubach and Birgit Gartner for fighting bureaucracy at the ICT and Dr. Leonie Barner, Jens Forberger, Johanna Gebhardt, Jördis Eisenblätter, Jochen Cäsar, Jeannette Kramlich, Alicia Malek, Spyridon Korres and André Blockhaus for being always helpful and having fruitful discussions. Further, I would like to thank Dr. Diego Marchetto and Eberhard Nold for their effort with XPS measurements at the Fraunhofer IWM and also Christopher Synatschke from the University of Bayreuth for conducting MALDI-TOF measurements.

I would also like to thank Prof. Dr. Scherge from the Fraunhofer IWM for the opportunity to work on an interesting research project.

Many thanks go out to the crew of the brave 17, who were so kind to proof read the current thesis: Dr. Nathalie Guimard, Dr. Sebastian Emmerling, Christiane Lang, Dr. Elise Lejeune, Dr. Guillaume Delaitre, Dr. Anja Goldmann, Christoph Dürr, Mathias Glassner, Michael Kaupp, Thomas Tischer, Kim Öhlenschläger, Christina Schmid, Bernhard Schmidt, Dominik Voll, Anna-Marie Zorn, Nicolas Zydziak, Özcan Altintas.

For the - sometimes a bit time consuming - support with Latex I would like to thank Thomas Tischer und Michael Kaupp.

Evelyn Stühling and Gabriele Herrmann were very helpful while fighting bureaucracy at the KIT.

I would also like to thank the whole *macroarc* crew. You are a great team, it is a pleasure to work with you. Keep the spirit alive.

I am grateful to my family for their support over the past years.

Finally, but most importantly, I want to thank Mareike for making my relocation from Freiburg to Karlsruhe so much more enjoyable as well as for her constant personal support during my difficult research times. Hopefully there are much more happy years to come.

